Study of Complex Dynamical Neural Networks and its application to Brain Development and Emergent Synchronization Phenomena.

Thesis submitted by Ana Paula Millán Vidal
For the degree of Doctor of Philosophy

Supervisor: Joaquín Javier Torres Agudo

Granada, June 2019

Dedicado a mi familia

Ana Paula

Agradecimientos

GRACIAS...

a mis directores de tesis, Joaquín J. Torres, por su enorme aportación a esta tesis y su ayuda en todas las sorpresas que han surgido por el camino, y Joaquín Marro, por todas las ideas, los consejos, y las discusiones científicas y no tanto;

a Miguel Ángel Muñoz, por el tiempo, la paciencia, y el buen ánimo;

al resto de compañeros del departamento, veteranos y no tanto: Paco de los Santos, Pablo Huertado, Anonio Lacomba, Dani, Carlos, Migue, Rubén, Nico, Víctor; también las que no están, Paula, Vir, Serena, Jordi;

a Pablo y Nico especialmente, porque no habría encontrado mi escritorio (ni hecho la matrícula, ni presentado el plan de doctorado, ni entendido la impresora) sin ellos;

a Sam, porque no hay frases mejores;

Mención especial a Pedro Garrido por recordarnos que aquí no hay laureles (ni de dormir ni de corona), y a Jose, por supuesto, por darme siempre una nueva oportunidad de quemar un ordenador.

Thanks are due also to many friends across the sea (or the ocean)...

to all the amazing people in Queen Mary; Paul, Fede, Giulia, Iacopo, Aguí, and specially to Diego and Owen for always knowing where the beer was (even in Whales), and Oli, who is responsible for any sentence in this thesis that doesn't sound like "something only Italians would say" (btw, my cat was magical and turned into a comet; we should get some pizza). London was a scary, dark and rainy place, and you helped me find the summer. And of course a huge thank you to my mentor there, Ginestra Bianconi, for teaching me so much and her strength and perseverance.

and a bit further away, to all my friends in California, Oscar, Bryan, Erick, Aishu. Thanks for the help, the laughs, and explaining me how roads and money worked. Thanks also to Giri, Seth and Maxim.

No podría haber habido tesis, ni papers, ni carrera, ni nada, sin el apoyo de todas las personas que he conocido en estos diez años en Granada; Naza, Miguel, Feiliciano, Pilar, Irina, gracias. Creo que crecimos juntas (sobre todo

aprendimos latex juntas que es lo que cuenta). Gracias a los que siguen aquí (en serio, se oían grillos ya); especialmente a Cristina, Feliz, David y Claudia por los cafés (en especial los de dos horas; pero en especial especial los de cerveza); a Sam, Pablo, Paloma, Agor, por intentar cada día llevarme a comedores y por esa fuerza y lucha incansables.

Nunca habría llegado hasta aquí sin los profesores maravillosos que tuve durante la carrera y también antes, en Lorca, en mi casa (todavía). En el instituto Ibañez Martín conocí a unos docentes increíbles que me transmitieron pasión y amor por la cultura, pero sobre todo rigor y entereza. Muchísimas gracias. Y por supuesto a mis amigas allí, Elena, Mabe, Irene. Os quiero.

Llego al final de unos agradacemientos que han sido sorprendemente fáciles de escribir; es el momento de la familia. Sé que no entendéis muy bien lo que hago pero que siempre habéis estado orgullosos de mí y habéis confiado en las decisiones que he tomado. No sé si sabéis lo importante que vuestra confianza es para mí, así que aquí está. Gracias. Gracias. Gracias. Os quiero.

Alex, tú también eres familia. Eres una de las mejores personas que he conocido nunca. Sé que siempre vas a estar, sé que confías en mí y sé que tus abrazos son los mejores. Gracias por lo demás – el agua, las mantas, los viajes en coche, los cafés. Y gracias por los hervidos, espero poder pagarte esa deuda algún día. Eyes up!

Preface

This act of thinking, of doubting one's own existence, served philosopher René Descartes (1596-1650) as proof of his own reality; while other knowledge, feeling or sensation could be a product of imagination, there has to be a thinking being – the self – for there to be a thought (Descartes, 1984). It is not only great philosophers who have wondered about the reality of the perceived world, for it seems that it comes to every consciousness – the question, what am I? One could not possibly count the number of works, from the ancient Greeks to today's self-aid best-sellers, that have tackled in this question.

This question is often paired with another: where am I? Where is this voice – that one identifies with one-self – coming from? It might seem a shallow question (as the voice is clearly a product of one's own brain) however in most ancient societies they would without doubt say it was the heart talking. According to Aristotle (384-322 b.C.), the *"mind"* resides in the heart, and the rational nature of man is owed to the great capacity of the brain to cool blood overheated by the heart[1] (Bear et al., 2007).

During the Renaissance, Descartes defined a mechanistic theory to explain animal behavior based on cerebral function. The brain would only control human behavior in its *animal part* though, since – according to Descartes – the man has an intellect, a soul (*"l'esprit"*) given by God, where their *special* abilities reside. Descartes started in this way two lines of thought that are still extraordinarily influential. On one side, the mechanistic philosophy, according to which knowledge of the "machine" is enough to know and explain its behavior. On the other, the *mind-body dualism*, that still persists in today's society (Bear et al., 2007).

The study of the mind followed the same path as other phenomena of Nature, and during the first half of the 19$^{\text{th}}$ a definite shift towards empirical knowledge occurred, necessarily assisted by fundamental experimental breakthroughs that

---

[1]Although Hippocrates (460-379 b.C.) already suggested that the brain might be responsible for thoughts and feelings, his views did not become universally accepted (Bear et al., 2007).

provided new ways to study the brain. In 1823 Jean Pierre Flourens (1794-1867) studied for the first time the functionality of different brain areas in a systematic manner by carrying out localized lesions in the brain of living animals, and describing their effects on motor functions, sensibility and behavior (Pearce, 2009). Shortly after, Paul Broca (1824-1880), after working with brain-damaged patients, suggested that certain regions of the brain were responsible for particular functions, that is, that the different cognitive abilities are distributed through the brain (Schiller, 1992). The hypothesis was also supported by observations of epileptic patients by John Hughlings Jackson (1835-1911) – who correctly inferred the organization of the motor cortex by watching the progression of seizures through the body (Critchley and Critchley, 1998) – and led to the division of the brain in the so-called *Broca areas* (Bear et al., 2007).

In parallel with this study of brain functionality and anatomy, research in a microscopic scale was for the first time possible thanks to the improvement of the microscope and the development of new experimental techniques that allowed us to visualize individual cells for the first time. Camillo Golgi (1843-1926) developed in 1873 an experimental procedure using a silver chromate salt to reveal the intricate structure of individual neurons (DeFelipe, 2015), that was used by Santiago Ramón y Cajal (1852-1934) in his seminal works (Ramón y Cajal, 1911). Golgi and Ramón y Cajal shared the Nobel Prize in Physiology in 1906 for their extensive observations, descriptions, and categorizations of neurons throughout the brain. Their work finally let up to the formation of the *neuron doctrine*, the hypothesis that the basic functional unit of the brain is the neuron, by Ramón y Cajal (Guillery, 2004).

During the 20th century, neuroscience began to be recognized as a distinct academic discipline in its own right, and the understanding of neurons and of the function of the nervous system became increasingly precise and molecular. For example, in 1952, Alan Lloyd Hodgkin (1914-1998) and Andrew Huxley (1917-2012) presented a mathematical model for the transmission of electrical signals in neurons of the giant axon of the squid, which they called *action potentials*, and how they are initiated and propagated, known as the *Hodgkin-Huxley model*, that granted them the Nobel Prize in Physiology in 1963. This model was shortly followed by many others that simplified the dynamical equations (FitzHugh, 1961), or included new functionality (Kandel et al., 2000).

It is worth noting the remarkable change in mentality that allows one to move from the mind-body dualism, that has so persistently soaked in modern society, to a doctrine that essentially goes on to say that consciousness – that is, how one perceives one-self – is "simply" owe to the dynamics – as complex as it might be – of a (roughly) $50\mu m$ cell (Kandel et al., 2000). The fundamental step, however, resides in the number of such cells (around 10^{11} in the human brain) and their non-trivial (i.e. non-linear) synaptic interactions, of which one can count up to 10^{15} (Kandel et al., 2000). As a matter of fact, ever since the

publication of Santiago Ramón y Cajal's drawings of neurons, it was clear that these are connected to one another forming networks, and that the consideration of neuron dynamics alone would not be enough to describe neural function, as the synaptic interactions among neurons enable them to cooperate and give rise to complex emergent phenomena – including consciousness (Boccaletti et al., 2006; Telesford et al., 2011; Gastner and ódor, 2016; Marro and Chialvo, 2017).

It seems convenient then to adopt the theoretical tools of statistical mechanics (Greiner et al., 2012), which deals with large systems of stochastically interacting microscopic elements (these being atoms, spins, birds, cells or even people (Field et al., 1995; Garcia-Ojalvo et al., 2004; Kiyono et al., 2005; Shmulevich et al., 2005; Vandermeer et al., 2008; Moussaïd et al., 2009)), to study brain function (Abbott and Kepler, 1990). Statistical mechanics does not seek to solve exactly the motion of all particles at the microscopic level, but aims to describe the emergent collective behavior – via a set of macroscopic observables (Marro and Dickman, 2005) – of the system. Within this context, networks of neurons – aka *neural networks* – are described by a graph in which nodes represent neurons and links stand for synapses (Boccaletti et al., 2006). Neural networks were initially defined as mathematical algorithms that tried to mimic brain function, partly inspired by mathematical models of spin systems (Sherrington and Kirkpatrick, 1975). These considered interacting entities (the spins) which a 2-state dynamics (up and down), that included a temperature or noise parameter to govern random fluctuations. The first of these was the Ising model, put forward in 1920 by Wilhelm Lenz (1888-1957) and studied by Ernst Ising (1900-1998) as a way to understand phase transitions and the behavior of magnets (Lenz, 1920; Ising, 1925). The model was shown to present a spontaneous symmetry breaking at a given temperature that corresponds to the phase transition – of a critical nature – between an ordered and disordered state (Onsager, 1944; Brush, 1967; Baxter, 2016). Making an analogy between spins and neurons (being both interacting particles with up and down states), and between an ordered magnetic state and a memory one, Shun'ichi Amari (1936) and then John J. Hopfield (1933) defined the first neural network models to exhibit the mechanism known as **associative memory**, that is, the ability of the brain to store and recall memories (Amari, 1972; Hopfield, 1982).

The consideration of the brain as a neural network has revealed itself to be extremely prolific, and to this date it has served to study several aspects of brain function, such as *associative* (Hopfield, 1982) and *working memory* (Pantic et al., 2002; Mongillo et al., 2008), the so-called cerebral up-and-down states with the associated brain rhythms (Buzsaki, 2006; Holcman and Tsodyks, 2006; Mejías et al., 2010; Torres and Marro, 2015), the role of sleep (Bazhenov et al., 2002), or the development of the brain itself (Chechik et al., 1998). Similar approaches are used to gain a system-level understanding of some brain disorders such as epileptic seizures (Volman et al., 2011), Alzheimer's disease (Greicius et al.,

2004; Stam et al., 2008), autism (Geschwind and Levitt, 2007) or schizophrenia (Faludi and Mirnics, 2011).

In most studied cases, brain function is found to be best reproduced when the considered models operate at – or near – a critical point (that is, the point of a second-order phase transition) (Chialvo, 2004; Eguiluz et al., 2005; Chialvo et al., 2008; Bonachela et al., 2010). This evidence has lead up to the so-called *criticality hypothesis*, according to which the brain – and other living systems, for that matter – would extract a large number of benefits such as maximal dynamical range, maximal sensitivity to environmental changes, or an optimal trade-off between stability and flexibility, from operating in the vicinity of a phase transition (aka, at this *"edge of chaos"*) (Chialvo, 2006; Muñoz, 2018). The question remains however of how the brain is placed (or tuned) at such a rather specific point. In this regard, the celebrated paradigm *Self-Organized Criticality* (SOC) seems to offer a framework that explains, without any fine tuning, the prevalence of critical points in Nature (Valverde et al., 2015; Muñoz, 2018)[2].

Interestingly, however, imaging studies of brain activity at the resting state have revealed that the brain actually wanders around a broad region near a critical point, instead of staying in it (Tagliazucchi et al., 2012). This suggests that the region where cortical networks operate is not just a critical point, but a whole extended region around it. In the framework of statistical mechanics, extended critical-like regions – known as *Griffiths phases* (GP) – can emerge from structural or quenched disorder (Griffiths, 1969; Noest, 1986), such as is the case of the patterns of connectivity in the brain (Muñoz et al., 2010; Villegas et al., 2014). Given that disorder is an intrinsic and unavoidable feature of neural systems, GPs are expected to have a relevant role in many dynamical aspects (Treviño III et al., 2012).

Nowadays, the underlying architecture of neural networks, as well as the question of how the structure and function of neural networks are related, is being considered in terms of large-scale *connectomes* or maps of connections (Bullmore and Sporns, 2009). Overall, biological neural networks have been found to display a structure that is not random nor regular, that at the same time segregates in different regions but presents short distances among them (i.e. a *small-world* structure), and splits in communities of regions more closely connected within themselves than with the rest of the brain in a hierarchical manner (a *hierarchical-modular structure*), and in which the relevant magnitudes, such as the number of neighbors, span many orders of magnitude (with indications of being *scale-free*) (Sporns et al., 2005; Achard et al., 2006; Bassett et al., 2006; Zhou et al., 2006; Stafford et al., 2014). Interestingly, recent

---

[2]As Per Bak put it in his seminal work, *"the aim of the science of self-organized criticality is to yield insight into the fundamental question of why Nature is complex, not simple, as the laws of physics imply"* (Bak et al., 1987).

studies on *in-vitro* cultures have also shown that its synchronization capabilities are strongly influenced by the *dimensionality* of the underlying network, suggesting that several features of brain dynamics might be a consequence of its 3-dimensional embedding (Severino et al., 2016).

Overall, these topological properties of the human connectome are thought to be fundamental to support both distributed processing and efficient integration of information (Bullmore and Sporns, 2012). Finding such networks of connections and relating their structural properties to the emerging cognitive functions is thus considered to be a fundamental question in neuroscience (Sporns, 2011; Gastner and ódor, 2016).

Neural networks are not static, as they change constantly in time subjected to internal and external stimuli. The formation of the brain, in particular, requires the creation of the enormous number of neurons and glia cells that conform it, and of all the synaptic connections among neurons. It does not seem realistic that the information needed to built an efficient network of such dimensions could be fully encoded in the genetic code – as large and complex as this might as well be (Kauffman, 1993; Shmulevich et al., 2005; Nykter et al., 2008). Consequently, one might ask whether the complex structure of the neural system could arise from simple growth mechanisms. Models in which networks are gradually formed, for instance by addition and/or deletion of nodes and edges, or by the rewiring of the latter, have long been studied in various contexts (Berg et al., 2004; Johnson et al., 2009; Navlakha et al., 2015). The idea behind all such evolving network models is that there should be general, relatively simple "microscopic" mechanisms which can give rise to these complex structures without the need for previous high levels of information or *a propos* tuning (Newman, 2003; Albert, 2005). Certain evolution rules have thus been shown to generate network topologies with particular properties, such as small-world, scale-free, or hierarchical-modular structures (Watts and Strogatz, 1998; Barabási and Albert, 1999; Bianconi and Rahmede, 2016). These rules often give rise to phase transitions, such that qualitatively different kinds of network topologies can ensue depending on parameters.

In most studied networks the evolution of the structure – or topology – is invariably linked to the state of the network and vice versa (Gross and Blasius, 2007). Consequently, models in which the evolution of network structure is intrinsically coupled with an activity model that runs on the nodes of the network – the so-called *co-evolving* or *adaptive* network models – have gained attention as a way to approximate the evolution of real systems (Sayama et al., 2013). Some interesting dynamic phenomena occur repeatedly in adaptive networks, such as the formation of complex topologies, robust dynamical self-organization, spontaneous emergence of different classes of nodes, generally through a complex mutual dynamics of both activity and topology (Vazquez et al., 2008; Su et al., 2013; Wiedermann et al., 2015).

Within this overall context, the aim of this thesis is to investigate, combining mathematical models and computational simulations, the collective behavior that may emerge in neural networks due to the symbiotic relationship between their complex, heterogeneous and time changing structure and the non-linear physiological dynamics of their components, as neurons and synapses.

In particular, the *main objectives of this thesis* are:

i) The development of a biologically-inspired adaptive model of brain maturation and evolution that couples neural activity and topology dynamics, and that can reproduce experimental temporal profiles of the synaptic density in the brain during infancy and young adulthood. We will also study its inherent emerging behavior due to the interplay between structural and physiological dynamics, and ask if new phases appear and how these – and the associated phase transitions – affect the memory capabilities of the system (chapter 2).

ii) The study of the determinant role of the synaptic density of the brain, both during infancy and adulthood, in its emergent cognitive abilities (chapters 3 and 4). The synaptic density of the brain varies largely during development, as a great number of synapses are created to be then gradually pruned. On this thesis we will study whether there are any computational advantages of going through such non-trivial evolution, and how the stability of the memories – both static and dynamic – depend on the intensity and extension of the pruning process and on the emergence of hubs (highly connected neurons) on the network. This is to be related to results in autism spectrum disorder, where a deficit in synaptic has been found, and schizophrenia, where there are evidences of an excessive pruning, and the cognitive impairment associated with these disorders.

iii) To develop a simple theoretical framework to study synchronization and frustrated synchronization phenomena in complex networks of neural oscillators, as a function of the topological features of the network, and relate them to similar phenomena observed in actual brain networks (chapters 5 and 6). One of the most studied features of brain dynamics is the emergence of synchronization at different rhythms, a phenomenon observed both in-vivo with EEG (electro-encephalogram) recordings and in in-vitro studies of neuronal activity. It has been argue that synchronization is fundamental for the brain to establish large-scale integration of distributed information (Varela et al., 2001). A characteristic feature is the emergence of temporal and spatial heterogeneous patterns of oscillations, which have been related to the non-trivial structure of the brain, but whose role and significance on brain dynamics is yet to be fully understood. In particular,

little is known of the effect of the non-trivial geometrical structure of the brain on its cognitive capabilities.

The *structure of the thesis* is as follows:

In **chapter** 1 we present an inductive, non-extensive picture of brain dynamics and its study, and we discuss the state of the art of some areas involved in brain research. We try to present a brief physiological description of the systems of interests, together with some archetypal or ground-breaking models, with particular attention to those that are used during the original chapters of this thesis. In particular, we start describing the basic dynamics of individual neurons and synapses (section 1.1), to then introduce the concept of neural networks and connectomes (section 1.2). We go on to consider how such networks might arise, and in section 1.3, we present some mathematical models of network evolution that give rise to non-trivial topologies. Finally, in section 1.4 we focus on the collective properties that may emerge on neural systems as a consequence of the non-linear microscopic dynamics and the complex changing structure described in the previous sections. In particular, we discuss the properties of associative memory and synchronization (presenting the Amari-Hopfield and Kuramoto models respectively to describe them), and the criticality hypothesis. Finally we present the mathematical framework of adaptive networks, in which the structure and dynamics of a system are naturally coupled, as a way to close our description of neural systems. Notice that this description is necessarily biased towards the results and models that are most relevant to the original chapters of this thesis. We do not seek to cover all aspects of brain function, physiology, or dynamics, but rather to present a convincing case for the relevance – and necessity – of statistical physics and complex system approaches in neuroscience.

In the chapters that follow, we present the original scientific contributions of this thesis.

In **chapter** 2 we present an adaptive model of brain evolution by combining a familiar auto-associative neural network with an evolving mechanism for the birth and death of synapses, that we use to describe *synaptic pruning* (an extensive decrease of synaptic density occurring during infancy). The question of how structure and function are related in neural systems is a fundamental question in neuroscience, and with this model we try to shed some light in this regard. We find that a feedback loop arises leading to two qualitatively different types of behavior. In one, the network structure becomes heterogeneous and dissasortative, and the system displays good memory performance; furthermore, the structure is optimized for the particular memory patterns stored during the process. In the other, the structure remains homogeneous and incapable of pattern retrieval. These findings provide an inspiring picture of brain structure and dynamics, are compatible with experimental results on early brain development,

and give a satisfactory explanation of synaptic pruning. We finally show that other evolving networks – such as those of protein interactions – might share the basic ingredients for this feedback loop and other questions, and indeed many of their structural features are as predicted by our model.

In **chapter** 3 we demonstrate that, as a consequence of the reported feedback-loop between form and function, hubs emerge in the system that greatly improve its tolerance to noise, and that are correlated to the patterns memorized in the network. Moreover, we also show that oscillations in the activity of the system among the memorized patterns of activity can occur, depending on model parameters, reminding mind dynamical processes. We show that such oscillations have their origin in the destabilization of memory attractors due to the pruning dynamics, that reduce the degree of the associated neuron hubs, inducing a kind of structural disorder or noise in the system at a long-term scale. This constantly modifies the synaptic disorder induced by the interference among the many patterns of activity memorized in the system. We also demonstrate that the observed new intriguing oscillatory behavior is to be associated only to long-term synaptic mechanisms during the network evolution dynamics, and it does not depend on short-term synaptic processes, as assumed in other studies and which are not present in our model. We finally show that the region of the parameter space associated with such oscillations is maximum when intermediate values of the stationary synaptic density are considered, since for sub-optimal connectivity network activity eventually becomes random, whereas for super-optimal ones the memories are stable and typically no oscillations are observed. We relate this result to some of the cognitive deficits associated with autism (where a defect of pruning has been observed) and schizophrenia (in which there are indications of an excess of pruning in some brain areas).

In **chapter** 4 we extend the proposed model for synaptic pruning to reproduce experimental profiles of temporal connectivity, including a transient period of relatively high connectivity during infancy, and to investigate if such initial growth has an important role on the emergent behavior of the system and on its computational properties. Thus, using a simple computational approach, we demonstrate that the consideration of this initial transient leads to an increased stability of the memory (ordered) states, such that there is a discontinuous phase transition between the ordered memory phase and a disordered one as a function of the transient density, with an associated bi-stability region. Furthermore, we prove that intermediate values of the initial synaptic density allow the system to reach the ordered state with a minimum energy consumption, a result that we also show to be robust to details of the synaptic pruning model considered. Finally, we show that the stationary state of the system is ultimately determined by the level of heterogeneity of the network prior the beginning of synaptic pruning. Our results here could thus explain why the experimental curves of synaptic density follow their characteristic profiles during infancy and, eventu-

ally, anomalies such as autism and schizophrenia associated, respectively, with a deficit or an excess of pruning that occur during early infancy and adulthood, respectively.

In the chapters that follow, we try to shed light on the origin of the complex spatio-temporal patterns of neural activity repeatedly observed in the cortex. In order to do so, we consider the relationship between the underlying geometrical structure of *in-vivo* neural networks and their synchronization capabilities. Biological neural network develop on a 3D space that is bounded by the cranium. However, typically *in-vitro* studies ignore this fact and consider 2D neuronal cultures. Similarly, the question of how the network's geometrical properties affect neuronal dynamics has been mostly unexplored from a theoretical point of view. Interestingly, however, recent *in-vitro* studies of neural activity indicate that the dynamics of networks of neuronal cultures are strongly dependent on the network geometry, and in particular on its dimensionality, so that 3D neuronal cultures produce more complex and varied patterns of oscillations than 2D ones.

In order to tackle this question from a theoretical point of view, in **chapter** 5 we consider a simple mathematical framework to study how the synchronization capabilities of a neural network might be affected by different features of its complex structure. In particular, we study the interplay between network geometry and the synchronization dynamics of coupled oscillators following Kuramoto dynamics. We use a complex network model called *Complex Network Manifold* that allows us to generate networks with a given geometrical and spectral dimension d_s, that are also small-world (and thus have an infinite Hausdorff dimension) and have a highly modular structure. We also demonstrate that CNMs with a given integer spectral dimension d_s can be embedded in a $d_s - 1$-dimensional euclidean space. Using this framework, we show that the synchronization properties of the network are directly affected by its spectral dimension, and that a wide region of *frustrated synchronization*, displaying complex patterns of oscillatory behavior, emerges for $d_s \geq 4$. Interestingly, these results imply that cortical networks, despite being embedded in a 3D space, could display a spectral dimension equal to four, the critical dimension for the onset of a global synchronous phase.

In **chapter** 6 we extend the numerical results obtained in chapter 5 and show that the spectral dimension of a complex network is determinant for the synchronization phenomena that it can display. In particular, we develop a mathematical framework to prove that the globally synchronized phase can only be thermodynamically stable for $d_s > 4$, whereas for $d_s > 2$ phase entrainment of the oscillators can occur. We then test our predictions on an extended framework of the Complex Network Manifolds model used in chapter 5. With the considered extension, the spectral dimension of the networks can hold fractional values as well, depending on the symmetries of the underlying structure. Consequently, these networks present a more tunable spectral dimension, and therefore

constitute an ideal framework to study the interplay between network geometry and synchronization.

Finally, in **chapter** 7 we present the main conclusions of this thesis, focusing on the fundamental role of the interplay between network structure and function, and on the possible implications of our findings. We finally discuss on the plausibility and possible extensions of the models considered and developed in this thesis.

Granada, June 2019

Resumen en castellano

"Cogito, ergo sum"
René Descates

Este pensamiento, el dudar de la existencia de uno mismo, sirvió al filósofo René Descartes (1596-1650) como prueba de su propia realidad; mientras cualquier otro conocimiento, sentimiento o sensación podía ser un producto de la imaginación, ha de haber un ser pensando – uno mismo – para que haya pensamiento (Descartes, 1984). Los grandes filósofos no han sido los únicos en preguntarse por la realidad del mundo percibido, ya que parece llegar a toda consciencia, la pregunta, ¿qué soy yo? Resultaría imposible contar el número de trabajos, desde la antigua Grecia a los actuales libros de auto-ayuda, que han intentado, con mayor o menor éxito, enfrentarse a esta pregunta.

Y es una pregunta que usualmente aparece acompañada por otra: ¿dónde estoy? ¿Dónde reside esta voz, que uno identifica consigo mismo? Puede parecer una pregunta banal, puesto que la voz es claramente un producto de mi cerebro, sin embargo en la mayoría de las culturas clásicas nos dirían, sin duda alguna, que es el corazón quien habla. De acuerdo con Aristóteles (384-322 a.C.), sin ir más lejos, la *"mente"* reside en el corazón, y la naturaleza racional del hombre se debe a la gran capacidad del corazón para enfriar la sangre "sobrecalentada" por el corazón[3] (Bear et al., 2007).

Ya durante el Renacimiento Descartes definió una teoría mecanicista para explicar el comportamiento animal basada en la función cerebral. No obstante, el cerebro sólo controlaría el comportamiento humano en su *parte animal* dado que, de acuerdo a Descartes, el hombre tiene un intelecto, un alma (*"l'espirit"*) dado por Dios, donde residen sus habilidades *especiales*. De este modo Descartes dio lugar a dos líneas de pensamiento que son aún tremendamente influyentes. Por un lado, la filosofía mecanicista, de acuerdo a la cual el conocimiento de la "máquina" basta para conocer y explicar su función. Por otro, el dualismo *mente-cerebro*, que aún persiste en la sociedad actual (Bear et al., 2007).

---

[3]Aunque Hipócrates (460-379 a.C.). ya sugirió que el cerebro podría ser responsable de los pensamientos y las sensaciones, sus teorías no fueron universalmente aceptadas (Bear et al., 2007).

El estudio de la mente, no obstante, siguió el mismo camino que otros fenómenos de la Naturaleza y durante la primera mitad del sigo XIX hubo un cambio definitivo en favor del conocimiento empírico, necesariamente asistido por el desarrollo de hitos experimentales que permitieron nuevas formas de estudiar el cerebro. En 1823 Jean Pierre Flourens (1794-1867) estudió por primera vez la funcionalidad de distintas áreas cerebrales de un modo sistemático, realizando lesiones localizadas en el cerebro de animales vivos y describiendo sus efectos en la función motora, la sensibilidad y el comportamiento del animal (Pearce, 2009). Poco tiempo después Paul Broca (1824-1880), tras trabajar con sujetos que presentaban daño cerebral, sugirió que ciertas regiones cerebrales eran responsables de funciones particulares, esto es, que las distintas habilidades cognitivas tiene lugar de forma distribuida en el cerebro (Schiller, 1992). La hipótesis fue reforzada por las observaciones experimentales de pacientes con epilepsia por John Hughlings Jackson (1835-1911), que infirió correctamente la organización del cortex motor observando la progresión de los ataques epilépticos en el cuerpo (Critchley and Critchley, 1998). Finalmente se formuló la división del cerebro regiones funcionales denominadas *areas de Broca* (Bear et al., 2007).

En paralelo con este estudio de la funcionalidad del cerebro y su anatomía, por primera vez fue posible investigar a escala microscópica gracias a la mejora del microscopio y al desarrollo de nuevas técnicas experimentales, que permitieron por primera vez visualizar células individuales. En concreto, Camillo Golgi (1843-1926) desarrolló en 1873 un procedimiento experimental basado en un cromato de plata para revelar la intrincada estructura de las neuronas individuales (DeFelipe, 2015), que fue después utilizado por Santiago Ramón y Cajal (1852-1934) en sus trabajos seminales (Ramón y Cajal, 1911). Golgi y Ramón y Cajal compartieron el premio Nobel en medicina en 1906 por sus extensas observaciones, descripciones y categorizaciones de las neuronas en el cerebro. Su trabajo finalmente llevó finalmente a Ramón y Cajal a formular la *doctrina de la neurona*, la hipótesis de que la unidad funcional básica del cerebro es la neurona (Guillery, 2004).

Durante el siglo XX, la neurociencia empezó a ser reconocida como una disciplina académica propia, y la compresión de las neuronas y de la funcionalidad del sistema nervioso empezó a ser cada vez más precisa y molecular. Por ejemplo, en 1952, Alan Lloyd Hodgkin (1914-1998) y Andrew Huxley (1917-2012) presentaron un modelo matemático para la transmisión de señales eléctricas en el axón gigante del calamar, que denominaron *potenciales de acción*, y cómo se inician y propagan, conocido como el *modelo de Hodgkin-Huxley*, por el que se les concedió el premio Nobel de medicina en 1963. Inspirados por este modelo, poco después se desarrollaron muchos otros simplificando las ecuaciones involucradas (FitzHugh, 1961), o incluyendo nueva funcionalidad (Kandel et al., 2000), por ejemplo.

Es remarcable el enorme cambio de mentalidad que permite pasar de la

dualidad mente-cuerpo, que tan persistentemente ha percolado en la sociedad moderna, a una doctrina, la de la neurona, que esencialmente viene a decir que la consciencia, esto es, cómo uno se percibe a sí mismo, es "simplemente" un fenómeno emergente debido a las dinámicas, tan complejas como puedan ser, de un célula con poco más de $50\mu m$ de tamaño (Kandel et al., 2000). El paso fundamental, no obstante, reside en el enorme número de dichas células (alrededor de 10^{11} en el cerebro humano) y en sus complejas interacciones sinápticas (no lineales), de las que uno puede contar más de 10^{15} (Kandel et al., 2000). De hecho, desde la publicación de los famosos dibujos de neuronas por parte de Santiago Ramón y Cajal, ha estado claro que éstas están conectadas entre sí formando redes, y que la consideración únicamente de la dinámica neuronal individual no será suficiente para describir la función neuronal. Así, las interacciones sinápticas entre las neuronas les permiten cooperar, dando lugar a comportamientos complejos emergentes, incluyendo la consciencia (Boccaletti et al., 2006; Telesford et al., 2011; Gastner and ódor, 2016; Marro and Chialvo, 2017).

Parece fundamental entonces adoptar las herramientas teóricas de la física estadística (Greiner et al., 2012), que ya trabaja con grandes sistemas de elementos microscópicos estocásticos que interactúan entre sí (ya sean átomos, espines, pájaros, células o incluso personas) (Field et al., 1995; Garcia-Ojalvo et al., 2004; Kiyono et al., 2005; Shmulevich et al., 2005; Vandermeer et al., 2008; Moussaïd et al., 2009)), para estudiar la funcionalidad del cerebro (Abbott and Kepler, 1990). La mecánica estadística no busca resolver de forma exacta el movimiento de todas las partículas involucradas a nivel microscópico, sino describir el comportamiento emergente, mediante un conjunto de observables macroscópicos (Marro and Dickman, 2005), del sistema. En este contexto, se definen las redes de neuronas, o *redes neuronales*, descritas por un grafo en el que los nodos representan neuronas mientras que las aristas representan sinapsis (Boccaletti et al., 2006). Las redes neuronales fueron inicialmente definidas como algoritmos matemáticos para reproducir la función cerebral, parcialmente inspirados por los modelos matemáticos de los sitemas de espines (Sherrington and Kirkpatrick, 1975). A su vez, éstos consideran partículas binarias (con estados "up" y "down", o arriba y abajo), que interactúan entre sí en presencia de un baño térmico a una temperatura dada o ruido que gobierna las fluctuaciones aleatorias. El primero de estos modelos fue el modelo de Ising, formulado en 1920 by Wilhelm Lenz (1888-1957) y estudiado por Ernst Ising (1900-1998) como una forma de entender los cambios de fase y el comportamiento de los imanes (Lenz, 1920; Ising, 1925). Pronto se demostró que el modelo presentaba una ruptura espontánea de la simetría a una temperatura dada, que corresponde con el cambio de fase, de naturaleza crítica, entre un estado ordenado y otro desordenado (Onsager, 1944; Brush, 1967; Baxter, 2016). Realizando una analogía entre espines y neuronas, siendo ambos partículas con dos estados que interactúan entre

sí, y entre un estado magnético ordenado y uno de memoria, Shun'ichi Amari (1936) primero y John J. Hopfield (1933) después definieron el primer modelo de red neuronal capaz de exhibir el mecanismo conocido como **memoria asociativa**, esto es, la habilidad del cerebro para almacenar y recuperar memorias (Amari, 1972; Hopfield, 1982).

La consideración del cerebro como una red neuronal ha demostrado ser extremadamente prolífica y, hasta la fecha, ha servido para estudiar diversos aspectos de la funcionalidad cerebral como la memoria *asociativa* (Hopfield, 1982) y *dinámica* (Pantic et al., 2002; Mongillo et al., 2008), los llamados estados "arriba" y "abajo" con los asociados ritmos cerebrales (Buzsaki, 2006; Holcman and Tsodyks, 2006; Mejías et al., 2010; Torres and Marro, 2015), el papel del sueño (Bazhenov et al., 2002) o el desarrollo del cerebro en sí mismo (Chechik et al., 1998). Perspectivas similares se usan para obtener un entendimiento global del sistema en casos de desordenes cerebrales como ataques epilépticos (Volman et al., 2011), la enfemedad del Alzheimer (Greicius et al., 2004; Stam et al., 2008), el autismo (Geschwind and Levitt, 2007) o la esquizofrenia (Faludi and Mirnics, 2011).

En la mayoría de los casos estudiados se ha encontrado que la funcionalidad del cerebro se reproduce de forma más natural cuando los modelos considerados operan en (o cerca de) un punto crítico, esto es, el punto correspondiente a una transición de fase de segundo orden) (Chialvo, 2004; Eguiluz et al., 2005; Chialvo et al., 2008; Bonachela et al., 2010). Esta evidencia ha llevado a formular la llamada *hipótesis de criticalidad*, de acuerdo a la cual el cerebro, y otros sistemas en general, extrae un gran número de beneficios al operar cerca de una transición de fase, en el llamado *"borde del caos"*. Entre estos destacan un máximo rango dinámico, sensibilidad máxima a estímulos o cambios externos, o un compromiso óptimo entre estabilidad y flexibilidad, por ejemplo (Chialvo, 2006; Muñoz, 2018). No obstante, aún es necesario esclarecer cómo se coloca o ajusta el cerebro en una configuración tan particular. En este contexto, el celebrado paradigma de *Criticalidad Auto-organizada* (SOC por sus siglas en inglés) parece ofrecer un marco teórico para explicar, sin necesidad de un ajuste preciso de los parámetros, la prevalencia de los puntos críticos en la naturaleza (Valverde et al., 2015; Muñoz, 2018)[4].

Recientes estudios de la actividad cerebral mediante fMRI han revelado que el cerebro, en su estado de reposo, no permanece en un único punto dinámico, sino que deambula en una amplia región a su alrededor (Tagliazucchi et al., 2012). De acuerdo a esta observación, la región en la que operan las redes corticales no sería solo un punto crítico, sino toda una región extendida a su alrededor. En el ámbito de la mecánica estadística, estas regiones pseudo-

---

[4] Como Per Bak escribió en su trabajo seminal, *"el objetivo de la ciencia de la criticalidad auto-organizada es ayudar a comprender la cuestión fundamental de por qué la naturaleza es compleja, y no sencilla, como las reglas de la física implican"* (Bak et al., 1987).

críticas, conocidas como *fases de Griffths* (GP por sus siglas en inglés), pueden emerger en sistemas con desorden estructural o "congelado" (Griffiths, 1969; Noest, 1986), como el producido por los patrones de conectividad no triviales en el cerebro (Muñoz et al., 2010; Villegas et al., 2014). Dado el desorden es una propiedad intrínseca e inevitable de los sistemas neuronales, las fases de Griffiths podrían tener un papel muy relevante en muchos de los aspectos dinámicos del cerebro (Treviño III et al., 2012).

Actualmente la arquitectura subyacente de las redes neuronales, además de la relación entre su estructura y función, se considera en términos de *"conectomas"* o mapas de conexiones a gran escala (Bullmore and Sporns, 2009). A partir de ellos se ha encontrado que las redes neuronales biológicas presentan una estructura que no es totalmente aleatoria ni tampoco regular, que está segregada en diferentes regiones que se mantienen a corta distancia (la llamada estructura de *"mundo pequeño"*) y se dividen en comunidades de regiones más estrechamente conectadas entre ellas que con el resto del cerebro de una manera jerárquica (estructura *jerárquico-modular*) en las cuales las magnitudes relevantes, como el número de vecinos, abarcan varios órdenes de magnitud (con indicaciones de ser *invariantes de escala*) (Sporns et al., 2005; Achard et al., 2006; Bassett et al., 2006; Zhou et al., 2006; Stafford et al., 2014). Curiosamente, estudios recientes en cultivos *in-vitro* han mostrado que sus capacidades de sincronización están fuertemente influenciadas por la *dimensionalidad* de la red subyacente, sugiriendo que diversas características de la dinámica del cerebro podrían ser consecuencia de su naturaleza tridimensional.

En general, las propiedades topológicas del conectoma humano podrían ser fundamentales para mantener tanto un procesamiento distribuido de la información como su integración eficiente (Bullmore and Sporns, 2012). Encontrar y caracterizar estas redes de conexiones, y relacionar sus propiedades estructurales con la funcionalidad cognitiva emergente, se considera por tanto un problema fundamental en neurociencia en la actualidad (Sporns, 2011; Gastner and ódor, 2016).

Las redes neuronales no son estáticas, sino que cambian constantemente sujetas a estímulos internos y externos. La formación del cerebro, en particular, requiere la creación de las enormes cantidades de neuronas y células de glía que lo conforman, y de todas las conexiones sinápticas entre neuronas. No parece realista pues que la información necesaria para construir una red eficiente de tales dimensiones pueda estar plenamente codificada en el código genético – por grande y complejo que éste sea (Kauffman, 1993; Shmulevich et al., 2005; Nykter et al., 2008). Por ello, cabe preguntarse si la compleja estructura del sistema neuronal podría surgir de mecanismos de crecimiento simples. Los modelos en los que las redes se forman gradualmente, por ejemplo mediante la adición o eliminación de nodos y enlaces, o mediante el reenlazado de estos últimos, se han estudiado ampliamente en varios contextos (Berg et al., 2004; Johnson et

al., 2009; Navlakha et al., 2015). La idea detrás de tales modelos es que deberían existir unas reglas generales relativamente simples de mecanismos "microscópicos" que den lugar a estas estructuras complejas sin la necesidad de grandes cantidades de información previa o ajuste de parámetros (Newman, 2003; Albert, 2005). Se ha encontrado, pues, que ciertas reglas evolutivas pueden dar lugar a topologías particulares, como la de mundo pequeño, la invarianza de escala o estructuras jerárquico-modulares (Watts and Strogatz, 1998; Barabási and Albert, 1999; Bianconi and Rahmede, 2016). Estas reglas a menudo dan lugar a transiciones de fase tales que pueden desarrollarse topologías de red cualitativamente diferentes en función de los parámetros del sistema.

En la mayoría de las redes estudiadas, la evolución de la estructura (o topología) está invariablemente ligada al estado de la red y vice-versa (Gross and Blasius, 2007). Así, los modelos en los que la evolución de la estructura de la red está intrínsecamente acoplada con un modelo de actividad neuronal que se desarrolla sobre ella (las llamadas redes *adaptativas* o *co-evolutivas*) se utilizan como forma de aproximar la evolución de sistemas reales (Sayama et al., 2013). Algunos fenómenos dinámicos ocurren de forma repetida en las redes adaptativas, como son la formación de estructuras complejas, la emergergencia de auto-organización dinámica robusta o la aparición de clases de nodos funcionalmente distintas (Vazquez et al., 2008; Su et al., 2013; Wiedermann et al., 2015).

Dentro de este contexto general, el objetivo de esta tesis es investigar, combinando modelos matemáticos y simulaciones computacionales, el comportamiento colectivo emergente en las redes neuronales biológicas debido a la relación simbiótica entre su estructura compleja, heterogénea y cambiante en el tiempo, y la dinámica fisiológica no-lineal de sus constituyentes, como son neuronas y sinapsis.

En particular, los *principales objetivos de esta tesis* son:

i) Desarrollar un modelo adaptativo, inspirado en las redes neuronales biológicas, de la maduración y evolución del cerebro, que acople la actividad neuronal con la dinámica de la topología de la red subyacente, y que reproduzca perfiles temporales experimentales de la densidad sináptica en el cerebro durante la infancia. También estudiaremos el comportamiento emergente en este modelo debido a la inter-relación entre la dinámica de la estructura y la fisiología, y analizaremos si aparecen nuevas fases y cómo éstas, y las transiciones de fase asociadas, afectan a la capacidad de memoria del sistema (capítulo 2).

ii) Estudiar el papel fundamental de la densidad sináptica del cerebro, tanto durante el desarrollo como en la madurez, en sus capacidades cognitivas emergentes (capítulos 3 y 4). La densidad sináptica del cerebro varía am-

pliamente durante el desarrollo, cuando se crean y destruyen (o podan) un gran número de sinápsis. En esta tesis estudiaremos las posibles ventajas computacionales que un desarrollo tan poco trivial puede tener. Así mismo, analizaremos cómo la extensión del proceso de poda y la posible aparición de nodos centrales altamente conectados (denominados "*hubs*") puede afectar a la aparición y estabilidad de las memorias, tanto estáticas como dinámicas.

iii) Desarrollar un marco teórico sencillo para estudiar la sincronización y fenómenos de sincronización frustrada en redes complejas de osciladores neuronales, como función de las características topológicas de la red, y relacionarlas a fenomenos similares observados en circuitos y redes cerebrales reales (capítulos 5 y 6). Una de las propiedades mejor estudiadas de la dinámica cerebral es la aparición de estados de sincronización en diferentes ritmos, un fenómeno observado *in-vivo* con grabaciones EEG (electroencefalograma) y en estudios *in-vitro* de la actividad neuronal. Se ha argumentado que la sincronización es fundamental para que el cerebro establezca una integración a gran escala de la información distribuida (Varela et al., 2001). Una propiedad característica es la aparición de patrones de oscilación temporas y espacialmente heterogéneos, los cuales se han relacionado a la estructura no trivial del cerebro, pero cuyo papel y significancia en la dinámica cerebral está todavía por entender. En particular, poco es sabido del efecto de las estructuras geométricas no triviales del cerebro en sus capacidades cognitivas.

La *estructura de esta tesis* es como sigue:

En el **capítulo** 1 presentamos una imagen inductiva y no extensiva de la dinámica cerebral y su estudio y discutimos las investigaciones más recientes sobre el cerebro. Intentamos presentar una descripción fisiológica breve de los sistemas de interés, junto a algunos modelos arquetípicos o revolucionarios con especial atención a aquellos que son utilizados en los capítulos originales de esta tesis. En particular, comenzamos describiendo la dinámica básica de neuronas y sinapsis individuales (sección 1.1), para después introducir el concepto de redes neuronales y conectomas (sección 1.2). Proseguimos considerando cómo surgen dichas redes y, en la sección 1.3, presentamos algunos modelos matemáticos de evolución de la red que dan lugar a topologías no triviales. Finalmente, en la sección 1.4 nos centramos en las propiedades colectivas que pueden emerger en sistemas neuronales como consecuencia de la dinámica microscópica no lineal y la compleja estructura cambiante descrita en secciones previas. En particular, discutimos las propiedades de la memoria asociativa y la sincronización (presentando los modelos de Amari-Hopfield y Kuramoto respectivamente para describirlos), y la hipótesis de criticalidad. Finalmente, presentamos el marco

matemático de redes adaptativas, en las cuales la estructura y la dinámica del sistema están naturalmente acopladas, como fin de nuestra descripción de los sistemas neuronales. Nótese que esta descripción está necesariamente sesgada hacia los resultados y modelos más relevantes para los capítulos originales de esta tesis. No buscamos cubrir todos los aspectos de la función cerebral, fisiología, o dinámica, sino presentar un esquema convincente de la relevancia – y necesidad – de la física estadística y de los sistemas complejos en la neurociencia.

En los capítulos que siguen presentamos las contribuciones científicas originales de esta tesis.

En el **capítulo** 2 presentamos un modelo adaptativo de la evolución del cerebro combinando un conocido modelo red neuronal auto-asociativa (el modelo de Amari-Hopfield) con un mecanismo para la creación y poda de sinapsis, y lo utilizamos para describir la *poda sináptica* (la extensa eliminación de sinapsis durante la infancia y la adolescencia). Con este modelo intentamos arrojar luz sobre la cuestión fundamental en neurociencia de cómo se relacionan la estructura y función de los sistemas neuronales. En concreto, encontramos que debido al acoplamiento entre forma y función emerge un bucle de retroalimentación que da lugar a dos comportamiento cualitativamente distintos. En uno, la estructura de la red es heterogénea y disasortativa, el sistema muestra la propiedad de memoria asociativa y, más aún, la estructura de la red es óptima para los patrones de actividad aprendidos en el proceso. En la otra, la estructura permanece homogénea y la red es incapaz de recuperar memorias. Estas evidencias son compatibles con los resultados experimentales en el desarrollo humano temprano, y sugieren una explicación satisfactoria de la poda sináptica. Para terminar, mostramos que otras redes evolutivas, como las redes de interacciones entre proteínas, podrían compartir algunos de los ingredientes básicos de este bucle de retroalimentación; y de hecho muchas de sus propiedades estructurales concuerdan con las predichas por nuestro modelo.

En el **capítulo** 3 demostramos que, como consecuencia del bucle de retroalimentación entre forma y función mostrado en el capítulo 2, aparecen *hubs* en la red que aumentan enormemente su tolerancia al rudio, y que además están correlacionados con los patrones memorizados por red. Además, mostramos que pueden aparecer oscilaciones en la actividad del sistema entre los patrones memorizados, dependiendo de los parámetros del modelo, que se asemejan a los procesos mentales dinámicos. Mostramos que el origen de estas oscilaciones está en la desestabilización de los atractores de memoria debido a la dinámica de la poda, que reduce el número de conexiones (o grado) de los *hubs* asociados con dicho patrón. Esto genera un ruido o desorden estructural a largo plazo y modifica constantemente el desorden inducido por la interferencia entre los distintos patrones aprendidos por el sistema. Este comportamiento se debe únicamente a los mecanismos de plasticidad estructural asociados a la evolución de la red, y no depende de otros mecanismos sinápticos o neuronales a cortas

escalas temporales, como sucede en otros estudios, ya que no están presentes en nuestro modelo. Para terminar, en este capítulo mostramos que el área en el espacio de parámetros asociada con dichas oscilaciones es máxima cuando se consideran valores intermedios de la densidad sináptica estacionaria, dado que para valores sub-óptimos la actividad de la red acaba dominada por el ruido, mientras que para valores mayores las memorias estáticas son estables y no se producen oscilaciones entre ellas. Estos resultados se relacionan con las observaciones experimentales en los trastornos del espectro autista y la esquizofrenia. En el primer caso se ha reportado un defecto de poda sináptica en algunas áreas cerebrales, mientras que en el segundo hay indicaciones de un exceso de poda.

En el **capítulo** 4 extendemos el modelo de poda sináptica propuesto en el capítulo 3 para reproducir los perfiles experimentales de densidad sináptica durante la infancia. En concreto, éstos incluyen un periodo inicial de alta conectividad, y en este captúlo investigamos el efecto que esto puede tener en el comportamiento emergente del sistema y sus propiedades computacionales. Mediante un enfoque computacional sencillo demostramos que la consideración de este periodo inicial de alta densidad aumenta considerablemente la estabilidad de las memorias, de modo que hay un cambio de fase discontinuo de una fase de memoria a una de ruido, como función de la densidad inicial, y con la aparición de la asociada región de bi-estabilidad. Además, probamos que valores intermedios de la densidad inicial permiten al sistema alcanzar el estado ordenado con un consumo mínimo de energía, y demostramos que este resultado es robusto frente a detalles del modelo de poda sináptica considerado. Finalmente mostramos que el estado estacionario del sistema está determinado en última instancia por el nivel de heterogeneidad en la red cuando comienza la poda sináptica. Nuestros resultados en este capítulo podrían explicar por qué las curvas experimentales de densidad sináptica siguen sus característicos perfiles durante la infancia y, eventualmente, relacionarlos con las anomalías observadas en el trastorno del espectro autista o la esquizofrenia, por ejemplo.

En los capítulos venideros, intentamos arrojar luz en el origen de los complejos patrones espacio-temporales de la actividad neuronal repetidamente observados en el córtex. Para ello, consideramos la relación entre la estructura geométrica subyacente en redes neuronales *ín vivo* y sus capacidades de sincronización. Las redes neuronales biológicas se desarrollan en un espacio 3D delimitado por el cráneo. Sin embargo, los estudios *in vitro* usualmente ignoran este hecho y consideran cultivos 2D. De una forma similar, la manera en que las propiedades geométricas de la red afectan a la dinámica neuronal ha sido casi inexplorada desde el punto de vista teórico. Curiosamente, estudios recientes *in vitro* de actividad neuronal indican que la dinámica de redes en cultivos neuronales es fuertemente dependiente de la geometría y, en particular, de su dimensionalidad, de manera que cultivos neuronales 3D producen patrones de oscilación más complejos y variados que los 2D.

Para afrontar esta cuestión desde un punto de vista teórico, en el **capítulo** 5 consideramos un marco matemático simple para estudiar cómo las capacidades de sincronización de una red neuronal pueden ser afectadas por diferentes aspectos de su estructura compleja. En particular, estudiamos la interrelación entre la geometría neuronal y la dinámica sincronización de osciladores acoplados siguiendo la dinámica de Kuramoto. Usamos un modelo de red compleja que genera redes que son variedades (llamado CNM por las siglas en inglés de *Complex Network Manifold*). Este modelo nos permite generar redes con una dimensión geométrica y espectral d_s dada, que son también de pequeño mundo (y, por tanto, tienen una dimensión de Haussdorf infinita) y tienen una alta estructura modular. Adicionalmente, demostramos que los CNMs con una dimensión espectral d_s dada pueden embeberse en un espacio euclídeo $d_s - 1$-dimensional. Usando este entorno, mostramos que las propiedades de sincronización de la red están directamente afectadas por su dimensión espectral y que una amplia región de *sincronización frustrada*, que exhibe patrones complejos de comportamiento oscilatorio, emerge para $d_s \geq 4$. De acuerdo con estos resultados, las redes neuronales corticales, a pesar de estar embebidas en un espacio 3 dimensional, podrían tener una dimensión espectral igual a cuatro, la dimensión crítica para la aparición de un estado sincronizado global.

En el **capítulo** 6 extendemos los resultados numéricos obtenidos en el capítulo 5 y mostramos que la dimensión espectral de una red compleja es determinante en los fenómenos de sincronización que pueden tener lugar sobre ella. En concreto, desarrollamos un marco matemático para demostrar que la fase globalmente sincronizada solo puede ser termodinámicamente estable para $d_s > 4$, mientras que para $d_s > 2$ puede ocurrir *arrastre* de fases de los osciladores. A continuación comprobamos nuestras predicciones teóricas dentro de un marco extendido de CNMs (capítulo 5). Con la expansión considerada, la dimensión espectral de las redes puede tomar valores fraccionarios, dependiendo de las simentrías subyacentes en la estructura. Por tanto, estas redes presentan una dimensión espectral altamente modificable, y constituyen un marco ideal para estudiar la relación entre la geometría de la red y fenómenos de sincronización.

Finalmente, en el **capítulo** 7 presentamos las conclusiones principales de esta tesis, centrándonos en el papel fundamental de la inter-relación entre la estructura y la función de una red, y en las posibles aplicaciones de los resultados obtenidos. Para acabar discutimos la plausibilidad y posibles extensiones de los modelos considerados y desarrollados en esta tesis.

Granada, junio de 2019

Contents

List of Figures

List of Tables

List of Boxes

Chapter 1

Actual perspectives in the study of neural systems

Made up by about 10^{11} neurons (and roughly the same number of glia cells) and 10^{15} synapses (Kandel et al., 2000), the brain is a paradigm of a complex system whose study involves the cooperation of many research fields, from biophysics to psychology, including physics mathematics and computer science. Descriptions of microscopic processes at the neuronal level are increasingly precise, and new experimental techniques allow the observation of brain activity at different levels. It is now more evident than ever that a comprehensive description of brain dynamics requires the consideration of the emergent behavior arising form the non-trivial cooperation among many elementary units such as neurons, synapses and glia cells. Departing from the occidental mechanistic point of view, *holistic* representations that consider brain functioning as a whole are becoming more relevant. As so, the brain is considered as a paradigmatic example of a complex system in which high level brain functions, such as cognition, emerge from the interaction among its microscopic components (Telesford et al., 2011; Marro and Chialvo, 2017).

At the mesoscopic level, the brain is made up by large, highly structured neuronal assemblies, and takes care of the processing of information and of high-level cognitive abilities (Bear et al., 2007). Experimental observations recurrently correlate many of these cognitive functions with the co-activation of different areas of the *cerebral cortex*, the outer layer of the mammal (and human) brain. The *cerebral cortex* (or simply the *cortex*) is mainly composed by the neuron cell bodies or *somas* (constituting the so-called *gray matter*), while internally the nerves (or axons) constitute the *white matter* (see panel 1). The study of the functioning of the cerebral cortex has been the focus of much attention since the pioneering works by Ramón y Cajal (Ramón y Cajal, 1911, 1995). Over a century ago K. Brodmann described a parcellation of the

cortex in the so-called "Broadmann areas", based on the cytoarchitectural organization of neurons (Strotzer, 2009). Many of these regions have since been associated with particular brain functions, such as vision or memory (Bliss and Collingridge, 1993; Kandel et al., 2000; Cardin et al., 2008). It is nowadays accepted however that brain functions are not restricted to a particular brain area, but occur distributed throughout the whole brain (Amit, 1989; Felleman and Van, 1991; Bullmore and Sporns, 2009; Stafford et al., 2014). As such, even in the resting state (that is, the brain's activity state when the subject is resting) it has been observed a consistent activation of several brain areas, that consequently are functionally inter-correlated constituting the commonly named *Resting State Networks (RSN)* (Fraiman et al., 2009).

The emergent observed behavior and dynamics of the brain is widely assumed to depend not only on the non-linear dynamics and interactions among its constituents, but also on the existence of an underlying complex and hierarchical structure of connections among the basic brain elements. This complex systems approach for the study of the brain is similar to those applied in other research areas combining concepts from network science, statistical physics and dynamical systems to study, e.g., social networks, epidemic spreading or the functioning of gene regulatory networks, to name a few. Within this approach, real-world systems are modeled as a collection of elements linked by pairwise connections. The underlying structure of connectivity powerfully shapes the patterns of interaction and the communication between the elements of the system, which in turn govern its global behavior. These patterns unfold dynamically across time in response to endogenous and exogenous perturbations. In particular, brain networks extend across a broad range of spatial and temporal scales, and can be assembled from various recording and mapping techniques that capture (usually pairwise) relationships among elements (Avena-Koenigsberger et al., 2018).

It has been recently observed that brain networks repeatedly show indications of a *small-world* structure (Sporns and Zwi, 2004; Achard et al., 2006; Stam et al., 2006; Achard and Bullmore, 2007; He et al., 2007; Wang et al., 2009) in which there are many short range connections but also some long-range ones, such that any two nodes in the network can be connected by a path with a small number of intermediate nodes. There are often also evidences of a *scale-free* structure, as it is observed in brain functional networks (Eguiluz et al., 2005) – in which most neuron make little connections but some are very highly connected, constituting the so called *hubs*.

Many natural systems of interconnected non-linear elements evolve over time into a critical state, characterized by avalanche dynamics that are scale-free and can be characterized by a power-law (Muñoz, 2018). According to the *criticality hypothesis*, this critical state might allow the system to satisfy the competing demands of information transmission and network stability. In the case of brain

dynamics, it has been suggested that the brain might also take advantage of the largest variety of metastable states that is found near a critical point, which would allow neuronal groups to generate a larger diversity of flexible collective behaviors (Fraiman et al., 2009). Different experimental evidences also seem to support this possibility (see Chialvo et al., 2008 and references therein). For instance, the propagation of spontaneous activity in cortical networks is often associated with avalanche processes with scaling exponents corresponding to those of a critical branching process, namely $-3/2$ for avalanche sizes and -2 for avalanche lifetimes, and scale invariance of network dynamics has been observed over many order of magnitude (Beggs and Plenz, 2003).

It has recently been suggested that a necessary requirement for the emergence of avalanches of neural activity is the balance between excitatory and inhibitory dynamics (Beggs and Plenz, 2004; Santo et al., 2018). However, the question remains of how the brain is posed at criticality. Mechanisms of *Self-Organized Criticality* (SOC) are often found to be in place in neural systems (Muñoz, 2018) as a means to achieve a critical state without any fine tuning (Bak et al., 1987). Other mechanisms have also been recently associated with the observed criticality in living systems. In particular, in a complex network structure with a hierarchical-modular architecture, as observed in the brain, the singular critical point is replaced by an extended critical-like region akin to a *Griffiths phase* (Moretti and Muñoz, 2013), providing an extended region of critical-like behavior.

The emergence of non-trivial structures, as well as complex emerging dynamics, is also a hallmark of *co-evolving networks*. In these systems, the underlying network also evolves in time in a way that is coupled with the dynamic state of its constituents. Examples of co-evolving systems are most communication networks, information networks such as gene or neural networks, and similarly social networks (Gross and Blasius, 2007). In the case of the brain, it has been widely reported that its network structure changes dramatically in time from conception to adulthood and elderly (Santos and Noggle, 2011). The brain is initially made up by a rapid proliferation of synapses after birth, which is then followed by an extensive process of **synaptic pruning**. This is thought to be some kind of optimization process to minimize the energy consumed by the brain and also the amount of genetic information that otherwise would be necessary to code an efficient network. This process goes on into adulthood, when synaptic connections continue to change, allowing for adaptation to a changing environment. Co-evolving systems have repeatedly been shown to present advantageous emerging dynamics, such as SOC, spontaneous division of labor (in which classes of topologically and functionally distinct nodes arise from homogeneous populations), formation of complex topologies and complex system dynamics due to the combination of local and topological degrees of freedom (Gross and Blasius, 2007; Vazquez et al., 2008; Wiedermann et al., 2015; Williams et al., 2019a).

In this chapter we deepen in these ideas and the experimental methods and models used to describe them, some of which we will use in the models developed in the original chapters of this thesis. We start in section 1.1 by giving a basic biological description of the main basic brain's constituents, neurons and synapses, and present a few archetypal mathematical models used to describe them. We then consider the structure of the neural system, aka *connectome*, and present the state of the art of connectome obtention and analysis on section 1.2. On section 1.3 we discuss the changes undergone by the brain during its development, and finally on section 1.4 we present the study of brain networks under the framework of statistical mechanics and complex systems and introduce some related models that are later used in this thesis.

The brain (Box 1.1)

The brain is the largest component and major functional unit of the Central Nervous System (CNS), and it is often the main structure referred to when speaking of the nervous system. It consists of[a] (Kandel et al., 2000):
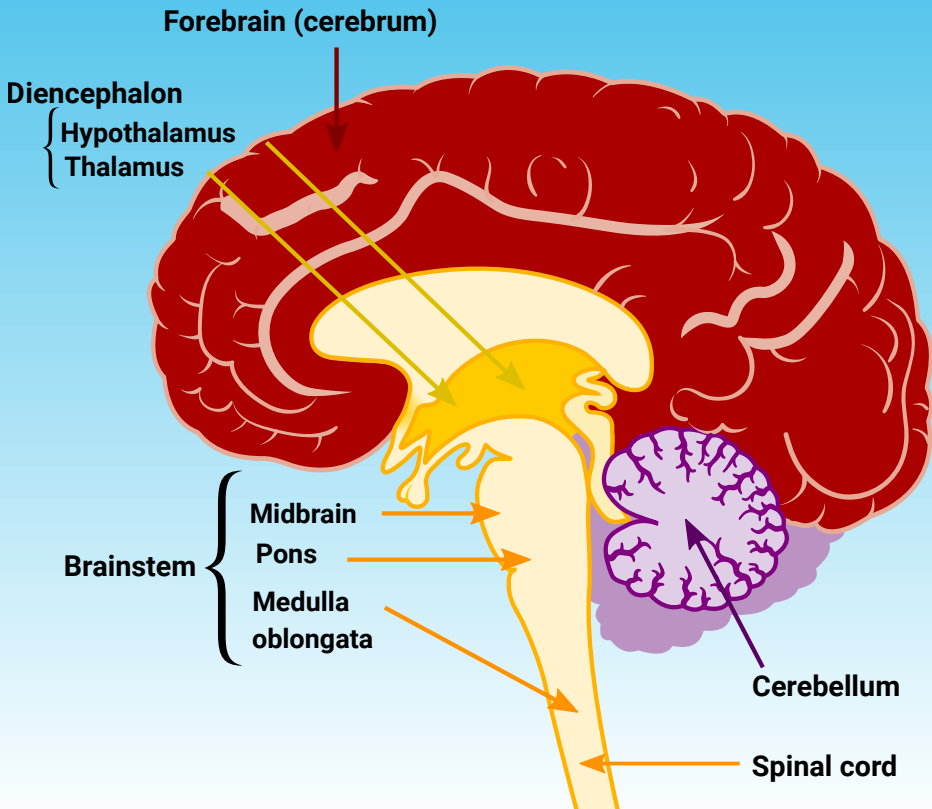
- The **brainstem**, constituted by the *medulla*, the *pons* and the *midbrain*, is involved in arousal and alertness mechanisms and it mediates autonomic control of the organs such as the heart, blood vessels, pupillae, among others.

- The **cerebellum** handles and processes sensory stimuli, motor information as well as balance, and it is also involved in language as well as cognitive functions. The body of the cerebellum holds more neurons than any other structure of the brain, but is also more extensively understood and includes fewer types of different neurons.

- The **diencephalon** is composed by the *thalamus* and the *hypothalamus*. The thalamus acts as a linkage between incoming pathways from the peripheral neural system to the cerebral hemispheres, and it connects the cerebellum and basal ganglia with the cerebrum. It is involved in wakefulness, consciousness and in motivation. It also engages in primitive emotions or feelings such as hunger, thirst and maternal bonding, partly regulated through the secretion of hormones from the pituitary gland.

- The **cerebrum** is composed by the two cerebral hemispheres and the *corpus callosum* connecting them. The hemispheres are made up by various structures, including the *cortex*, *basal ganglia*, *amygdala* and *hippocampus*. Together, they control a large portion of the functions of the human brain such as emotion, memory, perception and motor functions, and stand for the cognitive capabilities of the brain. In particular, the cortex, made up by gray matter covering the surface of the brain, is involved in several high level cognitive functions, such as planning and everyday tasks. The *hippocampus* is involved in storage of memories, the *amygdala* plays a role in perception and communication of emotion, and the *basal ganglia* play a major role in the coordination of voluntary movement.

---

[a]Figure adapted from (Commons, 2018).

1.1   A microscopic picture of the nervous system

The basic constituents of nervous systems – although not the only ones – are neurons and synapses. These are responsible for the processing and transmission of information by means of electrical and/or chemical signaling. Nowadays, there coexist highly detailed multi-dimensional mathematical models for neuronal activity and synaptic transmission, that specifically describe time variations of individual cell and synapse states, together with highly abstract models in the framework of statistical mechanics. In these last models, the dynamics of individual cells is highly simplified in order to study the emergent behavior of a system comprised by a great number of them, under different circumstances. Here, we introduce the basic characteristics of these elements and the interactions among them, and present some common individual neuron and synaptic mathematical model descriptions.

1.1.1   Neurons

A **neuron** is an electrically excitable cell that receives, processes and transmits information through electrical and chemical signals, and it is typically considered the basic element of information processing in the brain, according to the *neuron doctrine* (Ramón y Cajal, 1995).

A typical neuron, as represented in figure 1.1, consists on a central cell body or **soma**, a receiving pole consisting on a tree of soma extensions called **dendrites** and an output pole or **axon**, which is a long and thin extension of the soma. The soma houses the cell nucleus and most of the genetic expression and synthetic machinery to elaborate proteins, lipids, sugars and other constituents of cytoplasm environment. Its boundary constitutes the **membrane** of the cell, which presents communication sites or **channels** that connect the interior of the cell with the extracellular medium. These are constituted by specific transmembrane macro-molecules and control the level of excitability of the cell.

The axon typically extends from the soma forming a single branch that establishes connections or **synapses** to the dentrites of other neurons. The shape of a neuron can vary greatly. For instance, simplest neurons (appearing on the nervous system of invertebrates) present only a single process giving rise to the axon and dendrites, whereas the brain of vertebrates is mostly conformed by multipolar neurons, with multiple processes, which may give rise to more complex geometrical and topological structures (Mejías, 2009).

Neurons communicate with each other through the transmission of **action potentials (APs)** or **spikes**. These consist on rapid, self-regenerating electrical signals induced by the flow of ions through voltage-gated ion channels in the membrane of the neuron. Ion channels are specific protein structures in the membrane of the neuron that allow the flux of ions from the intracellular to the extracellular mediums, and vice-versa. Voltage-gated channels in particular
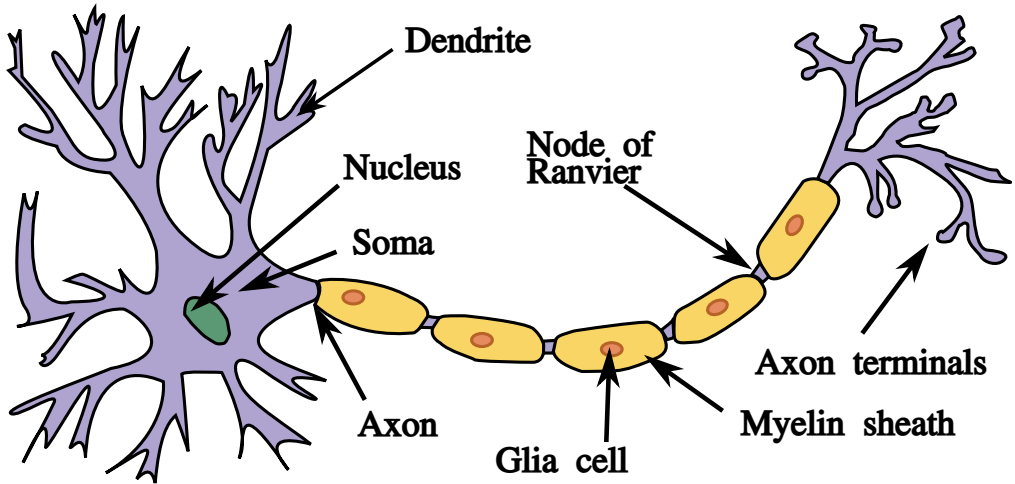
Figure 1.1: Schematic view of a typical neuron indicating the soma, the dendrites and the axon. As shown in the figure, many axons are covered with a layered myelin sheath made of Schwann cells – in the case of neurons in the peripherical nervous system (PNS) – or oligondendrocytes – in the case of neurons in the CNS – which are particular types of glia cells. The myeling sheath accelerates the transmission of electrical signals along the axon. These are separated by the *nodes of Ranvier*, which are gaps in the mylening sealth, highly rich in ionic channels, that serve to regenerate the action potentials travelling along the axon (Kandel et al., 2000). Figure adapted from (Commons, 2019).

are controlled by the voltage difference between both media, opening or closing according to its current value.

The voltage difference between the intra and extracellular media comes from different ion concentrations in each one, being Na^+ and Cl^- most abundant outside the cell, and K^+ and several organic anions inside. In the absence of an external stimulus, i.e. at the resting state, there is an excess of negative charges inside the cell, which is actively maintained by ion pumps spread out along the membrane. This causes the membrane potential at rest to have a typical value of approximately $-65mV$ (Koch, 2004). When a positive external current arrives at the cell, it depolarizes the membrane by increasing the positive charge in the intracellular medium. If the depolarization reaches the so called neuron *firing threshold*, there is an increasing activation of voltage-gated Na^+ channels that produces even further depolarization. This, in turn, makes more voltage-gated Na^+ channels open, leading to a fast feedback loop of increasing depolarization.

At this point the membrane potential is close to the Na^+ equilibrium potential, and two processes start to actively re-polarize the membrane: a high number of voltage-gated Na^+ channels close whereas voltage-gated K^+ channels open,

producing an increasing efflux of K^+ to the extra-cellular medium. This results in a positive net current from the neuron to the extra-cellular medium and in its fast hyper-polarization below the resting potential. At this low membrane potential many Na^+ channels activate again, resulting in a slow depolarization of the membrane until the resting potential is reached again. The overall variation of the membrane potential since the arrival of the external input at the neuron resting state, until this is reached again, constitutes the AP.

Once an AP is generated, it propagates along the axon due to the existence of many voltage-gated channels distributed along the membrane. When it reaches the pre-synaptic terminals of the pre-synaptic neuron, a number of biophysical processes take place to transmit the information encoded in the AP to the post-synaptic neuron, constituting the **synaptic transmission**.

1.1.2   Models of neurons

It is hardly surprising that during the last decades a huge number and variety of mathematical models have been developed to describe neuronal dynamics. These include different levels of detail (such as the neuron's varying morphology and functionality), range from simple binary models to high dimensional sets of coupled equations, and typically consider some source of non-linearity and stochasticity (Koch, 2004). Nowadays we count with highly detailed models for a great number of particular neurons, such as pyramidal neurons, interneurons, Purkinje cells, granule cells, or different types of motor neurons, to name a few (Masoli et al., 2015; Eyal et al., 2018; Haney et al., 2019). A comprehensive description of the literature is beyond the scope of this section, where we will just present some important neuron modeling milestones.

The **Hodgkin and Huxely model** constitutes a paradigmatic model for the generation of APs. First described in 1952, it is a phenomenological model that characterizes the ionic mechanisms underlying the generation of an AP by treating the neuron membrane as an electrical circuit. The dynamics of the membrane potential of the cell $V(t)$ is described as a set of nonlinear differential equations depending on the external current arriving at the cell $I(t)$ and a set of ion channels. The model includes the description of two voltage-gated ion channels, Na^+ and K^+, represented by electrical conductances $G_i(V, t)$ that depend on both voltage and time, and a passive leakage channel L represented by a linear conductance G_L (see figure 1.2).

HH-like neuron models constitute a successful phenomenological description of neural activity than can describe a wide range of phenomenology, and can also be improved by considering additional ionic currents. However, the high number of variables and non-linearities present in these models precludes an analytic treatment. Moreover, it was considered prohibitive for statistical physics analysis of even mesoscopic systems, when the HH model is used to define the neuron dynamics in a neural population. Therefore, more simplified scenarios

are typically considered, such as the **FitzHugh-Nagumo** model (FitzHugh, 1961; Koch, 2004), which reduces the system to a set of two coupled differential equations, or the so-called **threshold-firing** neuron models, such as the **integrate-and-fire** (Lapicque, 1907; Brunel and Van Rossum, 2007) or the **Izhikevich models** (Izhikevich, 2004). These models include an auxiliary condition for the generation of a spike, simplifying the non-linearities of the equations and allowing for faster and simpler computations (see the appendix A).

Further simplifications of the neuron dynamics can be taken, leading us to **binary neuron** models, in which the state of each neuron is a binary variable: the neuron can either fire ($S(t) = 1$) or be silent ($S(t) = 0$). The first model within this framework is the **McCulloch and Pitts** neuron model, proposed in 1943 (McCulloch and Pitts, 1943). This is simply an element that returns a Heaviside step function, $\Theta(t)$, of the sum of its inputs,

$$S(t + 1) = \Theta\left[RI(t) - \theta\right], \tag{1.1}$$

where R is the resistance and θ a voltage threshold parameter. This model soon received interest due to its simplicity. It was shown for instance that sets of these "artificial neurons" could be used to implement any logical gate (Peretto, 1992). It is commonly employed to construct *perceptrons* and other artificial intelligence structures, since it is computationally the fastest neuron model available (Amit, 1989).

Variations of this model are commonly used to analyze the emerging behavior of large sets – i.e. networks – of interacting neurons, such as in the Amari-Hopfield model (see section 1.4.1 and also Amari, 1972; Hopfield, 1982; Amit, 1989). These binary neural network models are widely used for instance when one seeks to explore the emergence of one characteristic collective behavior from the microscopic dynamics, such as *associative memory* or synchronization phenomena. In this framework even more abstract models are usually considered, such as the Kuramoto model (Kuramoto, 1975), the voter model (Castellano et al., 2009) or the contact process model (Gardiner et al., 1985; Muñoz et al., 2010). In this thesis we make use of such models – in particular of the Amari-Hopfield and the Kuramoto models – together with a complex underlying networked structure to study how the interplay between form (i.e. structure) and function may affect the emerging dynamics of neural systems.

1.1.3   Synapses

Synapses mediate the communication between neurons as they take care of transmitting APs from the pre-synaptic to the post-synaptic neuron. A typical neuron establishes about 1000 synaptic contacts with other neurons which gives 10^{14} synaptic connections over the whole brain (Kandel et al., 2000).

There are two basic mechanisms through which synapses transmit information: electrical and chemical. **Electrical synapses** are formed by specific

(a)

(b)

$$C_m \frac{dV(t)}{dt} = I(t) + \bar{G}_L \left[V_L - V(t)\right]$$
$$+ \bar{G}_{Na} m(t)^3 h(t) \left[V_{Na} - V(t)\right]$$
$$+ \bar{G}_K n(t)^4 \left[V_K - V(t)\right]$$
$$\frac{dx(t)}{dt} = \frac{x_\infty(V) - x(t)}{\tau_x(V)}$$

(c)
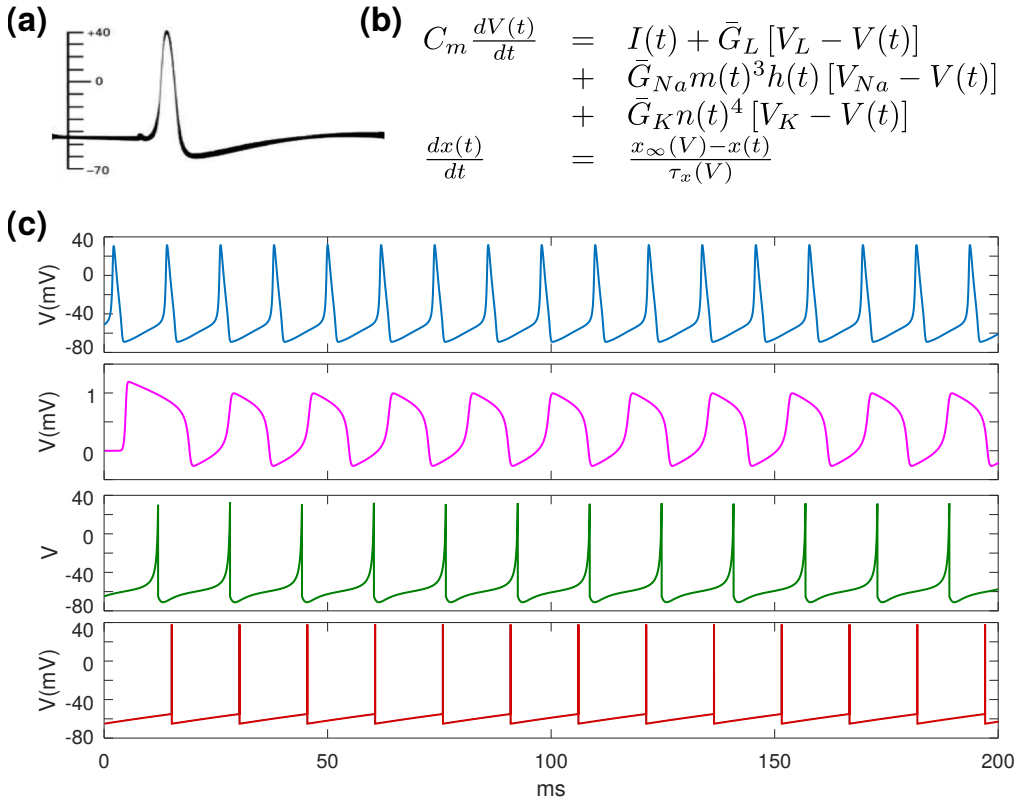
Figure 1.2:   **(a)** First published intracellular recording of an AP belonging to the squid giant axon (adapted from Hodgkin and Huxley, 1939). The vertical scale indicates, in mV, the potential of the internal electrode used to perform the recording. **(b)** Equations of the Hodgkin-Huxley model, where C_m is the membrane capacitance and $x = m, h, n$ are phenomenological variables that describe the activation and inactivation of the ionic conductantes as $G_{Na} = m(t)^3 h(t) \bar{G}_{Na}$, $G_K = n(t)^4 \bar{G}_K$. $\bar{G}_i$ and V_i are respectively the maximum conductance and the reversal potential of the corresponding ionic channel i. x_∞ are the steady state values of the active conductance variables, and τ_x the time constants for channel activation and inactivation. **(c)** Membrane potential dynamics as obtained with the Hodgkin-Huxley model (top panel), the FitzHugh-Nagumo model (second panel), the Izhikevich model (third panel) and the integrate-and-fire model (bottom panel).

protein structures called *gap junctions* that join the pre- and post-synaptic membranes directly, forming channels that connect the cytoplasm of both cells. The pre- and post-synaptic membranes therefore have to be close to each other, being the typical distance about $3.5nm$ (Kandel et al., 2000). The information is transmitted directly by the flow of ions from one cell to the other, making electrical synapses *bidirectional*. **Chemical synapses**, on the other hand, are unidirectional and do not involve a physical contact between the neurons (the membranes are typically separated $20 \sim 40nm$ by the *synaptic cleft* (Squire et al., 2012)), but are mediated by *chemical messengers* called *neurotransmitters*.

Chemical synapses are most commonly found in the long distance connections between neurons, allowing them to form complex networks of connections. On the contrary, electrical synapses typically constitute a form of local connectivity, and are mostly found between local clusters of inhibitory neurons (Galarreta and Hestrin, 2001; Connors and Long, 2004). Electrical synapses conduct nerve impulses faster, and therefore are commonly found in neural systems requiring fast responses, such as defensive reflexes (Purves et al., 2018). However, they lack gain – the signal in the postsynaptic neuron is usually smaller than that of the presynaptic neuron due to the membrane resistance.

In electrical synapses, the response is always the same sign as the source. On the contrary, when an AP arrives at a chemical synapse, it can produce either an excitatory or an inhibitory effect on the post-synaptic neuron. **Excitatory synapses** produce the depolarization of the post-synaptic neuron, thus making it more likely to spike. This is typically due to the influx of Na^+ or Ca^{2+} ions through the post-synaptic ion channels, increasing its membrane potential. **Inhibitory synapses**, on the other hand, induce the hyperpolarization of the post-synaptic cell, typically via an efflux of K^+ ions from the cell to the extracellular medium or an influx of Cl^- ions into the cell. In the majority of neural circuits (such as those of the hippocampus or several cortical regions), each neuron projects only one type of synapse, either excitatory or inhibitory (Sossin et al., 1990). This phenomenological principle (known as Dale's law) implies that neurons themselves can be classified as either excitatory or inhibitory. Interestingly, a balance between excitation and inhibition is thought to be necessary for the emergence of oscillations in the activity of neuronal populations, as observed experimentally (Brunel and Wang, 2003).

The effect of a synapse also depends on the time scale of the response, which is determined by specific post-synaptic repceptors. For instance, the major neurotransmitter involved in excitatory synpases is glutamate, and there exist mainly two kinds of receptors associated with it: *α-amino-3-hydroxy-5-methyl-4-isoxazolepropionic acid* (AMPA) receptors, which have a fast kinetics ($\sim 3ms$), and *N-Methyl-D-aspartic acid* (NMDA) receptors, with a much slower kinetics ($\sim 100ms$) (Koch and Segev, 1998). Therefore, the excitatory postsynaptic current can constitue a short event or be consistent in time. Similarly, the most
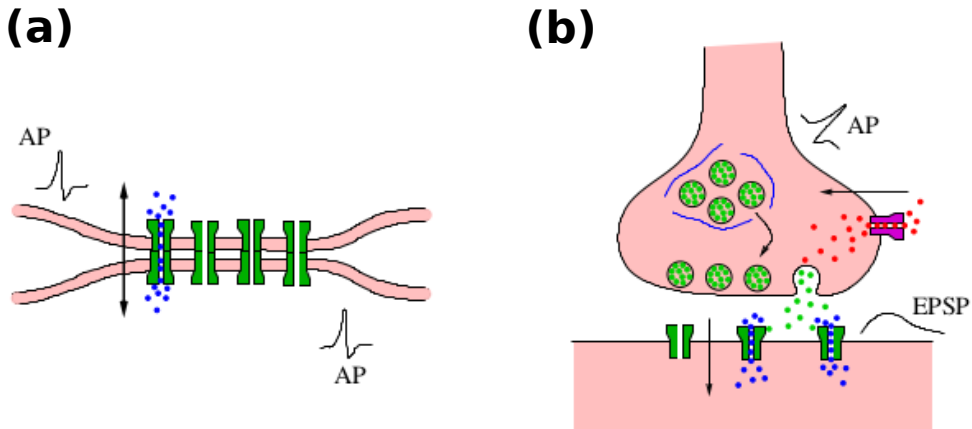
Figure 1.3: Schematic view of an electrical **(a)** and a chemical **(b)** synapse. In the electrical synapse there is a flux of intra-cellular ions (blue dots) through the gap junction (in green). In the chemical synapses the transmission occurs via the influx of Ca^{2+} ions (red dots) into the pre-synaptic terminal after the arrival of an AP. This induces the release of neurotransmitters (green dots), contained in synaptic vesicles located at the *ready releasable pool*, into the synaptic cleft. The neurotransmitters then bind to specific post-synaptic receptors (in green) which allow the entrance of extracellular ions such as Na^+ and K^+ (blue dots). The used vesicles are replaced by other vesicles coming from the *reserve pool* – depicted in the figure as the region delimited by blue lines, which in turn represent the *synapsin fibers* (Evergren et al., 2007) – or recycled to be used again. Figure adapted from Torres, 2010.

common neurotransmitter found in inhibitory synapses, *gamma-aminobutyric acid* (GABA), can bind to fast receptors (GABAa) or to slow ones (GABAb), producing instantaneous or prolonged hyperpolarizations in the postynaptic cell.

1.1.4   Synaptic plasticity

Synapses can change with time, either through the modification of the synaptic efficacy or **synaptic weight** – that is, the strength or amplitude of the synaptic connection – or the creation and elimination of synapses (structural plasticity). These changes are thought to be essential for learning and memory, and to present computational advantages as well (Abbott and Nelson, 2000; Zucker and Regehr, 2002).

Structural plasticity plays a major role on brain development, during which there is first a massive overproduction of synapses, later followed by extensive *synaptic pruning* as the individual matures (Huttenlocher and Dabholkar, 1997; Sowell et al., 2003). In humans, for example, synaptic density at birth is

about twice what it will be at puberty. Structural plasticity goes on into adulthood, where there is an ongoing experience-dependent creation and pruning of synapses that balance each other. This allows cortical networks to have variability to adapt and develop efficient structures (Knoblauch and Sommer, 2016), and it has also been associated with recovery from brain injuries (Holtmaat and Svoboda, 2009).

Synaptic strength also changes to adapt to external signals and perform different brain functions, such as memory (Abbott and Kepler, 1990; Song et al., 2000). Depending on the temporal scale at which changes occur, one can distinguish between **long-term synaptic plasticity (LTSP)** and **short-term synaptic plasticity (STSP)**. LTSP takes place at the time scale of minutes or more and leads to permanent changes in the synaptic weights, whereas STSP causes changes in the synaptic strengths at the time scale of hundreds of *ms*. Its study did not begin until the last decades of the 20th century, when it was reported that the amplitude of post-synaptic potentials at short time scales could depend on the activity of the presynaptic neuron (Bertram et al., 1996; Abbott and Regehr, 2004). Synapses which present this property are called activity-dependent synapses, or simply dynamic synapses.

1.1.4.1   Long-term synaptic plasticity

The biophysical mechanisms that provide long-term modifications at synapses are still debated, although the common assumptions include changes in the release probability of neurotransmitters, insertion or removal of post-synaptic receptors or changes in their conductances, to name a few (Gruart et al., 2006).

Long-term synaptic changes are thought to be behind the process of memory and learning; as first hypothesized by Donald Hebb (Hebb, 1949),

> *"Let us assume that the persistence or repetition of a reverberatory activity (or "trace") tends to induce lasting cellular changes that add to its stability. (...) When an axon of cell A is near enough to excite a cell B and repeatedly or persistently takes part in firing it, some growth process or metabolic change takes place in one or both cells such that A's efficiency, as one of the cells firing B, is increased."*

or, as it has since be summarized, *"neurons that fire together wire together"*. This hypothesis has lead to the theory of *Hebbian or associative learning*, according to which memories are held collectively in the neural network by the corresponding modifications of the synaptic weights. Mathematically, in a neural network made up by N neurons, the memories consist on a set of P patterns of activity that are set to be attractors of the activity dynamics of the system

(Hopfield, 1982). This can be attained by defining the synaptic weights as

$$w_{ij} = \frac{1}{Na_0 \, (1 - a_0)} \sum_{\mu=1}^{P} (\xi_i^\mu - a_0) \left(\xi_j^\mu - a_0 \right),$$
(1.2)

where $a_0 = \langle \xi_i^\mu \rangle$ is the mean activity of the patterns. This learning rule can be combined with a binary neuron model such as the McCulloch and Pitts model (as defined in Eq. 1.1) to define a neural network with the associative memory property (see section 1.4.1).

The definition 1.2) constitutes the final step of a learning process that can be implemented as a synaptic plasticity mechanism. A prolific one is **spike timing-dependent plasticity (STDP)**, which explicitly defines the long-term changes in the synaptic efficacies induced by the relative firing patterns of the pre-synaptic and post-synaptic neurons. An important aspect of the STDP theory is the temporal causality in the firing of the neurons: firing of the post-synaptic neuron following repeated arrival of pre-synaptic spikes induces long-term potentiation, whereas if this firing precedes the arrival of the pre-synaptic spikes, it leads to the long-term depression of the synapse. The change in the synaptic weight is then given by

$$\Delta w_{ij} = \sum_{f=1}^{N} \sum_{n=1}^{N} W \left(t_i^n - t_j^f \right),$$
(1.3)

where t_j^f are the arrival times of the pre-synaptic spikes at the synapse, and t_i^n are the firing times of the post-synaptic neuron. $W(x)$ is called the STDP function that characterizes the change in the synaptic efficacy. A common choice is

$$W(x) = \begin{cases} A_+ \exp(-x/\tau_+) & \text{if } x > 0, \\ A_- \exp(x/\tau_-) & \text{if } x < 0, \end{cases}$$
(1.4)

which has been used to fit experimental data (Zhang et al., 1998), with typical values for the time constants $\tau_+ = \tau_- = 10ms$. STDP rules are often paired with homeostatic mechanisms to prevent saturation or divergence of the synaptic weights, which could lead to epileptic-like behavior. STDP mechanisms have been observed in different species, including the rat, locust, cat and human, and in different brain regions, such as the cortex or hippocampus (Sjostrom et al., 2008).

1.1.4.2 Short-term synaptic plasticity

Short-term synaptic plasticity appears under repetitive pre-synaptic stimulation, and can lead to a decrease in the post-synaptic response (**short-term depression, STD**) or to an increase (**short-term facilitation, STF**) (Abbott et al., 1997; Markram et al., 1997; Abbott and Regehr, 2004). STD is

caused by the depletion of neurotransmitters consumed during synaptic signaling at the axon of the pre-synaptic neuron, and it has been found to be involved in selective attention (Buia and Tiesinga, 2005), neural population oscillations (Pantic et al., 2002) and up and down cortical transitions, for instance (Holcman and Tsodyks, 2006; Mejías et al., 2010). STF in turn is caused by the influx of Ca^{2+} into the axon terminal after spike generation, which increases the release probability of neurotransmitters (Tsodyks and Markram, 1997). It has been related to working memory tasks (Romani et al., 2006), slow oscillations (Melamed et al., 2008) and an increased storage capacity (Mejías and Torres, 2009; Mejías et al., 2012).

Synapses in different cortical areas can have varied forms of plasticity, showing either STF or STD, or a mixture of both forms. The combination of STD and STF leads to a competition between both opposite tendencies, producing a maximum of the post-synaptic response for a given pre-synaptic firing rate (Tsodyks and Markram, 1997). Therefore, STSP provides a synapse-level mechanism to control the gain of post-synaptic responses in an activity dependent manner (Abbott et al., 1997). The time-scale of STSP concurs with many neural processes such as motor control, speech recognition and working memory (Romani et al., 2006; Mongillo et al., 2008; Brunel and Lavigne, 2009). It is therefore plausible that STSP might serve as a neural substrate for processing of temporal information on the relevant time scales.

One of the most successful models of dynamic synapses was proposed by Tsodyks and Markram (Tsodyks and Markram, 1997; Tsodyks et al., 1998). It consists in a phenomenological coarse-grained description of the neurotransmitters concentration via a set of coupled differential equations. Under this model, neural networks with STSP have been found to present richer dynamical behaviors, such as the emergence of network bursts of activity (or population spikes), avalanches, or dynamical memories (Pantic et al., 2002; Torres et al., 2007a). In particular, STF allows synapses to hold the memory trace of an input without recruiting persistent firing of neurons, providing a very economical working memory (Mongillo et al., 2008), whereas STD has been shown to help discrimination between rhythmic inputs of different periods (Karmarkar and Buonomano, 2007). Moreover, in attractor neural networks, STD has been shown to degrade the memory capacitiy of the network, i.e.the maximum number of memories that can be effectively stored and retrieved (Torres et al., 2002), whilst inducing hoping (or wandering) among different memories (Pantic et al., 2002; Cortes et al., 2006; Marro et al., 2007b; Torres et al., 2007a; Torres et al., 2007b). Interestingly, the inclusion of STF can compensate for the lost of memory capacity (Mejías, 2009; Mejías and Torres, 2009; Mejías et al., 2012).

1.2   The structure of the neural system

In the previous section we have presented a brief description of the basic constituents of a neural system, neurons and synapses, and we have emphasized the relevance of synapses on the transmission of information, memory, and other high level brain cognitive abilities. However, it is not only the existence of such connections that is necessary for the brain's emergent dynamics. On the contrary, the underlying network structure made up by these connections is thought to be essential for brain functioning as well (Damoiseaux and Greicius, 2009; Sporns, 2011; Shen et al., 2015). This line of thought is not exclusive to brain research, as the conceptual simplicity of a network is widely used to capture the essence of cooperation in many complex systems, such as social, ecological or industrial networks (Wasserman and Faust, 1994; Albert et al., 1999). These systems share intricate microscopic dynamics – which, as we have seen in the case of neurons and synapses, are characterized by non-linear dependencies – together with a non-trivial network structure, which is thought to be essential for the emerging dynamics of the system.

In the brain, the underlying structure – or map – of connections, usually referred to as *connectome*, has been the focus of attention of much experimental and theoretical research in the last decades. Modern brain mapping techniques include **Magnetic Resonance Imaging (MRI)** techniques (Mori and Tournier, 2013) and **Electro- and Magnetic- encephalograms (EEG and MEG)** (Niedermeyer and Silva, 2005; Boto et al., 2018). They produce increasingly large data-sets of anatomical connections, describing actual physical interactions among brain areas, and functional connectivity describing correlations among the activity of different neural populations or brain areas. Structural or anatomical connectivity describes physical connections between neurons that range from the microscopic scale of local circuits to large-scale networks of mesoscopic pathways. Functional connectivity, on the other hand, represents correlations between the activity of pairs of regions that may or may not be physically connected, and that are distributed over the brain and often spatially afar (Friston, 1994). The emerging network thus depends on the specific task that the individual is engaged on when the data is recorded. For instance, a network that recurrently appears on resting state studies of brain activity is the so-called *default mode network (DMN)*. The DMN is composed by regions that usually decrease their activity during task performance when compared with the average brain activity at rest (Shulman et al., 1997) and has been associated with self-conscious and social tasks, such as thinking about oneself, remembering the past or planning for the future (see Raichle et al., 2001; Smith et al., 2009 and also panel 1.2.3 .

Characterizing the relationship between functional and anatomical connectomes at different scales may be useful to explore the emergent dynamics of the

system due to its structural connectivity (Zhou et al., 2006; Honey et al., 2007; Honey et al., 2009). Moreover, its use in clinical research, using the comparison with control populations, could be useful, for instance, to reveal connectivity abnormalities in neurological and psychiatric disorders (Stam et al., 2008; Leistedt et al., 2009; Wang et al., 2009).

The analysis of structural and functional connectivity in the cerebral cortex of mammals, including the rat (Burns and Young, 2000), cat (Scannell et al., 1999), monkey (Felleman and Van, 1991) and human (Crick and Jones, 1993) has revealed common organizational principles that are also shared with social, biological, and technological networks (Newman, 2011). These include a *small-world* structure, in which clusters of nodes segregate into tightly coupled neighborhoods, yet maintain very short distances among nodes across the entire network (Tononi et al., 1994); a *community structure* so that different communities of modules can be identified; or a *scale-free* structure, such that there are nodes with very different number of neighbors (and often the distribution of such number follows a power-law) and there exist highly connected nodes or *hubs* (Barabási and Albert, 1999). Other recurrent properties are the presence of non-trivial correlations among the nodes (either assortative or dissasortative) or the emergence of hierarchical structures.

Overall, these properties indicate a structure that is not random nor regular, therefore deemed as a *complex network*. This structure is though to be essential to support the emergence of complex dynamics on natural systems. In the brain, for instance, a community structure is thought to be fundamental for a distributed processing of information (such that each module takes case of a different functional process). Similarly, a small-world structure is related to the co-expression of segregated processing of information – which usually requires tightly coupled clusters of nodes – with the integration of information coming form different systems, a fact that requires long-distance shortcuts (Sporns and Zwi, 2004; Achard et al., 2006; Bassett et al., 2006; He et al., 2007; Deuker et al., 2009). In the following, we will characterize some common statistical measures of a network's topological structure that are useful for brain research, as it is detailed in subsection 1.2.1. We then present the most common experimental methods used to obtain functional and structural connectomes in subsection 1.2.1 and analyze the main features that characterize the topological structure of connectomes in section 1.2.3.

Complex Networks (Box 1.2)

The presence of the small-world (SW) and scale-free (SF) properties is a constant in the underlying structure of many systems. SW networks present an admixture of properties of two trivial network structures: lattices (fully ordered) and random networks (fully disordered). **Lattices** are ordered graphs with a geometric structure. Mathematically, a lattice is a graph whose drawing, embedded in an Euclidean space $\mathbb{R}^n$, forms a regular tiling. On the opposite site, **random networks**, such as Erdos-Renyi (ER) networks, are constructed simply by randomly connecting pairs of nodes with an uniform probability (Newman, 2011). Lattices typically have high clustering and long characteristic paths, whereas ER networks have small clustering and small characteristic paths. SW networks are characterized by short distances between nodes, equivalent to ER networks, but relatively large clustering, equivalent to lattices. Firstly found in large social networks (Travers and Milgram, 1967), SW networks are ubiquitous in Nature and society, having since been found in genetic, metabolic, ecological and information systems. Watts and Strogatz first proposed a mathematical graph that depicted the emergence of small-world properties. Such graph combined ordered lattice-like connections with a small admixture of random links (Watts and Strogatz, 1998).

Random   **Small-World**   **Lattice**
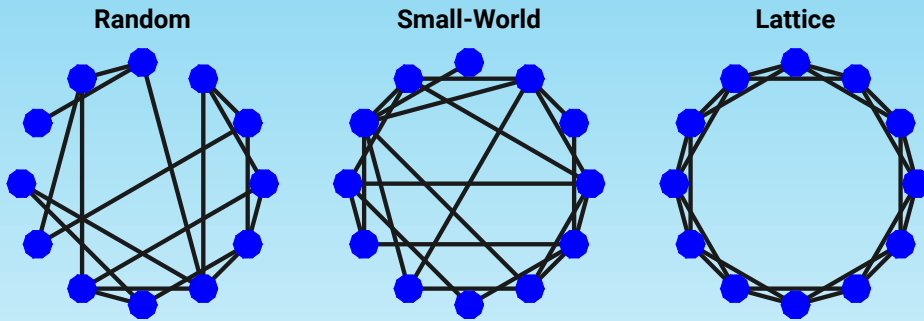
Similarly, whereas both lattices and ER networks have an homogeneous topology (all nodes have similar, or equal, degrees), many real world systems present heterogeneous topologies, characterized by nodes with very different degrees and the emergence of *hubs* (highly connected nodes). In some cases, the distribution of these degrees follows a power-law, and thus the corresponding networks are deemed scale-free, since nodes with all possible degrees are present in the network in the large-size limit. Scale-free networks are robust with respect to random deletion of nodes but highly vulnerable to targeted attack on the hubs, often resulting in disintegration of the network (Barabási and Albert, 1999). Note that the topology of scale-free networks cannot be efficiently captured

by random sampling, since most nodes are low degree, and hubs will be under-represented. Scale-free networks are also known to show facility of synchronization and fast processing (Lago-Fernández et al., 2000).

Interestingly, many systems have also been found to posses a **modular structure**: their nodes can be divided in sets of modules so that the number of intra-module connections is much higher than that of inter-module connections. A modular structure is thought to be necessary for the segregated processing of information.

Small-worldness, degree heterogeneity and a community structure are hallmarks of a *complex network*, signs of a structure that is not random nor fully ordered. They are commonly found for instance in the C-elegans and the sapiens connectomes, as shown below (figure 1.4).
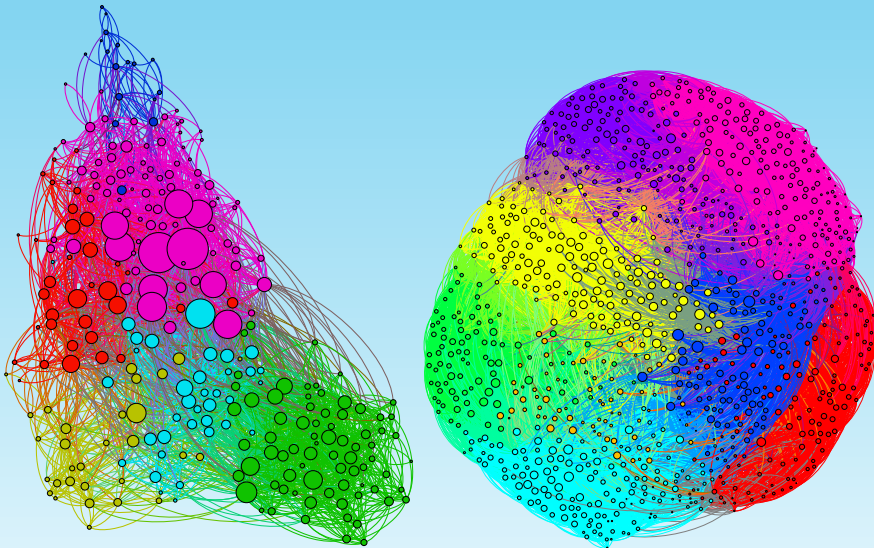
Figure 1.4: A representation of the *C-elegans* worm structural connectome (left) and the sapiens functional one (right) highlying the community structure of the networks (by indicating each community's nodes in a different color) and heterogeneous structures, with node sizes proportional to their degree (Li et al., 2004; Hagmann et al., 2008).

1.2.1   Some relevant network definitions

A network is a graph indicating the connections (links or edges) of a set of N nodes. It can be defined by its adjacency matrix e_{ij}, with $e_{ij} = \{1, 0\}$ indicating the presence or absence of an edge among nodes i and j, respectively. The network is said to be *undirected* if $e_{ij} = e_{ji} \forall (i, j)$, and *directed* other-

wise. Most biological networks, such as trophic, genomic, or neural networks, are directed. There are however some real-world networks that are naturally undirected, such as the network of electrical synapses in the brain, functional connectomes and most social networks. Moreover, undirected networks allow for deeper mathematical approaches, including the definition of a Hamiltonian description (Amit, 1989). Similarly, according to the nature of the links, networks can be further classified as *binary*, if they only consider the existence or not of a link, or *weighted*, if the links can have different strengths depending on some assumptions. For instance, in functional brain networks the strength of an edge may represent the level of correlation between the activity of the two nodes (see section 1.2.2). In this section we focus on the definition of common used network measures for undirected binary networks (Newman, 2011).

Firstly, a network is **connected** if there exists a *path* between every pair of nodes, where a path is an ordered sequence of distinct nodes and edges linking a source node j to a target node i. In a **disconnected network** (i.e., not connected), there often exists a **giant component** which is a connected sub-network that contains most of the nodes in the network. In the following, we will consider the network to be connected.

The most basic measure of a network is its nodes' **degrees**, $k_i = \sum_{j=1}^{N} e_{ij}$. The degrees of all nodes in the network characterize the **degree distribution**, $p(k)$. Its mean value, $\kappa = N^{-1} \sum_{i=1}^{N} k_i$, is usually considered a measure of the edge density of the network. According to the degree distribution, a network can be **homogeneous**, if all nodes have similar (or equal) degrees, or **hetero-geneous**, if there exist nodes with different degrees (see panel 1.2). This can be measured with the **homogeneity parameter** $g = \exp(-\sigma_k^2/\kappa^2)$, where σ_k^2 is the variance of the degrees of the nodes. Homogeneous networks present $g \to 1$ (with $g = 1$ in the case of sparse networks with $p(k) = \delta_{k_0,k}$), whereas $g < 1$ for heterogeneous networks. **Scale-free** networks are a particular example of heterogeneous networks which are very common in Nature, and exhibit degree distributions that are roughly power-law (and therefore $g \to 0$). A hall-mark of heterogeneous networks is the emergence of high degree nodes or **hubs**, which play an important role in integrating information in the network. These basic network characteristics usually strongly influence higher order measures, so that network statistics are usually compared to those of *null-models* (Gotelli and Graves, 1996; Dormann et al., 2009). These have simple random or ordered topologies whilst preserving the basic network's characteristics: size N, density κ, and typically also degree sequence (Maslov and Sneppen, 2002).

Network dimensions (Box 1.3)

The common concept of the **Euclidean dimension** often need to be extended to more general spaces. In topological spaces without a metric, for instance, the concept of dimension is generally associated with the **Lebesgue covering dimension**, which is a topological invariant. First define an open cover of a topological space X as a family of open sets whose union contains X. The *order* of a cover is the smallest number n (if it exists) such that each point of the space belongs to at most n sets in the cover. A refinement of a cover C is another cover, each of whose sets is a subset of a set in C. The covering dimension of X is the minimum value of n such that every open cover C of X has an open refinement with order $n+1$ or below. If no such minimal n exists, the space is said to be of infinite covering dimension. The Lebesgue dimension is integer, as the Euclidean dimension.

Early in the 20th century the **Hausdorff or fractal dimension** was introduced as a measure of roughness or chaos by mathematician Felix Hausdorff. This extends the euclidean dimension to non-integer metric spaces by measuring the local size of a space X taking into account the distance between points. Consider the number $N(r)$ of balls of radius at most r required to cover X completely. When r is very small, $N(r)$ grows polinomially with $1/r$. For a sufficiently well-behaved X, the Hausdorff dimension is the unique number d_H such that $N(r)$ scales as r^{d_H} as $r \to 0$.

Interestingly, the Hausdorff dimension is commonly extended to complex networks changing the concept of *area* by that of *neighbors*, and that of *distance* for *jumps* over the network (so it is equivalently to consider an implicit metric in which each link in the network has length equal to 1). Therefore, the **topological dimension** on a network measures how the number of neighbors of any given node grows when moving 1 2, 3, ..., r steps away from it: $N_r(r) \sim r^{d_T}$ for large values of r. Networks with the SW property have local neighborhoods quickly covering the whole network, that is, N_r grows exponentially with r, formally corresponding to $d_T \to \infty$. Instead, large-worlds have a finite topological dimension, while $d_T = 0$ describes fragmented networks.

Finally, the concept of dimensionality can also be applied to the spectral properties of the network. The **spectral dimension** d_S characterizes the scaling of the eigenvalues of the associated Laplacian matrix $\boldsymbol{L}$, with elements $L_{ij} = \delta_{ij} - e_{ij}/k_i$. $\boldsymbol{L}$ has real eigenvalues $\lambda_1 \leq \lambda_2 \leq ... \leq \lambda_N$, with $\lambda_1 = 0$ by construction. For many complex networks λ_2 remains finite as the networks size N grows; the network is then said to display a *spectral gap*. In networks with a hierarchical ordering of clusters, however, the spectral gap approaches zero as $N \to \infty$. This ensures that one

can define the spectral dimension d_S, which characterizes the power-law scaling of the density of eigenvalues $\rho(\lambda)$ for $\lambda \ll 1$ as $\rho(\lambda) \approx \lambda^{d_S/2-1}$. The spectral dimension characterizes the propagation of a random walk on the network, as well as its synchronization capabilities.

In the case of the brain, dimensionality is known to play a major role on its emerging behavior, and several features of brain dynamics are a consequence of its 3D embedding (Severino et al., 2016). The mammalian cerebral cortex, in particular, is a profoundly convoluted and compact six-layered surface. The classical explanation for its folded appearance is that it is a solution to the problem of packing a large surface area into a restricted volume. However, inter-layer connections create a non-trivial geometry that shows a fractal architecture – recent measures give a dimension $D = 2.8 \pm 0.05$ (Kiselev et al., 2003) – that is thought to heavily influence brain function (Griffin, 1994). The extent of folding of the mammalian cerebral cortex, which is characterized by the fractal dimension, is an important factor that influence a species' cognitive abilities and sensori-motor skills (Toro et al., 2008; Sun and Hevner, 2014). In humans, for instance, the complexity of the cortex folding increases with normal brain development (Blanton et al., 2001).

Consequently, considering the 3D embedding of biological networks might be highly relevant to study brain function. In particular, *in-vitro* studies comparing 2 and 3D neuronal cultures indicate that the latter exhibit morphological and biochemical features resemblant of *in-vivo* systems that are lost in 2D ones (Irons et al., 2008; Puschmann et al., 2013; Severino et al., 2016; Kuehn and Sereno, 2018). Moreover, 3D cultures minimize cellular stress, an inherent feature of standard 2D cell culture systems, and have been shown to support richer dynamical repertoires (Severino et al., 2016). Similarly, the synchronization properties of a network are known to be influenced by the network topological and spectral dimension (Barahona and Pecora, 2002; Chavez et al., 2005; Donetti et al., 2005). Consequently, it is clear that the underlying dimensions of neural systems play a determinant role of their dynamics. In chapters 5 and 6, we tackle on the issue of how the different dimensions of neuronal networks may affect their emergent collective behavior.

On a higher level or organization, **network motifs** can be analyzed to identify highly frequent patterns of local interconnections potentially indicating common models of information processing. Biological and technological networks contain several characteristic motifs such as feed-forward loops, feed-back loops and bidirectional loops, with distinct frequencies of individual loops likely having specific functional implications (Gollo and Breakspear, 2014).

More elaborate network statistics aim at measuring functional integration and segregation, quantifying centrality of individual regions or pathways, or testing the network's resilience to damage. In the following subsections we present some common topological measures used in brain research and their possible interpretation in functional and structural connectomes. In table 1.1 there is a summary of these magnitudes and their calculations.

1.2.1.1   Functional segregation

Functional segregation in the brain represents the ability of specialized processing within densely interconnected groups of brain regions. In anatomical networks, the presence of clusters suggests the potential for segregated functional activity, whereas in functional networks, it might be indicative of a segregated neural processing (Sporns, 2011).

Measures of segregation therefore quantify the presence of clusters or modules. The simplest one is the **clustering coefficient**, C, which measures the number of triangles in the network, that is, the proportion of a node's neighbors that are connected themselves[1]. High clustering indicates a high probability of local connections, suggesting a more dense connectivity with local nodes than with the rest of network (Watts and Strogatz, 1998). Interestingly, many real world networks have been found to present high clustering, whereas random sparse networks have a vanishing clustering coefficient as their size increases (in fact $C \sim N^{-1}$ as $N \to \infty$; see Newman, 2011).

Many networks have been found to have a macroscopic structure organized in communities, called **community** or **modular structure**, made up by groups of nodes that are more densely connected among themselves than with the rest of the network (see panel 1.2). The modular structure of a network is measured with the **modularity** Q (Newman, 2004). Modularity algorithms try to find a division of the network that maximizes the number of within-group links, whilst minimizing the inter-group links (Girvan and Newman, 2002), maximizing Q. However, the optimal modular partition of most large networks cannot be found and it is typically estimated with optimization algorithms (Danon et al., 2005) that usually sacrifice accuracy for computational speed (Newman,

---

[1]The mean clustering coefficient is normalized individually for each node and may be therefore disproportionately influenced by nodes with a low degree in heterogeneous networks. A classical variant of the clustering coefficient, known as the **transitivity**, T, is normalized collectively and consequently does not suffer from this problem (Newman, 2003).

Measures of topological structure	
Degree	$k_i = \sum_j e_{ij}$
Characteristic path length	$\ell = \frac{1}{N} \sum_{i=1}^{N} \ell_i = \frac{1}{N} \sum_{i=1}^{N} \frac{1}{N-1} \sum_{j \neq i} d_{ij}$

d_{ij}: distance between i and j, i.e. minimum number of jumps necessary to go from i to j in the network

Global efficiency	$E = \frac{1}{N} \sum_{i=1}^{N} E_i = \frac{1}{N} \sum_{i=1}^{N} \frac{1}{N-1} \sum_{j \neq i} d_{ij}^{-1}$
Modularity	$Q = \sum_{u \in M} \left[a_{uu} - \left(\sum_{v \in M} a_{uv} \right)^2 \right]$

M: set of non-overlapping modules

a_{uv}: proportion of links that connect nodes in module u with nodes in module v

$$Q = \frac{1}{l} \sum_{ij} \left(e_{ij} - \frac{k_i k_j}{l} \right) \delta_{m_i, m_j}$$

m_i: module containing node i

Clustering coefficient	$C_i = \frac{2t_i}{k_i(k_i-1)}$

for $k_i > 2$, and 0 otherwise

t_i: number of triangles around node i, $t_i = \frac{1}{2} \sum_{j,h} e_{ij} e_{jh} e_{ij}$

Mean clustering coefficient	$C = \frac{1}{N} \sum_{i=1}^{N} C_i$
Transitivity	$T = \frac{\text{\# of closed triples}}{\text{\# of all triplets}}$

where a triplet is a set of 3 nodes connected by either 2 (open triplet) or 3 (closed triplet) undirected links

Closeness centrality	$\ell_i^{[-1]} = \frac{N-1}{\sum_{j \neq i} d_{ij}}$
Betweenness centrality	$b_i = \frac{1}{(n-1)(n-2)} \sum_{h,j \neq i} \frac{\rho_{hj}(i)}{\rho_{hj}}$

ρ_{hj}: number of shortest paths between h and j

$\rho_{hj}(i)$: number of shortest paths between h and j that pass through i

Participation coefficient	$y_i = 1 - \sum_{m \in M} \left(\frac{k_i(m)}{k_i} \right)^2$

M: set of modules

$k_i(m)$: number of links between i and all nodes in module m

Degree distribution	$p(k) = \sum_{i=1}^{N} \delta_{k,k_i}$
Average neighbor degree	$k_{nn,i} = \frac{\sum_j e_{ij} k_j}{k_i}$
Assortativity coefficient	$r = \frac{l^{-1} \sum_{(i,j) \in L} k_i k_j - \left[l^{-1} \sum_{(i,j) \in L} 1/2(k_i + k_j) \right]^2}{l^{-1} \sum_{(i,j) \in L} 1/2(k_i^2 + k_j^2) - \left[l^{-1} \sum_{(i,j) \in L} 1/2(k_i + k_j) \right]^2}$
Small-world coefficient	$S = \frac{C/C_{rand}}{\ell/\ell_{rand}}$

Table 1.1: Mathematical definitions of complex network measures. These definitions correspond to binary undirected networks; expanded definitions for directed and/or weighted networks exist for most of these magnitudes: clustering and transitivity (Onnela et al., 2005; Fagiolo, 2007), modular structure (Leicht and Newman, 2008), assortativity (Barrat et al., 2004; Leung and Chau, 2007).

2006; Blondel et al., 2008). Some algorithms also detect overlapping modular structure, acknowledging the fact that single nodes may simultaneously belong to multiple nodes (Palla et al., 2005).

1.2.1.2   Functional integration

Functional integration in the brain is the ability to combine specialized information arriving from distributed regions (Sporns et al., 2005). Distances in the network are thought be indicatives of the capability for functional integration, since short distances indicate easily achievable communication[2]. In a network, the **topological distance** between two nodes, d_{ij}, is the number of nodes in the shortest path between them. The most common measure of functional integration is the **characteristic path length** ℓ of the network, that is, the average shortest path length between all pairs of nodes (Watts and Strogatz, 1998). ℓ only exists for connected networks, as it diverges for disconnected ones. In such cases, the **global efficiency** E (the average of the inverse shortest path lengths) is used. Given that ℓ is primary influenced by long paths and E by short ones, it has been suggested that E might be more meaningful as a measure of integration (Achard and Bullmore, 2007).

The scaling of ℓ with the size of the network N gives information on the **topological dimension** of the network (see panel 1.2.1). If $\ell \sim N^{1/d_T}$, the network is said to have (finite) topological dimension d_T. For instance, in a lattice $\ell \sim N^{1/d_E}$, where d_E is the Euclidean dimension of the lattice. In random and SW networks, however, the scaling of ℓ with N is slower due to the *long-range* connections, and the topological dimension is infinite. For SW networks, in particular, $\ell \sim \ln(N)$. In fact, the small-world property can be alternatively defined as the scaling $\ell \sim \frac{\ln N}{\ln\langle k \rangle}$. Given that $\ln N \ll N$ as $N \to \infty$, this implies that distances in a random network are orders of magnitude smaller than the size of the network (Newman, 2011).

1.2.1.3   Measures of centrality

Measures of **centrality** detect nodes that are important for different tasks, and the simplest of them is simply the node's degree, k_i. In modular networks, degree-based measures of within and between module connectivity are used to classify nodes in distinct functional groups (Guimerà and Amaral, 2005). For instance, the **participation coefficient** y_i indicates the fraction of a node's intermodular links. It therefore reflects the diversity of intermodular connections

---

[2]It is worth noting, however, that functional connectomes already contain information about integrated activity, since two correlated regions will appear as connected in these networks. Paths in these networks represent sequences of statistical associations and may not correspond to information flow, so that they are less straightforward to interpret (Honey et al., 2009).

of individual nodes, so that nodes with high participation coefficient act as connector hubs.

Another common measure of centrality is the **closeness centrality** $\ell_i^{[-1]}$, defined as the inverse of the average shortest path length from one node to all other nodes. Similarly, the **betweenness centrality** b_i measures the fraction of all shortest paths in the network that go through a given node. Its definition can be naturally extended to links to detect important anatomical of functional connections (Brandes, 2001). Centrality is also an indicator of integration, since central nodes tend to facilitate integration.

1.2.1.4   Measures of network resilience

Anatomical brain connectivity influences the capacity of neuro-pathological lesions to affect functional brain activity. Measures of resilience quantify anatomical features that reflect network vulnerability to damage. One of such features is the **degree distribution** $p(k)$ (Barabási and Albert, 1999). For instance, complex networks with power-law degree distributions may be resilient to gradual random deterioration, but highly vulnerable to disruptions of high-degree central nodes. Most real-life networks do not have perfect power-law degree distributions but ones that locally behave power-law-like. Another useful measure of resilience is the **assortativity coefficient** r, which measures the correlation between the degrees of connected nodes (Newman, 2002). Assortative networks, with $r > 0$, are likely to have a comparatively resilient core of interconnected high-degree hubs. On the contrary, dissasortative networks, with $r < 0$, are likely to have widely distributed and consequently vulnerable high-degree hubs (Pastor-Satorras et al., 2001; Piraveenan et al., 2008). Most real-world networks are dissasortative, with the exception of social networks. Interestingly, dissasortativity has been shown to emerge naturally on scale-free (and more generally heterogeneous) networks (Johnson et al., 2011).

1.2.2   Connectome generation

A *connectome* is a map of connections between different brain areas. It may refer to physical connections among the units (structural connectivity) or to functional connections, reflecting the effective relation in the activity of the nodes. This concept is expected to help to understand how the underlying structure of a neural network allows for and affects the functional states of the brain (Hagmann, 2005; Sporns et al., 2005).

The information encoded by a connectome depends greatly on the technique used for its construction and the scale of the map of connectivity. Mapping microscopic connections is highly invasive, and their immense number makes obtaining microscopic maps of whole brain areas experimentally intractable with current techniques. Moreover, these connections are highly dynamic, making

it difficult to define and extract a static network. Therefore, information at this level is only available for individual, small brain areas or in-vitro neuronal cultures, and the construction of a whole connectome has only been possible for the worm *Caenorhabditis elegans* (Li et al., 2004; Varshney et al., 2011). Most brain studies have considered either macroscopic or mesoscopic approaches, with regions ranging from anatomically distinct brain areas to sets of hundreds of neurons. There is growing evidence that in this scale many of the functional and cognitive properties of the brain emerge due to the collective activity of many neurons. However, this adds the problem of defining the nature of the nodes and links in the connectome, which typically requires combinations of brain mapping methods, anatomical parcellation schemes, and measures of connectivity. Nodes should ideally represent brain regions with coherent patterns of external connections (so that they share most of their neighborhoods), and they should completely cover the surface of the cortex without overlapping. Given that the eventual parcellation is study-dependent, comparison across different studies (for inter-subject or inter-species comparisons, for instance) is difficult (Horwitz, 2003).

The two most used techniques nowadays to extract connectome data are Magnetic Resonance Imaging (MRI) and Electro- and Magnetic-encephalograms (EEG and MEG). **Magnetic Resonance Image (MRI)** techniques are based on the response of water, a main component of biological tissue, to magnetic fields due to the magnetic moment $\boldsymbol{\mu}$ of the protons conforming the water molecule. They are commonly used to measure the structure of biological tissue in hospitals, including guided stereo-tactic surgery and radio-surgery for treatment of intracranial tumors (Brown and Nelson, 2016) or control for Alzheimer's disease and epilepsy (Sadek, 2013). In brain research, MRI techniques provide 3D structural pictures of the brain and also functional information of the relation between different regions, providing the foundation for both structural and functional connectomes, respectively using fMRI (functional MRI) or DTI (diffusion tensor imaging) procedures.

DTI techniques make it possible to estimate the location, orientation, and anisotropy of the brain's white matter tracts – or nerves – in a non-invasive manner. Nerves are covered in a myeling shield that facilitates the diffusion of water through them (see figure 1.1). Once the image has been taken, a diffusion tensor $\boldsymbol{D}$ can be obtained in each voxel that describes diffusion anisotropy. The direction (and directionality) of the nerve is indicated by the main eigenvector of $\boldsymbol{D}$, providing a directed network of anatomical connections. DTI has also various clinical applications requiring the localization of white matter tracts.

It is also possible to obtain functional connectomes with MRI techniques using fMRI, which measures the blood flux in biological tissue. The blood flux indicates the local level of oxygen consume, which in turn is used as a proxy for neural activity. Given the temporal activity of each voxel x, $V(x,t)$, a correlation

matrix between voxels can then be obtained as

$$r\left(x_1, x_2\right) = \frac{\langle V(x_1,t)V(x_2,t)\rangle - \langle V(x_1,t)\rangle \langle V(x_2,t)\rangle}{\sigma_{x_1}\sigma_{x_2}}, \qquad (1.5)$$

where $\langle \cdot \rangle$ represents a temporal average and $\sigma_x \equiv \langle V(x,t)^2\rangle - \langle V(x,t)\rangle^2$. Two voxels x_1 and x_2 are said to be correlated if $r(x_1, x_2)$ is greater than a threshold value r_c (Dodel et al., 2002). The threshold is arbitrarily determined, and ideally networks should be characterized across a wide range of values. Given that the correlation matrix is symmetric, functional connectomes are undirected networks. The connection can either be positive or negative, depending on the sing of the correlation.

Another important technique is EEG recordings, which measure brain activity via external electrodes. It provides information on functional connectivity only and with lower spatial resolution than MRI since individual electric potentials are low, making it necessary to integrate the activity of mesoscopic regions made up by millions of neurons. However, it is non-invasive, nor does it imply any risks or exposure to radiation and, furthermore, it can provide better temporal resolution than fMRI. Similarly, MEG techniques detect the magnetic fields generated by ionic currents using SQUID sensors (superconducting quantum interference devices) and it is also non-invasive. MEG images have higher spatial resolution than EEG and similarly high temporal resolution.

1.2.3   Connectome characterization

Systematic investigations of structural and anatomical cortical networks show the recurrent appearance of small-word characteristics[3] (Hilgetag et al., 2000; Chialvo, 2004; Sporns and Zwi, 2004; Eguiluz et al., 2005), and common occurrence of feed-back and feed-forward loops, given the high frequency of reciprocal connections (Kötter and Stephan, 2003) and abundance of short cycles (Sporns et al., 2000). These distributed cluster structures provide pathways for efficient recurrent processing, supporting the coordinated expression of both functional segregation and integration (Tononi et al., 1998; Sporns et al., 2000), and it might support synchronous processing (Kaiser and Hilgetag, 2004; Masuda and Aihara, 2004) or efficient information exchange (Latora and Marchiori, 2001) as well.

Several studies have also revealed a hierarchical community structure (Bassett et al., 2008), as well as a backbone of densely interconnected hubs, thus providing a shortest path structure that facilitates coordinated processing of information (Heuvel et al., 2012). Hub nodes are of particular importance in

---

[3]It is worth mentioning however the study by Gallos et al., 2012, suggesting that functional brain networks consist of a myriad of densely connected local moduli, which altogether form a large world structure; however, incorporating weak ties into the network converts it into a small-world preserving an underlying backbone of well-defined moduli.

multiple cognitive domains (Fornito et al., 2012), and disruption of hub connectivity is increasingly recognized as a hallmark of neurological and psychiatric disorders (Rubinov and Bullmore, 2013). The fundamental role of anatomical hubs in brain dynamics often implies that they act as functional hubs as well (Honey et al., 2009; Shen et al., 2015).

Despite the common existence of hubs, a scale-free structure has only been partially found on structural networks, where hubs have low maximum degrees, due to the saturation of the number of synaptic connections (Sporns and Zwi, 2004). On the contrary, functional networks exhibit robust power-law like degree distributions, indicating that there is always a small but finite number of brain sites having broad "access" to most other brain regions. In particular, functional networks of the human visual and motor cortex where found to present a scale-free degree distribution with a power-law exponent of -2, and also a power-law scaling of the number of neighbors at a given distance (notice however that linear metric in the cortex is unclear due to extensive folding of brain tissue) (Eguiluz et al., 2005). These networks where also shown to have small ℓ (comparable with those of equivalent random networks), large C and assortative correlations (Newman, 2002). The properties above have been found to be robust within subjects, tasks and brain locations, and over a wide range of thresholds used to define the associated connectivity matrices (Eguiluz et al., 2005).

A recurrent question in connectome analysis is how the underlying anatomical structure gives rise to the network of functional connections (Sporns, 2012) and how spontaneous brain dynamics at large scale organize into the relatively few spatiotemporal patterns revealed experimentally (Fox and Raichle, 2007). Direct comparison between anatomical and functional connectomes is not straightforward: functional networks tend to be denser than anatomical ones (they typically contain numerous connections between anatomically unconnected regions (Damoiseaux and Greicius, 2009)), whereas anatomical networks typically present higher efficiency and stronger connections (Honey et al., 2007). A way to study the emergence of functional connections from the anatomical ones is by simulating neural dynamics over a structural network and inferring the functional network from it, which can then be compared to those obtained from experimental data (Jirsa and Kelso, 2000; Sporns, 2004). These hybrid modeling studies (Chialvo, 2010) often suffice to capture relevant spatio-temporal aspects of brain dynamics – such as the emergence of strucutres having a well-established neurobiological meaning as the cortical DMN (see panel 1.2.3) – provided that the dynamical regime is critical. This contributes to the plausibility of the so-called *criticality hypothesis*, according to which the brain operates near a critical a point, which would hold computational and dynamical benefits (see section 1.4.3).

Across subject comparisons of connectivity maps can be useful to detect possible abnormalities of network connectivity associated with various brain

disorders (Bassett et al., 2008), although the differences in methodology across studies still make between-subject comparisons difficult (Sporns et al., 2005).

Interestingly, during the past decade there has been a great number of experimental descriptions of connectomes of different species, with a growing degree of precision, opening the gate for inter-species connectome comparison. In the macaque, for instance, anatomical and functional networks alike show modular structure and extensive overlap, and anatomical modules correspond to groups of specialized functional areas, a result also found for other species such as the cat and rhesus monkey (Young, 1992; Hilgetag et al., 2000; Stephan et al., 2000). A first level inter-species comparison relates to the structure of the underlying network, with the question of whether the differences in connectivity are associated with differences in brain functionality. However, the limitations in across-subjects studies magnify for inter-species comparisons as connectomes of different species are obtained through different techniques and at different scales, and therefore describe different things. For instance, the *C-elegans* connectome describes neuron-neuron synaptic interaction, whereas available data on the macaque and the cat describe correlations among macroscopic regions.

Default mode network (Box 1.4)

The cerebral cortex exhibits spontaneous activity even in the absence of any apparent task or external stimuli (Raichle, 2011). The large scale networks of these interacting regions make up the **Resting State Networks (RSN)**, of which the most widely studied one is the **default mode network (DMN)** (shown in figure 1.5, see also Acerra and Moseley, 2005). The DMN is composed by regions that usually decrease their activity during task performance (Shulman et al., 1997) when compared with the average brain activity at rest, suggesting the existence of a "default mode" of brain function that remains active during rest in an organized manner (Raichle et al., 2001). It is particularly associated with self-conscious and social tasks, such as thinking about oneself, remembering the past or planning for the future (Raichle et al., 2001).

The DMN is marked by a balance of positive and negative correlations and is disrupted in many disorders (Fox and Raichle, 2007), including autism (Kennedy et al., 2006), Alzheimer's disease (Greicius et al., 2004), depression (Greicius et al., 2007), schizophrenia (Williamson, 2007), and attention deficit hyper-activity disorder (Tian et al., 2006), as well as the comatose state (Norton et al., 2012). It has also been shown to be disrupted in patients suffering from long-term pain (Foss et al., 2006), which may indicate that the long-term interference with DMN (caused by the constant pain perception) may eventually cause plastic changes in the brain. Such brain state alterations can be regarded as a displacement from an optimal dynamical point (Haimovici et al., 2013). It has been proposed that, in the normal brain, the DMN proves "a balance of opposing forces" to enhance "the maintenance of information for interpreting, responding to, and even predicting environmental demands" (Raichle and Mintun, 2006). Therefore, an unbalanced DMN suggests that these functions may be compromised.
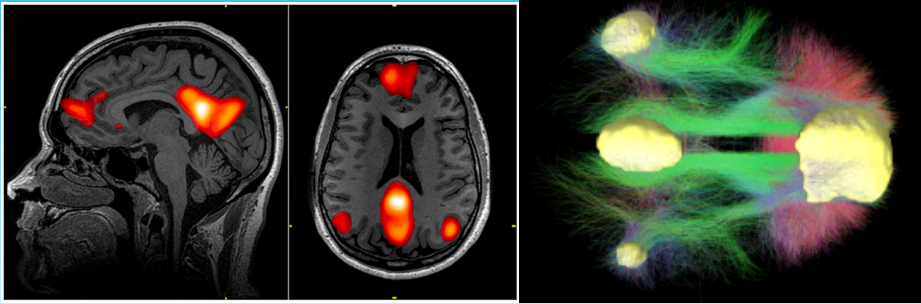
Figure 1.5: Representations of the functional DMN (left) obtained with fMRI and its anatomical substrate (right), as obtained with DTI.

1.3   Non-equilibrium neural networks

Most networks are not static, they are instead subjected to an undergoing dynamical process of addition and removal of nodes and links that may depend on a non-trivial manner on topological, dynamical and environmental factors (Holme and Saramäki, 2012; Williams et al., 2019b). The development of the vertebrate brain for instance – and in particular of the cerebral cortex – reflects a complex interplay of experiential and genetic factors. Pre- and pots-natal environmental events – such as sensory stimuli, hormones, parent-child relationships, stress or psychoactive drugs – affect cerebral development (Kolb et al., 2012).

It is typically assumed that the majority of neurons in the brain are produced during fetal development. Synaptic density however keeps increasing after birth, reaching a peak during infancy. Then an extensive process of **synaptic pruning** begins which eliminates roughly half of all synaptic connections (Rakic et al., 1986; Huttenlocher and Dabholkar, 1997; Iglesias et al., 2005). It therefore affects hugely the structure of the underlying network and its emerging cognitive abilities, and deficits in this process have been related to some neurological disorders (Keshavan et al., 1994; Geschwind and Levitt, 2007; Faludi and Mirnics, 2011; Tang et al., 2014; Presumey et al., 2017).

There are multiple models in the literature that simulate the development of a neural network, from topological models such as the Barabási-Albert model (BA) (Barabási and Albert, 1999), to biologically plausible models that try to mimic microscopic phenomena (Iglesias et al., 2005; Morrison et al., 2008). Topological models typically ignore any biological mechanism or constrain to reproduce some properties of the underlying structure, such as the evolution of the mean degree or the scaling of the distributions of degrees, weights or distances in the network, among others (Holtmaat and Svoboda, 2009; Johnson et al., 2010a; Navlakha et al., 2015). Biologically inspired models of synaptic pruning consider more detailed physiological processes. For instance, less efficient synapses can be pruned following competitive learning rules together with STDP and some sort of homeostasis mechanism (Chechik et al., 1998, 1999; Iglesias et al., 2005; Morrison et al., 2008).

Different mechanisms have been related to the growth and pruning of synaptic connections during brain development. In particular, glia cells in the brain (known as *microglia*) play a major role in shaping and rewiring synaptic connections as they phagocytose pre- and post-synaptic components of "weak" synapses (Paolicelli et al., 2011). Microglia are highly motile cells (Nimmerjahn et al., 2005), and they interact extensively with synapses in an activity-dependent manner that affects the functional maturation of the synapse (Miyamoto et al., 2013), influencing synaptic transmission (Wake et al., 2009; Tremblay et al., 2010). Interestingly, synaptic pruning co-occurs with an increased density of microglia in the CNS, and involves extensive microglial phagocytosis of synapses. Defects

in microglia physiological function have been related to brain diseases, so that a reduction in the function and number of synapses, along with an activation of microglia, is an early event in the pathogenesis of Alzheimer's disease, Huntington's disease, and other neurodegenerative diseases (Perry and O'Connor, 2010). Similarly, microglia mal-function has been related to autism spectrum disorder and obsessive compulsive disorder (Chen et al., 2010; Derecki et al., 2012), and it has been suggested to play a role in schizophrenia as well (Derecki et al., 2012).

Similaryl, spontaneous and sensory-evoked pre-synaptic activity, as well as glutamate, act as trophic factors to guide new synaptic spines growth (Lee et al., 1980; Frank, 1997; Klintsova and Greenough, 1999; De Roo et al., 2007), and other mechanisms of cooperation among neurons have also been proposed, such as STDP (see section 1.1.4 and also Deger et al., 2012, 2016). Similarly, synaptic pruning can be promoted by apoptosis[4], the programmed death of the cells, which has been observed ubiquitously in developing nervous systems (Cowan et al., 1984; Luo and O'Leary, 2005; Low and Cheng, 2006). Alternatively, neurons might eliminate whole processes, or disassemble individual synaptic contacts, in what constitutes an extremely dynamic process that targets weaker synapses (Low and Cheng, 2006), allowing for a fine-tuning of the synaptic circuitry. These mechanisms are promoted by complex neurochemical pathways of cell signaling, that might depend on different dynamic functions such as the timing of action potentials or the cell's activity.

Long-term high resolution imaging studies of *in-vivo* neuronal structure (Holtmaat et al., 2005; Holtmaat and Svoboda, 2009) have evidenced that synaptic turnover goes on into adulthood, providing the brain with **structural plasticity** as synaptic circuits continue to stabilize. Whereas the overall statistics of synaptic density and the large-scale structure of cortical neurons, made up by axonal and dendritic branches, are relatively stable, small synaptic structures, such as dendritic spines and axonal boutons are highly dynamic (Deger et al., 2012; Miyamoto et al., 2013). Such an extraordinarily long phase of developmental reorganization has implications on the impact of environmental events on the development of human cognitive and emotional capacities, as well as the late onset of human-specific neuropsychiatric disorders (Petanjek et al., 2011).

Structural plasticity also provides another mechanisms for the formation of long-term memory in the cortex. Apart from changes in the connection strengths, learning could also depend on learning-induced changes in the cortical wiring diagram (Chklovskii et al., 2004; Arcangelis et al., 2006). In this

---

[4]Apoptosis is thought to be responsible for the removal of a large percentage of excess projections during early development (Cowan et al., 1984; Yuan et al., 2003), when there is a neuronal competition for different growth factors such as the nerve growth factor, released in limited amounts at the synapse and necessary for neuronal survival during development (Oppenheim, 1989; Singh and Miller, 2005).

learning mode, the storage capacity lies in the system's flexibility to choose which pre-synaptic units provide input to each postsynaptic unit. Weight and wiring changes are not mutually exclusive, and experimental evidence suggests that neurons and their synapses might be engaged in both forms of learning. Given that in most areas of the brain, including the cerebral cortex, neurons are sparsely connected, ongoing structural plasticity could improve substantially the storage capacity compared with plasticity due to changes in synaptic strength alone (Chklovskii et al., 2004; Knoblauch et al., 2010).

Similarly, recent studies have shown that the consideration of the underlying geometrical restrictions found in neural networks can also have important effect on their emergent structure. For instance, it was been shown that networks that include information of the geometrical space of the cortex reproduce better the clustering coefficients and characteristic path lengths found in cortical networks (Kaiser and Hilgetag, 2004). The consideration of the underlying geometric structure can also have implications on the emerging properties of the network, such as its capability to reach a synchronized state (Millán et al., 2018a).

In the following subsections we present three statistical physics models of network development that are latter used in the original chapters of this thesis to model network structure. These models can be used to reproduce some features of the underlying structure in the brain, such as its emerging topological or geometrical properties, or to reproduce synaptic pruning. We finish the section discussing the relevance of adaptive networks to model brain function.

1.3.1 Topological models of network growth

There are various examples in Nature of systems that develop scale-free patterns of connectivity, including neural networks (Amaral et al., 2000), protein-protein interaction networks (Newman, 2003), the world wide web and some social networks (Barabási and Albert, 1999). As discussed in section 1.2.1, scale-free networks are characterized by hubs whose existence implies that the mean minimum path is typically small when compared to random networks or lattices (Boccaletti et al., 2006), however they are highly vulnerable to damage to the hubs (Mitra et al., 2008).

One of the most famous generative models for scale-free topologies is the so called **Barabási-Albert preferential attachment network model** (BA) (Barabási and Albert, 1999). It generates scale-free networks in systems of increasing size $N(t)$, by means of a local attachment rule applied to the new nodes added to the network. More precisely, initially the network is made up by N_0 randomly connected nodes. At each time step a new node is added to the network and linked to m ($m \leq N_0$) existing nodes with a probability $\Pi(k_i)$,

$$\Pi(k_i) = \frac{k_i}{\sum_{j=1}^{N(t)} k_j}. \tag{1.6}$$

Consequently, heavily linked nodes are more likely to gain a new edge, while nodes with only a few links are unlikely to be selected. Notice however that the number of low-degree nodes grows linearly with time, in such a way that the asymptotic degree distribution is scale-free:

$$p(k) \propto k^{-\gamma}, \tag{1.7}$$

with $\gamma = 3.0 \pm 0.1$ (Barabási and Albert, 1999). The distribution of the clustering coefficient per node degree, defined as $C(k) \equiv \langle C_i \rangle_{\{i:k_i=k\}}$ also behaves as a power law,

$$C(k) \propto k^{-1}. \tag{1.8}$$

This implies that low-degree nodes have higher clustering, so that they form dense sub-graphs, that are interconnectes through hubs. BA networks are also part of the small world networks family: the average path length is small, eventually shorter than in a random graph and, at the same time, the clustering coefficient is significantly higher than for random networks.

1.3.2   Synaptic pruning

Synaptic pruning is thought to play a major role in the development of the mammalian brain and the emergence of its cognitive abilities (Mimura et al., 2003; Low and Cheng, 2006; Santos and Noggle, 2011). It has been shown that it may represent an optimization strategy to minimize the energy consumed by the existing synapses, which in a human at rest can account for a quarter of the total energy consumed by the individual (Chechik et al., 1998, 1999), and also the genetic information that otherwise would be needed to build an efficient and robust network (Chechik et al., 1999; Navlakha et al., 2015). Synaptic pruning is also a major mechanism to induce diversity in the synaptic connections and to give rise to complex, heterogeneous synaptic circuits (Petanjek et al., 2011). Given its relevance on brain development, certain brain disorders, such as autism and schizophrenia, have been related to details of this process (Keshavan et al., 1994; Geschwind and Levitt, 2007; Faludi and Mirnics, 2011; Kolb et al., 2012; Fornito et al., 2015).

Modeling of synaptic pruning processes has attracted the attention of the neuroscience community in the last decade. However, until now there is not a clear theoretical framework in which synaptic pruning can be studied in depth. This is one of the main objectives of the present thesis. To do so, we depart in chapter 2 from a topological model that describes the creation and elimination of edges in a network, much in the framework of the BA-model (Johnson et al., 2010a). The model considers the evolution of a N-node network in which nodes gain and lose edges according to stochastic rules that only consider information (local and global) on the degrees. In order to implement this in a general way, each node has a probability P_i^l to lose a randomly selected edge, and a

probability P_i^g to gain one to a randomly selected node. These probabilities are assumed to factorize in two terms as

$$P_i^g = u(\kappa)\pi(k_i)$$
$$P_i^l = d(\kappa)\eta(k_i), \tag{1.9}$$

where π and η are normalized functions, namely $\sum_{k=1}^{N} \pi(k) = \sum_{k=1}^{N} \sigma(k) = 1$.

Every time an edge is added into the network, two nodes increase their degrees: the original node i selected according to $\pi(k_i)$, and the randomly selected node j that i is connected to, selected with probability $(N - k_i)^{-1}$, which in the infinity size limit ($N \to \infty$, $\kappa \to cte$), is approximately N^{-1}. Similarly, every time an edge is removed from the network two nodes decrease their degree, the node i with probability $\sigma(k_i)$ and the node j with probability $k_j/(N\kappa)$. Therefore, one can define the effective probabilities

$$\widetilde{\pi}(k) \equiv \pi(k) + \frac{1}{N}$$
$$\widetilde{\sigma}(k) \equiv \sigma(k) + \frac{k}{\kappa N}, \tag{1.10}$$

which measure the probability that the degree k of a node is modified in one unit.

Network evolution can now be seen as a one-step process (Van Kampen, 1992) with transition rates $u(\kappa)\widetilde{\pi}(k)$ for an increment and $d(\kappa)\widetilde{\sigma}(k)$ for a decrement of the degrees. The expected value for the variation in $p(k,t)$ at each time step, which we equate with a temporal derivative, defines a master equation for the degree distribution (Johnson et al., 2010a):

$$\frac{dp(k,t)}{dt} = u(\kappa)\widetilde{\pi}(k-1)p(k-1) + d(\kappa)\widetilde{\sigma}(k+1)p(k+1)$$
$$- [u(\kappa)\widetilde{\pi}(k) + d(\kappa)\widetilde{\sigma}(k)]\, p(k,t). \tag{1.11}$$

If $p(k,t)$ evolves to a stationary distribution $p_{st}(k)$, it must satisfy detailed balance, given that it is a one step process (Van Kampen, 1992). Therefore, the flux of probability from k to $k+1$ must equal the flux from $k+1$ to k, $\forall k$ (Marro and Dickman, 2005). This condition is also sufficient for $\frac{dp(k,t)}{dt}$ to be zero, and it can be written as

$$\frac{\partial p_{st}(k)}{\partial k} = \left[\frac{u(\kappa_{st})\widetilde{\pi}(k)}{d(\kappa_{st})\widetilde{\sigma}(k+1)} - 1 \right] p_{st}(k), \tag{1.12}$$

where we have substituted a difference for a partial derivative and defined $\kappa_{st} \equiv \sum_{k=1}^{N} k p_{st}(k)$. Setting $\widetilde{\pi}$ and $\widetilde{\sigma}$ to be normalized to 1, i.e. $\sum_{k=1}^{N} p(k)\widetilde{\pi}(k) = \sum_{k=1}^{N} p(k)\widetilde{\sigma}(k) = 1$ $\forall t$, which is equivalent to saying that at each time step

exactly $Nu(\kappa)$ edges are created and $Nd(\kappa)$ are destroyed, then in the stationary state one must have

$$u(\kappa_{st}) = d(\kappa_{st}), \tag{1.13}$$

since the the total number of edges is conserved. In this case, $p_{st}(k)$ will have an extremum at k_e if $\widetilde{\pi}(k_e) = \widetilde{\sigma}(k_e + 1)$. This can be a maximum or a minimum depending on the ratio between the numerator and the denominator in equation 2.19: it will be a maximum if the first is smaller than the latter for $k < k_e$, and viceversa for $k > k_e$. Assuming only one extremum, a maximum then implies a relatively homogeneous distribution, while a minimum means that $p_{st}(k)$ is split in two, and therefore highly heterogeneous. Intuitively, if nodes with high degree have a higher probability of gaining new edges than of losing them, their degrees will continue to grow indefinitely, leading to heterogeneity. If, on the other hand, highly connected nodes always lose more edges than they gain, the network will be quite homogeneous. From this reasoning one can see that there is a particularly interesting case, which turns out to be critical, when $\pi(k)$ and $\sigma(k)$ are such that

$$\widetilde{\pi}(k) = \widetilde{\sigma}(k) \equiv \nu(k) \;\; \forall k. \tag{1.14}$$

According to Eq. 2.19 this means that, for large k, $\partial p_{st}(k)/\partial k \to 0$, and $p_{st}(k)$ flattens out – as a power law does.

The standard Fokker-Planck approximation for the one step process defined by Eq. 2.19 is (Van Kampen, 1992):

$$\begin{aligned}
\frac{\partial p(k,t)}{\partial t} =& \frac{1}{2} \frac{\partial^2}{\partial k^2} \left\{ [d(\kappa)\widetilde{\sigma}(k) + u(\kappa)\widetilde{\pi}(k)] \, p(k,t) \right\} \\
&+ \frac{\partial}{\partial k} \left\{ [d(\kappa)\widetilde{\sigma}(k) - u(\kappa)\widetilde{\pi}(k)] \, p(k,t) \right\}.
\end{aligned} \tag{1.15}$$

For transition rates that meet the condition in Eq. 1.14, this can be rewritten as

$$\begin{aligned}
\frac{\partial p(k,t)}{\partial t} =& \frac{1}{2} \left[u(\kappa) + d(\kappa) \right] \frac{\partial^2}{\partial k^2} \left[\nu(k)p(k,t) \right] \\
&+ \left[u(\kappa) - d(\kappa) \right] \frac{\partial}{\partial k} \left[\nu(k)p(k,t) \right].
\end{aligned} \tag{1.16}$$

Ignoring boundary conditions, the stationary solution must satisfy, on one hand, $\nu(k)p_{st}(k) = Ak + B$, so that the diffusion is stationary and, on the other, $u(\kappa_{st}) = d(\kappa_{st})$, to cancel out the drift. For this situation to be reachable from any initial condition, $u(\kappa)$ and $d(\kappa)$ must be monotonous functions, decreasing and increasing respectively. Interestingly, experimental studies of synaptic pruning in the neo-cortex also show that pruning rates are decreasing over time, so that a greater number of synapses are pruned early in development and circuits are fine-tuned later in development. In this manner most of the synapses are pruned early reducing energy consumption, whereas the network can slowly fine-tune the relevant pathways, ultimately leading to more efficient and robust

routing networks when learning is distributed throughout the network (Navlakha et al., 2015). Decreasing pruning rates are also consistent with the developmental time-course of myelination, which shows sharp sigmoidal growth soon after pruning begins (Dean III et al., 2014). By pruning aggressively early, myelin is not unduly wasted on axons that may ultimately be lost.

This model has been used before to reproduce some topological aspects of the process of synaptic pruning, such as the temporal evolution of the mean connectivity or the scaling of the degree distribution in the mature brain. In chapter 2 we present an extension of this model that includes the consideration of the physiological activity of neurons, which is coupled with the network evolution. Interestingly, we show that the interplay between form and function can affect the phase diagram of the system, leading for instance to a stronger noise tolerance or to an oscillatory activity, as shown in chapter 3.

1.3.3 Network geometry

Growing evidence indicates the need to go beyond traditional network schemes and consider generalized network structures such as multilayer networks, formed by several co-interacting networks (Boccaletti et al., 2014), and higher order networks that go beyond pairwise interactions (Bianconi and Rahmede, 2015; Wu et al., 2015; Bianconi and Rahmede, 2016). These can be essential to analyze brain networks, where sets of regions can interact together forming large complexes that co-activate simultaneously (Giusti et al., 2016; Severino et al., 2016), and other systems such as protein interaction networks, where typically biological reactions involve the chemical interaction among several different proteins (Wan et al., 2015).

There is simultaneously a growing interest in *network geometry*, and in particular in characterizing *network curvature*, with indications that several complex networks have an hyperbolic structure which is believed to be beneficial for routing algorithms and navigability (Boguna et al., 2009; Serrano et al., 2012).

Interestingly, both network geometry and the co-interaction of more than two nodes can be described by **simplicial complexes**, which naturally introduce *d*-node interactions and an underlying network geometry. Instead of considering only nodes and links, simplicial complexes are made up by *d***-dimensional simplexes**. These are generalizations of triangles (in $2D$) and tetrahedra (in $3D$) to arbitrary dimensions, and consider the co-interaction of their $d+1$ nodes. dimensional simplex is a triangle and so on. Each simplex considers the co-interaction of the $d+1$ nodes conforming it. A simplicial complex has the following two additional properties:

i) If a simplex α belongs to the simplicial complex $\mathcal{K}$ (i.e. $\alpha \in \mathcal{K}$), then also all its faces $\alpha' \subset \alpha$ belong to the simplicial complex $\mathcal{K}$ (i.e. $\alpha' \in \mathcal{K}$).

ii) If two simplices α and α' belong to the simplicial complex (i.e. $\alpha, \alpha' \in \mathcal{K}$), either their intersection is null, i.e. $\alpha \cap \alpha' = \emptyset$ or their intersection belongs to the simplicial complex, (i.e. $\alpha \cap \alpha' \in \mathcal{K}$).

In particular, the theoretical framework of **Network Geometry with Flavor (NGF)** (Bianconi and Rahmede, 2016) introduces a purely combinatorial non-equilibrium evolution model of simplicial complexes in which an hyperbolic geometry emerges naturally. The skeleton of the NGF, or dual network, is formed by the nodes and links.

Network Geometry with Flavour

A NGF of dimension $d \geq 1$ is a simplicial complex formed by d-dimensional simplices glued along their $(d-1)$-dimensional faces. For example, a NGF of $d = 1$ is formed by links glued at their end nodes, a NGF of $d = 2$ is formed by triangles glued along their links, and a NGF of $d = 3$ is formed by tetrahedra glued along their triangular faces. Each δ-face α can be characterized by its *generalized degree* $k_{d,\delta}(\alpha)$, which is the number of d-dimensional simplices incident to α. For instance, in $d = 1$ $k_{1,0}(\alpha)$ is the number of links incident to a node α, i.e. its degree. Similarly, in $d = 2$, $k_{2,1}(\alpha)$ and $k_{2,0}(\alpha)$ are the number of triangles incident to a link or a node, respectively. By assigning to each node a fixed *energy* ϵ_i from a distribution $g(\epsilon)$ (so that each face has energy $\epsilon_\alpha = \sum_{i \in \alpha} \epsilon_i$) NGFs can have heterogeneous properties.

NGFs evolve in time according to a non-equilibrium dynamics that at each time t adds a new d-dimensional simplex that is attached to a $(d-1)$-face α chosen with probability

$$\Pi_\alpha^{[s]} = \frac{1}{Z^{[s]}(t)} e^{-\beta \epsilon_\alpha} \left(1 + s n_\alpha\right), \tag{1.17}$$

where $\beta \geq 0$ is a parameter of the model called equivalent to an inverse temperature, $s = \{-1, 0, 1\}$ is the **flavor** of the NGF and $n_\alpha = k_{d,d-1}(\alpha) - 1$ is the number of d-dimensional simplices incident to α minus one. $Z^{[s]}(t)$ is the normalization,

$$Z^{[s]}(t) = \sum_{\alpha \in \mathcal{S}_{d,d-1}} e^{-\beta \epsilon_\alpha} \left(1 + s n_\alpha\right). \tag{1.18}$$

The new simplex is formed by the nodes of α plus a new node i that is linked to each node $j \in \alpha$. Therefore, the total number of nodes $N(t)$ at time t is $N(t) = t + d$, considering that initially $(t = 0)$ the NGF is formed by one d-simplex.

The flavor s of the NGF has a strong influence on its geometrical and statistical properties. For instance, for $s = -1$ only 2 d-simplices can be attached to each phase, and the resulting networks are manifolds. For $s = 1$, on the
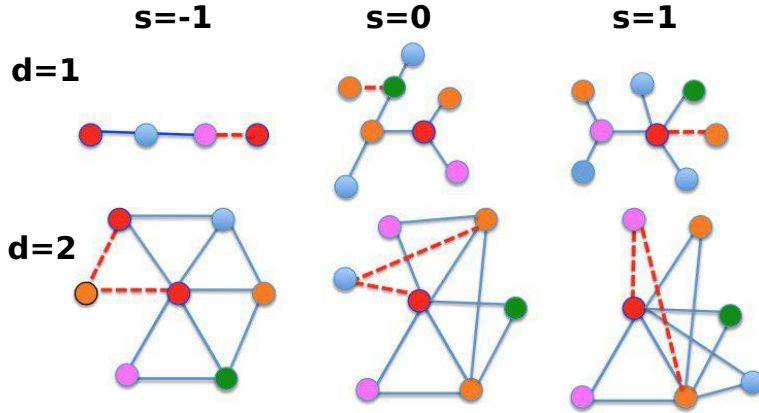
Figure 1.6: Schematic picture of the temporal evolution of NGFs of flavor s in dimension $d = 1, 2$. Figure adapted from (Bianconi and Rahmede, 2016).

δ \ s	-1	0	1
$d-1$	B	E	PL
$d-2$	E	PL	PL
$\leq d-3$	PL	PL	PL

NGF (d, s, β)	Equivalent Network
$(1, 0, 1)$	BA model
$(1, > 0, 1)$	Bianconi-Barabási model
$(3, 0, -1)$	Stochastic Apollonian network

Table 1.2: On the left, the scaling of the distribution of the generalized degrees $k_{d,\delta}$ in NGF with flavor s and $\beta = 0$, indicating a binomial (B), exponential (E) or power-law (PL) scaling. For $d \geq d_c^{[\delta,s]} = 2(\delta + 1) - s$ the power-law distributions are scale-dree, i.e., the second moment of the distribution diverges. On the right, some examples of NGFs whose network skeleton is equivalent to known network models (Andrade Jr et al., 2005; Krioukov et al., 2010; Bianconi and Rahmede, 2015).

other hand, $\Pi_\alpha^{[0]}$ is proportional to its generalized degree $k_{d,d-1}(\alpha)$, providing a generalization of the preferential attachment mechanism.

Using the master equation approach, it can be shown for $\beta = 0$ that, depending on d, δ and s, the generalized degrees $k_{d,\delta}$ can follow either a binomial, exponential or power-law distribution (see table 1.2). In particular, NGFs are scale-free as long as

$$d \geq d_c^{[0,s]} = 2 - s. \tag{1.19}$$

Therefore, NGFs are scale-free for $d \geq 3, 2, 1$ respectively for $s = -1, 0, 1$. This result also indicates that an explicit preferential attachment rule is not necessary to generate scale-free networks in $d > 1$.

NGFs generated with these model have been used in a variety of scenarios, including the modeling of quantum gravity (Bianconi et al., 2015). Moreover, a

generalization of NGFs has been recently been proposed considering complexes formed by gluing together not only simplicial complexes but also regular convex polytopes, which are called **cell complexes**. These are less densely connected that simplices and have been used to characterize self-assembled nanostructures (Šuvakov et al., 2018) or granular materials (Papadopoulos et al., 2018), and are also used for interdisciplinary applications such as protein interaction and social networks. Note that cell-complexes in general can be formed by using any convex polytope, and that a given cell-complex might be not pure, i.e. it can be formed by different types of convex polytopes.

Simplicial and cell complexes thus provide an ideal theoretical setting to analyze how the network underlying symmetries, dimensionality and geometry might affect brain dynamics. Moreover NGFs have a tunable spectral dimension (Mulder and Bianconi, 2018) and non-trivial spectral properties, and they can be embedded in an euclidean space with a well-defined dimension. Consequently, in this thesis we make use of their known geometrical and spectral properties to study how these relate to the synchronization properties of a neural network in chapters 5 and 6.

1.4 Emergent dynamics in neural systems

The previous picture suggests that the brain, composed by a large number of interacting elements, each one exhibiting nonlinear dynamics, might be studied under the framework of complex systems, as it displays many signatures of complexity and criticality. This framework has also been of use to study for instance the emergence of **associative memory** in neural systems. This is the ability to learn and remember the relationship between unrelated items, such as people's names, and is related, for instance, to the existence of *internal representations* – of brain activity – of objects and concepts. Another recurrent property of neural systems is the emergence of neural oscillations, consisting on oscillations in the neural activity, which are observed throughout the CNS at different scales. They have been related to several cognitive processes as varied as memory, self-consciousness and vision; and overall are thought to provide a means towards the integration of distributed information.

The variety of behaviors observed in the brain could be concomitant with the existence of a critical state at which neural dynamics are posed. This idea, known as the *criticality hypothesis*, suggests that the brain may take computational advantage by operating near a critical point. Interestingly, it has been suggested that the emergence of a complex behavior can also be related to a complex interplay between structure a dynamics (Hilgetag and Grant, 2000).

In this section we review the emergence of associative memory and synchronization in neural systems, and present two archetypal models used to describe them, which constitute an important part of the theoretical framework we are going to use in the development of the original chapters of this thesis. We then introduce the criticality hypothesis and finish the section and the chapter with a short review of adaptive networks. and SOC in neural systems and present some statistical physics models used to described them.

1.4.1 Associative memory: The Amari-Hopfield model

In the 1980s Hopfield formulated a neural network model that included the hypothesis of Hebbian learning in order to study associative memory (Hopfield, 1982). The model consists in a network composed by N binary neurons, whose states are given by $s_i = \{0, 1\}$, that indicate respectively a silent (resting potential) or firing (emitting an action potential) neuron. $\boldsymbol{S} = \{s_1, ..., s_N\}$ is the state of the set of neurons. In its original definition, the model considers a *fully connected network* where each neuron i is connected to all other neurons but self-connections are not allowed.

The model assumes the linear summation of sub-threshold inputs, so that the incoming current at a neuron i (Kandel et al., 2000) or its *local field potential*

is given by $h_i(t)$, defined as

$$h_i(t) = \sum_{j=1}^{N} w_{ij} e_{ij}(t) s_j(t). \tag{1.20}$$

In the stochastic version of the model, the state of each neuron follows a probabilistic dynamics according to

$$P\left[s_i(t+1) = 1\right] = \frac{1}{2}\left\{1 + \tanh\left[T^{-1}\left(h_i(t) - \theta_i(t)\right)\right]\right\}, \tag{1.21}$$

where

$$\theta_i(t) = \frac{1}{2}\sum_{j=1}^{N} w_{ij} e_{ij}(t) \tag{1.22}$$

is the neuron's threshold for firing. The noise parameter or *temperature T* ($T > 0$) sets the level of stochasticity on the activity of the neurons (Bortz et al., 1975). If $T = 0$ the evolution of the system is deterministic and the state of a neuron at time t is completely determined by the states of its neighbors at time $t - 1$. For $T > 0$, however, the evolution is stochastic and, as T is increased, the thermal noise has a stronger effect. Computationally, the model has been implemented essentially with two different updating protocols: parallel updating, also called *Little dynamics*, and randomly sequential updating, i.e. *Glauber dynamics*, although other hybrid updating schemes have also been explored (Marro et al., 2008; Torres et al., 2008).

Within this framework, a **memory** is represented by a pattern of activity $\boldsymbol{\xi} \equiv \{\xi_i, ..., \xi_N\}$, with $\xi_i \in \{0, 1\}$, that corresponds to a particular configuration of the system. A set of P of such patterns, $\{\boldsymbol{\xi}^\nu\}_{\nu=1,...,P}$, can be stored in the system by the thoughtful definition of the synaptic weights, using for instance the hebbian learning rule in Eq. 1.2. Via this rule, the activity patterns are stored in the synaptic weights w_{ij}, that are reinforced by a positive quantity $\delta = (\xi_i^\nu - a_0)(\xi_j^\nu - a_0) > 0$ when a certain pattern ν contemplates both neurons i and j in the same state, and are weakened when the same are in different states, with $\delta < 0$.

In the case of symmetric connections ($w_{ij} = w_{ji} \ \forall i, j$), as produced by the hebbian learning rule, one can define the Hamiltonian of the system, very similar to that of the Ising model, that can be written as

$$H(\boldsymbol{S}) = -\frac{1}{2}\sum_{i=1}^{N}\left[h_i(\boldsymbol{S}) - \theta_i\right] = -\frac{1}{2}\sum_{i,j\neq i} w_{ij} s_i s_j + \sum_{i=1}^{N}\theta_i s_i. \tag{1.23}$$

In the deterministic limit $T \to 0$ the state of the neural network always reaches a minimum of the associated Hamiltonian $H(\boldsymbol{S})$. The macroscopic state of the

system can thus be characterize by its **overlap** with each of the patterns,

$$m^\mu(\boldsymbol{S}, t) \equiv \frac{1}{N a_0 \left(1 - a_0\right)} \sum_{i=1}^{N} \left(\xi_i^\mu - a_0\right) s_i(t). \tag{1.24}$$

Let us consider a case with weak noise, i.e. low T, and few stored patterns, or small *memory load* $\bar{\alpha} \equiv P/N$. If the initial state of the network $\boldsymbol{S}$ is close to the pattern configuration $\boldsymbol{\xi}^\mu$, $m^\mu(\boldsymbol{S}) \approx 1$, the network will evolve towards such a memory, being the state $\boldsymbol{\xi}^\mu$ the attractor of network dynamics. For $T = 0$ there is a point-wise convergence to the memory attractors, both when using Little and Glauber dynamics.

Each stored memory yields the appearance of two attractors in the dynamics of the system, one associated with the corresponding activity pattern $\boldsymbol{\xi}^\mu$ and the other with the antipattern $-\boldsymbol{\xi}^\mu$. Due to this association between stored activity patterns and dynamical attractors, Hopfield-like models are commonly denoted as **Attractor Neural Networks (ANN)**.

In the rest of the parameter space, the Amari-Hopfield model can be analytically solved within the statistical mechanics theory for *spin-glasses* using a mean-field replica trick (Amit, 1989) in the replica symmetry limit. This mean-field treatment allows us to characterize for instance the phases of the system, the stability of such phases, or the **maximum storage capacity** $\bar{\alpha}_{\max}$, i.e. the maximum number of patterns that can be recovered efficiently at a certain temperature. A global picture of the network phases in the $(T, \bar{\alpha})$ diagram is reported in figure 1.7, where one can observe four qualitatively different phases:

i) The **memory** or ferromagnetic phase (M), where the network exhibits associative memory, corresponding to the region below the T_c line. The memory states (also known as Mattis states) in which only the overlap with a given pattern $\boldsymbol{\xi}^\mu$ is non zero are the stable solutions corresponding to the absolute minima of the free energy. This phase is (mathematically) equivalent to the *ferromagnetic* or *ordered phase* of interacting spin networks (as in the Ising model).

ii) The **spin-glass** phase (SG) corresponds to the region between T_M and $T_g = 1 + \sqrt{\bar{\alpha}}$. The storage of a large number of different patterns in the network gives rise to *quenched noise* as a consequence of the interference between them in w_{ij}, which can destabilize such memory phase. Here the absolute minima of the free energy correspond to "spurious" or mixed states, in which the state of the system does not correspond to any of the memories but to infinite combinations of them. Thus, the system is not able to recover any memory. Note that even in the deterministic case, at $T = 0$, there is a critical load parameter $\bar{\alpha}_{\max} = 0.138$ upon which associative memory fails. $\bar{\alpha}_{\max}$ defines the maximum storage capacity of

the network Amit, 1989, that is, the maximum quantity of information that can be stored and effectively retrieved from the network.

iii) The **unstable memory** phase (M+SG) corresponds to the region between T_c and T_M lines, where the spurious SG states are the absolute minima, but memory solutions appear as local minima as well.

iv) The disordered, noisy or paramagnetic phase (P) corresponds to the region over T_g, which indicates a continuous phase transition from an ordered phase (either M or SG) to the paramagnetic one. Here the dynamics of the system is disordered and completely dominated by thermal noise (Amit, 1989).
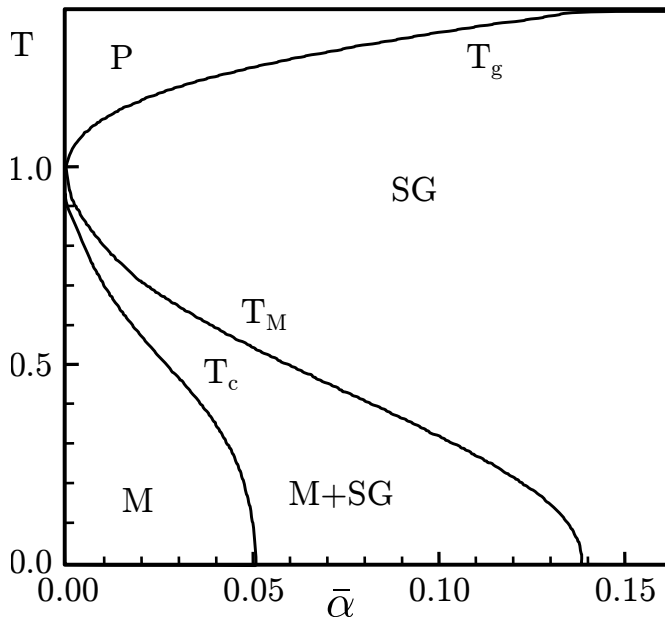
Figure 1.7: Phase diagram of the Hopfield model indicating the stable memory phase (M), the unstable memory phase (M+SG), the spin-glass phase (SG) and the paramagnetic disorder phase (P) in the case of a fully connected binary network.

The emergent behavior of the Amari-Hopfield model has also been studied on non-trivial network topologies, such as scale-free and small-world networks (Torres et al., 2004; Boccaletti et al., 2006; Oshima and Odagaki, 2007). Such systems have been shown to present the same phases as the canonical fully connected model, with transition lines that depend on the topology. In particular, it has been reported that, for heterogeneous networks and a single stored pattern, the overlap reduces for $T < T_c$, so that memory is recovered but with more

errors than in a fully connected network. However, the critical temperature diverges, $T_c \to \infty$ as $N \to \infty$, due to the presence of hubs that retain pattern information. Therefore, the memory phase expands to much higher values of thermal noise. On the other hand, the capacity of the network is known to decrease as the mean connectivity of the network decreases (Torres et al., 2004).

Although the steady state of the general model defined above represents an equilibrium system in the sense of the statistical mechanics, some non-equilibrium versions of such model can be studied considering for instance synaptic plasticity. In this case, the phase diagram changes qualitatively, with the emergence of new non-equilibrium dynamic phases, chaotic switching among memory patterns and criticality (Marro et al., 2008; De Franciscis et al., 2010). In chapters 2, 4 and 3 we consider a form of structural plasticity coupled with the Amari-Hopfield model, and we show that the time-varying structure (as produced by structural plasticity) can lead to the emergence of new phases and extend the stability of the memory states to higher values of noise, for instance.

1.4.2 Brain rhytms and synchronization: The Kuramoto model

One of the most studied features of brain dynamics is the emergence of synchronization at different rhythms, observed both in-vivo and in-vitro, and consisting on alternate periods of coherence – during which many neurons fire within a narrow time window – inter-spaced by periods of relative quiescence (Linkenkaer-Hansen et al., 2001; Buzsaki, 2006). EEG and MEG recordings repeatedly report oscillations at particular frequencies, defining "bands" of frequencies such as delta $(0.5 - 3.5 \text{ Hz})$, theta $(3.5 - 7 \text{ Hz})$, alpha $(8 - 13 \text{ Hz})$, beta $(15 - 25 \text{ Hz})$, and gamma $(30 - 70 \text{ Hz})$ bands. Specific oscillation patterns are associated with particular cognitive processes: theta and gamma rhythms with memory encoding and retrieval, alpha and gamma rhythms with attentional suppression and focusing, whereas the gamma band is associated with global synchronization and consciousness (Ward, 2003). Synchronization is also known to play a major role in vision (Steinmetz et al., 2000; Matias et al., 2015), the circadian rhythms in mammals (Komin et al., 2010) and pathologies such as epilepsy (Kandel et al., 2000).

Synchronization is arguably how the brain achieves the large-scale integration of its many parallel, distributed information-processing activities, allowing coherent cognition and behavior (Varela et al., 2001), being fundamental for cognitive processes such as memory, attention, decision-making, and even conscious awareness (Ward, 2003). Therefore, shedding light on the origin, nature, and functional meaning of such an intricate synchronization dynamics is a fundamental challenge in neuroscience (Buzsaki, 2006).

The archetypal Kuramoto model allows us to model synchronization with a minimal design (Kuramoto, 1975, 2003; Acebrón et al., 2005), providing a mathematical description of a large set of coupled oscillators. Its formulation

was motivated by the behavior of systems of chemical and biological oscillators (Kuramoto, 2003), and it has found widespread applications such as in neuroscience (Strogatz, 2000). The model makes several assumptions, including that there is weak coupling, that the oscillators are identical or nearly identical, and that interactions depend sinusoidally on the phase difference between each pair of objects. In its usual formulation, the Kuramoto model consists in a set of N coupled oscillators described by the following set of differential equations

$$\dot{\theta}_i(t) = \omega_i + k \sum_{j=1}^{N} \sigma_{ij} \sin\left(\theta_j(t) - \theta_i(t)\right) \quad (1.25)$$

where $\theta_i(t)$ is the phase of oscillator i at time t, ω_i is its natural or internal frequency and $k\sigma_{ij}$ is the coupling strength between oscillator j and i. The internal frequencies can be identical $\omega_i = \omega$ or more in general they can be extracted from a predefined probability distribution $g(\omega)$.
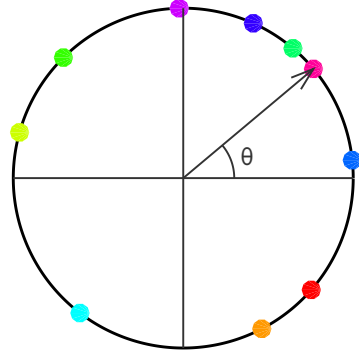
The level of synchronization in the system is measured with the Kuramoto order parameter, defined as

$$Z(t) = R(t)e^{i\phi(t)} = \frac{1}{N} \sum_{j=1}^{N} e^{i\theta_j(t)} \quad (1.26)$$

where $0 \leq R \leq 1$ gauges the overall coherence and $\phi(t)$ is the average phase of global oscillations.

Theoretical results are known for different limits of the Kuramoto model. In an infinitely large population of fully connected oscillators, full synchronization ($\omega_i = \omega \ \forall i$) is only possible in the case of homogeneous frequencies ($\omega_i = \omega \ \forall i$) (Steinmetz et al., 2000). On the other hand, with frequency heterogeneity the model exhibits a phase transition at a given value of k that separates a coherent steady state ($R > 0$) from an incoherent one ($R = 0$).

Synchronization dynamics has also been studied on lattices. In particular, in regular lattices of dimension d, it has been shown that global synchronization is only possible for $d > 4$; in dimensions $2 < d \leq 4$ only entrained frequency synchronization, but not phase synchronization, is observed, whereas in dimension $d \leq 2$ synchronization is not observed (Hong et al., 2005; Hong et al., 2007). Interestingly, regimes of partial synchronization have also been found to emerge in ring lattices. In such cases *chimera states*, consisting on incongruous interconnected parts, in which regions of coherent (phase and frequency locked) and incoherent (drifting) oscillators coexist (Abrams and Strogatz, 2004; Abrams et al., 2008; Laing, 2009) in simple variations of the Kuramoto model (Panaggio and Abrams, 2015).

In chapters 5 and 6 we show that a regime of frustrated synchronization, characterized by global oscillations of $R(t)$, can emerge in complex networks with hierarchical and modular structure (Moretti and Muñoz, 2013; Villegas et al., 2014) depending on their spectral dimension.

1.4.3   The criticality hyphotesis

Upon experimentally enhancing the spatio-temporal resolution of activity recordings, Beggs and Plenz made the remarkable finding that, actually, synchronized outbursts of neural activity could be decomposed into complex spatio-temporal patterns, thereon named *neuronal avalanches* (Beggs and Plenz, 2003). These present a scale-free distribution of sizes, with an exponent of $-3/2$, and also a scale-free distribution of lifetimes, with an exponent close to -2, in agreement with a critical branching process (Beggs and Plenz, 2003, 2004; Petermann et al., 2009; Hahn et al., 2010).

Scale-free avalanches of neuronal activity have since been consistently reported to occur across neural tissues, preparation types, experimental techniques, scales, and species (Hahn et al., 2010; Haimovici et al., 2013). They are observed during the earliest time of the development of superficial layers in the cortex requiring the presence of dopamine (a neuro-modulator) and a certain balance between excitatory and inhibitory synaptic transmission (Beggs and Plenz, 2003; Gireesh and Plenz, 2008). Moreover, EEG recordings indicate that, under healthy conditions, no temporal scale is predominant and the power spectra of brain activity decays as $1/f$ noise (Bullock et al., 2003). Scale-invariance is also shown in human cognition (Ward, 2002), human motion (Nakamura et al., 2007) and animal motion (Anteneodo and Chialvo, 2009).

These observations have been taken as empirical evidence backing the *criticality hypothesis*. That is, the conjecture that the awake brain might extract essential functional advantages – including maximal sensitivity to stimuli, large dynamical repertoires and optimal computational capabilities – from operating close to a critical point, separating two different phases (Chialvo, 2004, 2010). Critical dynamics has been documented in species evolution (Bak, 2013), traffic flow in highways (Bak, 2013), the internet (Takayasu et al., 2000) or rainfall dynamics (Peters and Neelin, 2006), among others (Beckers et al., 1990; Rauch et al., 1995; Malamud et al., 1998; Lux and Marchesi, 1999; Cavagna et al., 2010). The complexity of the brain might be yet another signature of an underlying critical process. As the largest number of metastable states exists at a point near the transition, the brain can then be accessing the largest repertoire of behaviors in a flexible way (Chialvo, 2010; Expert et al., 2010; Bak, 2013). Importantly, criticality is found to be associated with maximal information transfer (Beggs and Plenz, 2003) and thus high efficacy of neuronal information processing.

Furthermore, some relevant aspects of brain dynamics have been be predicted from the structure assuming that the underlying dynamics are critical

(Haimovici et al., 2013). Networks derived from correlations of fMRI signals in human brains are indistinguishable from networks extracted from Ising models at critical temperature (Baliki et al., 2008). Consequently, the paradigm of self-organized criticality (SOC) has been profusely adopted in neuroscience, and interesting models inspired in SOC have been proposed to account for the empirically observed scale-free avalanches of neuronal activity (Jensen, 1998; Harris, 2002; Brunel and Hakim, 2008).

However, what those phases are, and what the nature of the putative critical point is, are questions that still remain to be fully settled. The nature of such critical point is usually assumed to be the separation between a quiescent and an active phases, however several experimental investigations found evidence that scale-free avalanches emerge in concomitance with collective oscillations, suggesting the presence of a synchronization phase transition (Santo et al., 2018). Similarly, it is not clear whether the observed exponent values appear as a generic consequence of how temporally-defined avalanches are measured (involving thresholding, time binning to discriminate their beginning and end, or sub-sampling due to technological and empirical limitations). Further explanations relate cortical dynamics to the point of marginal percolation of activity (Poil et al., 2012) or the Ising model (Destexhe, 2009; Fraiman et al., 2009).

1.4.4　Criticality in disordered media

The paradigm of self-organized criticality (SOC) has revealed itself to be rather prolific when applied to the understanding of living systems, as it provides a framework to explain, without the necessity of any fine tuning, the prevalence of the critical point (Bak et al., 1987). Interestingly, however, fMRI analysis of brain activity at the resting state have revealed that the brain actually wanders around a broad region near a critical point, instead of staying in it (Tagliazucchi et al., 2012). This suggests that the region where cortical networks operate is not just a critical point, but a whole extended region around it.

The existence of an extended critical-like region is a well-known result in the context of statistical mechanics when disordered media are considered (Griffiths, 1969; Noest, 1986), known as a *Griffiths phase* (GP). GPs are broad regions in the parameter space exhibiting critical-like features and, thus, not requiring of a too-precise fine tuning. Given that disorder is an intrinsic and unavoidable feature of neural systems, GPs are expected to have a relevant role in many dynamical aspects (Treviño III et al., 2012).

Computational and theoretical studies of spreading dynamics on top of both artificial hierarchical-modular networks and the *C. elegans* connectome have shown the emergence of an extended region characterized by generic power-laws, akin to a GP (Vojta, 2006; Muñoz et al., 2010; Moretti and Muñoz, 2013). It is noteworthy that disorder needs to be present at very different scales for

GPs to emerge (otherwise rare-regions cannot be arbitrarily large); this is why a hierarchy of levels is required (Muñoz, 2018). Plain modular networks without the broad distribution of cluster sizes, characteristic of hierarchical structures, are not able to support GPs.

Stretched critical regions, stemming from structural disorder, yield enhanced functionality in a generic way, facilitating the task of self-organizing, adaptive and evolutionary mechanisms selecting for criticality (Muñoz et al., 2010). Furthermore, functional advantages usually ascribed to criticality, such as a huge sensitivity to stimuli, are reported to emerge generically all along the GP. The existence of a GP thus provides a more robust basis for the ubiquitous presence of scale-free behavior in neural recordings, and might give us the key to understanding why broad regions around criticality are observed in fMRI experiments of the brain resting state (Levina et al., 2007; Bonachela et al., 2010; Millman et al., 2010; Tagliazucchi et al., 2012) .

GPs have previously been associated with large-world networks (that is, networks with a finite topological dimension). In chapter 5 we demonstrate that broad regions of frustrated synchronization, resembling a GP, can appear on small-world networks too, and in chapter 6 we investigate how the existence and properties of this region depend on the network's spectral dimension.

1.4.5   Adaptive neural networks

There are many systems in which the evolution of their underlying networked structure is invariable linked to the dynamical state of their nodes and links, and vice-versa. These are called **adaptive** or **co-evolutionary networks**. One familiar example are transport network, such as roads, power-grids, or wireless communication networks, as well as the internet network (Gross and Blasius, 2007). In all these systems a high load on one connection can cause it to fail, being an incentive for new additional connections. The same mechanisms can arise in natural and biological distribution networks, such as the vascular system and genetic and neural networks, and in chemistry and biology, including protein interaction and ecological networks. Similarly, in social sciences networks different social states among the nodes can lead to the break-up of the interactions.

Despite the diversity of scenarios in which adaptive networks appear, there are a number of hallmarks associated with them. These include self-organization towards critical behavior, frequently concomitant with the appearance of power-law distributions, the formation of complex topologies and complex system-level dynamics (Gross and Blasius, 2007; Wiedermann et al., 2015). Given that the information can be stored and read from the topology, the dynamics of adaptive networks involves local as well as topological degrees of freedom and it can be more complex than that of similar non-adaptive models. In particular, the dynamics on the network makes topological degrees of freedom accessible in

every node, spreading information on topological properties across the network. The local topological evolution can then react on this information and drive the topology to a topological phase transition at which the dynamics on the network is critical (Vazquez et al., 2008). It could explain, for instance, how neural and genetic networks manage to exhibit dynamics that in many models appears only in critical states at the edge of chaos (Gross and Blasius, 2007; Tetzlaff et al., 2010; Muñoz, 2018). Similarly, the capability of adaptive networks to form complex topologies could offer a highly elegant way to build up large-scale structures from simple building blocks, such as in the growth of vascular networks (Wiedermann et al., 2015).

Another recurrent property of adaptive networks is the spontaneous division of labor with the emergence of classes of topologically and functionally distinct nodes. It has been suggested that this is driven by the self-organization towards a phase transition at which the critical slowing down of the turnover times between emergent properties of nodes occurs (Gross and Blasius, 2007).

More fundamental work is still needed in order to understand how all these properties emerge from the transfer of information between state and topology and the subtle interplay between different time scales. Since adaptive networks appear in many different fields and are already implicitly contained in many models, a theory of adaptive networks can be expected to have a significant impact on several areas of active research.

In chapter 2 of this thesis we present an adaptive model for synaptic pruning in the brain, that can also account for structural plasticity. This naturally produces heterogeneous degree distribution (where two distinct classes of nodes appear, hubs and low-degree nodes), and it further shows the emergence of new qualitative behavior such as a region of bistability between different phases or an oscillatory region (see chapter 3).

Chapter 2

Concurrence of form and function in developing networks and its role in synaptic pruning

In this chapter we investigate the fundamental question in neuroscience of how the structure and function of neural systems are related. We study this interplay by combining a familiar auto-associative neural network with an evolving mechanism for the birth and death of synapses. A feed-back loop then arises leading to two qualitatively different types of behavior. In one, the network structure becomes heterogeneous and dissasortative, and the system displays good memory performance; furthermore, the structure is optimized for the particular memory patterns stored during the process. In the other, the structure remains homogeneous and incapable of pattern retrieval. These findings provide an inspiring picture of brain structure and dynamics, are compatible with experimental results on early brain development, and may help to explain synaptic pruning. Other evolving networks – such as those of protein interactions – might share the basic ingredients for this feed-back loop and other questions, and indeed many of their structural features are as predicted by our model. The study presented here has been published in Millán et al., 2018c.

2.1   Introduction

In the previous chapter we have briefly introduced some relevant mathematical models that are typically used for the study of brain dynamics. As we have seen, viewing the brain as a complex network allows us to understand how some characteristic cognitive processes may emerge from the collective behavior of neurons and synapses (Amari, 1972; Hopfield, 1982; Marro and Chialvo, 2017). The structural properties of this underlying network thus affect the behavior of the system in various ways (Modha and Singh, 2010; Telesford et al., 2011; Voges and Perrinet, 2012; Gastner and ódor, 2016).

A main process that determines the properties of the underlying network is *synaptic pruning* and the associated *structural plasticity* (Chechik et al., 1998, 1999), whose major role on brain maturation has been discussed in section 1.1.4. Namely, synaptic pruning is a mechanism of network adaptation and development – from a highly dense network to a sparser, more structured one – that shapes the connectivity structure of the brain during infancy and young adulthood. This provides the brain with structural plasticity, that is, the ability to develop, change and learn due to changes in its underlying structure (Holtmaat et al., 2005; Holtmaat and Svoboda, 2009). The effect of synaptic pruning on the brain's cognitive capabilities can hardly be overestimated, being necessary for the emergence of the diverse and complex connectivity structure that is characteristic of biological neural networks and thought to be determinant for their function (Iglesias et al., 2005; Holtmaat and Svoboda, 2009; Santos and Noggle, 2011; Sporns, 2012; Navlakha et al., 2015). Moreover, defects in the pruning process have been found in some cognitive disorders such as autism and schizophrenia, which we discuss further in chapter 3 (Geschwind and Levitt, 2007; Sekar et al., 2016). Notice that neural circuits continue to change in the mature brain, which also shows structural plasticity to some extend, as they maintain the ability to grow and break synapses (Knoblauch and Sommer, 2016).

Synaptic pruning induces temporal changes in the structure of connections (new synapses grow and others disappear) in response to spontaneous and sensory-evoked neural activity (Lee et al., 1980; Frank, 1997; Klintsova and Greenough, 1999; De Roo et al., 2007; Deger et al., 2012). Consequently, it is reasonable to think that the evolution of network structure is intrinsically coupled with the activity dynamics on the network. It is thus also natural to consider a *co-evolving* neural network when seeking for a more precise mathematical model to describe network evolution (see section 1.4.5 and also Gross and Blasius, 2007; Vazquez et al., 2008; Sayama et al., 2013). Previous studies of co-evolving brain networks have studied the temporal evolution of the mean degree (Huttenlocher and Dabholkar, 1997), particular microscopic mechanisms (Chechik et al., 1999), the development of certain computational capabilities

(Eguiluz et al., 2005), or the effects of specific growth rules (Iglesias et al., 2005). Other recent works have suggested evidence for the role of bistability and discontinuous transitions in the brain, for instance in synaptic plasticity mechanisms involved in learning (Litwin-Kumar and Doiron, 2014; Zenke et al., 2015).

In this chapter we present a novel co-evolving model for synaptic pruning and structural plasticity that combines the Amari-Hopfield neural network (see section 1.4.1 and also Amari, 1972; Hopfield, 1982) with a plausible model of network evolution (as presented in section 1.3.2; see also Johnson et al., 2010a). In order to do so, we set the probabilities of synaptic growth and death to depend on neural activity, as it has been empirically observed (Holtmaat and Svoboda, 2009). We consider the emergence of some general properties observed in actual neural networks, including degree heterogeneity that roughly accords with scale-free distributions, and negative degree-degree correlations i.e. dissasortativity (see section 1.2.3), which strongly influence the dynamics of the system (Torres et al., 2004; Franciscis et al., 2011).

Taken separately, the two models used to describe neuron and network dynamics exhibit a continuous phase transition: from a phase of memory to one of noise in the case of the Amari-Hopfield model, and from heterogeneous to homogeneous networks in the case of the synaptic pruning model. Taken together, the topological state of the networks affects the activity one, and viceversa. We find that, for certain parameter ranges, the phase transition between memory and randomness becomes discontinuous (i.e. resembling a first order thermodynamic transition). Depending on initial conditions, the system can either evolve towards heterogeneous networks with good memory performance, or homogeneous ones incapable of memory, as a consequence of a feed-back loop between structure and function. To the best of our knowledge, this is the first time that this feed-back loop, and the ensuing discontinuous transition, have been identified. Also, in our model networks are generated which have optimal memory performance for the specific memory patterns they encode, thus allowing for a greater memory capacity than would be possible in the absence of such a mechanism. Our results thus suggest a more complete explanation of synaptic pruning.

Finally, we also discuss the possibility that other biological systems – in particular, protein interaction networks – also owe their topologies to a version of the feed-back loop between form and function that we identify here, due to the network properties that they share with neural networks.

2.2 Model construction

We define a co-evolving model of synaptic pruning that couples a traditional associative memory model, the Amari-Hopfield model (AH) (see section 1.4.1

and also Amari, 1972; Hopfield, 1982), with a preferential attachment model for network evolution (see section 1.3.2; see also Johnson et al., 2010a). The model is defined in this chapter to describe the basic mechanisms of synaptic pruning, and we further use it in chapters 3 and 4 to explore other consequences of the co-evolving dynamics. More precisely, in chapter 3 we will use this model to investigate in detail the effect of combining thermal and quenched disorder (arising from the competition among different stores memories), and in chapter 4 we analyze in depth the consequences of the initial overgrowth of synaptic density that precedes synaptic pruning on the dynamics of the system, and on its emergent behavior.

Our system consists in a time-dependent, symmetric, undirected, N-node complex neural network (Boccaletti et al., 2006) where nodes stand for neurons and edges represent synapses. The network is defined at time t by the adjacency matrix $\boldsymbol{e}(t)$, with elements $e_{ij}(t) = \{0,1\}$, according to whether there exists or not an edge between the pair of nodes (i,j), respectively. The **degree** of node i at time t is defined as

$$k_i(t) = \sum_{j=1}^{N} e_{ij}(t) \tag{2.1}$$

and the **mean degree** of the network is

$$\kappa(t) = \frac{1}{N} \sum_{i=1}^{N} k_i(t). \tag{2.2}$$

2.2.1   The neural network model

Following the familiar AH prescription presented in section 1.4.1 (Amit, 1989), each neuron i is modeled as a stochastic binary unit, $s_i(t) = \{0,1\}$, representing respectively a silent and a firing neuron. Each edge (i,j) is characterized by its **synaptic weight** w_{ij}, which defines the strength of the synapse. This is a real variable defined by means of a set of P binary patterns of neural activity, $\xi_i^\mu \in \{0,1\}$, $\mu = 1,...,P$, according to the Hebbian learning prescription (see section 1.1.4.1):

$$w_{ij} = [\kappa_\infty a_0 (1 - a_0)]^{-1} \sum_{\mu=1}^{P} (\xi_i^\mu - a_0)\left(\xi_j^\mu - a_0\right), \; i \neq j$$
$$w_{ii} = 0, \tag{2.3}$$

where $\kappa_\infty = \kappa(t \rightarrow \infty)$ and a_0 is the mean activation of the patterns, i.e. $a_0 = \langle \xi_i^\mu \rangle$. As seen in the previous chapter, this definition of the synaptic weights makes the patterns ξ_i^μ attractors of the activity dynamics of the system, and therefore it is the final step of a process of "learning" or "storing" the memories in the synaptic weights. Given that $w_{ij} = w_{ji}$ by construction (and that e_{ij} is also

symmentric, as previously defined), the network is symmetric, in the spirit of previous studies (Sompolinsky and Kanter, 1986). This is for simplicity and also as a reference to compare with the canonical AH model (Amari, 1972; Hopfield, 1982). Earlier studies suggest that the inclusion of asymmetry could lead to the induction of chaos, affecting learning, for instance causing the system to oscillate among different states (Sompolinsky and Kanter, 1986). Here we have decided to simplify the picture and consider symmetric networks, and we expect that, given a reasonable definition of asymmetry, the main results of our work would hold.

The **local field** at neuron i quantifies the incoming input from neighbor neurons, and it is given by

$$h_i(t) = \sum_{j=1}^{N} w_{ij} e_{ij}(t) s_j(t). \tag{2.4}$$

The equation is analogous to the canonical AH one (Eq. 1.20) with the inclusion of the network's topology through $e_{ij}(t)$. The states of all neurons are updated in parallel at every time step according to the probabilistic dynamics

$$P\left[s_i(t+1) = 1\right] = \frac{1}{2} \left\{ 1 + \tanh\left[T^{-1}\left(h_i(t) - \theta_i(t)\right)\right] \right\}, \tag{2.5}$$

where

$$\theta_i(t) = \frac{1}{2} \sum_{j=1}^{N} w_{ij} e_{ij}(t) \tag{2.6}$$

is a neuron's **threshold** for firing. The noise parameter or **temperature** T ($T > 0$) sets the level of stochasticity on the activity of the neurons (Bortz et al., 1975), so that if $T = 0$ the evolution of the system is deterministic and the state of a neuron at time t is completely determined by the states of its neighbors at time $t - 1$. For $T > 0$, however, the evolution is stochastic and, as T is increased, the thermal noise has a stronger effect (see figure 1.7).

The definition in equation 2.6 is typically considered, in the case of static networks, when the biologically plausible $\{0, 1\}$ code is used instead of the canonical $\{\pm 1\}$ one, since it allows one to recover the phase diagram of the canonical, fully connected AH model (Amit, 1989). Therefore, we maintain it when extending the model to a time dependent topology, and it naturally leads to a *dynamic threshold*. This is not a strong assumption since dynamic or adaptive thresholds have been widely described in several neural systems. For instance, they have been shown to create a nontrivial motion between the attractors of the system (Horn and Usher, 1989; Itskov et al., 2011) and to have a major role in stochastic resonance (Mejías and Torres, 2011) and in the functioning of sensory systems (Fricker et al., 1999; Azouz and Gray, 2000, 2003; Cardin et al., 2008; Kobayashi et al., 2009). Mechanisms of threshold adaptation have been found

to help to avoid saturating activity during developmental changes (Turrigiano et al., 1998), and to be related to homeostatic regulation mechanisms observed in cortical neurons (Abbott and LeMasson, 1993; Turrigiano et al., 1998) and to the emergence of self-organized criticality in neural systems (Uhlig et al., 2013; Hobbiss et al., 2018). In our context, $\theta_i(t)$ depends only on the existing synapses, which can be seen as a means of *homeostasis* since the response of a neuron is regulated by the number and strength of its synaptic contacts, thus avoiding silencing low-degree neurons and saturation of hubs. Furthermore, in our model the term $e_{ij}(t)w_{ij}$ in Eq. 2.6 characterizes the intensity of the synaptic transmission between neurons i and j, so that the threshold dynamics depends indirectly on the neural activity.

The **overlap** of the network state with each of these patterns determines the global state of the system,

$$m^{\mu}(t) = [Na_0(1 - a_0)]^{-1} \sum_{i=1}^{N} (\xi_i^{\mu} - a_0) \, s_i. \tag{2.7}$$

It follows from this definition that $-1 \leq m^{\mu}(t) \leq 1$. We say that the system is in a *memory state* or, equivalently, that it has *retrieved* pattern μ, if $m^{\mu} > 2/3$ and $m^{\nu} \to 0 \; \forall \nu \neq \mu$. This indicates that the activity state of the network strongly resembles that of pattern μ.

The canonical setting of this model, in the case of a fully connected network and random orthogonal patterns, is described in detail in the previous chapter (see subsection 1.4.1). In summary, it exhibits three characteristic phases. In the absence of thermal noise, $T = 0$, the patterns ξ_i^{μ} are stable attractors of the dynamics of the system for $P < P_c = 0.138N$, and the system is in what is called the *memory phase*. P_c defines the *maximum storage capacity* of the network (Amit, 1989), that is, the maximum quantity of information – or number of patterns – that can be stored and effectively retrieved from the network. This phase is (mathematically) equivalent to the *ferromagnetic* or *ordered phase* of interacting spin networks (as in the Ising model). The storage of a large number of different patterns in the network gives rise to *quenched noise* as a consequence of the interference between them in w_{ij}, which can destabilize such memory phase. Therefore, if P is further increased above P_c there is a discontinuous phase transition to a *spin-glass (SG) phase*, in which there appear metastable states – consisting in combinations of a macroscopic number of stored patterns (therefore also called *mixed states*) – that trap the dynamics of the system. Similarly, in the case of $P = 1$ there is a continuous phase transition as the temperature increases from the memory phase to a noisy or *paramagnetic phase* (also called *disordered phase*), at $T_c = 1$. In the paramagnetic phase there are no stable attractors, and the dynamics of the system is driven by noise (Amit, 1989). Finally, in the more general case in which both $T > 0$ and $P > 1$, the location of the phase transitions depends both on T and P (see figure 1.7 in

chapter 1). We here consider an evolving network whose structure, contrary to the canonical model above, changes constantly in time subjected to the pruning dynamics, as we shall describe in the next section.

2.2.2   Activity dependent synaptic pruning model

The network structure changes in time following a preferential attachment process that is a generalization of the topological synaptic pruning model presented in the previous chapter (see subsection 1.3.2). At each time t, each node has a probability $P_i^g(t)$ of being assigned a new edge to another node, randomly chosen, and a probability $P_i^l(t)$ of losing one of its edges. These are given by

$$
\begin{aligned}
P_i^g &= u\left(\kappa\right)\pi\left(k_i, I_i\right), \\
P_i^l &= d\left(\kappa\right)\eta\left(k_i, I_i\right),
\end{aligned}
\tag{2.8}
$$

where the time dependency has been dropped for clarity. In this equation the local probabilities π and η can depend on the node's degree k_i but also on the physiological variable $I_i = |h_i - \theta_i|$. This is the scaled input that each neuron receives as a consequence of the coupling with its neighbors, a sort of recurrent current in the network, which is a measure of the present activity of the neural medium reaching neuron i. In this way we couple the evolution of the network with the neural dynamics, following the empirical observations that synaptic growth and death are determined by neural activity (Lee et al., 1980; Frank, 1997; Klintsova and Greenough, 1999; De Roo et al., 2007). The probabilities π and η are normalized over the network: $\sum_{i=1}^{N}\pi(k_i, I_i) = \sum_{i=1}^{N}\eta(k_i, I_i) = 1$.

The first terms on the right-hand side of each equation represent a global dependence to account for the fact that such processes rely in some way on diffusion of different molecules through large areas of tissue, and we take the mean degree $\kappa(t)$ at each time as a proxy. In order to describe synaptic pruning, we choose these probabilities to be consistent with empirical data describing synaptic density in mammals during infancy (Huttenlocher and Dabholkar, 1997; Navlakha et al., 2015). The simplest choice is (Johnson et al., 2010a; Millán et al., 2015; Millán et al., 2018c)

$$
\begin{aligned}
u(\kappa(t)) &= \max\left\{\frac{n}{N}\left(1 - \frac{\kappa(t)}{2\kappa_\infty}\right), 0\right\} \\
d(\kappa(t)) &= \frac{n}{N}\frac{\kappa(t)}{2\kappa_\infty},
\end{aligned}
\tag{2.9}
$$

where n is the number of edges to be added or removed at each step, which sets the speed of synaptic turnover, and $\kappa_\infty = \kappa(t \to \infty)$ is the stationary mean degree. Notice also that equation 2.9 assures that $u(\kappa) \geq 0 \ \forall \kappa$.

The definitions in Eq. 2.9 take into account that synaptic growth and death relay in some way on the concentrations of various molecules (that can have an

important role in synaptogenesis, as axonal growth factors), which can diffuse through large areas of tissue and therefore cannot in general be considered local (Klintsova and Greenough, 1999). Here, therefore, we consider $\kappa(t)$ as a proxy for the amount of resources consumed by the existing synapses in the network. In an environment with a finite presence of nutrients, it is reasonable to think that there is a competition for the existing resources, and that neurons are sensitive to the amount of nutrients available to them, so that synapses are less likely to grow, and more likely to atrophy, when the connectivity is high, and viceversa, as assumed by equation 2.9. Finally, we note that experimental studies (Huttenlocher and Dabholkar, 1997) have revealed a fast initial overgrowth of synapses associated with the transient existence of different growth factors. This and other particular mechanisms could be accounted for by adding extra factors in Eqs. 2.9. For example, an initial overgrowth of the synaptic density can be reproduced by adding the term $a \exp(-t/\tau_g)$ in the growth probability (Johnson et al., 2010a). This is analyzed in more detail in section 2.3.2.

2.2.3   Monte Carlo simulations

In practice, numerical simulations are carried out via a Monte Carlo method as follows [in particular, we make use here of the BKL algorithm (Bortz et al., 1975)]. The initial conditions for the neural states are randomly distributed. For the network topology we draw an initial degree sequence from a distribution $p(k, t = 0)$, and then place edges between nodes i and j with a probability proportional to $k_i(0)k_j(0)$, as in the configuration model (Newman, 2011; Courtney and Bianconi, 2016). Then, at each time step t, the number of edges to be created and destroyed is sorted according to two Poisson distributions with means $Nu(\kappa)$ and $Nd(\kappa)$, respectively. As many times as needed according to this draw, we choose a node i with probability $\pi(k_i, I_i)$ to be assigned a new edge to another node randomly chosen; and similarly we choose a new node j according to $\eta(k_j, I_j)$ to lose an edge from one of its neighbors, randomly chosen. This process is done in a serial manner, and the same node can be selected more than once (Bortz et al., 1975).

Notice that for each node i that gains or looses an edge e_{ij}, the degree of the second node j to which that edge links also changes accordingly. Therefore, there are in fact two paths that can lead to the change of a node's degree: either through the primary process with probability $\pi(k_i, I_i)$ for a gain (or $\eta(k_i, I_i)$ for a loss), or when it is randomly connected to (or disconnected from) an already chosen node. These secondary processes lead respectively to the probabilities $1/(N - k_i - 1) \approx 1/N$ and $k_i/(\kappa N)$, disregarding degree-degree correlations.

The effective values of the second factors in equation 2.8 are consequently

$$\widetilde{\pi}_i = \frac{1}{2}\left[\pi(k_i, I_i) + \frac{1}{N}\right],$$
$$\widetilde{\eta}_i = \frac{1}{2}\left[\eta(k_i, I_i) + \frac{k_i}{\kappa N}\right],$$

(2.10)

where the $1/2$ factor is included to assure normalization.

For the sake of simplicity, we shall consider $\widetilde{\pi}$ and $\widetilde{\eta}$ to be power-law distributed (Johnson et al., 2010a), which allows one to move smoothly from a sub-linear to a super-linear dependence with a single parameter,

$$\widetilde{\pi}_i = \frac{I_i^\alpha}{\langle I^\alpha \rangle N},$$
$$\widetilde{\eta}_i = \frac{I_i^\gamma}{\langle I^\gamma \rangle N},$$

(2.11)

which are normalized over the network, $\sum_{i=1}^{N} \widetilde{\pi}_i = \sum_{i=1}^{N} \widetilde{\eta}_i = 1$.

This leads to

$$\pi(I_i) = \frac{1}{Z_\pi} \max\left\{2\frac{I_i^\alpha}{\langle I^\alpha \rangle N} - \frac{1}{N}, 0\right\},$$
$$\eta(I_i, k_i) = \frac{1}{Z_\eta} \max\left\{2\frac{I_i^\gamma}{\langle I^\gamma \rangle N} - \frac{k_i}{\kappa N}, 0\right\},$$

(2.12)

which hold that $\pi(I_i)$, $\eta(I_i, k_i) > 0$ $\forall i$. The factor $1/Z_x$ is included to assure normalization: $\sum_{i=1}^{N} \pi(I_i) = \sum_{i=1}^{N} \eta(I_i, k_i) = 1$. Notice that by construction the death probability η depends on both I_i and k_i, whereas the growth probability π is independent of the degree. Given that, in the memory regime of the AH model, $I_i \propto k_i$, as shown in figure 2.1c, one could consider the approximation $\eta \to \eta(I_i)$ too. These definitions are most important, as they characterize the coupling between neural activity and structure. However, the particular functions are an arbitrary choice and other ones could be considered.

In our scenario, the parameters α and γ characterize the dependence of the local probabilities on the local currents and account for the different proteins and factors that control synaptic growth. These could be obtained experimentally, although to the best of our knowledge this has not yet been done.

Finally, we impose further restrictions on the network. First of all, e_{ij} is a binary matrix, so that only one edge per pair of nodes is allowed and the strength of the connection between two neurons, resembling the number of multiple contacts between actual neurons (Fares and Stepanyants, 2009), is considered to be given by w_{ij}. Moreover, we set the minimum degree of the network, $k_i = 1$, so that there cannot be any disconnected nodes, and we forbid self-connections, $e_{ii} = 0$ $\forall i$. The maximum degree a node can have is therefore $N - 1$. We do not

impose a hard bound on it as other works have done (Knoblauch et al., 2014; Knoblauch and Sommer, 2016). This would exclusively affect hubs, reducing their connectivity. This might affect the memory capabilities of the network in the limit $P \to \infty$ but, since we do not work on this limit, we do not expect any changes on the qualitative behavior and main findings of our model.

2.2.4   The macroscopic state

The time scale for structure changes is set by the parameter n in Eq. 2.9, whereas the time unit for activity changes, h_s, is the number of Monte Carlo Steps (MCS) that the states of all neurons are updated according to the Hopfield dynamics between each structural network update. Our studies show a low dependence on these parameters in the cases of interest, so we only report results here for $h_s = 10$ MCS and $n = 10$. We have also considered both *Little* and *Glauber* dynamics to integrate the neural activity, with the same results (Amit, 1989).

The macroscopic activity state is characterized by the overlap, as defined above. Results in the main section of this chapter are for $P = 1$, so we simplify the notation and use $m = m^1$. A discussion on the effect of learning more patterns is included in subsection 2.4.2, whereas in chapter 3 we carry on an in depth analysis of the combination of thermal (as given by $T > 0$) and quenched ($P > 1$) disorder, showing that it can lead to the emergence of an oscillatory regime (Millán et al., 2019b).

The network macroscopic state is described via the **degree distribution** $p(k,t)$ ($p(k,t) \geq 0 \; \forall k, t, \sum_{k=1}^{N} p(k,t) = 1 \; \forall t$) and some of the network properties defined in the previous chapter (see subsection 1.2.1). In particular, it is of interest here the **homogeneity** $g(t)$,

$$g(t) = \exp\left(-\sigma^2(t)/\kappa^2(t)\right), \tag{2.13}$$

where $\sigma^2(t) = \langle k^2(t) \rangle - \kappa^2(t)$; the node's **clustering coefficient**, C_i,

$$C_i(t) = \frac{2t_i(t)}{k_i(t)\,(k_i(t) - 1)}, \tag{2.14}$$

where t_i is the number of triangles incident to node i ($t_i = 1/2 \sum_{j,h} a_{ij} a_{ih} a_{jh}$); the degree dependent clustering coefficient,

$$C(k,t) = \frac{1}{p(k,t)} \sum_{i=1}^{N} C_i(t) \delta_{k,k_i}; \tag{2.15}$$

and the **Pearson correlation coefficient** applied to the edges,

$$r(t) = \frac{[k_l k_l'] - [k_l]^2}{[k_l^2] - [k_l]^2}, \tag{2.16}$$

where $[\cdot] = \frac{1}{\kappa N} \sum_l (\cdot)$ stands for the average over edges (Boccaletti et al., 2006) and the time dependence has been dropped for clarity. The homogeneity parameter indicates the degree of homogeneity and heterogeneity of the degree distribution. In homogeneous networks all nodes have similar degrees and consequently $\sigma(t)$ is small and g approaches one, with the trivial case of $g = 1$ if $p(k,t) = \delta_{k,k_1}$. For heterogeneous networks, on the other hand, there are big fluctuations in the degrees of the nodes and $g(t) \to 0$.

Finally, we notice that in this model r can be estimated as (Johnson et al., 2010a)

$$r(t) = \langle k \rangle \frac{\left\langle k^2 k_{nn}(k) - \langle k^2 \rangle^2 \right\rangle}{\langle k \rangle \langle k^3 \rangle - \langle k^2 \rangle^2}, \qquad (2.17)$$

where $k_{nn}(k)$ is the neighbors mean degree function,

$$k_{nn,i} = \frac{1}{k_i} \sum_j a_{ij} k_j. \qquad (2.18)$$

The Pearson correlation coefficient characterizes the degree-degree correlations, which have important implications for network connectedness and robustness. That is, whereas most social networks are assortative ($r > 0$), almost all other networks, whether biological, technological or information-related, seem to be generically dissasortative ($r < 0$), meaning that high degree nodes tend to have low degree neighbors, and vice-versa. Previous studies showed that heterogeneous networks favor the emergence of dissasortative correlations (Boccaletti et al., 2006; Johnson et al., 2010b; Williams and Del Genio, 2014).

In this chapter we will consider as order parameters the stationary overlap, $\overline{m} = m(t \to \infty)$, the stationary homogeneity, $\overline{g} = g(t \to \infty)$ and the stationary Pearson's coefficient $\overline{r} = r(t \to \infty)$. Measures of the global variables on the stationary state are obtained by averaging during a long window of time: $\overline{f} = \Delta t^{-1} \sum_{t=t_0}^{t_0+\Delta t} f(t)$.

2.3 Preliminary analysis

2.3.1 Topological limit

Consider first the topological limit of the model, which is equivalent to the model defined in section 1.3.2. In this case network structure is de-coupled from neural activity, so that the topology of the network is independent from its neural state. In our model, this limit is obtained by substituting $I_i \to k_i$, so that $\widetilde{\eta}_i = \widetilde{\eta}(k_i)$ and $\widetilde{\pi}_i = \widetilde{\pi}(k_i)$, whereas the global probabilities are still given by Eq. 2.9.

Following section 1.3.2, we can construct a master equation for the evolution of the degree distribution by considering network evolution as a one step process with transition rates $u(\kappa)\widetilde{\pi}(k)$ for degree increment and $d(\kappa)\widetilde{\sigma}(k)$ for

the decrement. Approximating the temporal derivative for the expected value of the difference in a given $p(k,t)$ we get, as in section 1.3.2:

$$
\begin{aligned}
\frac{dp(k,t)}{dt} = \; & u\left(\kappa\right)\widetilde{\pi}\left(k-1\right)p\left(k-1,t\right) \\
& + d\left(\kappa\right)\widetilde{\eta}\left(k+1\right)p\left(k+1,t\right) \\
& - \left[u\left(\kappa\right)\widetilde{\pi}\left(k\right)+d\left(\kappa\right)\widetilde{\eta}\left(k\right)\right]p\left(k,t\right),
\end{aligned}
\tag{2.19}
$$

which is exact in the limit of no degree-degree correlations between nodes (Johnson et al., 2010a).

Depending on the parameters, three qualitatively different behaviors, leading in practice to different phases, are possible for $k_i \gg 1$ (see figure 2.1a):

i) If $\gamma > \alpha$, then $\widetilde{\eta}(k_i) > \widetilde{\pi}(k_i)$, and high degree nodes are more likely to lose than to gain edges. Consequently, $p_\infty(k) = p(k, t \to \infty)$ is homogeneous, $\bar{g} \to 1$, and the probability of having high degree nodes vanishes rapidly from a maximum. This situation corresponds to the case $\alpha = 0.8$, $\gamma = 1.0$ (purple circles) in figure 2.1a.

ii) If $\gamma < \alpha$, then $\widetilde{\eta}(k_i) < \widetilde{\pi}(k_i)$, and high degree nodes are more likely to continue to gain than to lose edges. Since the stationary number of edges $N\kappa(t)$ is fixed, this leads to a bimodal $p_\infty(k)$, with $\bar{g} \to 0$, as shown by the blue squares in figure 2.1a, for $\alpha = 1.2$ and $\gamma = 1.0$.

iii) In the case $\gamma = \alpha$, $\widetilde{\eta}(k_i) = \widetilde{\pi}(k_i)$ and very connected nodes are as likely to gain as to lose edges. Excluding low degrees, $p_\infty(k)$ then decays as a power-law with exponent $\mu \approx 2.5$, in accordance with long-range connections observed in the human brain (Gastner and ódor, 2016) and measures of protein interaction networks (Albert, 2005). This situation is illustrated by the green diamonds in figure 2.1a, corresponding to $\alpha = \gamma = 1.0$.

In figure 2.1b we show $\bar{g}(\alpha)$ as obtained for the topological limit of the model ($\gamma = 1.0$, purple squares), displaying the continuous phase transition (from homogeneous networks with $\bar{g} > 0$ to heterogeneous ones with $\bar{g} = 0$) described above. Interestingly, we have found that the condition $\widetilde{\pi}(k_i) = \widetilde{\eta}(k_i)$ is mandatory to obtain a critical behavior, despite previous preliminary studies assuming the contrary (Johnson et al., 2010a). In particular, in the same figure we show in green $\bar{g}$ for a different set of local probabilities ($\pi(k) = k^\alpha/(\langle k^\alpha \rangle N)$ and $\eta(k)$ as before) that do not meet the aforementioned condition. The transition in this case is a discontinuous one, which fails to produce scale-free networks. The indicated lines in this panel follow from integration of the corresponding master equations, whereas points are from Monte Carlo data. Deviations from simulations are due to the emergence of small degree-degree correlations that are not taken into account by the master equation.
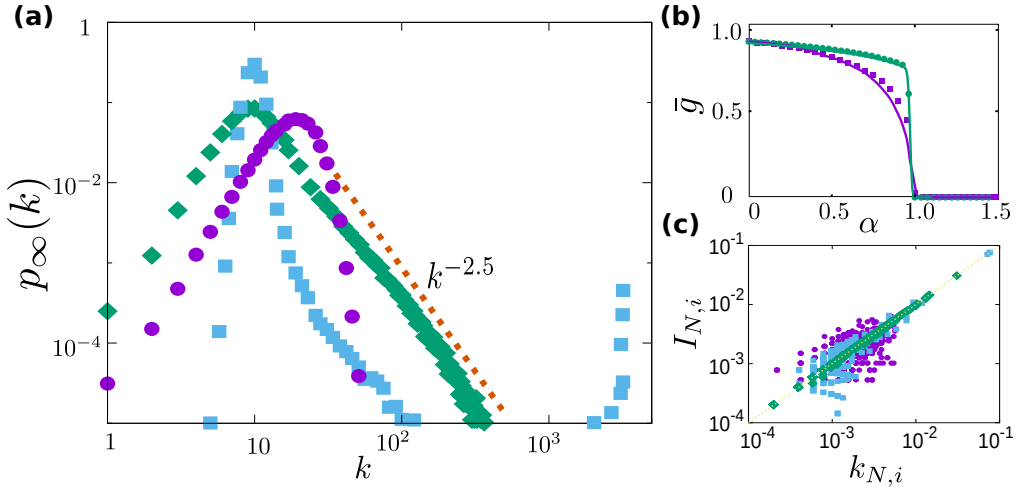
Figure 2.1: **Topological limit and activity-topology coupling. (a)** Stationary degree distributions $p_\infty(k)$ for $\gamma = 1.0$ and the three different observed phases: subcritical ($\alpha = 0.8$, purple circles), critical ($\alpha = 1.0$, green diamonds) and supercritical ($\alpha = 1.2$, blue squares). **(b)** $\bar{g}(\alpha)$ for the topological limit of our model ($\gamma = 1.0$, purple squares), and for a different set of local probabilities as indicated in the main text, not inducing criticality (green circles). **(c)** Normalized current of each neuron, $I_{N,i}$, as a function of its normalized degree, $k_{N,i}$, showing the correlation between neural activity and topology that emerges in our model system. The normalization is made by averaging over the total current ($\langle I \rangle N$) and degree ($\langle k \rangle N$) of the network, respectively. Labels as in panel (a). Results are for $N = 3200$ and $\gamma = 1.0$, and data from Monte Carlo simulations have been averaged over 100 realizations. Error bars corresponding to s.d. are too small to be appreciable.

Interestingly, in this topological limit the network structure is determined by α and γ and this, in turn, characterizes the memory transition (see figure 2.2). In this way, for $\alpha < 1$, networks are homogeneous, and there is a continuous transition from memory to noise. The critical temperature for this transition moves from $T_c = 1$ for completely homogeneous networks for $\alpha \ll 1$, to higher T as the nodes degrees gain some heterogeneity, according to previous studies (Torres et al., 2004). Similarly, for $\alpha > 1$ the phase transition is delayed for increasing α and N and it finally diverges in the thermodynamic limit (Leone et al., 2002).

Finally, we notice also that, in this topological limit, $\gamma = 1$ corresponds to choosing links at random for removal, given that the probability of choosing an edge (i, j) is then $p_{ij} = \frac{1}{k_i}\tilde{\eta}(k_i) + \frac{1}{k_j}\tilde{\eta}(k_j) = \frac{1}{\langle k \rangle N}$. This can be seen as a first order approximation to the pruning dynamics, where edges are randomly
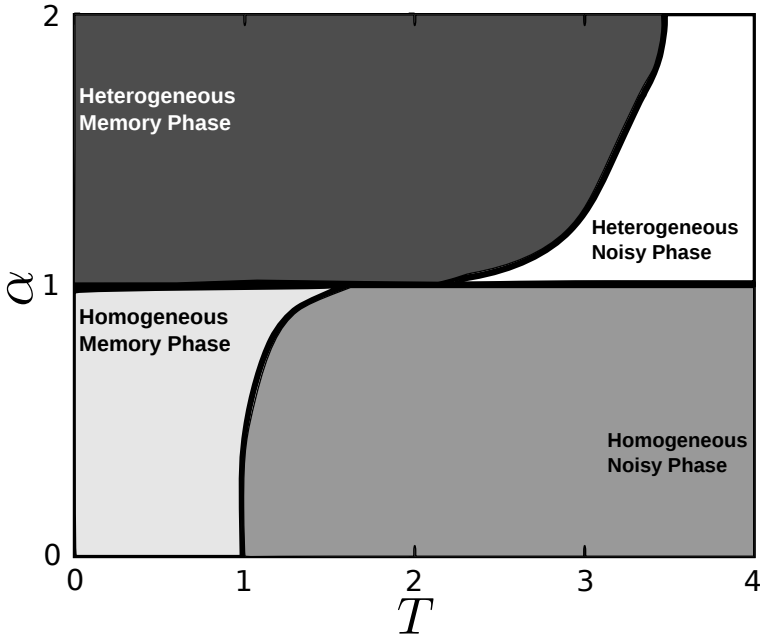
Figure 2.2: **Phase diagram of the topological limit.** Phase diagram of the system in the topological limit $I_i \rightarrow k_i$. Without the physiology-structure coupling, network structure is simply determined by α and γ and, this, in turn, characterizes the memory transition. Data: $N = 1600$, $\gamma = 1$, $\kappa_0 = 20$, $\kappa_\infty = 10$, $n = 5$.

removed, with the advantage that it induces powerful simplifications during computations. Furthermore, the relevant parameter determining the behavior of the system is the ratio between α and γ, whereas their absolute values only affect quantitatively (see Supplementary Figure A.1). Therefore, in the following we use $\gamma = 1$ and leave α as the control parameter of the network evolution.

2.3.2   Model fitting of experimental synaptic pruning profiles

The time evolution of $\kappa(t)$ is controlled in our model by the global probabilities $u(\kappa)$ and $d(\kappa)$, which can be chosen to model experimental data on synaptic density during brain development (Johnson et al., 2010a; Millán et al., 2018c). In particular, here we analyze and fit two experimental data-sets (figure 2.3):

i) A post-morten study of the synaptic densisty, $\rho(t) \propto \kappa(t)$, on the human infant auditory cortex (Huttenlocher and Dabholkar, 1997). Measures of synaptic density were obtained in autopsies by directly counting synapses in tissues from different layers of the auditory cortex, and in partitular, here we show the data for layes 1 (L1) and 2 (L2) in panel a.
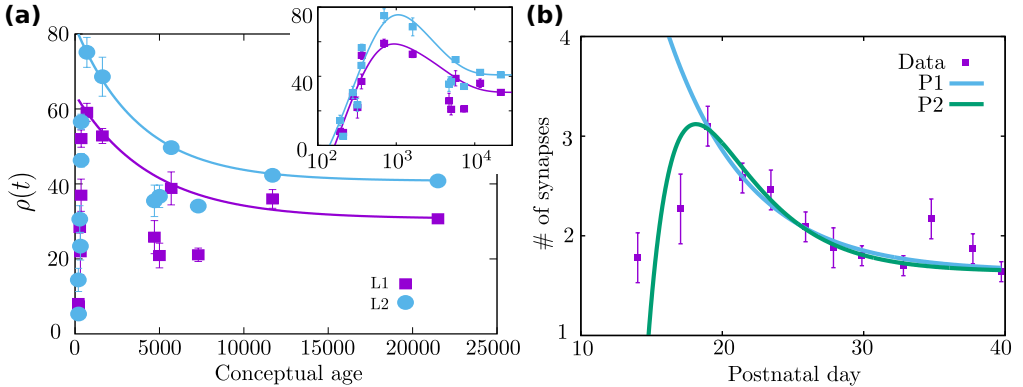
Figure 2.3: **Synaptic pruning profiles derived with our model.** Experimental data-sets on connectivity during infancy (points) and model fit (solid lines). **(a)** Postmortem synaptic density in layers 1 (L1) and 2 (L2) of the human auditory cortex (Huttenlocher and Dabholkar, 1997). Inset on the right shows the fit of the maximum on a log-log scale, labels as in the main plot. **(b)** Synaptic density in the developing mouse somatosensory cortex (Navlakha et al., 2015). We show the fit with the linear model (P1) and including the growth factor (P2). Error bars of the data-points in both panels correspond to s.d. as obtained in the original works.

ii) An electron microscopy imaging study of the mouse somatosensory cortex that quantifies the number of longe-range synaptic connections (Navlakha et al., 2015), shown in panel *b*.

Even though they correspond to different animals and have been obtained through different techniques, both data-sets show the same overall behavior: an extreme initial growth of synapses, followed by a maximum when pruning begins and connectivity starts decreasing, until a plateau is reached. Synaptic density decays roughly exponentially during pruning, and can be fitted by $u(\kappa)$ and $d(\kappa)$ as given by Eq. 2.9. These describe the case in which synapses are less likely to grow, and more likely to atrophy, when the connectivity is high, and vice-versa, a situation that could easily arise in the presence of a finite quantity of nutrients.

The evolution of the mean degree is given by

$$\frac{d\kappa(t)}{dt} = 2\left[u\left(\kappa(t)\right) - d\left(\kappa(t)\right)\right]. \tag{2.20}$$

By substituting Eq. 2.9 into Eq. 2.20, we obtain the time evolution of $\kappa(t)$,

$$\kappa(t) = \kappa_\infty \left[1 - \left(1 - \kappa_0/\kappa_\infty\right) e^{-t/\tau_p}\right], \tag{2.21}$$

Model 1				
Data	κ_0	t_0	κ_∞	τ_p
L1	59.1	700	30.7	1600(300)
L2	1.2(2)	40.8	75.1	3800(100)
MSC	3.10	18.97	1.64	5.72(1)

Model 2				
Data	κ_∞	τ_p	a	τ_g
L1	30.7	300(200)	33(5)	210(20)
L2	75.1	290(40)	700	2700(100)
MSC	1.64	2.2(2)	1.7(1)	4.0(2)

Table 2.1: **Synaptic pruning profiles fitting parameters.** Parameters used for the fit in figure 2.3; κ_0, t_0 and κ_∞ are obtained directly from the experimental data. The three lower points in figure 2.3a (for $t \approx 5000$) and the third point from the right in figure 2.3b have been excluded from the fits.

where $\tau_p = N\kappa_\infty/(2n)$, so that $\kappa(t)$ decays exponentially from κ_0 to κ_∞, assuming that $\kappa_0 > \kappa_\infty$ as in the case of interest. The best fit of Eq. 2.21 to the two experimental data-sets is shown by the solid lines of the figure, the corresponding parameters are indicated in table 2.1 (model 1).

The initial overgrowth of synapses that is observed in the experimental data (Fig. 2.3) can be related to the transient existence of some growth factors. It can be accounted for in our model by including a non-linear, time dependent term, $c(t) = a \exp(-t/\tau_g)$, in the growth probability $u(\kappa)$. The solution is now

$$\kappa(t) = \kappa_\infty \left[1 + b \exp(-t/\tau_g) - a \exp(-t/\tau_p)\right], \tag{2.22}$$

with $b = a\tau_g/(\tau_g - \tau_p)$, $a = 1 - \kappa_0/\kappa_\infty + b$, and τ_p as before. With the inclusion of this term, the evolution of $\kappa(t)$ on both data-sets can be fully reproduced, as shown in figure 2.3 (inset of panel a, on a log-log scale, and green line of panel b (P2), the corresponding parameters are indicated in table 2.1 under model 2).

Summarizing, the present model can approximate the evolution of the mean density of synapses in the mammal brain during infancy, and with the inclusion of an initial growth factor it also reproduces the fast growth and early maximum of the connectivity. Notice that this framework also goes in line with previous studies that have highlighted the computational benefits of a pruning process in which the pruning rate decreases with time, as in our model, which can optimize both efficiency and robustness when growth takes place locally throughout the network (Navlakha et

al., 2015). In our model the decreasing rate is naturally obtained via a simple, physiologically-inspired master equation for $p(k, t)$. Even when an extra growth factor is included, once pruning begins its rate decreases over time, in accordance with (Navlakha et al., 2015).

In this chapter we focus on the effect that the coupling with neuronal physiological activity has on network development and vice-versa, in the framework of co-evolving growth models. Consequently, we consider here the simplest version of the model, with linear dependence of $u(\kappa)$ and $d(\kappa)$ on $\kappa(t)$, to illustrate the effect of coupling structure and physiology. Non-linear global probabilities could also be considered, but would add an extra level of complexity which we will not explore here. In chapter 4 we study the effect of more realistic pruning probabilities that consider the effect of the transient period of high connectivity during infancy.

2.4   Emergent behavior of the co-evolving synaptic pruning model

2.4.1 (T, α) phase diagram

In the presented coupling model, where pruning depends on I_i (see section 2.2), computer simulations depict a rich emergent phenomenology depending on stochasticity (T) and emerging degree heterogeneity (α). The effect of the number of memorized patterns P is analyzed later in section 2.4.2 (and more deeply in chapter 3), and we discuss the effect of γ in the supplementary figure $A.1$. Other parameters, such as κ_∞ or a_0, were found to have only a quantitative effect on the resulting phase diagram, and they are set as in a previous study (Johnson et al., 2010a). Preliminary simulations suggested dependence on the heterogeneity of the initial condition for the network structure (IC), so we consider two different types of IC, namely, homogeneous, $p(k, t = 0) = \delta(k - \kappa_0)$, and heterogeneous, $p(k, t = 0) \propto k^{-2.5}$, networks, with fixed κ_0.

Our coupling dynamics leads to a rich phenomenology, including discontinuous transitions and multistability. Three different phases can be identified by monitoring the steady-state order parameters $\bar{g}(\alpha, T)$, $\overline{m}(\alpha, T)$ and the Pearson correlation coefficient, $\bar{r}(\alpha, T)$, as illustrated in figure 2.4 (data for $\bar{r}(\alpha, T)$ is not shown here since it provides similar information as $\bar{g}(\alpha, T)$). Analysis of these and similar curves for different parameter values leads to the phase diagram in figure 2.5. That is, there is a **homogeneous memory phase** for low α and T that is characterized by high $\overline{m}$, high $\bar{g}$ and low (negative, almost zero) $\bar{r}$ (Fig. 2.4a, c for $\alpha = 0.5$ and low T, and in Fig. 2.4b, d for $T < 1.2$ and low α). The system is then able to reach and maintain memory, while the topological

processes lead to a homogeneous network configuration. Due to the existence of memory, there is a strong correlation between the physiological state of the network, as measured by the currents I_i, and its topology, as reflected by the degrees k_i (see figure 2.1c).

A continuous increase in α leads through a topological phase transition from homogeneous final networks (with roughly Poisson degree distributions) to heterogeneous ones (with bimodal degree distributions). At the critical point $\alpha = \alpha_c^t(T)$ the emergent networks are scale-free (i.e. with power-law-like degree distributions). The phase transition is revealed in $\bar{g}(\alpha)$ (Fig. 2.4b for $T = 0.9, 1.0$ and 1.1) as a fast (and continuous) decay to zero, and it also appears in $\overline{m}(\alpha)$ (Fig. 2.4d) where, after an initial growth with α, $\overline{m}$ then decreases at the transition, and finally approaches a constant value for $\alpha > \alpha_c^t(T)$. This is a consequence of the strong coupling between structure and memory, and it shows that scale-free networks optimize memory recovery for a given set of control parameters. We call this the **heterogeneous memory phase**, characterized by high $\overline{m}$, very low (almost zero) $\bar{g}$ and high negative $\bar{r}$, indicating a memory state with heterogeneous (bimodal) dissasortative structure. Interestingly, this phase expands up to high noise levels as a consequence of network heterogeneity, which increases memory performance as discussed in section 1.4.1 (Torres et al., 2004; Franciscis et al., 2011). Moreover, memory recovery in turn favors network heterogenization in a feed-back manner due to the microscopic dynamics, enhancing the stability of the state. This is because I_i becomes proportional to k_i in the memory regime, whereas this correlation is reduced in disordered neural states (see figure 2.1c).

As T is further increased, the dynamics is finally governed by noise, and the stationary network is then homogeneous, resulting in the **homogeneous noisy phase**, characterized by low (almost zero) $\overline{m}$, high $\bar{g}$ and low (almost zero) $\bar{r}$ (Fig. 2.4a, c for $\alpha = 0.5$ and 1.0 and high T, and Fig. 2.4b, d for $T > 0.9$ and low α).

A particularly interesting aspect of this phenomenology is that the nature of the phase transition with T depends on α. For low α ($\alpha < \alpha_c^t(T)$) there is a continuous (second order) transition with increasing T from a homogeneous memory phase to a homogeneous noisy one through $\alpha = \alpha_c^m(T)$ (Fig. 2.4a, c for $\alpha = 0.5$). On the other hand, at higher α ($\alpha > \alpha_c^t(T)$) the transition from the heterogeneous memory phase to the heterogeneous noisy one is discontinuous (first order), and includes a **bi-stability region** (striped area in figure 2.5). In this region simulations starting from heterogeneous IC reach the heterogeneous memory state, whereas those starting from homogeneous ones fall into the homogeneous noisy one (Fig. 2.4b, d for $T = 1.2$, and Fig. 2.4a, c for $\alpha = 1.5$).

The existence of multistability illustrates how memory promotes itself in a heterogeneous network, which is a direct consequence of the coupled dynamics in our model, and it is lost in the topological limit (see figure 2.2). This is
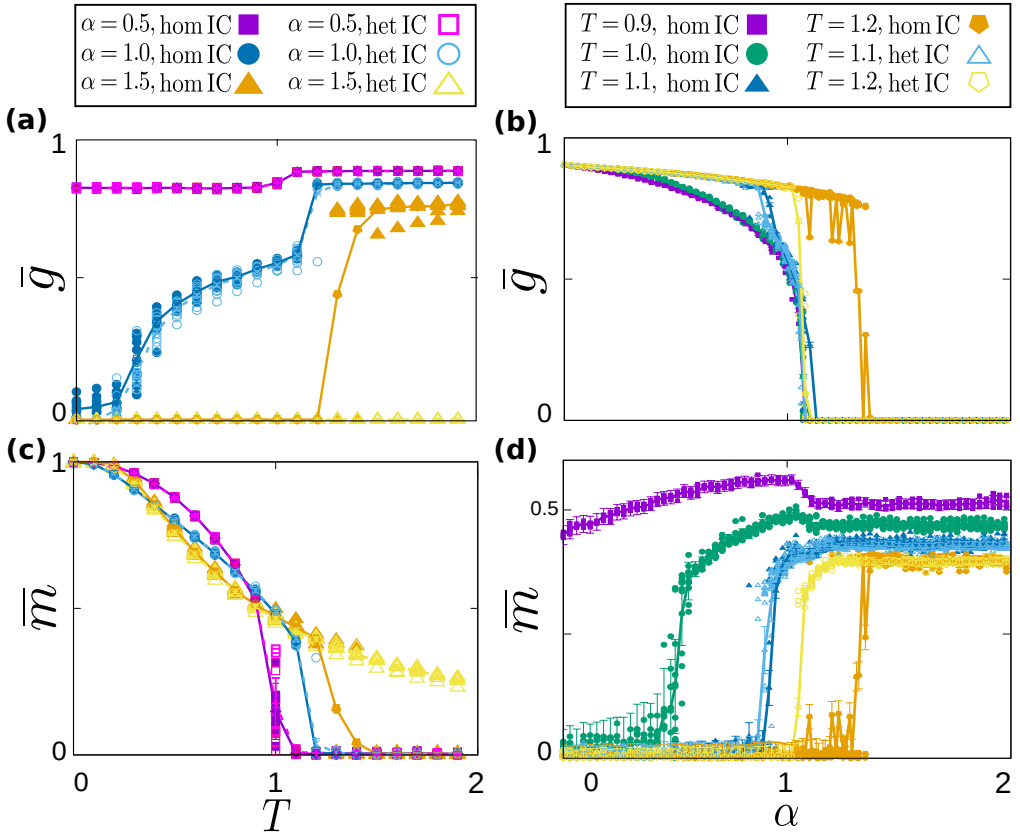
Figure 2.4: **Analysis of the transition lines in the phase diagram.** Behavior along the dotted lines marked in figure 2.5, for $N = 1600$, $\kappa_\infty = 10$ and $n = 5$. Panels **(a)** and **(c)** show $\bar{g}(T)$ and $\overline{m}(T)$ respectively for different values of α, as indicated. Panels **(c)** and **(d)** correspond respectively to $\bar{g}(\alpha)$ and $\overline{m}(\alpha)$, for different temperatures as indicated. Solid points are for homogeneous IC and empty ones for heterogeneous IC, in every panel. Notice that some isolines go through the three phases: for $T = 1.0$ and 1.1 (panels b and c) the system is initially in the homogeneous noisy phase, and an increase in α leads through $\alpha_c^m(T)$ to networks that are heterogeneous enough to maintain memory, which further increases heterogeneity due to the feed-back loop ($\bar{g}(\alpha)$ decreases). A final increase in α leads through $\alpha_c^t(T)$ to heterogeneous networks. Similarly in panels a and c, the system visits for $\alpha = 1$ the three phases: at very low T, α is high enough to develop heterogeneous memory networks, but a slight noise increase suppresses heterogeneity, until the noise is too high and memory is also lost, leading to the homogeneous noisy phase. Data-points are averaged over 30 realizations and error-bars correspond to the s.d.
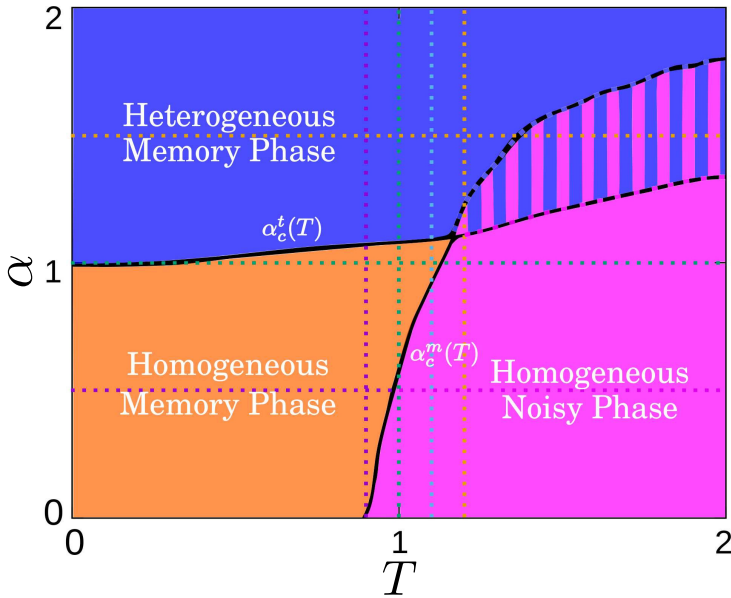
Figure 2.5: (T, α) **phase diagram of the coupled model** as obtained from analysis of the control parameters ($\overline{m}$, $\overline{g}$ and $\overline{r}$). The transition lines $\alpha_c^t(T)$ and $\alpha_c^m(T)$ are indicated either with solid or dashed lines regarding to whether they correspond to continuous or discontinuous transitions. The horizontal and vertical dotted lines correspond to the cases illustrated in figure 2.4. Parameters as in figure 2.4. Data-points are averaged over 10 realizations.

because heterogeneous networks present higher memory recovery than homogeneous ones for high noise levels, particularly for $T > 1$ (Torres et al., 2004; Franciscis et al., 2011). At the same time, given that in our model the growth and death of links depend on the activity of the nodes, the evolution of the structure of the network is driven by its activity state. In this way, an ordered state of the activity of the system – that is, a memory state – is needed in order to allow for the formation of heterogeneous (ordered) structures. Hence, if the network is in a noisy state, edge birth and death are random processes, and thus lead to a homogeneous network configuration. On the contrary, in the memory state there is a direct correlation between I_i and k_i (Fig. 2.1b) that allows for the emergence of structure – as given by the local probabilities. Correspondingly, the physiological state directly depends on the network structure through the currents I_i, thus closing a memory-heterogeneity feed-back loop. As a consequence, homogeneous and heterogeneous IC evolve differently, which translates into a multistability region for high α and T, and the presence of memory for $T > 1$. A schematic view of this feed-back loop is shown in figure 2.6.
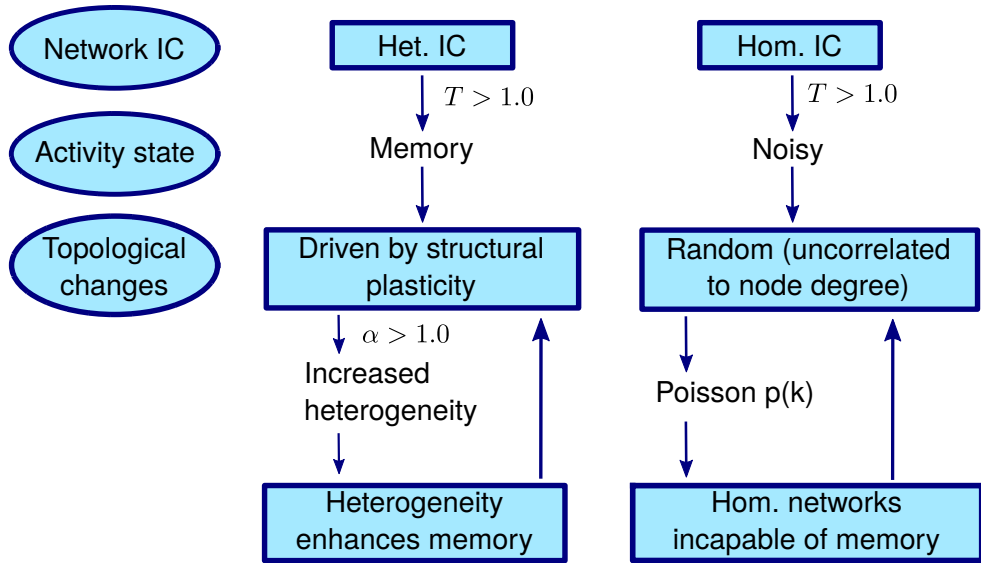
Figure 2.6: Schematic view of the form-function coupling in the bi-stability region $(\alpha, T > 1.0)$ of the presented coupled model. Homogeneous IC fall into the noisy state since $T > 1.0$, and this leads to a random topological process that does not increase heterogeneity, rendering the networks in the homogeneous noisy state. Heterogeneous IC, on the other hand, are capable of initial memory, which leads to further heterogeneization due to the structural plasticity, in a feed-back loop manner that deems the heterogeneous memory state stable.

Therefore, a main observation here is that the model shows an intriguing relation between memory and topology which induces complex transitions that might be relevant for understanding actual brains. In particular, the inclusion of a topological process allows for memory recovery when $T > 1$, whereas the presence of thermal noise shifts the topological transition, which in the topological limit occurs at $\alpha = 1$, to $\alpha > 1$. These findings can also have implications for network design – for instance, to help memory recovery optimization in noisy environments. It is worth noting also that one does not need to know the specific patterns that induce the synaptic weights in order to have a memory state, so that the definition of memories is not essential – only an ordered state of neural activity. Therefore, our results could be extended to other models of microscopic activity, not necessarily based on a Hebbian learning, or to other systems such as protein interaction networks (see section 2.5), as long as they present a transition between an ordered and a disordered activity state.

2.4.2   Memory storage capacity analysis

We have so far considered $P = 1$ for the sake of simplicity. However, for neural networks – whether natural or artificial – to be useful, they must generally store many different memory patterns. Something analogous seems also to be true for other complex systems, such as gene regulatory networks, which switch between different configurations. We therefore go on to study the memory storage capacity of the network – that is, how its memory capability depends on the number of memorized patterns P.

As shown in figure 2.7a, the performance (as measured by the overlap $\overline{m}$ of the recovered pattern) drops fast with P for random uncorrelated memory patterns ($a_0 = 0.5$) (Morelli et al., 2004). This is because networks in the model are highly sparse, with values of $\kappa/N \in \left[10^{-3}, 10^{-2}\right]$, and can also be heterogeneous, depending on α. Both sparseness and heterogeneity damage severely the memory retrieval ability of the neural network. In this structures the performance diminishes fast with P compared with the case of highly connected and homogeneous neural networks, as discussed in section 1.4.1 (Stauffer et al., 2003; Castillo et al., 2004; Morelli et al., 2004; Torres et al., 2004; Oshima and Odagaki, 2007; Akam and Kullmann, 2014).

However, there is experimental evidence that the configurations of neural activity related to particular memories in the animal brain involve many more silent neurons, $\xi_i = 0$, than active ones, $\xi_i = 1$ (Akam and Kullmann, 2014). In this case there is a positive correlation between different patterns due to the sparseness, since $a_0 \neq 0.5$, which is also known to improve the storage capacity of a neural network (Knoblauch et al., 2014; Knoblauch and Sommer, 2016), and in particular that of heterogeneous and sparse neural networks (Morelli et al., 2004). Consequently, we consider here this kind of activity patterns, and we further define them as non-overlapping regions of active neurons, each consisting of N/P neurons, so that they cover the whole network (and therefore the mean activity of the patterns is $a_0 = P^{-1}$). This corresponds to a particular definition of sparse or biased patterns, which in other works have been considered to be randomly distributed with a given a_0 (Knoblauch et al., 2014; Knoblauch and Sommer, 2016), that allows for a good visualization of the activity of the network by means of the raster plots.

In figure 2.7b we show $\overline{m}(P)$ as obtained with this configuration, and find that good memory performance can be maintained at higher P depending on α. These curves are combined with analogous ones for $\bar{g}(P, \alpha)$ to define the phase diagram of panel c. This shows that for $\alpha < 1$ memory is preserved only for small P; the structural noise (or quenched disorder) introduced by the patterns having a similar effect to that of the thermal noise in figure 2.5. This leads to a continuous (second order) transition from homogeneous-memory to homogeneous-noisy networks as P is increased. On the other hand, for $\alpha > 1$ the competition between different patterns boosts network heterogeneity, and

(a)

(b)

(c)

(d)
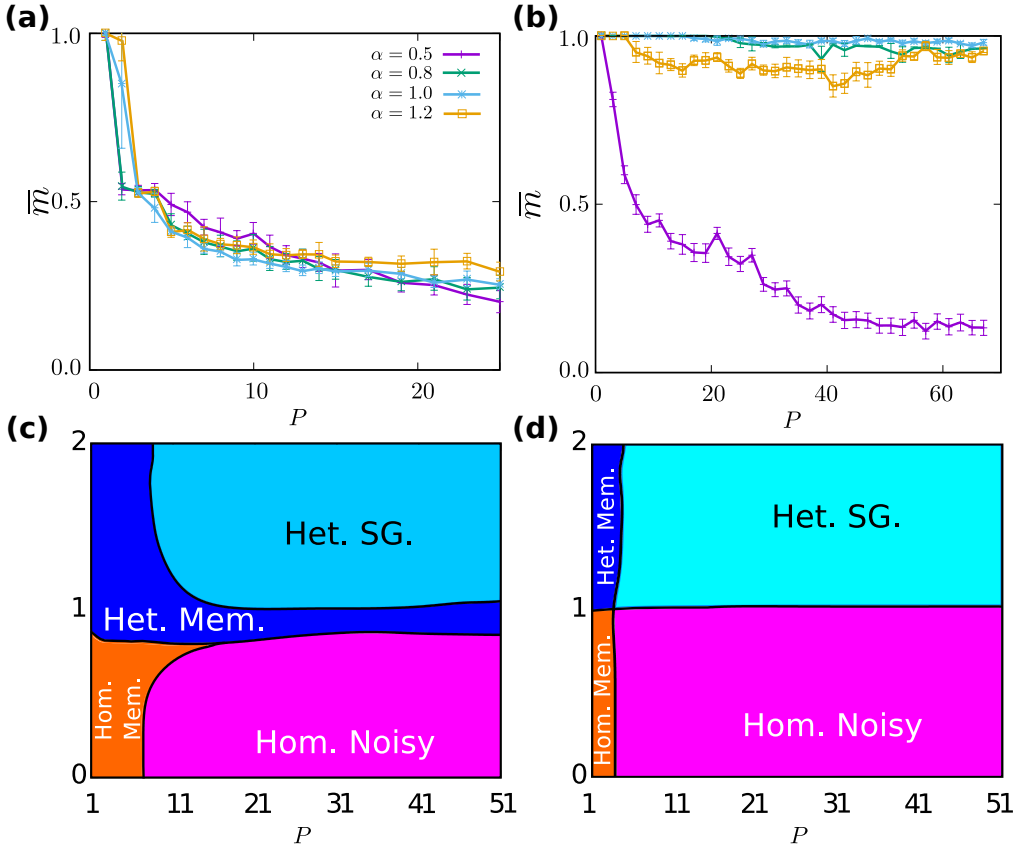
Figure 2.7: **Memory storage capacity analysis.** Capacity curves $(T = 0)$ for **(a)** randomly distributed patterns $(a_0 = 0.5)$, and **(b)** patterns distributed in small sets of active neurons $(a_0 \approx 1/P)$. $\overline{m}$ corresponds to the recovered pattern in each case. Results are for $N = 800$ and are averaged over 50 realizations of the system, with other parameters as before. Error bars correspond to the s.d. Panels **(c)** and **(d)** show the phase diagram of the system, obtained as in figure 2.5, as a function of α and P, respectively for the full model and the topological limit, and for activity patterns defined as in panel *b*. Data-points have been averaged over 10 realizations.

the capacity of the network increases greatly. There is a transition from a pure memory state to a spin-glass-like state (SG), in which a few patterns are partially retrieved at the same time. However, due to the presence of hubs and the correlation among patterns, this corresponds to high overlap which each of the patterns $(\overline{m} \approx 1)$, instead of a moderate value as one would expect in a typical spin-glass phase[1] (Amit, 1989).

---

[1]Interestingly, as we show in the following chapter, when larger values of the stationary

This result is only possible thanks to the form and function coupling introduced by the model. In the topological limit, as defined in section 2.3.1, on the other hand, memory is lost for $P > 4$ ($N = 800$, Fig. 2.7), leading to much more narrow memory phases (whether homogeneous for $\alpha < 1.0$ of heterogeneous for $\alpha > 1.0$). Moreover, the SG states correspond in this case to moderate overlap values ($\overline{m^\mu} \approx 0.6$), thus indicating a real SG state. Therefore, the memory storage capacity analysis reveals another significant difference between the topological and coupled versions of the model, since the coupled one allows for good memory retrieval even at much larger numbers of patterns ($P > 50$) for $\alpha \simeq 1$ – that is, for the limiting case in which the emerging networks are approximately scale-free. It follows that the emerging network topologies in the coupled version do not owe their good memory performance solely to their power-law degree distributions. Rather, the network is tuned for good memory performance on the specific patterns encoded in the synaptic weights. In the following chapter we consider in more detail the effect of quenched disorder in the system, when different parameters are considered, and in particular study its interplay with thermal noise considering also $T > 0$.

2.5   Protein interaction networks

Many complex systems can be described as networks which evolve under the influence of node activity, and it is likely that the described structure-function feed-back loop plays a role in these settings too. In particular, it could be compatible with experimental and theoretical studies concerning protein interaction networks, which gather different types of metabolic interactions among proteins. These can be either inhibitory or excitatory and also have different strengths, as edges in our model. Moreover, network structure changes on an evolutionary time scale, during the evolution of the species, and these changes combine a random origin, typically due to mutations, with a "force" driven by natural selection, which is likely to be activity dependent (Albert, 2005). The similarities between this picture and our model suggest a parallelism concerning the resulting network topologies as well.

Measurements on protein interaction networks show power-law distributions of some important topological magnitudes:

i) degree distribution $p(k) \propto k^{-\mu}$, with $\mu \approx 2.5$ (Albert, 2005);

ii) clustering coefficient $C(k) \propto k^{-\psi}$, with $\psi \approx 1$ (metabolic networks) or 2 (protein interaction networks) (Maslov and Sneppen, 2002; Albert, 2005);

iii) and neighbors mean degree $k_{nn}(k) \propto k^{-\nu}$, with $\nu \approx 0.6$ (Berg et al., 2004).

mean connectivity κ_∞ are considered, the pure memory states gain stability in this region (Millán et al., 2019b).
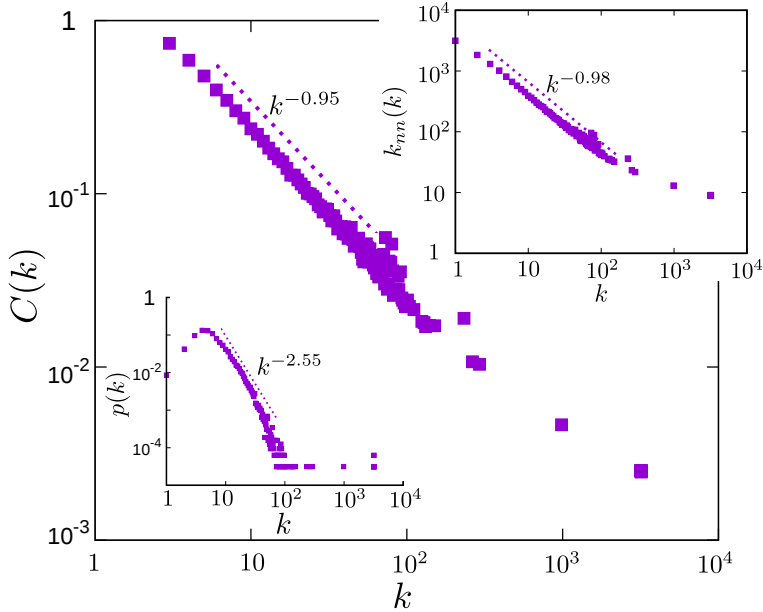
Figure 2.8: **Statistical comparison of the present co-evolving network model with protein interaction networks:** clustering coefficient $C(k)$ (main plot), neighbours mean degree $k_{nn}(k)$ (top inset) and probability distribution $p(k)$ (bottom inset) after a long transient of network evolution for a point in $\alpha_c^t(T)$ ($T = 0.5$, $\alpha = 1.05$), including a power-law fit of the tails. Data-points are averaged over 100 realizations of the system.

We find that these magnitudes are also power-law distributed for networks in our model near the transition $\alpha_c^t(T)$ (figure 2.8), with exponents $\mu_M = 2.55 \pm 0.01$, $\psi_M = 0.98 \pm 0.01$ and $\nu_M = 0.95 \pm 0.02$, so there is a good agreement with μ and ψ. Moreover, $k_{nn}(k)$ decays in our model as a power-law for almost every value of the parameters, which is related to the intrinsic topological dynamics of the model, that creates an asymmetry between the nodes that gain and loose edges (Berg et al., 2004). We find $\nu \approx 0.5$ for homogeneous networks and $\nu \approx 1.5$ for bimodal ones, whereas scale-free networks lie in between, with $\nu \approx 1.0$. It is likely that this parameter could be better reproduced with further adjustments in the local probabilities, so as to reflect degree-degree correlations among different proteins.

Interestingly, several studies have recently shown that there are specific patterns in protein interaction networks that can be determined experimentally (Turanalp and Can, 2008; Liu et al., 2017), and which could allow us to identify important biological substructures in the network (Ren et al., 2013; Xiong et al., 2014). This information could be used, together with the model proposed here, to determine the relevance of such patterns and of the complex interplay

between the underlying structure of the network and its functional role, as in the present study.

> In conclusion, there are definite indications that some of the main topo-
> logical properties of protein interaction networks could be qualitatively
> reproduced with simple adjustments or extensions of our model. This
> suggests a general mechanism underlying the dynamics of different bio-
> logical systems, which is likely to extend as well to other contexts.

2.6   Discussion

It is well known that the brain stores information in synaptic conductances, which mediate neural activity; and that this in turn affects the birth and death of synapses. To explore what this feed-back might entail, we have coupled an auto-associative or attractor neural network model with a model for the evolution of the underlying network topology, which has been used to describe synaptic pruning. Neural network models have long provided a means of relating cognitive processes, such as memory, with biophysical dynamics at the cellular level (see section 1.4). This coupled model includes the further ingredient of a changing underlying network structure, in such a way that it can be used as a more general and complete study of synaptic pruning and structural plasticity. The intention behind our theoretical framework is to identify a minimal set of ingredients which can give rise to observed phenomena. Specif details of a given system could be added to the model, such as more realistic neuron and synaptic dynamics (Sec. 1.1).

Taken separately, each of the two models involved exhibits continuous phase transitions: between a phase of memory and one of noise in the neural network, and between homogeneous and heterogeneous network topologies in the pruning model. Our coupled model continues to display both of these transitions for certain parameter regimes, but a new discontinuous transition emerges, giving rise to a region of coexistence of phases (also known as hysteresis). In other words, situations with the same parameters but slightly different initial conditions can lead to markedly different outcomes. In this case, whether the attractor neural network is initially capable of memory retrieval influences the emerging network structure, which feeds back into memory performance. There is therefore a crucial feed-back loop between structure and function, which determines the capabilities of the eventual system which the process yields. Our picture thus addresses how neural activity can impact on early brain development, and relates specific dynamic processes in the brain to well-defined mathematical properties, such as bistability and critical-like regions, or the emergence of a feed-back loop.

The models we have coupled in this work are the simplest ones able to

reproduce the behavior of interest – namely, associative memory (Sec. 1.4.1) and network topologies with realistic features (Sec. 1.3.2). However, there are no indications to believe that this feed-back will disappear when using more complex models, including the consideration of asymmetric networks, or more realistic choices of the synaptic weights. Hebbian synapses have been considered here as a standard way to define memory attractors, and therefore a useful tool to understand the effect of heterogeneity, and its coupling with memory, on network dynamics. More realistic scenarios could include time dependent synapses, considering for instance learning (Song et al., 2000) or fast synaptic noise (Cortes et al., 2006), which would indubitably add more complexity to the model. Similarly, particular definitions of the memories could boost the capacity of the network, and even create topologically induced oscillations. In the following chapter, for instance, we go on to study the interplay between thermal and quenched disorder in this model. The quenched disorder arises naturally when considering $P > 1$ stored patterns of activity and $T > 0$, and it leads to an oscillatory behavior for some parameter ranges, which can be associated with oscillations of neural activity.

Interestingly, neural systems may not be the only ones to display the properties we have found to be sufficient for the existence of this feed-back loop between structure and function. Networks of proteins, metabolites or genes also adopt specific configurations (often associated to attractors of some dynamics), and the existence of interactions between nodes might depend on their activity. One may expect that the interplay between form and function we have described in this work could play a role in many natural, complex systems. In this regard, we have shown some evidence that protein networks seem to have topological features which emerge naturally from the coupled models we have considered here.

Finally, an unresolved question in neuroscience is why brain development proceeds via a severe synaptic pruning – that is, with an initial overgrowth of synapses, followed by the subsequent atrophy of approximately half of them throughout infancy. Fewer synapses require less metabolic energy, but why not begin with the optimal synaptic density? Navlakha and co-authors have shown that network properties such as efficiency and robustness can be optimised by a pruning rule which favors short paths (Navlakha et al., 2015). However, in order for synapses to "know" whether they belong to short paths, some kind of back-propagating signal must be postulated. Our coupled model provides a simple demonstration of how network structure can be optimized by pruning, as in Navlakha's model, with a rule that only depends on local information at each synapse – namely, the intensity of electrical current. Moreover, this rule is consistent with empirical results on synaptic growth and death (Lee et al., 1980; Frank, 1997; Klintsova and Greenough, 1999; De Roo et al., 2007). In this view, a neural network would begin life as a more or less random structure with a

sufficiently high synaptic density that is capable of memory performance. This is in keeping with the description given by neuroscientists such as Kolb and Gibb, who say of the initial 10^{14} synapses in the human brain: *"This enormous number could not possibly be determined by a genetic program, but rather only the general outlines of neural connections in the brain will be genetically predetermined"* (Kolb and Gibb, 2011). Throughout infancy, certain memory patterns are stored, and pruning gradually eliminates synapses experiencing less electrical activity. Eventually, a network architecture emerges which has lower mean synaptic density but is still capable, by virtue of a more optimal structure, of retrieving memories. Moreover, the network structure will be optimized for the specific patterns it stored and, when the emerging networks are scale free, it becomes possible to store orders of magnitude more memory patterns via this mechanism as compared to the networks generated with the uncoupled (topological) version of the model. This seems consistent with the fact that young children can acquire memory patterns (such as languages or artistic skills) which remain with them indefinitely, yet as adults they struggle to learn new ones (Gómez and Gerken, 2000; Kolb and Gibb, 2011). In chapter 4 we show the fundamental effect that a long transient period of high connectivity, as observed experimentally, may have on the cognitive abilities displayed by the system.

Chapter 3

How Memory Conforms to Brain Development

The brain is an illustrative example of a system in which a dynamic complex network develops by the generation and pruning of synaptic contacts between neurons while memories are acquired and consolidated. In this chapter we consider how the mechanisms responsible for the evolution of brain structure affect and are affected by memory storage processes. To do so we make use of the adaptive neural network model presented in the previous chapter. We have already seen that such model, based on recent experimental observations, assumes that the basic rules for adding and removing synapses depend on local synaptic currents at the respective neurons, in addition to global mechanisms depending on the mean connectivity. In this way a feed-back loop between "form" and "function" spontaneously emerges that influences the ability of the system to optimally store and retrieve sensory information in patterns of brain activity or memories. In particular, in this chapter we report that, as a consequence of such feed-back-loop, oscillations in the activity of the system among the memorized patterns can occur, depending on parameters, reminding mind dynamical processes. Such oscillations have their origin in the destabilization of memory attractors due to the pruning dynamics, which induces a kind of structural disorder or noise in the system at a long-term scale. This constantly modifies the synaptic disorder induced by the interference among the many patterns of activity memorized in the system. The work presented here has been published in Millán et al., 2019b.

3.1　Introduction

The complex interrelation between *form* and *function* plays an important role in Nature and neural systems (Gross and Blasius, 2007; Vazquez et al., 2008; Sayama et al., 2013). The idea has been efficiently developed in the field of adaptive networks, in which a sort of coupling feed-back loop sets in between the network dynamic activity and its topological structure. Outstanding phenomena then emerge, some of which we have discussed in section 1.4.5. These include self-organization into complex topologies that exhibit robust dynamics, spontaneous differentiation of the nodes, or complex mutual dynamics in both activity and topology, in any case mimicking many different conditions in Nature (Bullmore and Sporns, 2009; Sayama et al., 2013; Millán et al., 2018c). This framework has proved useful in understanding fundamental questions concerning mammal brains, e.g., how structural and functional properties relate to each other both at the level of models involving sets of neurons and synapses and at the coarse-grained scale of *connectomes* and functional nets which is captured by imaging techniques (Bullmore and Sporns, 2009; see also 1.2.

In the previous chapter we have addressed the question of how an efficient brain network might develop by *synaptic pruning* after a sort of "wild" proliferation of synaptic connections between neurons following conception (Chechik et al., 1998; Iglesias et al., 2005; Santos and Noggle, 2011; Presumey et al., 2017; see also section 1.3.2). Interestingly, certain brain disorders, such as autism spectrum disorder (ASD) and schizophrenia, have been related to details of synaptic pruning (Keshavan et al., 1994; Geschwind and Levitt, 2007; Faludi and Mirnics, 2011; Kolb et al., 2012; Fornito et al., 2015). In particular, ASD has been associated with a defect of synaptic pruning in certain brain areas (Tang et al., 2014), whereas schizophrenia could be related to an excessive pruning (Sekar et al., 2016).

In any case, it now seems clear that such synaptic pruning involves in some way an optimization process, probably aimed at minimizing both energy consumption and the genetic information that otherwise would be needed to build an efficient and robust network (Chechik et al., 1999; Chklovskii et al., 2004; Johnson et al., 2010a; Knoblauch et al., 2010; Navlakha et al., 2015). In particular, in the previous chapter we have shown that this process could greatly improve memory retrieval under a noisy environment, such as it is the case in biological systems (Millán et al., 2018c). Moreover, ongoing structural plasticity in the adult brain has also been suggested to improve substantially the storage capacity (Chklovskii et al., 2004; Knoblauch et al., 2010), and has been related to graded amnesia, catastrophic forgetting, and the spacing effect (Knoblauch et al., 2014; Knoblauch and Sommer, 2016). These results are based on the fact that the number of potential synapses a neuron could develop, i.e. its potential connectivity, is much greater than the actual number of synapses, and structural

plasticity allows the system to explore different wiring possibilities (Stepanyants et al., 2002; Fares and Stepanyants, 2009).

Here we analyze how the dynamical processes of adding and removing synapses during brain development can affect the ability of the network to store and optimally retrieve a given set of memories. To do so we make use of the adaptive network model defined in chapter 2. This combines the auto-associative Amari-Hopfield neural network (see section 1.4.1 and also Amari, 1972; Hopfield, 1982) with a preferential-attachment dynamics for network evolution in a way that has been shown to accurately reproduce the observed variation of neuron connectivity data on human brains during infancy (see section 1.3.2 and also Johnson et al., 2010a; Millán et al., 2018b). As empirically observed (see Holtmaat and Svoboda, 2009 and references therein) this model assumes that the probabilities of growth and death of synapses depend on both the mean connectivity in the system and the neural activity. In chapter 2 we have analyzed the effect of thermal noise in the system and its emergent behavior. We have shown that the coupling between neuronal activity and connectivity creates a feed-back loop between form and function since the system activity influences its topology and, in turn, is affected by the network structure through the synaptic currents the neurons receive (Millán et al., 2018c). The system is then able to produce heterogeneous networks with the presence of hubs, similar to the ones observed in actual neural systems (Van Den Heuvel and Sporns, 2011; Crossley et al., 2014; Oh et al., 2014; Stafford et al., 2014), with high memory retrieval and noise tolerance, depending on parameters.

Here we develop on the effect that synaptic (or quenched) disorder resulting from the interference among many patterns of activity – stored by *Hebbian* learning on the synaptic weights – has on the emergent behavior of the system. We show that, as a consequence of the interplay between structural (i.e. pruning), thermal and quenched disorder, oscillations can emerge in the activity of the model which imply visiting different memorized patterns, an emergent behavior that had not been reported before in this model. This intriguing behavior is precisely due to long-term synaptic mechanisms associated with the network evolution dynamics, and not to short-term synaptic processes, such as synaptic depression and facilitation (Pantic et al., 2002; Marro et al., 2007a; Torres et al., 2007a, 2008; Torres and Marro, 2015) or spike frequency adaptation (Knoblauch and Palm, 2002; Ha and Cheong, 2017), which are not present in our model. These have already been described to induce oscillations among stored patterns of network activity, however the biophysical mechanisms behind them are different from the topological rewiring process considered here, and in particular they act on shorter time-scales – on the order of *ms* as opposed to the time scale of hours or days in which synaptic rewiring can operate in actual brains (Lee et al., 1980). It would be straightforward to extend the present study by adding short-term mechanisms, and we hypothesize that the

interplay between different neuron and synaptic processes during learning and brain evolution could give rise to other types of oscillatory phenomena associated with non-equilibrium phases not yet reported, a fact that we glimpse could have strong computational implications.

3.2 Model and Methods

In this chapter, we make use of the evolving brain network model defined in the previous one, but focus on the emerging behavior as a consequence of a finite memory load ($\bar{\alpha} = P/N \neq 0$ when $N \gg 1$) and on the effect of the stationary mean connectivity on the emerging dynamics of the system. Here we will review the basic definitions of the model and introduce the new magnitudes used in this chapter; the detailed derivation of the model can be found in section 2.2.

The system consists on a time-dependent, symmetric, undirected N-node complex network (Boccaletti et al., 2006), defined at time t by the adjacency matrix $e_{ij}(t) = \{0, 1\}$, in which each node represents a neuron and each existing edge ($e_{ij}(t) = 1$) stands for a synapse. The topology changes in time following a Markov process given by the probabilities $\widetilde{P}_i^g$ and $\widetilde{P}_i^l$ that each node has to increase and decrease its degree, namely

$$\widetilde{P}_i^g = u(\kappa)\widetilde{\pi}_i, \quad \widetilde{P}_i^l = d(\kappa)\widetilde{\eta}_i. \tag{3.1}$$

where $\kappa(t)$ is the mean connectivity as before, and the time dependence has been dropped for clarity. $\widetilde{\pi}_i$ and $\widetilde{\sigma}_i$ are functions of the incoming current at each neuron from its neighbors, $I_i(t)$ – which depends on the neural activity state. The global probabilities $u(\kappa)$ and $d(\kappa)$ determine the evolution of the mean connectivity $\kappa(t)$, and they can be defined to fit experimental measures of synaptic density during infancy as in the previous chapter, namely

$$
\begin{aligned}
u(\kappa) &= \max\left\{\frac{n}{N}\left(1 - \frac{\kappa}{2\kappa_\infty}\right), 0\right\} \\
d(\kappa) &= \frac{n}{N}\frac{\kappa}{2\kappa_\infty},
\end{aligned}
\tag{3.2}
$$

where κ_∞ defines the stationary mean connectivity. Selecting an initial condition $\kappa_0 > \kappa_\infty$, equations 3.2 describe and exponential decay from κ_0 to κ_∞ (as given by Eq. 2.21), according to the experimental data (see Sec. 2.3.2).

The local probabilities, on the other hand, set the degree structure of the network, and here we consider

$$
\begin{aligned}
\widetilde{\pi}_i &= \frac{I_i^\alpha}{\langle I^\alpha\rangle N}, \\
\widetilde{\eta}_i &= \frac{I_i}{\langle I\rangle N},
\end{aligned}
\tag{3.3}
$$

which are normalized over the network, $\sum_{i=1}^{N} \widetilde{\pi}_i = \sum_{i=1}^{N} \widetilde{\eta}_i = 1$. The power-law relation in $\widetilde{\pi}_i$ allows us to explore both sub-and super-linear responses by just modifying a single parameter, namely α. The probability $\widetilde{\eta}_i$, on the other hand, is fixed in a linear response, which corresponds to edges being chosen at random for removal, which can be seen as a first order approximation to the pruning dynamics (Millán et al., 2018c). The macroscopic state of the network structure is measured by the homogeneity parameter,

$$g(t) = \exp\left(-\sigma_k^2(t)/\kappa(t)\right), \tag{3.4}$$

where $\sigma_k^2(t)$ is the variance of the degrees of the nodes. $g(t)$ equals 1 if $p(k) = \delta_{k_0,k}$ (homogeneous network) and tends to 0 for highly heterogeneous (bimodal) networks. As we saw in the previous chapter, in the topological limit of the model 2.3.1, there is a phase transition from homogeneous networks with $g \to 1$ to heterogeneous ones with $g \to 0$ as α increases.

Each neuron follows a stochastic Amari-Hopfield dynamics, where the level of stochasticity is characterized by a noise parameter or temperature T; $T = 0$ corresponding to the deterministic limit (Amit, 1989). This is the control parameter for the activity dynamics. Each synapse has associated a synaptic weight w_{ij}; these are defined to store a set of P patterns of activity ξ_i^{μ} following the hebbian learning rule (Sec. 1.1.4.1; see also Hebb, 1949; Amit, 1989). Consequently, the macroscopic activity state of the system is measured by the **overlap** of the network state with each of the memorized patterns,

$$m^{\mu}(t) = [Na_0(1-a_0)]^{-1} \sum_{i=1}^{N} (\xi_i^{\mu} - a_0)\, s_i. \tag{3.5}$$

In this chapter it will also be of interest the degree dependent overlap, $m^{\mu}(k,t)$, defined as

$$m^{\mu}(k,t) = [Np(k,t)a_0(1-a_0)]^{-1} \sum_{i=1}^{N} (\xi_i^{\mu} - a_0)\, s_i \delta_{k,k_i} \tag{3.6}$$

where $p(k,t)$ is the degree distribution of the network. Therefore, $m^{\mu}(t) = \sum_{k=1}^{N} p(k,t)m^{\mu}(k,t)$. $m^{\mu}(k,t)$ indicates the contributions to the overlap of nodes with different degrees k. Notice also that in general $m^{\mu}(k,t)$ is not bounded by ± 1, unless the patterns of activity are homogeneously distributed through the neurons.

As in the previous chapter (Sec. 2.4.2), we consider a set of P activity patterns with small mean activity a_0 (so that they involve more silent that firing neurons) and define them as non-overlapping regions of N/P active neurons, so that they cover the whole network (and therefore $a_0 = P^{-1}$). This is following the experimental evidence that the configurations of neural activity related to

particular memories in the animal brain involve many more silent neurons, $\xi_i^\mu = 0$, than active ones, $\xi_i^\mu = 1$ (Chklovskii et al., 2004; Akam and Kullmann, 2014). Conveniently, it also introduces a positive correlation between different patterns, which is known to improve the storage capacity of a neural network (Knoblauch et al., 2014; Knoblauch and Sommer, 2016), and in particular that of heterogeneous and sparse neural networks (Morelli et al., 2004). This definition also allows for a good visualization of the activity of the network by means of the raster plots.

Interestingly, the activity patterns defined here are such that when a number P_r of them are recovered at the same time, in a SG-like state, the maximum overlap that they can have is less than one. In order to see this, one can decompose equation (3.5) in P sums, each over the neurons corresponding to the region associated with each of the activity patterns, as

$$m^\mu = [Na_0(1 - a_0)]^{-1} \sum_{\nu=1}^{P} \sum_{i=1}^{\mathcal{N}} \left(\xi_{\mathcal{N}\nu-\mathcal{N}+i}^\mu - a_0 \right) s_{\mathcal{N}\nu-\mathcal{N}+i}, \qquad (3.7)$$

where $\mathcal{N} = a_0 N = N/P$ is the size of each region and the time dependency has been dropped for clarity. Here, the first sum is over the P patterns stored in the network, whereas the second one goes over the $\mathcal{N}$ neurons in the region associated with each pattern. If the pattern μ is recovered together with other $P_r - 1$ patterns, then the sum over ν can be split in three terms: the region associated with the pattern μ, the ones corresponding to the other retrieved patterns, and finally those of the non-retrieved patterns (which do not contribute to the sum). Therefore, the overlap corresponding to this pattern is $m^\mu = \left(1 - P^{-1}\right)^{-1} \left[1 - P^{-1} - (P_r - 1) P^{-1}\right]$. This yields

$$m^\mu = 1 - \frac{P_r - 1}{P - 1} \leq 1, \qquad (3.8)$$

which only meets the equality in the case $P_r = 1$, that is, if only the pattern μ is retrieved.

This scheme also allows us to define another measure of the overlap between the state of the system and the memorized patterns, considering only the corresponding active neurons, as

$$m_1^\mu(t) \equiv \frac{1}{a_0 N} \sum_{i=1}^{N} s_i(t)\xi_i^\mu, \qquad (3.9)$$

with $m_1^\mu \in [0, 1]$. If is also of interest its binarized extension, m_B^μ, defined as

$$m_B^\mu(t) \equiv \begin{cases} 1, & \text{if } m_1^\mu(t) > m_{th} \\ 0, & \text{otherwise.} \end{cases} \qquad (3.10)$$

Therefore, $\mathbf{m_B(t)} = \left(m_B^1(t), m_B^2(t), ..., m_B^P(t) \right)$ indicates, in a binary code, which combination of patterns is recovered at time t. Equivalently, the decimal variable d_s can be defined,

$$d_s(t) \equiv \sum_{\mu=1}^{P} 2^{\mu-1} m_B^\mu(t), \qquad (3.11)$$

which one can interpret as a one-dimensional variable indicating the global memory state of the system.

In the previous chapter we have shown that, within this framework, three phases emerge depending on α, the parameter controlling pruning dynamics, and T, which sets the thermal noise in the neuronal activity. These are a homogeneous memory phase when both α and T are low ($T, \alpha < 1$), in which the network is capable of memory retrieval and the topology dynamics keeps a homogeneous configuration; a heterogeneous memory phase for high α ($\alpha > 1$) in which the dynamics leads to bimodal networks (with the appearance of hubs or highly connected nodes); and a homogeneous noisy phase for high noise T. However, as we will depict in the next section, the combination of thermal noise together with the introduction of a larger number of patterns of activity – which induces interference among them – induces other non-reported non-equilibrium phases characterized by the emergence of complex oscillations among the activity associated with the stored patterns.

3.3 Results

In the previous chapter we have shown that the storage capacity of the network can be greatly improved when the feed-back loop between structure and function is considered (Millán et al., 2018c). This is because the interplay between form and function gives rise to a topological structure that enhances the stability of the memory attractors which are recovered during the evolution of the system. In order to explore this interesting picture under other conditions, here we analyze in detail the phase diagram of the system with respect to four relevant parameters in the model, namely, α, κ_∞, T and P. The first two characterize the network structure dynamics, whereas the temperature, T, and the number of stored patterns, P, account respectively for thermal and quenched disorder. The last one is a consequence of the interference among many stored patterns, and it can affect the recall process.

3.3.1 Steady state solutions for $T = 0$

We first analyze the behavior of the system at $T = 0$, that is, in the absence of thermal fluctuations that can affect the stability of the fixed point solutions
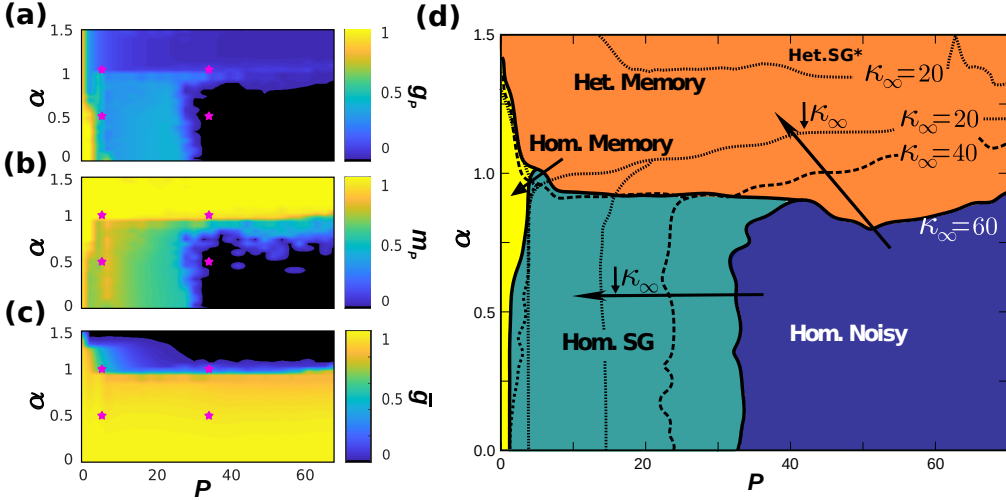
Figure 3.1: **(P,α) phase diagrams of the system $(T = 0)$.** The phase diagrams depict the steady-state of the system with respect to P and α at $T = 0$ and for $\kappa_\infty = 60$. **(a-c)** Fraction of patterns retrieved after a given transient, g_P (panel a); average overlap with these recovered patterns, m_P (panel b) and stationary homogeneity $\bar{g}$ (panel c). The pink stars on the diagrams indicate the (P,α) points corresponding to the time series shown in figure 3.2. A memory phase appears as a blue region in the diagram of g_p and a high value of m_p, indicated by a yellow color. A SG phase appears as a blue region in g_p and a lower value of m_p, indicated by a green color, whereas a noisy phase appears as black in g_p and m_p. Similarly, homogeneous structures take place for high values of $\bar{g}$, indicated by a yellow region in the corresponding diagram, whereas heterogeneous structures are for low values of $\bar{g}$, indicated by a black region. **(d)** Combined phase diagram using the information from panels a-c, each phase indicated for a different color. The phase regions depicted here correspond to $\kappa_\infty = 060$, with the phase transitions indicated by the solid lines. The corresponding phase transitions for $\kappa_\infty = 40$ and $\kappa_\infty = 20$ are respectively shown by the dashed and dotted lines, as indicated in the figure. The heterogeneous SG-like phase (Het.SG) appears only for small κ_∞ ($\kappa_\infty = 20$ in this case). The original diagrams for $\kappa_\infty = 20$ and 40 used to make this figure are shown in $B.1$ (appendix B). The network size was set here to $N = 1600$ and each point has been averaged over 10 realizations of the system.

of the system dynamics. As stated above, there are, however, other sources of noise in our system which can have a prominent influence in its behavior. One is the interference among stored patterns, which can significantly reduce the memory retrieval ability of the system (Amit, 1989). Another is the pruning dynamics; this is an intrinsic, structural noise that emerges due to the stochastic

adding and removal of synapses associated with the network dynamics during brain development, and which can dynamically affect the performance of the system during memory acquisition and consolidation.
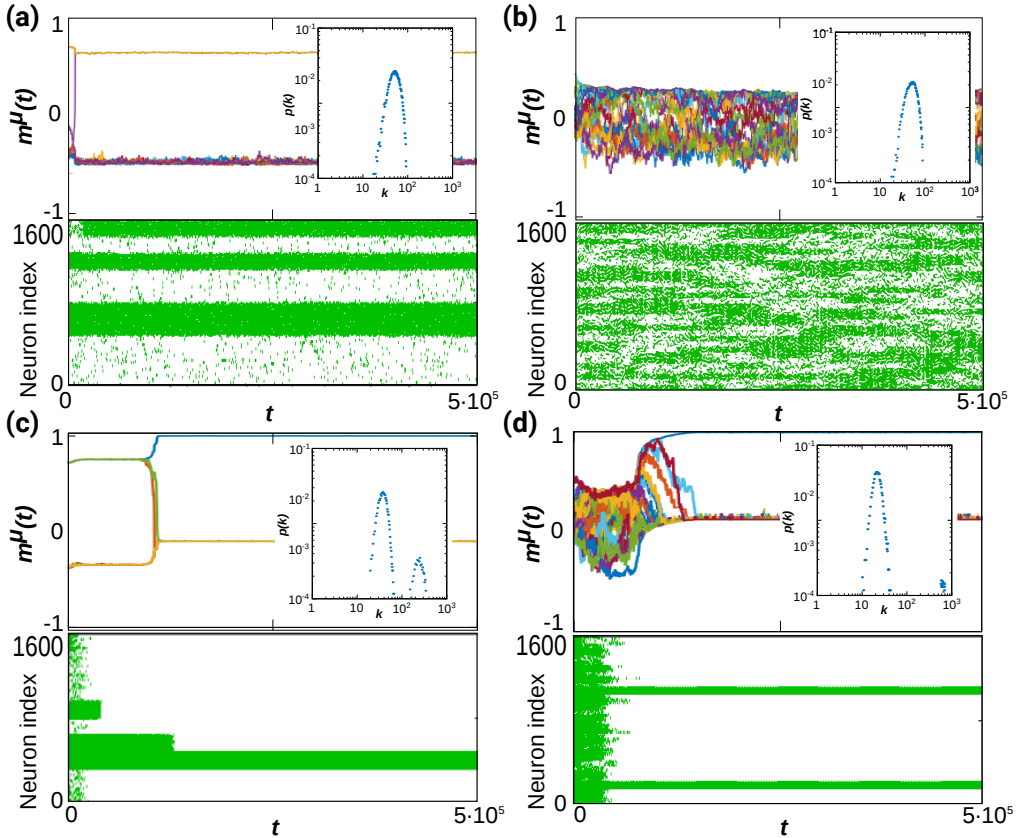
Figure 3.2: **Exemplary time series of the behavior of the system at $T = 0$.** We show the time evolution of the system at $T = 0$ and $\kappa_\infty = 60$ in four typical cases corresponding to different values of α and P, as marked with pink stars in the phase diagrams of figure 3.1. Each composite panel illustrates the overlap time series, $m^\mu(t)$, (top graph), raster plots of neuron activity (bottom graph) and the steady-state degree distribution of the network (inset), computed at $t = 10^6$ Monte Carlo Steps and averaged over 10 realizations of the system. The panels correspond respectively to $\alpha = 0.5$ and $P = 10$ **(a)**, $\alpha = 0.5$ and $P = 30$ **(b)**, $\alpha = 1.5$ and $P = 10$ **(c)**, and $\alpha = 1.5$ and $P = 30$ **(d)**. In all presented simullations we set $N = 1600$.

In this section we thus extend the study presented in section 2.4.2 (chapter 2), where we shown that the memory storage capacity of the network is optimized when the activity-topology feed-back coupling is taken into account, and

sparse correlated patterns are considered. Here, however, we seek a deeper understanding of the dynamics of the system due to the interplay between quenched and structural disorder and to define a framework that we will exploit when considering also the presence of thermal noise in the system (section 3.3.2). Furthermore, in this chapter we analyze also the role of the stationary mean connectivity, κ_∞, on the associated emergent dynamics and the stability of the phases reported in chapter 2. The parameter κ_∞, which is equivalent to the synaptic density, holds physiological interests since it can be taken as a measure of the extension of the process of synaptic pruning. From this point of view, a brain that has undergone a more drastic synaptic pruning would have smaller κ_∞ than one that has been less pruned. This can be related to recent experiments that have associated an excessive pruning in certain brain areas with schizophrenia (Sekar et al., 2016), whereas ASD has been related to a defect of synaptic pruning (Tang et al., 2014).

In order to undertake this analysis, in panels a, b and c of figure 3.1 we show the corresponding phase diagrams of the system (depicting different phases or kinds of behavior) with respect to P and α, for $\kappa_\infty = 60$, and similar diagrams can be found in appendix 3 for $\kappa_\infty = 20$ and 40 (Fig. B.1). These depict some non-equilibrium phases associated with different computational abilities during memory recall. Panel a shows, in the steady state, the ratio of patterns that can be retrieved with high overlap ($m^\mu \geq 0.66$), namely

$$g_P \equiv P_r/P, \tag{3.12}$$

where P_r is the number of retrieved patterns. A value $g_P = 1/P$ indicates a pure memory state, whereas larger values correspond to mixtures and SG-like states (Amit, 1989), and $g_P = 0$ corresponds to the noisy or non-memory state. Meanwhile, panel b shows the mean overlap of the recovered patterns during memory recall, namely m_P, and finally panel c shows the stationary mean homogeneity, $\bar{g}$.

These diagrams show up different types of dynamical behavior. In order to illustrate the characteristics of each one, in figure 3.2 we depict the time series $m^\mu(t)$ (top graph of each panel), raster plots showing the whole activity of the system (bottom graph of each panel) and the steady-state degree distribution (inset of each panel) for some particular values of α and P (and $\kappa_\infty = 60$) as indicated by the pink starts on the phase diagrams illustrated in figure 3.1.

Characterization of the non-equilibrium phases:

The integrated analysis of figures 3.1a, b, c and 3.2 shows the emergence of four different non-equilibrium phases in the system, as indicated in the combined phase diagram of figure 3.1d.

i) The **homogeneous memory phase** emerges for very small P ($P \to 1$) and $\alpha < 1.5$. It is characterized by high overlap with the recovered pattern m_p and large homogeneity $\bar{g}$.

ii) The **homogeneous SG phase**[1] appears for small P ($30 > P > 1$) and small α ($\alpha < 1.0$). In this region SG-like or *mixture* states – in which some of the memories are partially retrieved at the same time – start to emerge, as illustrated in figure 3.2a ($\alpha = 0.5$, $P = 10$). As a consequence, both g_P and m_P take intermediate values; the former since only a finite number of patterns is retrieved, $g_p < 1$ (light blue region of the diagram in figure 3.1a), the later because these patterns are retrieved at the same time, and therefore the overlap is reduced, $m_p < 1$ (green and light-blue region of the diagram in figure 3.1b). In general, however, the observed SG-like states present high values of the overlap with all the recovered patterns due to the high correlation between memories we have considered in this work. In this phase, the resulting network structure of the system is homogeneous since $\alpha < 1$, so that $\bar{g}$ approaches 1 and the degree distribution resembles a Poisson distribution (see figure 3.1c and the inset of figure 3.2a).

iii) The **homogeneous noisy phase** appears for $\alpha < 1.0$ and large P ($P > 30$). When P is increased the memories lose stability until there is a transition from the SG-like state to the noisy one, where the network structure remains homogeneous, as shown in figure 3.2b for the point $\alpha = 0.5$ and $P = 30$. This is indicated by $g_P \to 0$ (black region in figure 3.1a), $m_P \to 0$ (black region in figure 3.1b) and $\bar{g} \to 1$ (yellow region on the bottom-right side of figure 3.1c).

iv) For $\alpha \geq 1.0$, on the other hand, there is a **heterogeneous memory phase** in which just one (or very few) pattern is retrieved[2], with $m_P \approx 1$. The network structure is heterogeneous since $\alpha > 1$ (see inset of figure 3.2c). As a consequence, $g_P \to 1/P$ (dark-blue region in figure 3.1a), m_P approaches 1 (yellow region in figure 3.1b), and $\bar{g} \to 0$ (black region in figure 3.1c). Memory is achieved due to heterogeneity and the presence of hubs (see the inset of figure 3.2d, showing the appearance of hubs, and figure 3.1c, indicating $\bar{g} \to 0$), which can maintain the information content of the retrieved pattern even in the presence of the strong noise induced by the interference with other stored patterns and the dynamic changes of the network structure. Therefore, when P is increased the recovered

---

[1]Notice that this region was not previously observed or reported in chapter 2 since κ_∞ was too small for it to be appreciable, as we go on to discuss.

[2] Consequently, we deem it a memory phase instead of a spin-glass-like one, since even when a few patterns are recovered together, the overlap with each one of them is high, due to the correlation among patterns.

patterns remain stable, so that m_P remains close to 1 and g_P decreases as $1/P$ since only one pattern is retrieved.

The description of the different phases appearing on our system here shows up two main differences with the phase diagram previously illustrated in figure 2.7 in chapter 2. First of all, the appearance now of the homogeneous-SG phase between the homogeneous memory and homogeneous noisy phases. Secondly, what was previously reported to be a heterogeneous SG-like state (for high α and P) appears now clearly as a memory-like phase. These differences are only imputable to the different stationary mean connectivity, which in the previous work reported in chapter 2 was set to a relatively small value of $\kappa_\infty = 10$, whereas now in the present work we have considered a larger value $\kappa_\infty = 60$. Consequently, there are indications of a strong influence of κ_∞ on the particular features of the emerging non-equilibrium phases in the system, as we discuss next.

The role of κ_∞ on the non-equilibrium phases for $T = 0$:

In order to see the influence of κ_∞ on the nature of different emerging phases, in figure 3.1d we show the integrated phase diagrams obtained for $\kappa_\infty = 60$ (solid lines), 40 (dashed lines) and 20 (dash-dotted lines). These have been made by integrating information from the g_p, m_p, $\bar{g}$ and also P_r ($P_r = g_p P$) diagrams, which can be seen in the appendix B (figures $B.1$ and $B.2$).

Larger values of κ_∞ increase the tolerance of the system to quenched disorder, so that a bigger number of patterns can be stored. This is in line with the known result that the information is stored in the synaptic weights, and therefore increasing the number of synapses also increases the amount of information that the system can store (Amit, 1989). Consequently, when κ_∞ is diminished, the homogeneous SG region shrinks (in favor of the homogeneous noisy one), until it is effectively lost for $\kappa_\infty = 10$ as in Fig. 2.7 (chapter 2). Similarly, when smaller values of κ_∞ are considered the heterogeneous memory states (for large P and α) lose stability, and SG-like states in which a few patterns are recovered at the same time become more likely (see figure $B.2$ in appendix B). Hence, in our previous study with $\kappa_\infty = 10$ and $N = 800$ (Fig. 2.7, chapter 2), SG-like states were more likely to occur than pure memory states (that appear for larger values of κ_∞.

Finally, it is worth noting too that the qualitative state of the system is approximately independent of P for $P > 20$, as shown in figure 3.1, where one can see that g_p, m_p and $\bar{g}$ remain essentially constant as P is increased with constant α above $P = 20$, in agreement also with the previous studu in chapter 2. Therefore, in the following we restrict our analysis to the most interesting region $P < 20$ and do not analyze the large storage limit of the system (Knoblauch et al., 2014; Knoblauch and Sommer, 2016). This is because our interest here is

in characterizing the dynamic behavior arising as a consequence of the interplay between structure and function under the presence of thermal and quenched noise, rather than its storage capacity.

> In summary, for $T = 0$, that is, when there are only two sources of noise in the system (structural and quenched disorder), the stationary state for a given P depends strongly on the network structure, determined by α and κ_∞. As so, for $\alpha > 1$, the networks develop heterogeneous structures in which hubs arise that are very densely connected with the rest of the network, and can maintain information about the memories even when P is very high. For $\alpha < 1$, on the other hand, the network is always homogeneous, with every node having similar, low degree, and a SG-like phase soon arises, which is then suddenly lost as the quenched disorder becomes too strong and finally the system falls into the noisy state. Meanwhile, small values of κ_∞ can affect the stability of the memory states, leading to the shrinkage of the homogeneous SG phase (for $\alpha < 1$) and the conversion of pure heterogeneous memory states to heterogeneous SG-like states (for $\alpha > 1$).

3.3.2 Behavior of the system for $T > 0$

Our previous analysis has determined the phase diagram of the system at $T = 0$, which characterizes the effect of the dynamical topological structure on the memory capabilities of the system. In this section, we consider the effect of thermal noise in our system's emergent behavior. In order to do so, we analyze the (T, α) phase diagrams of the system for different values of κ_∞ and P, namely $P = 5$, 10, 15 and 20, and for three values of $\kappa_\infty = 20$, 40 and 60, as before. The selected values of P correspond to the left region of diagrams in figure 3.1, where the phase transitions from memory to the SG and noisy states takes place. In particular, in panels a, b and c of figure 3.3 we show the g_p, m_p and $\bar{g}$ diagrams corresponding to $\kappa_\infty = 20$ and $P = 10$, that show up the emergent phases on the system. The diagrams for the other values of κ_∞ and P are shown in appendix B (Fig. $B.3$).

In order to illustrate better the behavior of the system in the cases of interest, we also include in figure 3.4 the time series of $m^\mu(t)$ is some exemplary (T, α) points as indicated by the pink starts in the diagrams of figure 3.3. More examples of the time evolution of the system for $\kappa_\infty = 20$ and other values of P are also shown in appendix B (Fig. $B.4$).

In the following, we first discuss the emergent behavior of the system as a consequence of the combination of thermal, quenched and structural disorders, to then analyze the role of the stationary synaptic density and the number of stored patterns on such behavior.
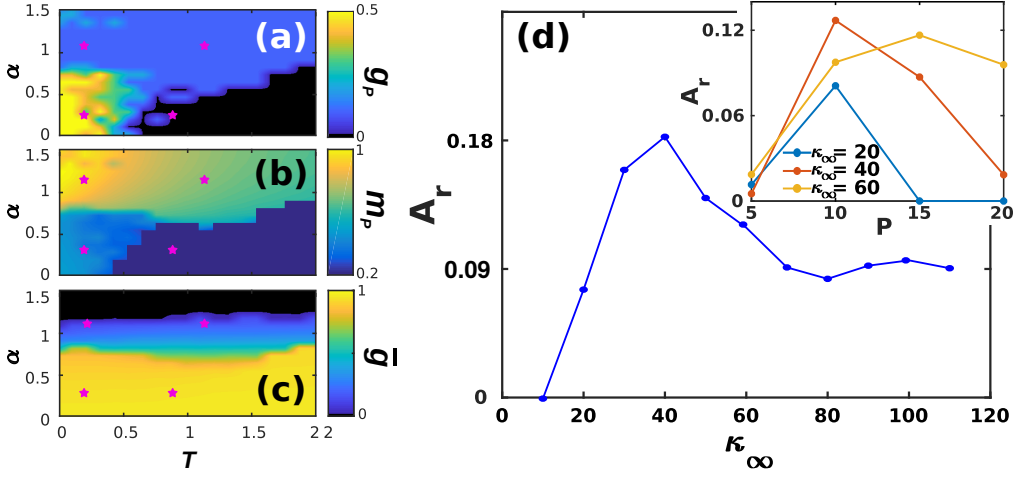
Figure 3.3: **Emergent behavior of the system. (a-c)** Phase diagrams of the system with respect to α and T for $P = 10$ and $\kappa_\infty = 20$, corresponding respectively to g_p, m_p and $\bar{g}$, as indicated in the label of the color bar. Pink stars in the panels indicate the (T, α) point of the corresponding time series in figure 3.4. Results are for $N = 1600$ and have been averaged over 5 realizations of the system dynamics. In these panels a memory phase appears as a blue region in the diagram of g_p and a high value of m_p, indicated by a yellow or green color. A SG phase appears as an orange region in g_p and a lower value of m_p, indicated by a green or blue color, whereas a noisy phase appears as black in g_p and dark-blue in m_p. Finally, the oscillatory phase appears for high values of g_p (light yellow region) and relatively low values of m_p (blue region). Similarly, homogeneous structures take place for high values of $\bar{g}$, indicated by a yellow region in the corresponding diagram, whereas heterogeneous structures are for low values of $\bar{g}$, indicated by a black or dark blue region. **(d)** Relative area of oscillatory behavior (as defined in the main text) as a function of κ_∞ (main plot, corresponding to $P = 10$), and P (inset, with κ_∞ as indicated in the legend).

Emergence of neural activity oscillations:

The diagrams in figure 3.3 indicate the emergence of at least 4 different phases, as we go on to describe. Firstly, in panel a we analyze $g_p(T, \alpha)$, that is, the number of patterns visited by the system after the transient evolution takes place. For $\alpha > 1$, we find that this number remains finite, and greater than zero, up to very high values of the temperature ($T \approx 2.0$), corresponding to the blue region of the diagram. This indicates that the system is in a **memory state** (or in a SG-like state in which only a small number of patterns are retrieved), such as the one depicted in figure 3.4c and d. The stability of the memory

state for $T > 1$ is possible due to the emergence of heterogeneous structures (since $\alpha > 1$), and consequently hubs, as indicated by $\bar{g} \to 0$ for $\alpha > 1$ (black region in figure 3.3*c*). Notice also that the overlap corresponding to these states, m_P, decreases as T is increased (Fig. 3.3*b*), indicating that these states are also becoming less stable as the thermal noise becomes stronger. In these conditions, only the more densely connected hub nodes are able to maintain information about the memories, and these are the ones contributing the most to the overlap.

As α is decreased, however, the behavior shown in the diagrams becomes more complex and different regions (phases) start to emerge. We find, as expected, that memory is completely lost for $T \gg 1$, i.e., due to the strong noise the system falls into the **noisy** or **non-memory state**. Consequently, $g_p \to 0$ (black region in Fig. 3.3*a*) and $m_p \ll 1$ (dark-blue region in Fig. 3.3*b*). In fact, now networks are homogeneous (since $\alpha < 1$) and there are no hubs that preserve memory, as indicated by $\bar{g} \to 1$ in figure 3.3*c*, evidencing that the degree distribution is homogeneous. A typical time series of $m^\mu(t)$ for this situation is shown in figure 3.4*b*.

For small values of T and α (T, $\alpha < 1$), on the other hand, $g_P \to 1$ (orange and yellow region on figure 3.3*a*), indicating that a great number of patterns are being retrieved ($P_r \to P$) with a moderate value of the overlap m_P, as indicated by the green and blue region in figure 3.3*b*. Moreover, results in figure 3.3*a* indicate that, at least in some cases, g_P actually increases when T goes from 0 to 1 (see, e.g., the yellow area in figure 3.3*a*). That is, as the temperature increases, more memories take place in the state of the system, with a relatively high overlap m_P. This is because, for $\alpha < 1$, there is a wide region of **oscillatory behavior** between the SG-like and the noisy phases corresponding to the yellow area in the g_p diagram in figure 3.3. An exemplary series of oscillations is illustrated in figure 3.4*a*. Note that the observed oscillations occur at level of the neuronal population as measured by the global network parameter $m^\mu(t)$, and not on the single neuron level – which appear as small, high-frequency oscillations of $m^\mu(t)$.

The oscillatory state emerges as a consequence of the interplay between structural and thermal noise and the activity of network, since the process of addition and removal of synapses, that creates a dynamical network structure, together with the thermal noise, can make the recovered patterns unstable. Moreover, given that $\alpha < 1$, the structure of the networks remains homogeneous and no real hubs emerge. Notice however that due to the non-trivial interplay between activity and topology, in the region of oscillatory behavior the networks display a more heterogeneous structure, and $\bar{g} < 1$. This effect will be discussed in more detail in section 3.3.3.
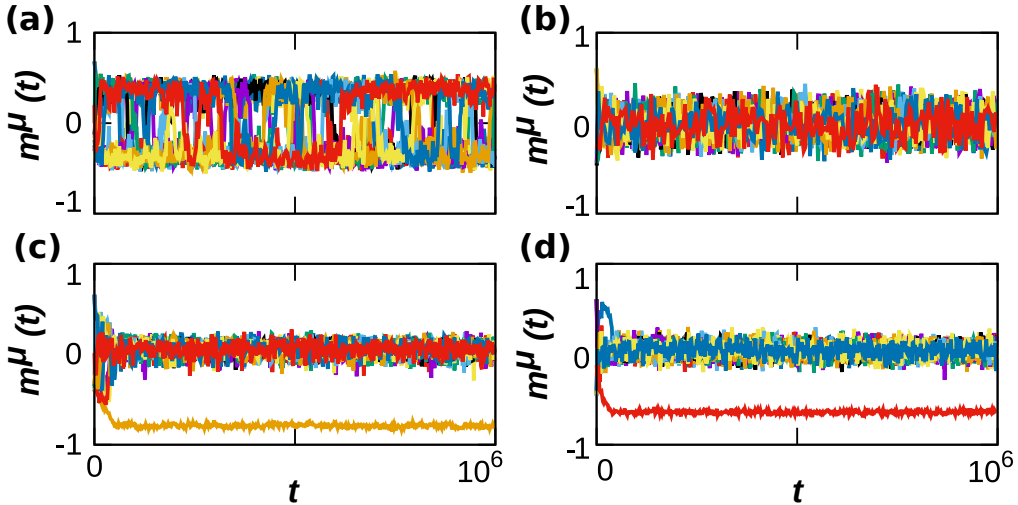
Figure 3.4: **Exemplary time series for $T > 0$.** Time series of the overlap $m^\mu(t)$ for some representative cases of the system dynamical behavior, corresponding to $\kappa_\infty = 20$ and to $P = 10$ and 4 points of the (T, α) space, as indicated by pink starts in the phase diagrams of figure 3.3. Namely, panels **(a-d)** correspond respectively to the points $(0.3, 0.3)$, $(0.9, 0.3)$, $(0.3, 1.1)$, $(1.1, 1.1)$. Results are for $N = 1600$.

The role of κ_∞ on the neural oscillations for $T > 0$:

As in the case with $T = 0$, we have also analyzed the role of the stationary mean connectivity, κ_∞, on the phase diagram of the system for $T > 0$. In particular, we have measured the relative **area of the oscillatory region**, A_r, as a function of κ_∞ and P, as shown in figure 3.3d (see also figure $B.3$ in appendix B). A_r is defined as the ratio between the number of points in the (T, α) space that display oscillatory behavior and the total number of points in the considered region (which corresponds to $0 \le T \le 1.5$, $0 \le T \le 1.5$).

We find in our model that the area associated with the oscillatory behavior (for $\alpha, T < 1$) for a given κ_∞ is maximum at intermediate values of P (see the inset of Fig. 3.3d): for very small P there is a dominance of stable SG-like states, whereas for large P the system falls easily on the noisy phase (see Fig. $B.3$ in appendix B). Similarly, for a given P the greater extension of the oscillatory phase is found for an intermediate κ_∞, as indicated by the maximum of $A_r(\kappa_\infty, P = 10)$ in figure 3.3d. For instance, for $P = 10$ the noisy phase extends to $T < 1$ for $\kappa_\infty = 20$ (Fig. 3.3b) and the oscillatory region is small, whereas for $\kappa_\infty = 60$ (Fig. 3.3j) there is a combination of stable SG-like states and oscillations for $\alpha, T < 1$. Finally for $\kappa_\infty = 40$ (Fig. 3.3f) the oscillatory phase is most robust.

Consequently, the absence of dynamical memories in the system could be

associated with a defect of the pruning process that causes κ_∞ to be greater than usual, and could be therefore associated with the cognitive abilities of subjects with ASD. Interestingly, it has been recently reported that short-term memory and episodic memory are impaired in ASD subjects (Poirier et al., 2011; Lind et al., 2014), which is consistent with our findings here since, in order to be able to recall a sequence of memories, it is first necessary to destabilize the already recalled ones so as to allow the system to remember new ones. On the other hand, schizophrenia is typically associated with erratic behavior (Loh et al., 2007), which could be related to the high frequency memory oscillations found here for smaller values of κ_∞.

> In summary, in this section we have found that the combination of thermal, structural and quenched disorder, associated with the interference among patterns, can give rise to oscillations among the memorized patterns for $\alpha < 1$ – that is, when the networks are homogeneous – and $T < 1$, corresponding to the yellow region in figure 3.3a. The robustness of the oscillatory region is maximum at both intermediate values of P and κ_∞. The effect of κ_∞ hints a possible relation with the deficit and excess of synaptic pruning observed in autism and schizophrenia (Loh et al., 2007; Tang et al., 2014)

3.3.3   Emergence of hubs

The appearance of hubs and heterogeneity plays a significant role in the emergent dynamics of the system. In particular, with a given level of noise ($T > 0$), the topological structure of the network determines whether the system relaxes to a memory state, wanders among different patterns or falls into a noisy state. Therefore, here we discuss in more detail the emergence of hubs during the network evolution and their effect on the emergent state of the system.

We first notice that, according to the previous analysis, for $\alpha < 1$ networks are homogeneous, as evidenced by the homogeneous degree distributions shown in the insets of figure 3.2a, b. This is also revealed by the high value of the homogeneity parameter $\bar{g}$ shown in figures 3.1 and 3.3 for $\alpha < 1$, indicating that the variance of k_i is small. As a consequence, no real hubs can be defined, since all nodes have similar low degree (given that $\kappa_\infty \ll N$, so that the connectivity of the nodes is bounded). On the contrary, for $\alpha > 1$ and in the case of memory, networks are heterogeneous as evidenced by $\bar{g} \to 0$ (black regions in the corresponding diagrams $\bar{g}(\alpha, P)$ and $\bar{g}(\alpha, T)$ respectively in figures 3.1 and 3.3). This indicates that there are nodes with very different degrees and, in particular, the degree distribution $p(k, t)$ is bimodal and it splits in two, as shown in the insets of figure 3.2c, d, with the emergence of hubs. Therefore, one can set the connectivity threshold k_{th} – that defines the minimum node's degree to

characterize it as a hub – at the value of k at which $p(k, t \to \infty)$ presents a local minimum between the two modes. This establishes a clear separation between high and low degree nodes. In particular, in all cases studied here, we find that a threshold $k_{th} = 2\kappa_\infty$ also suffices to differentiate between homogeneous and heterogeneous structures, since for $\alpha < 1$ (homogeneous case) the maximum degree of a network is always below $2\kappa_\infty$.
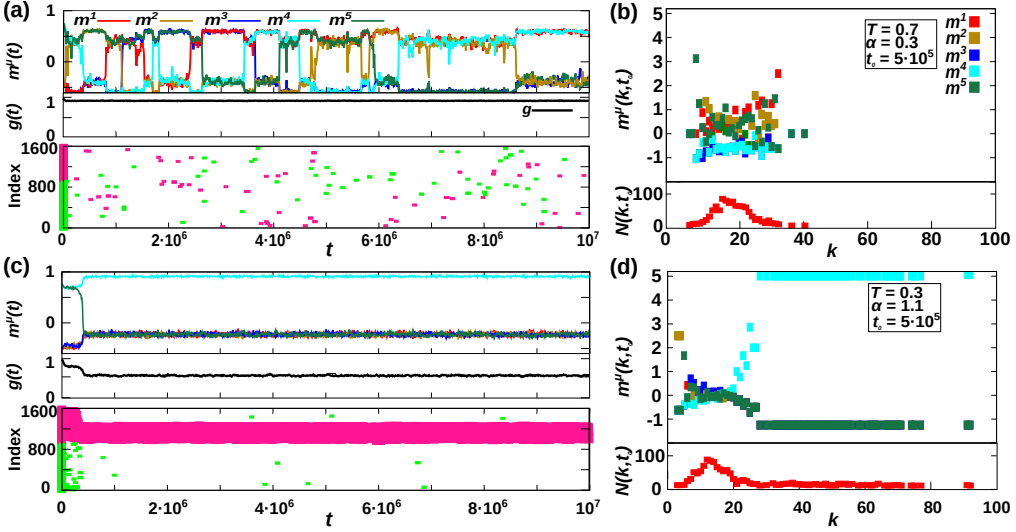
Figure 3.5: **Emergence and effect of hubs in the system. (a,c)** Temporal evolution of the system in two representative cases of the dynamics for $P = 5$ and $\kappa_\infty = 20$, corresponding to the emergent oscillatory behavior for $T = 0.7$ and $\alpha = 0.3$ (panel a) and to the heterogeneous memory phase for $T = 1.1$ and $\alpha = 1.1$ (panel c). In these panels, the top plots represent $m^\mu(t)$, the middle ones the homogeneity parameter $g(t)$ and finally the bottom ones show the existing hubs in the network at each time t, where active and inactive hubs are plotted in different colors (respectively pink and green). **(b,d)** Snap-shot of the state of the system in panels a and c, respectively, at time $t_0 = 5 \cdot 10^5$, as represented by the degree-dependent overlap $m^\mu(k, t_0)$ and the number of nodes with degree k, $N(k, t_0) = Np(k, t_0)$. Results are for $N = 1600$.

Interestingly, due to the underlying stochastic rewiring process and to the system's finite size, there is always some variability in the degrees of the nodes and, particularly in the region of oscillatory behavior, there is a relative increase in the variability of k_i with respect to the SG phase (as evidence by a decreased $\bar{g}$ in the corresponding diagrams of figure 3.3). We argue that this is due to the intrinsic coupling between activity and topology, and to the combination of thermal (since $T > 0$), topological (due to the ongoing rewiring process) and quenched (due to the learning of different patterns) disorder in the system. In

the region of oscillatory behavior, the instability of the memories influences the synaptic currents I_i creating variability, thus causing the observed increased heterogeneity. This causes the emergence of relatively-high degree nodes that correspond to the tail of the homogeneous distribution $p(k, t \to \infty)$ and that might have an important effect on the system. Therefore, in order to explore as well the dynamics of these relatively-high degree nodes, we have selected a lower threshold, $k_{th} = 1.75\kappa_\infty$, for the analysis of hub dynamics.

Hubs (and relatively-high degree nodes for the homogeneous case) dynamics is investigated in figure 3.5, where we compare two different cases for $P = 5$ and $\kappa_\infty = 20$:

i) The first one (panels a and b) corresponds to the region of oscillatory behavior for homogeneous networks ($\alpha < 1$) and it is for $T = 0.7$ and $\alpha = 0.3$ (corresponding to the bottom-left graph of figure $B.4a$).

ii) The second one (panels c and d) corresponds to the heterogeneous-memory phase ($\alpha > 1$), and it is for $T = 0.3$ and $\alpha = 1.1$ (corresponding to the top-left graph of figure $B.4a$).

For each of these cases we show:

i) The temporal evolution of the system (panels a and c) as given by the overlap $m^\mu(t)$, the homogeneity $g(t)$ and the hub raster plots, where we represent the existing hubs at each time t, in different colors according to their active or inactive state (respectively pink and green).

ii) The system's state at a particular time $t_0 = 5 \cdot 10^6 \text{MCS}$ (panels b and d) as given by the degree-dependent overlap $m^\mu(k, t_0)$ (defined in Eq. 3.6) and the degree histogram $N(k, t_0) = Np(k, t_0)$.

We observe, for $\alpha > 1$ (panel c), that a great number of hubs emerge in the system, and that almost all hubs correspond to the active nodes of the retrieved pattern. Moreover, in this case $m^\mu(k, t_0)$ of the recovered pattern μ is larger for high-degree nodes (figure 3.5d), indicating that they contribute most to the overlap $m^\mu(t_0)$. On the contrary, for the non-recovered patterns ν, $m^\nu(k, t_0)$ remains small for all k. On the other hand, for $\alpha < 1$, no real hubs emerge and only transient relatively-high degree nodes are observed in figure 3.5a. These do not only correspond to the recovered patterns but are scattered throughout the network, and no significant correlation can be measured between the pattern oscillations and the hubs dynamics. This causes instabilities that ultimately lead to the oscillatory behavior (see figure 3.5b, indicating that relatively high-degree nodes contribute more to $m^\mu(k, t)$ of the recovered patterns but not only).

> In summary, figure 3.5 shows that, for $\alpha > 1$, there are active hubs in the system that correspond to the recovered pattern, making it stable. On the other hand, for $\alpha < 1$ no real hubs can emerge in the system, and the transient relatively-high degree nodes are scattered throughout the network, not only corresponding to the recovered pattern, thus inducing the observed oscillatory behavior.

3.3.4   Quantitative analysis of the oscillatory behavior

In the previous sections we have shown the emergence of oscillations for $\alpha < 1$ and $T > 0$, and their relation to the existence of transient relatively-high degree nodes on the network. Here, we develop further on the structure and patterns of these oscillations. For simplicity, we focus on the case of $\kappa_\infty = 20$ and $P = 5$ as before, and in figure 3.6 we show a long time series corresponding to this oscillatory phase ($T = 0.7$ and $\alpha = 0.3$ as in the top graph of Fig. *B.4a* and in Fig. 3.5*a*). Plots of the active-overlap parameter $m_1^\mu(t)$ (defined in Eq. 3.9; panel *a*), its binearized version $m_B^\mu(t)$ (Eq. 3.10; panel *b*) and the global memory state parameter $d_s(t)$ (Eq. 3.11; panel *c*) indicate that the state of the system corresponds to oscillations between SG-like states in which either 2 or 3 patterns are transiently retrieved. These plots also evidence that the oscillations do not follow any clear periodic or regular pattern.

   In order to analyze the pattern of oscillations, we show in figure 3.6*d* the power spectra of $m_B^\mu(t)$, $S_\mu(f)$, and of $d_s(t)$, $S_s(f)$. Both of them display a power-law decay with an exponent equal to -0.9, indicating that there is not a dominant frequency of the oscillations, but that jumps between different patterns occur at all time scales. This is in accordance with previous studies that have repeatedly reported $1/f$-type noise in brain activity under healthy conditions, as discussed in section 1.4.3. It has been reported, for instance, in electroencephalogram (EEG) and functional magnetic resonance (fMRI) measures of human brain activity (Linkenkaer-Hansen et al., 2001; Voytek et al., 2015) and also in behavioral processes related to human cognition and motion as well as animal motion (Chialvo, 2010). $1/f$ noise indicates the existence of temporal correlations within the data, and has been related to emerging self-organized criticality in the brain (Chialvo, 2010).

   Moreover, we also investigate the frequency of appearance of each global state, as seen in figure 3.6*e*, which indicates that global states have different probabilities of occurrence in each realization of the system. However, when averaged over realizations, the mean probability of each state, $\bar{p}_s$, converges to a uniform distribution $\bar{p}_s \to 1/N_s$, where $N_s = 20$ is the total number of possible 2- and 3-pattern states ($\bar{p}_s = 0.054(3)$ when averaged over 20 realizations). Similarly, individual patterns may have different probability of appearance, p_μ,

in each realization of the dynamics, but when averaged over realizations $\bar{p}_\mu$ converges to $1/P$ ($\overline{p_\mu} = 0.21(1)$). Finally, we also computed the transition matrix between global SG-like states (figure 3.6f) which indicates that, in a given realization of the system, some transitions are preferred by the system depending on the emergent coupling between activity and topology.
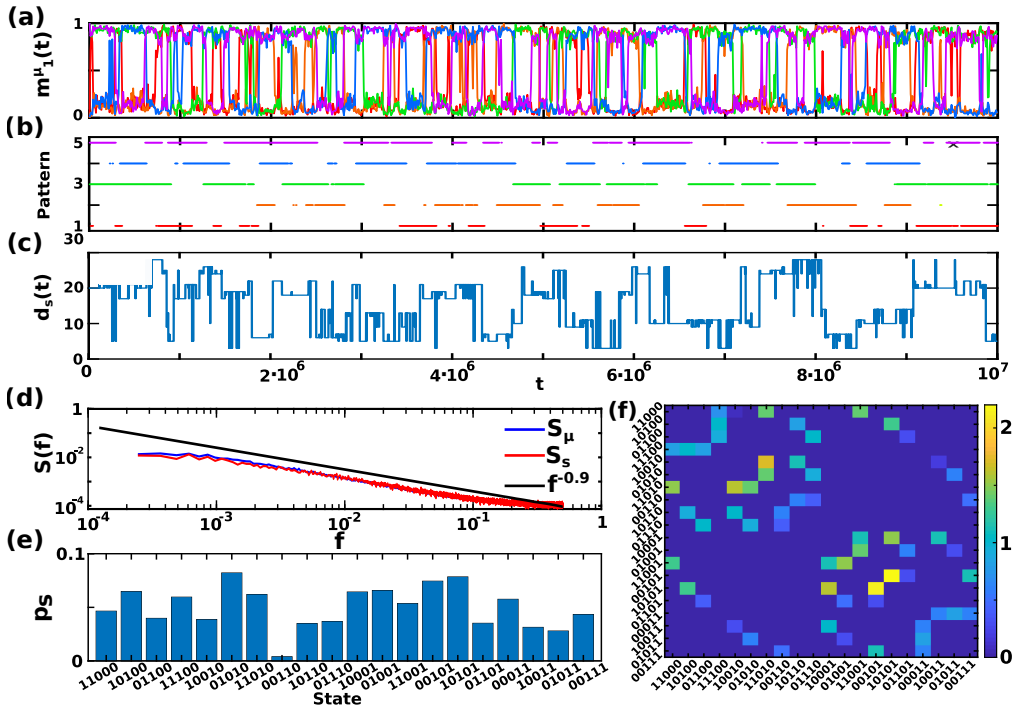
Figure 3.6: **Analysis of the oscillatory behavior of the system** in a representative point ($T = 0.7$, $\alpha = 0.3$, $P = 5$, $\kappa_\infty = 20$). **(a-c)** Temporal evolution of the system as given respectively by the retrieved patterns at each time, $m_1^\mu(t)$, the binearized variable $m_B^\mu(t)$ indicating whether each pattern is active or not, and finally the global memory state $d_s(t)$ as defined in the text, for a total time of 10^7 MCS. These show that the system wanders through the different attractors without a periodic order. **(d)** Power spectra of $m_B^\mu(t)$, $S_\mu(f)$, and of $d_s(t)$, $S_s(f)$, indicating a power-law scaling of $S_\mu(f)$ and $S_s(f)$ with an exponent of -0.9. **(e)** Probability of appearance of each global state, evidencing that only $2-$ and $3-$pattern SG states are recovered. **(f)** Transition matrix of global states, that is, the probability of jumping (times 10^{-3}) from a given global state s to another s'. Results are for $N = 1600$, and have been averaged over 20 realizations of the system in panels d and f.

In summary, these results show that the oscillations are not periodic, but occur at all time scales, and that all SG-like states are visited in a non-periodic order. Interestingly however, in a given realization of the system not all transitions are allowed, but only some of them occur. It could be interesting to analyze in more detail in further studies whether the coupling between structure and activity induces a particular pattern of oscillations, and how the scaling of the frequency of oscillations depends on the parameters of model.

3.4   Discussion

In this chapter we have reported on recent studies on the emergent behavior of developing brain models in which structure and function cooperate and influence each other through a feed-back loop, thus affecting the system's memory storage and retrieval abilities (Millán et al., 2019b). We have made used of the co-evolving synaptic pruning model defined in the previous chapter (Sec. 2.2) to analyze how the learning of a larger number of memories, in combination with thermal and structural disorder, affects the emergent behavior of the system, and also the conditions under which such feed-back loop can enhance the storage and retrieval of a set of correlated patterns. The emergent dynamics and behavior of the system is therefore a consequence of the interplay between structural, quenched and thermal disorder during its maturation. This is a prominent example of how inter-synaptic factors at the network level can affect the processing of information in developing brains in a nontrivial way.

The results presented in this chapter demonstrate that a heterogeneous network can greatly improve the stability of the memory patterns, since its structure is optimized to preserve information about them in the network hubs which, as we have shown, correspond to the active neurons of the retrieved memories during the recall process. Moreover, due to the structural plasticity, once a pattern is retrieved, the ability of the system to recall it again increases thanks to pruning optimization. This illustrates the constructive role of synaptic pruning to consolidate memories in the *memory phase* of the system.

Our study also shows that the interplay between thermal noise, the interference among stored patterns and the dynamics driving the evolution of the topology creates instabilities on the memory attractors, which can make the system wander among different configurations for certain values of the parameters.

Discussion of the emerging oscillatory behavior of the system

The oscillations among stored patterns observed in our system are caused by the topological synaptic plasticity due to the death and birth of synapses, which change the energy landscape of the system. In fact, in the absence of this rewiring process, this oscillatory phase is not present and the model would reduce to an Amari-Hopfield model on top of a non-trivial fixed topology. This has been shown to present the same phases as the canonical fully connected version of the model, with transition lines that depend on the topology, so that for instance the critical temperature diverges, $T_c \to \infty$ as $N \to \infty$, due to the presence of hubs that retain pattern information, as discussed on section 1.4.1 (see also Amit, 1989).

Interestingly, the observed oscillatory behavior appears on the homogeneous networks phase of the system. However, it is associated with an increased heterogeneity of the underlying structure due to the existence of transient relatively-high degree nodes (whose degree is however smaller than typical hubs) that emerge and disappear in time. Moreover, these relatively-high degree nodes do not correspond in general to the active nodes of the transiently recovered patterns, but appear distributed throughout the whole network, corresponding also to active nodes of the rest of non retrieved patterns. This creates a non-trivial time-dependent competition among the different patterns which, together with the subsequent removal of some synapses during brain development, can make the currently recalled attractor less stable, thus inducing the observed wandering among the memories.

We have also analyzed the characteristics of these oscillations and shown that the oscillatory pattern is not periodic but presents a power spectrum following a power law scaling decay with an exponent of -0.9, so there are not any preferred frequencies. This in accordance with previous studies repeatedly reporting $1/f$ noise in brain activity under healthy conditions (Linkenkaer-Hansen et al., 2001; Voytek et al., 2015) and also in behavioral processes (Chialvo, 2010), which is related to the existence of temporal correlations within the data, and has been related to emerging Self-Organized Criticality (SOC) in the brain (Chialvo, 2010), as discussed in chapter 1 (section 1.4.3).

Interestingly, the appearance of an oscillatory phase characterized by dynamical memories could be useful to enhance the learning and recalling of sequences of patterns of activity, as in episodic memories, without the necessity of any external input or current forcing the retrieval of the memories in the sequence. This type of oscillations has already been reported for brain models with synapses enduring short-term synaptic plasticity, STSP (see section 1.1.4.2 and also Pantic et al., 2002; Cortés et al., 2006; Marro et al., 2007a; Torres et al., 2007a, 2008). This occurs at the synapse level and depends on the activity of the pre-synaptic neuron – which therefore depends closely on the synaptic current I_i used in our model (Amit, 1989). However, STSP is caused by biophysical mechanisms controlling the release and recycling of neurotransmitters

at the synapses during synaptic transmission and operates at short time scales of the order of *ms* (Tsodyks and Markram, 1997). The activity dependent topological plasticity reported here, however, is the result of the interplay between form and function in a developing brain, and the ongoing synaptic rewiring in mature brains, which happens at the time scale of hours or days (Holtmaat and Svoboda, 2009). Moreover, topological or structural plasticity allows the system to explore more efficiently its dynamical phase space and it has been shown to improve the capacity of neural networks by allowing them to organize in a more efficient structure. Both mechanisms could happen at the same time in actual systems, together with neuron level phenomena such as spike adaptation (Knoblauch and Palm, 2002; Ha and Cheong, 2017). We hypothesize that the combination of these mechanisms could lead to the extension of the oscillatory behavior to other regions of the phase diagram, although results would strongly depend on the relative time scale between structural plasticity and STSP, and it could be an interesting approach for future works.

It is also worth noting that the reported oscillations in our system are for the overlap function that is a measure of the activity of the whole neuron population during memory recall processes. These occur in actual neural systems at a long time scale – normally days or even years – as it is the case in our model. Temporal changes at the single neuron level appear in our system as high frequency fluctuations in the time dependent value of the overlap parameter. If the level of stochasticity is low (low T) and the network size is large enough ($N \gg 1$), such single neuron fluctuations are very unlike to be significant on $m^{\mu}(t)$. In any case, the model output could be easily tuned up to obtain faster of slower oscillations in the overlap function to match more realistically actual experiments during learning and recalling. This could be done by varying some model parameters to make the recall process more or less efficient in time, or to allow the system to recall dynamic memories – such as episodic memories – that are learned and recalled at different stimuli input frequencies.

Relation of the synaptic density κ_{∞} with neurological disorders

We have analyzed in detail how the dynamical behavior of the system depends on the synaptic factors affecting the addition and removal of synapses and on the number of stored patterns. In particular, the stationary mean connectivity of the network, κ_{∞}, has been shown to have a great effect on the emergent behavior of the system. For instance, we have found that the absence of dynamical memories in the system, or the presence of memory oscillations with long periods, is associated with a defect of the pruning process. Similarly, we have shown that high frequency oscillations among patterns and more tendency to noisy behavior occur when there is a pruning excess. The destabilization

of recovered memories is necessary for instance to recall a sequence of memories, each during a short period of time, so as to allow the system to remember new ones. One thus may argue that the induced instability and the associated oscillatory behavior observed in our system could be positive for information processing. This would allow neuronal media to explore different memories or attractors, for instance following hetero-clinic orbits and, consequently, to process more complex information, such as spatio-temporal patterns of information (see Rabinovich et al., 2006 and references therein). Such emergent behavior could also be useful to respond more efficiently to changing external stimuli, as in episodic memory tasks, as it has been widely stated in previous works in different neural systems (Cortés et al., 2006; Marro et al., 2008; Torres et al., 2008).

The effect of the synaptic connectivity on the emergent behavior of the system could perhaps be associated with cognitive abilities related to autism spectrum disorders (ASD) and schizophrenia. It has recently been reported that short-term memory and episodic memory are impaired in ASD subjects (Poirier et al., 2011; Lind et al., 2014) and a pruning defect has also been observed in some brain areas (Tang et al., 2014). The results presented in this chapter could link both observations since they imply that in a less pruned brain, which will consequently have a higher synaptic density, the memory attractors are more stable. This implies a lower ability to remember sequences of patterns, as described in episodic memory tasks in ASD patients, because it is harder for the brain to forget the already recalled pattern due to its strong stability. Results in our model also indicate that a lightly pruned brain could be forced out of the memory phase into an oscillatory regime with an increase in the number of stored patterns (see figure 3.3). These observations might provide an interesting insight for experimental psychologists to design a cognitive strategy or therapy to learn and recall sequences of patterns, that might improve the cognitive abilities of patients with ASD.

On the other hand, we have demonstrated that high frequency oscillations among patterns occur when there is a pruning excess, and this could be perhaps associated with the erratic behavior observed in schizophrenia (Loh et al., 2007), in which case the brain seems to present some areas with an excess of pruning (Sekar et al., 2016). In this case our results here suggest that a learning therapy based on increasing the number of stored memories would not be useful but may in fact be detrimental, as it would make the memory activity patterns more unstable. A learning therapy that moves the patient brain state near to its stable memory phase, for instance, by stabilizing a few old useful memories, could therefore be more convenient.

Limitations and possible extensions of the model

It is worth noting that some drastic assumptions have been made in order to

simplify the relevant scenario. Firstly, our study is for sparse correlated patterns, as suggested by experimental studies (Chklovskii et al., 2004; Akam and Kullmann, 2014), which are also known to improve the memory retrieval capabilities of the network (Knoblauch et al., 2014; Knoblauch and Sommer, 2016) and particularly so in the case of highly sparse and heterogeneous networks (Morelli et al., 2004). Moreover, we have selected the patterns of activity to be non-overlapping regions of activity, following previous works (Torres and Marro, 2015). This set up corresponds to a particular case that allows for a better visualization of the network dynamics and that has proven out to be useful to investigate the interplay between structure and dynamics, i.e., between form and function, together with the presence of thermal and quenched disorder, on a developing neural network. Similarly, results are for the low storage regime of the neural network, $P \ll N$, what allows us to study in detail the dynamical behavior of the system that gives rise to memory wandering. However, given that our qualitative results depend little on P for $P > 20$, we expect them to hold when P is increased.

Further extensions of this work could also include the consideration of different details of the synaptic pruning process, including for instance the growth of synapses taking place after birth (Millán et al., 2018b), multiple synaptic contacts between neurons (Knoblauch et al., 2014; Knoblauch and Sommer, 2016), or a hard bound on the maximum degree of the nodes (Stepanyants et al., 2002; Fares and Stepanyants, 2009). Moreover, more elaborated definitions of the probabilities of growth and death of synapses (Eq. 2.11 and 2.9) could also be considered, such as a mechanism of self-organization towards the stationary mean connectivity (Chechik et al., 1999; Arcangelis et al., 2006; Lewis and Todd, 2007; Tetzlaff et al., 2010) or by explicitly including a dynamics for the available nutrients (Tetzlaff et al., 2010). However these definitions would still need to reproduce the basic characteristics of brain development and synaptic pruning, that is, an initial fast decay of connectivity and an ongoing rewiring of edges after the stationary mean connectivity has been reached. We expect that our main results (existence of a feed-back loop between structure and activity, bistability and emergence of oscillations) would still hold, at least qualitatively, with these modifications, in accordance with previous studies (Millán et al., 2018b). The consideration of a limit of the nodes' maximum degree, for instance, would primarily affect the hubs of bimodal networks. However, these typically form a highly connected core in the network, so that the average path length between nodes would not increase heavily. Therefore, we expect that this bound would not have an important effect in the regime $P \ll N$ in which we set the system here.

In the following chapter we tackle the first of these considerations, and consider a more realistic definition of the global probabilities $u(\kappa)$ and $d(\kappa)$ (Eq. 3.2) that also includes the initial overgrowth of the synaptic density that occurs

in mammals following birth, as in Eq. 2.22 in chapter 2. One could also consider biologically inspired pruning functions, that characterize for instance a specific dependence on the concentration of different proteins and growth factors controlling synaptic growth. These could be obtained experimentally, although to the best of our knowledge it has not yet been done. Results in this chapter could thus motivate neurobiologists to design experiments to describe the exact probabilities involved in synaptogenesis and pruning, information that could be easily incorporated in our theoretical framework. Similarly, it could also be particularly interesting to include a learning dynamics that is also coupled to the development of the neural network, thus modeling learning during infancy, or to include an external current on the system, that could certainly be time dependent, to analyze the effect of external inputs on associative memory and memory wandering.

Chapter 4

Growth strategy determines aspects of brain performance.

The interplay between structure and function is crucial in determining some emerging properties of many natural systems. As we have seen in previous chapters, different aspects of such interplay have a strong influence on the emergent behavior of evolving brain models, and can induce the emergence of new intriguing dynamical phases. In addition, such interplay can well reproduce experimental temporal profiles of synaptic density. Following this motivation, in chapter we go deeper into the study of the influence that new aspects associated with the evolution of actual brains have on their cognitive properties. Consequently, we adapt here the evolving neural network model presented in chapter 2 to include an initial transient period of relatively high synaptic connectivity, as it is observed experimentally. Using a simplified framework, we prove that the existence of this transient is critical in providing ordered stationary states that have the property of being able to store stable memories. In fact, there is a discontinuous phase transition between the ordered memory phase and a disordered one as a function of the initial transient synaptic density. We also show that intermediate synaptic density values are optimal in order to obtain these stable memory states with a minimum energy consumption, and that ultimately it is the transient heterogeneity in the network what determines the stationary state. Our results here could explain why the pruning curves observed in actual brain areas present their characteristic temporal profiles and, eventually, anomalies such as autism and schizophrenia associated, respectively, with a deficit or an excess of pruning. A preprint of the results presented in this chapter can be found in Millán et al., 2018b.

4.1   Introduction

Aoong the thesis we have emphasized the relevance of considering a complex networked structure to study natural and human systems; almost every biological and social system, as well as many man-made structures, develops intricate relations among its components, resulting in a network configuration that is usually far from being homogeneous (Boccaletti et al., 2006; Newman, 2011). It is then hardly surprising the tremendous amount of attention that research on complex networks has received over recent decades, in order both to understand and protect natural networks and to optimize technical designs.

In chapter 1 we have shown how most studied networks, and in particular brain networks, present non-trivial topological features, such as high clustering and short minimum paths (small-worldness), modular structure, and cost-efficient wiring (see section 1.2 for a more detailed discussion on the relevance of complex networks in neuroscience, and also Albert, 2005; Eguiluz et al., 2005; Gastner and ódor, 2016). The majority of known networks exhibit also highly heterogeneous degree distributions (where the degree of a node is its number of neighbors) and, except in the case of social networks, negative degree-degree correlations – a property known as disassortativity (Ódor, 2013). In other words, many networks of interest include a small number of highly connected nodes, called *hubs*, which tend to be connected to low-degree nodes (Newman, 2003). These properties influence the emerging dynamics of complex systems. For instance, both degree heterogeneity and degree-degree correlations strongly influence the signal to noise ratio in certain dynamical systems (Maslov and Sneppen, 2002; Torres et al., 2004; Franciscis et al., 2011), for instance, whereas the synchronization properties of a complex network strongly depend on its dimension, as we discuss on the following chapters (Eytan and Marom, 2006; Millán et al., 2019b).

In order to understand how such non-trivial networked structures come about, much work has gone into investigating mechanisms of network evolution, some of which have been reviewed in chapter 1 (Berg et al., 2004; Johnson et al., 2009; Navlakha et al., 2015), and have been the topic of the two previous original chapters (2 and 3) of this thesis. In particular, we have already seen that one main process that takes places in the development of neural systems is *synaptic pruning* (section 1.3.2). This consists in an extensive pruning of synaptic connections than takes place during infancy, which results in the elimination of about half the synapses in the brain. The process goes on into adulthood, as mature brain circuits maintain the ability to generate new synapses, allowing for *structural plasticity* in the brain. Both processes involve the growth and death of synapses over time in an activity-dependent manner. Recent studies have suggested that details of synaptic pruning may have large implications on high-level brain functions, and they have been related to the emergence of some

neurological disorders such as autism and schizophrenia (Faludi and Mirnics, 2011; Tang et al., 2014; see also section 3.4 in chapter 3). However, little is so far known about the influence of synaptic pruning and the relatively high synaptic connectivity during early brain development on its performance. It is believed that the reason for reducing synaptic density is becoming more energetically efficient (Chechik et al., 1999). But then a question arises, why not begin life with the optimal synaptic density?

In order to analyze how details of this process might affect the cognitive abilities of a neural system, in chapter 2 we have presented an original adaptive neural-network model that describes synaptic pruning. In our model, the evolution of the structure of the network depends on its activity state, and viceversa. This creates a feed-back loop in which structure and function influence each other. The proposed computational model combines a familiar associative memory model, the Amari-Hopfield model (see sections 1.4.1 and 2.2.1), with a preferential attachment model for network evolution (see section 1.3.2; see also Millán et al., 2018c; Millán et al., 2019b), based on the fact that synaptic growth and death are related to neural activity (Klintsova and Greenough, 1999). This setup creates a feedback loop between structure and dynamics, leading to two qualitatively different kinds of behaviors, as it has been previously shown (Millán et al., 2018c; Millán et al., 2019b). In one of them, the network structure becomes heterogeneous and dissasortative, and the system then displays good memory performance. In the other, the structure remains homogeneous and incapable of pattern retrieval. In chapter 3 we have further shown how the combination of thermal and quenched disorder in the system can create instabilities in the memory atractors, giving rise to an oscillatory behavior as observed experimentally.

In this chapter we extend the aforementioned adaptive network model to consider the period of high synaptic connectivity that takes place during infancy, before synaptic pruning begins. We show that, even in a simple case, the transient period of high synaptic density can lead to an increased network performance, in terms of memory retrieval, even in the presence of high levels of noise.

The basic mechanism which our model illustrates needs not be restricted to neural networks, but may help understanding also how other structures form, e. g., in the case of protein interaction networks which also change in evolutionary time scales in a way that is related to their physiological activity (Berg et al., 2004), as we already discussed in section 2.5. In fact, as it is the case of our model, most biological networks change with time, so that pruning may be a general mechanism for network optimization trying to minimize energy consumption in an environment of limited resources without the need for a great amount of information specifying the initial topology.

4.2   Synaptic pruning model

In this chapter we make use of the adaptive network model defined in chapter 2 to study the effect of the initial transient period of high connectivity. The full derivation of the model can be found in 2.2; here we will review the most relevant concepts and explain in detail the changes and new definitions introduced in this chapter for the present study.

The system thus consists of a N-node undirected binary network whose structure is given by the adjacency matrix $e_{ij}(t)$. The state of each neuron is given by the stochastic binary variable $s_i(t)$, which follows an Amari-Hopfield dynamics (as introduced in section 1.4.1) where the level of stochasticity is characterized by a noise parameter or temperature T, with $T = 0$ corresponding to the deterministic limit (Amit, 1989). Each synapse is characterized by its strength, given by the synaptic weight w_{ij}. These are defined so that the network *learns* or *stores* a pattern of activity ξ_i, that is, to make ξ_i an attractor of the dynamics of the system[1].

The macroscopic state of the system may thus be characterized by the overlap of the network with the memorized pattern, $m(t)$, and its stationary value[2], $\overline{m} = m\,(t \to \infty)$. Namely,

$$m(t) = \frac{1}{Na_0(1 - a_0)} \sum_{i=1}^{N} (\xi_i - a_0)s_i, \tag{4.1}$$

where $a_0 = \langle \xi_i \rangle$ is the mean activation of the pattern, introduced for normalization purposes. $m(t) = 1$ indicates that the state of the network is equal to the pattern, and the system is in a memory state, whereas $m(t) = 0$ corresponds to the non-memory state. In a low noise situation, ξ_i is an atractor of the dynamics of the system, whereas the inclusion of thermal and quenched disorder can destabilize it, as discussed in chapters 2 and 3.

The topology changes in time following a Markov process given by the probabilities $\widetilde{P}_i^g$ and $\widetilde{P}_i^l$ that each node i has to gain and loose an edge at time t, namely

$$\widetilde{P}_i^g = u(\kappa)\widetilde{\pi}_i \quad \widetilde{P}_i^l = d(\kappa)\widetilde{\eta}_i. \tag{4.2}$$

where we have dropped the time dependency for clarity. Here $\kappa(t)$ is the mean connectivity of the network as before, and $\widetilde{\pi}_i = \widetilde{\pi}(I_i)$, $\widetilde{\sigma}_i = \widetilde{\sigma}(I_i)$, where $I_i(t)$ stands for the incoming current at each neuron from its neighbors.

As we have seen previously (section 2.2), the evolution of the mean connectivity $\kappa(t)$ only depends on the global variables $u(\kappa)$ and $d(\kappa)$ (provided that

---

[1]We decide to set the number of memorized patterns P to one for the sake of simplicity. In chapters 2 (Sec. 2.4.2) and 3 we have already discussed the effect of learning more patterns, which can lead to emergence of spin-glass phases and population neural activity oscillations.

[2]Measures of the global variables on the stationary state are obtained by averaging during a long window of time: $\bar{f} = \Delta t^{-1} \sum_{t=t_0}^{t_0 + \Delta t} f(t)$.

$\widetilde{\pi}$ and $\widetilde{\eta}$ are normalized over network), and it is given (Johnson et al., 2010a; Millán et al., 2018c) by

$$\frac{d\kappa}{dt} = 2\left[u\left(\kappa\right) - d\left(\kappa\right)\right]. \tag{4.3}$$

Experimental evidence indicates a fast growth of the synaptic density following birth and preceding synaptic pruning, whose impact on brain development is yet to be fully clarified (Tang et al., 2014; Navlakha et al., 2015). In chapter 2 we have reproduced these profiles of synaptic density by considering an initial, fast growth of synapses followed by synaptic pruning, namely (see section 2.3.2)

$$
\begin{aligned}
u\left(\kappa\right) &= \frac{n}{N}\left(1 - \frac{\kappa(t)}{2\kappa_\infty} + a_g \exp(-t/\tau_g)\right) \\
d\left(\kappa\right) &= \frac{n}{N}\frac{\kappa(t)}{2\kappa_\infty},
\end{aligned}
\tag{4.4}
$$

where τ_g and a_g control the time-scale and intensity of the initial growth, κ_∞ is the stationary mean connectivity, and n/N characterizes the speed of synaptic growth and death. This leads to

$$\frac{d\kappa}{dt} = \frac{2n}{N}\left[1 - \frac{\kappa(t)}{\kappa_\infty} + a_g \exp(-t/\tau_g)\right], \tag{4.5}$$

which has the solution

$$\kappa(t) = \kappa_\infty\left[1 - b\exp(-t/\tau_g) + c\exp(-t/\tau_p)\right], \tag{4.6}$$

where $\tau_p = N\kappa_\infty/2n$ sets the temporal scale of the pruning process, $b = a_g\tau_g\left(\tau_p - \tau_g\right)^{-1}$ and $c = \kappa_0/\kappa_\infty + b - 1$. This model for $\kappa(t)$ – shown by the dashed black line in figure **??**a – has been shown to reproduce experimental data of the mean synaptic density in the cortex in humans and rodents (see section 2.3.2 and also Johnson et al., 2010a; Millán et al., 2018c).

The local probabilities $\widetilde{\pi}$ and $\widetilde{\eta}$ introduce a dependence on the physiological state of the neurons, and account for local heterogeneity in the network. Following previous studies, we take $\widetilde{\pi}(I_i) \propto I_i^\alpha(t)$ ($\alpha > 0$), $\widetilde{\eta}(I_i) \propto I_i(t)$, which correspond to synapses being chosen at random for removal, which can be seen as a first order approximation of pruning dynamics (Johnson et al., 2009). The global order parameter used in this chapter to describe network structure is the homogeneity parameter $g(t)$, and its stationary value $\bar{g} = g\left(t \to \infty\right)$. Namely,

$$g(t) = \exp\left(-\sigma_k^2(t)/\kappa(t)\right), \tag{4.7}$$

where $\sigma_k^2(t)$ is the variance of the degrees of the nodes. $g(t)$ equals 1 if $p(k) = \delta_{k_0,k}$ (homogeneous network) and tends to 0 for highly heterogeneous (bimodal) networks. In the topological limit of this model there is a continuous phase transition from homogeneous networks ($\bar{g} \to 1$) to heterogeneous ones ($\bar{g} \to 0$) as α increases, with a critical point $\alpha_c = 1.0$ in which scale-free networks emerge, as reported in chapter 2, figure 2.1 (see also Johnson et al., 2010a; Millán et al., 2018c).

4.2.1   Emerging dynamics of the model

In chapter 2 we have analyzed the effect of the coupling between the local structure of the network and the physiological dynamics (Millán et al., 2018c; Millán et al., 2019b) during synaptic pruning ($a = 0$ in Eq. 4.4). Depending on α, the parameter controlling the heterogeneity of the pruning dynamics, and the temperature T setting the thermal noise in the system, three phases appear:

  i) A homogeneous memory phase when both α and T are low, in which the network displays memory and its structure is homogeneous.

  ii) A heterogeneous memory phase for high α, in which the network is bimodal (appearance of hubs).

  iii) A homogeneous noisy phase for high noise T.

Finally, a bistability region emerges between the heterogeneous memory and the homogeneous noisy phases, corresponding to moderate α values, $1 < \alpha < 2$, and high temperature, $T > 1$, as a consequence of the coupling introduced by the model. This is because heterogeneous networks are more tolerant to thermal noise than homogeneous ones, so that the critical temperature T_c separating the memory and non-memory phases diverges from $T_c = 1$ for homogeneous networks to $T_c \to \infty$ for heterogeneous ones, where the presence of *hubs* stabilizes the memories (Torres et al., 2004; Franciscis et al., 2011; see also Sec. 1.4.1).

In the bi-stability region the stationary state of the system depends on its initial network configuration: networks that are initially heterogeneous display memory and enhanced heterogeneity during the whole evolution of the system, whereas homogeneous ones fall into the noisy state. Consequently, the initial overgrowth of synapses could have important consequences in the emerging behavior of the system in this region, since it changes the state of the system when synaptic pruning begins. That is, the structure and memory state at which the system is when synaptic pruning starts may depend on details of the process that has let it there, such as the maximum number of synaptic contacts or its duration. Therefore, in this chapter we analyze the effect of the non-trivial transient of high connectivity preceding synaptic pruning on the dynamics of the system on the bistability region (in particular, we fix $\alpha = 1.2$, $T = 1.3$).

4.2.2   Linear approximation

One can easily see that $\kappa(t)$ as given by Eq. 4.6 presents a maximum $\kappa^* = \kappa(t^*)$, where

$$t^* = \frac{\tau_g \tau_p}{\tau_p - \tau_g} \ln\left(\frac{\tau_p b}{\tau_g c}\right). \tag{4.8}$$
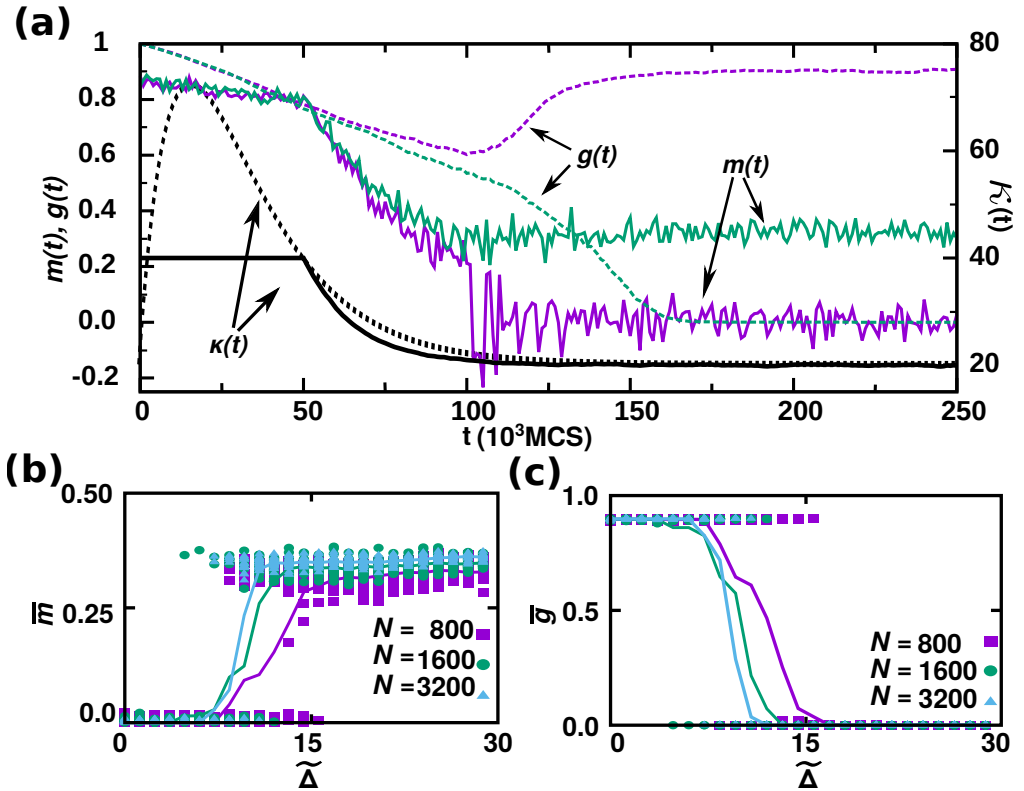
Figure 4.1: **Frozen-initial-density model of synaptic pruning.** **(a)** The black lines represent $\kappa(t)$ as given by the realistic model (dashed line) and the linear approximation model (solid line). The colored lines show two exemplary temporal evolutions of the linear model with $\kappa(t)$ as given by the black solid line. We represent $m(t)$ (colored solid lines) and $g(t)$ (colored dashed lines) for two realizations leading to two qualitatively different steady states: in green, a series in which the network keeps memory ($\overline{m} = 0.35$) and heterogeneity ($\bar{g} = 1.0$) in the steady state and, in purple, the opposite example. All parameters are the same in both situations ($N = 1600$, $n = 2$, $\kappa_0 = 40$ and $\kappa_\infty = 20$ and $\Delta = 5 \cdot 10^4 MCS$). Panels **(b)** and **(c)** show, respectively, $\overline{m}(\widetilde{\Delta})$ and $\bar{g}(\widetilde{\Delta})$ for different system sizes, where $\widetilde{\Delta} = \Delta/\tau_p$. Results are for $\kappa_0 = 40$ and $\kappa_\infty = 20$. The parameter n is scaled with the network size, so that $n = 5, 10, 20$ respectively for $N = 800, 1600, 3200$.

Both t^* and κ^* depend non-trivially on a, τ_g and τ_p (since b and c are also functions of a, τ_p and τ_g). Therefore, in order to study the effect of the non-trivial transient of high connectivity on the emergent state of the system, here we consider a first order approximation to this realistic pruning profile. In particular, $\kappa(t)$ is kept constant (and high), $\kappa(t) = \kappa_0$, at the onset of the

evolution (see solid black line in figure 4.1*a*), during a *frozen-density* time Δ, by imposing that the same number of edges are created and destroyed, namely

$$u(t) = d(t) = d_0 \ \forall t < \Delta, \tag{4.9}$$

where $d_0 = $ const and, in particular, we consider here $d_0 = n/N$. Thereafter, the mean degree is allowed to vary following the pruning dynamics. This allows us to easily control the width (Δ) and height ($\kappa^* = \max(\kappa_t)$) of the pruning process, which fully characterize it.

4.3   Crucial role of the high-density transient

An exemplary evolution of the coupled system is shown in figure 4.1*a*. During the initial *frozen-density* period ($t < \Delta$) the mean connectivity is kept constant ($\kappa(t) = \kappa_0 \geq \kappa_\infty$) but the network structure is allowed to vary, since $d_0 N$ edges are created and destroyed at each time step, providing a non-trivial transient of network evolution. If κ_0 is sufficiently large, the system can perform memory retrieval throughout this period even though $T > 1$ – as indicated by $m(t)$ significantly different from zero. Given that $\alpha > 1$ too, the underlying topological dynamics starts creating hubs and heterogeneity throughout this period, and thus $g(t)$ decreases. Notice that the network only heterogenizes if it is able to maintain memory, since otherwise the topological rewiring process is lead by noise and the network remains homogeneous, as discussed in chapter 2. This a consequence of the coupling between neural dynamics and topology.

Once $t > \Delta$ synaptic pruning begins and $\kappa(t)$ decays towards κ_∞. Given that $T > T_c = 1.0$, a fully homogeneous network would no be able to maintain memory. In a highly heterogeneous network, however, the critical temperature diverges with the system size, and the memory states can be stable even with $T > 1.0$. Therefore, at this point the system can either fall into the noise state and lose its heterogeneity (purple lines in figure 4.1*a*), or remain in the heterogeneous memory state (green lines), showing multistability. If the system remains in the memory state, it continues to heterogenize ($g(t) \to 0$), to the point that it can maintain memory performance as $\kappa(t) \to \kappa_\infty$ (dashed green line in figure 4.1*a*). On the other hand, if the neural network falls into the noisy state ($m(t) \approx 0$), neural activity – and hence synaptic growth and death – becomes uncorrelated with node degree, and the topology reverts gradually to a more homogeneous configuration ($g(t) \to 1$, dashed purple line), incapable of memory.

In particular, we show in figure 4.1*b, c* that, for a given κ_0, there is a discontinuous phase transition as a function of Δ. Note that we have re-scaled Δ with τ_p as $\tilde{\Delta} = \Delta/\tau_p$ in these panels. As Δ is increased the system moves from a phase governed by noise, $\overline{m} \to 0$, in which networks are homogeneous, $\bar{g} \to 1$ (which we shall call the **homogeneous noisy phase**), to one where networks

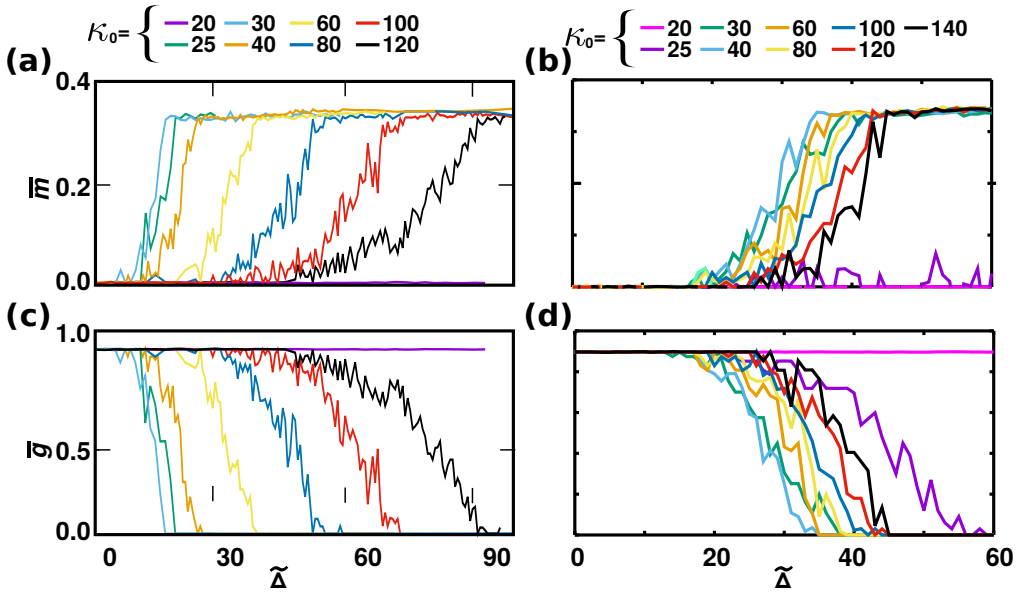Figure 4.2: **Transition curves for models A and B.** Stationary mean values of the overlap, $\overline{m}$ **(a,b)**) and homogeneity, $\bar{g}$ **(c,d)**) respectively for models A (panels *a* and *c*) and B (panels *b* and *d*). Results are shown as function of $\widetilde{\Delta}$ and for different values of κ_0 as indicated by the labels on top of the diagrams. $N = 1600$ and other parameter values as in figure 4.1.

are heterogeneous, $\bar{g} \to 0$, and they display memory, $\overline{m} > 0$ (therefore called **heterogeneous memory phase**) . A finite size analysis shows that the results hold for increasing network size (figure 4.1*b, c* is for $N = 800$, 1600 and 3200).

4.3.1 Non-linear effect of the initial density

The initial density κ_0 has a major effect on the dynamics, determining whether the system will be able to maintain memory retrieval and the minimum $\widetilde{\Delta}$ necessary for it (see figure 4.2).

In the case $\kappa_0 = \kappa_\infty$, $\kappa(t)$ is trivially constant and, given that $T > 1$, the system falls into the noisy state regardless of $\widetilde{\Delta}$ (see $\kappa_0 = 20$ in figure 4.2*a, c*). This continues up to slightly higher initial densities (up to $\kappa_0 = 25$), where the memory state is reached even for very low $\widetilde{\Delta}$. One might expect that the memory state would become easier to reach with higher κ_0 but, in fact, the opposite effect is obtained, and networks with increasing κ_0 take longer $\widetilde{\Delta}$ to reach the heterogeneous memory phase, for $\kappa_0 \gg \kappa_\infty$. This apparent paradox is explained after a deeper look at the system. In fact, large κ_0 implies that networks are initially more homogeneous and take more time to become heterogeneous under the topology dynamics. Besides, more edges have to be
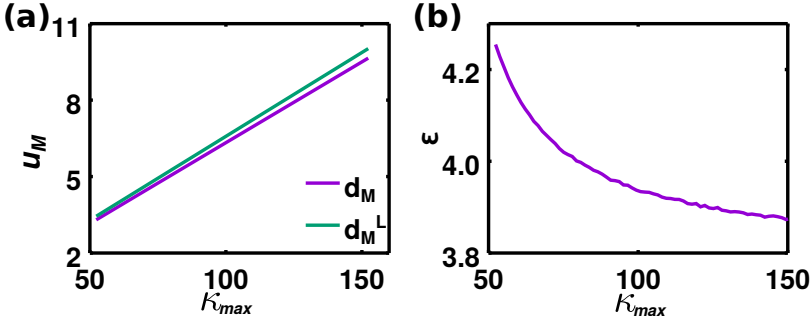
Figure 4.3: **Error of the linear approximation.** **(a)** Mean proportion of edges removed between t_1 and t_2 in the realistic model (d_m, purple line) and the linear approximation (d_m^L, green line). **(b)** Normalized error associated with the linear approximation ε. Parameters as in figure 4.2.

pruned to make a significant change in the network, which slows down network evolution. In consequence, very highly connected networks are more likely to fall into the noise state for a given $\widetilde{\Delta}$.

4.3.1.1   Validity of the results

One relevant question at this point is how this result depends on the particular definition of d_0, since so far we have considered $d_0 = \text{const } \forall \kappa_0, \Delta$. However, one may argue that the density of synaptic turnover should depend on the number of existing synapses, $d_0 = f(\kappa_0)$. In particular, in a more realistic scenario, one can define d_0 so as to approximate the mean number d_m of links added and removed in the realistic model between the two times t_1 and t_2 such that $\kappa(t_1) = \kappa(t_2) = \kappa_0$, $t_1 < t_2$; namely

$$d_m \equiv \frac{1}{t_2 - t_1} \sum_{t=t_1}^{t_2} d(\kappa(t)). \tag{4.10}$$

A parabolic approximation of $\kappa(t)$ as given by Eq. 4.6 around κ^* gives, for d_m,

$$d_m \approx d_m^L \equiv \frac{1}{4\tau_p}\left(\kappa^* + \frac{1}{6}D\Delta_\kappa^2 \kappa_\infty\right), \tag{4.11}$$

where

$$D = \tau_g^{-2}\left(\frac{\kappa^*}{\kappa_\infty} - 1\right) - c\left(\frac{1}{\tau_g^2} - \frac{1}{\tau_p^2}\right)e^{-t^*/\tau_p} \tag{4.12}$$

and $\Delta_\kappa = \kappa^* - \kappa_0$. As shown in figure 4.3, the percentage of error associated with the linear approximation,

$$\varepsilon \equiv 100\frac{|d_m - d_m^L|}{d_m}, \tag{4.13}$$

is small.

Equation 4.11 suggests a scaling relation $d_0 \propto \kappa_0$, and in particular one can consider $d_0 = n\kappa_0/N$. In the following we refer to this definition as **model B**, and to the former with $d_0 = n/N$ as **model A**. We show for both models the corresponding phase transition curves in panels b and d of figure 4.2. Interestingly, even though with model B the number of links rewired at each time depends linearly on κ_0, our main results hold as there is also in this case an optimal, intermediate κ_0 that requires a minimum time Δ to achieve the stationary memory state, confirming the non-linear effect of the initial density on the emerging behavior of the system.

4.3.2   Convergence to the memory state

The non-linear (or second order) effect of κ_0 also implies that the complementary representation $\overline{m}(\kappa_0)$ for a given $\widetilde{\Delta}$ shows a bell shape for intermediate $\widetilde{\Delta}$, with a maximum at $\kappa_0^A \approx 27$ and $\kappa_0^B \approx 40$ respectively for models A and B (see figure 4.4 panels a and b). From $\overline{m}(\widetilde{\Delta})$ one can explicitly measure the minimum value of $\widetilde{\Delta}$ needed to achieve memory for a given density. More generally, we define $\widetilde{\Delta}_{\min}^a(\kappa_0)$ as the minimum value of $\widetilde{\Delta}$ needed to reach a stationary mean overlap equal to $m_a = 0.1a\,\overline{m}$, $a = 1, 2, .., 10$ for a given κ_0. This definition aims to measure how much time it takes for a given configuration to organize into the heterogeneous state. Minimal values of $\widetilde{\Delta}_{\min}^a$ indicate an optimal initial configuration to reach memory with a minimal energy consumption. Our measures (figure 4.4 panels c and d) indicate a minimum $\widetilde{\Delta}_{\min}^a$ for the same connectivity as the maximum of $\overline{m}(\kappa_0)$, namely κ_0^A and κ_0^B in both alternative model descriptions. Therefore, memory is not only reached faster but it is also stronger for the optimal κ_0.

Finally, an integrated view of the effect of network dynamics and the emergent behavior of the system can be obtained by the phase diagram of the system, as shown in figure 4.5e, f, as a function of the control parameters $\widetilde{\Delta}$ and κ_0. These have been obtained by the integrated analysis of $\overline{m}(\widetilde{\Delta}, \kappa_0)$ and $\overline{g}(\widetilde{\Delta}, \kappa_0)$, which indicates the existence of a region of stationary memory and heterogeneous networks for both high $\widetilde{\Delta}$ and high κ_0. The phase transition between noise and memory moves to higher $\widetilde{\Delta}$ for higher κ_0 in an approximately linear manner, as previously discussed, leading to the contraction of the heterogeneous memory region. On the other hand, very small κ_0 never leads to memory, due to the high thermal noise.

Summing up, our results show the benefit of intermediate densities with respect to very high ones in order to achieve memory in a noisy environment. Interestingly, results hold when the density of synaptic turnover d_0 is re-scaled linearly with the density of synapses κ_0, indicating that the
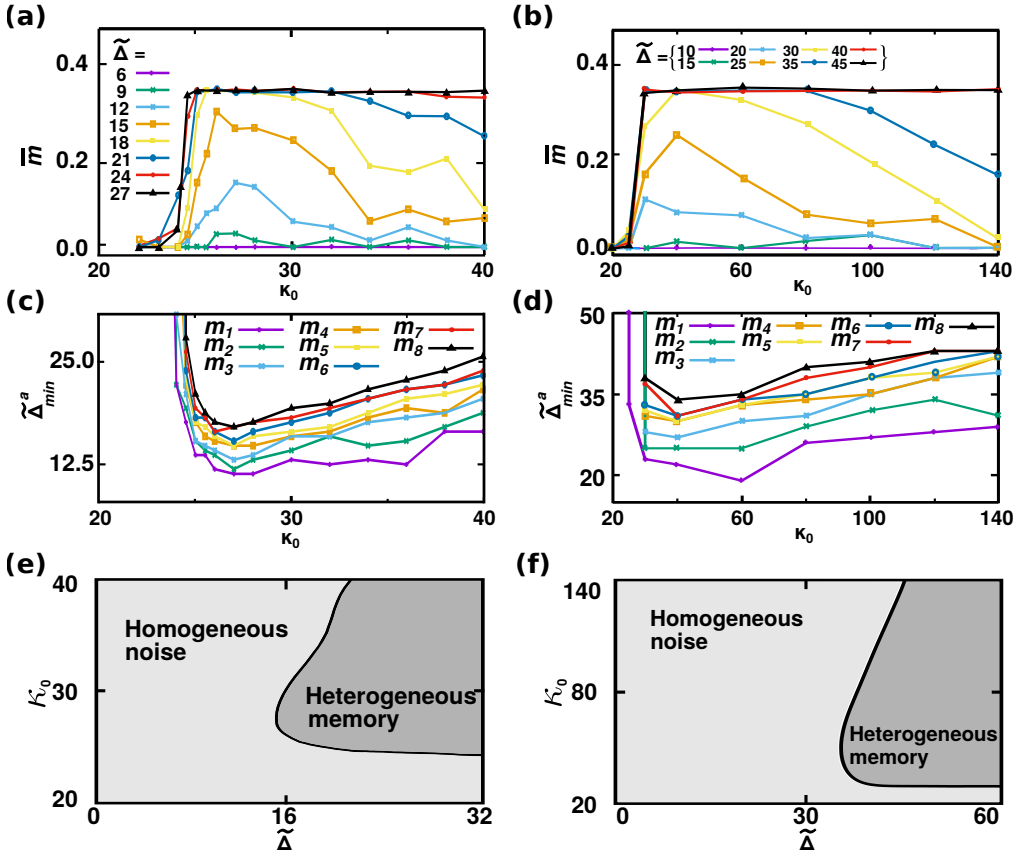
Figure 4.4: **Crucial role of the high-density transient.** **(a,b)** $\overline{m}(\kappa_0)$ for different values of Δ, respectively for models A and B. **(c,d)** $\widetilde{\Delta}^a_{min}(\kappa_0)$ for different values of Δ, respectively for models A and B, with smaller times indicating a faster stabilization of the memory state. **(e,f)** Two dimensional phase diagram of the system, respectively for models A and B. These are obtained through analysis of $\overline{m}(\widetilde{\Delta}, \kappa_0)$ and $\bar{g}(\widetilde{\Delta}, \kappa_0)$, so that the heterogeneous memory phase is defined by $\overline{m} > 0$ (in particular, $\overline{m} \geq 0.35$) and $\bar{g} \to 0$, whereas the homogeneous noisy one has $\overline{m} \to 0$ and $\bar{g} \to 1$. Parameter values as in Fig. 4.2. $\widetilde{\Delta}$ for model B is defined as $\widetilde{\Delta} = \Delta/1000$.

longer transient time needed to reach the heterogeneous memory phase for higher κ_0 is not only due to the higher number of synapses that need to be rewired. This result suggests why for an evolving network such as the infant brain it is detrimental to initially grow a very high density of synapses, since this increases the energy costs during growth and also during the pruning process, and it does not improve memory retrieval or
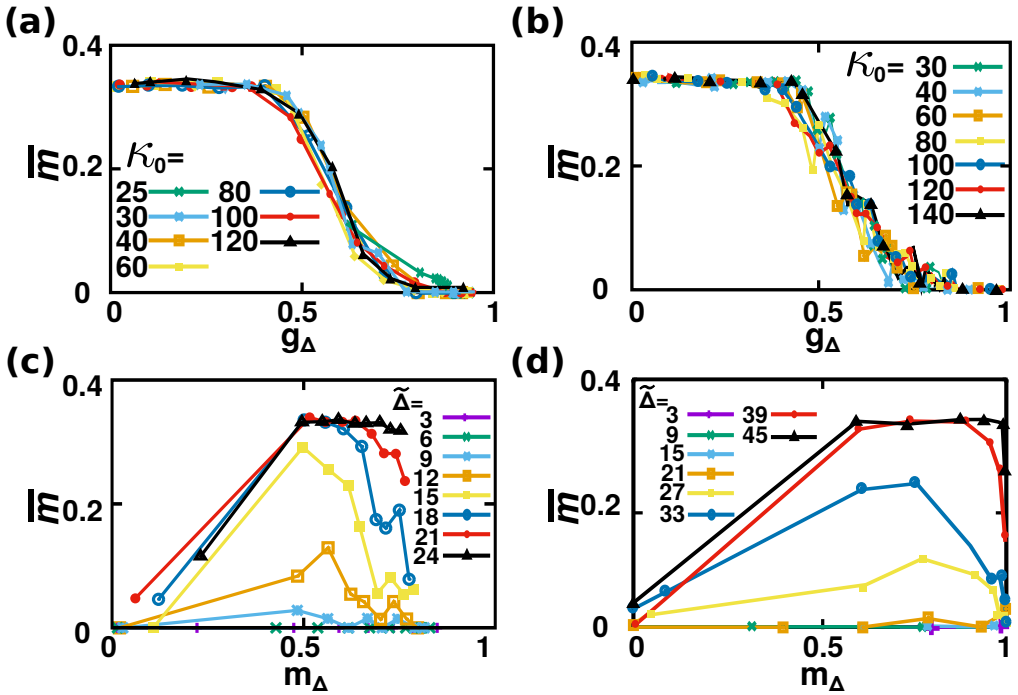
Figure 4.5: **Transient heterogeneity determines network performance.** **(a,b)** $\overline{m}(g_\Delta(\widetilde{\Delta}))$ for different values of κ_0, respectively for models A and B, as defined in the main text. **(c,d)** $\overline{m}(m_\Delta(\kappa_0))$ for different values of $\widetilde{\Delta}$, respectively for models A and B.

network structure. On the contrary, a neural network with intermediate values of transient synaptic density would perform more efficiently during pruning. Moreover, this would also be convenient in terms of energy consumption.

4.4   Transient heterogeneity determines network performance

We have shown a quadratic dependence of the system stationary state on κ_0 (see figure 4.4), and discussed the presence of multistability for intermediate values. However, what determines, on a given trial, the stationary state of the system? Based on the results shown above, we propose that it is the transient level of heterogeneity (that is, the heterogeneity at the onset of the pruning) what determines the probability that the network will maintain memory.

In order to explore this hypothesis, we first define g_Δ and m_Δ as the values

of g and m at the beginning of the pruning, that is,

$$g_\Delta \equiv g(t = \Delta), m_\Delta \equiv m(t = \Delta). \tag{4.14}$$

These definitions allow us to explore how the stationary state depends on the transient evolution of the system. In particular, for each value of $\widetilde{\Delta}$ and κ_0 we measure the onset heterogeneity g_Δ and the stationary overlap $\overline{m}$. In figure 4.5a, b we show, respectively for models A and B, the measured values of $\overline{m}$ as a function of g_Δ, with each curve corresponding to a fix value of κ_∞ and varying $\widetilde{\Delta}$, namely $\overline{m}\left(g_\Delta\left(\widetilde{\Delta}\right)\right)$. These panels show up two main findings. Firstly, a continuous transition from the heterogeneous memory state to the homogeneous noisy one as a function of g_Δ; and, secondly, a collapse of the curves for different κ_0. In consequence, g_Δ determines whether the network will be able to maintain memory once the pruning begins: high onset heterogeneity (small g_Δ) implies stationary memory, whereas low heterogeneity (high g_Δ) implies a stationary noisy state. These results are independent of κ_0 and of the model used, indicating that g_Δ is a strong indicator of stationary memory.

Notice that g_Δ depends not only on κ_0 and $\widetilde{\Delta}$, but also on m_Δ, since the rewiring process only promotes heterogeneity when the network displays memory. This is shown in figure 4.5c, d, where we display $\overline{m}\left(m_\Delta(\kappa_0)\right)$, with each curve corresponding to a given value of $\widetilde{\Delta}$, and respectively for models A and B. Since m_Δ does not unequivocally determine the stationary state, the curves do not collapse in this case. What it is obtained is a quadratic dependence of $\overline{m}$ on m_Δ, indicating an optimal value of transient memory of $m_\Delta \approx 0.5$. This emerges because $m_\Delta \approx 0.5$ strongly correlates with a minimum g_Δ, so that the value of $\widetilde{\Delta}_{\min}^a$ necessary for a stationary memory state is minimal for this value. In this sense, if $m_\Delta \ll 0.5$, there is no transient memory because κ_0 is too small and, therefore, there is insufficient heterogeneity. On the other hand, if $m_\Delta \approx 1$, this is so because κ_0 is large and the network is still very homogeneous when pruning begins. In both cases, the network evolves towards a homogeneous configuration. Note that this qualitative result does not depend on the particular definition of d_0 since it holds for both models A and B.

4.5   Discussion

In this chapter we have analyzed the fundamental role of the high synaptic-density period that the brain undergoes during infancy. In order to do so, we have made use of the adaptive network model for synaptic pruning defined in chapter 2, and first presented in (Millán et al., 2018c). The model creates a dependence of the final network structure and performance on the transient synaptic density, as one should probably expect in Nature. In this model, the introduction of a high fixed-density transient allows for network heterogenization and for the settlement of a memory state under noisy conditions. We have

analyzed in detail a point of the (T, α) phase space corresponding to the bi-stablity area between heterogeneous memory and homogeneous noisy states (as depicted on figure 2.4), where the system is most sensitive to the details of the evolution and the initial conditions. This happens to correspond to high noise T and also to large α, so that the system can heterogenize.

In these conditions, we have found that the model exhibits a discontinuous (first order) phase transition as one varies the length of the transient period of fixed density, $\widetilde{\Delta}$, and the value of this density, κ_0. In fact, there is a quadratic effect of κ_0, such that medium values provide a faster and more stable evolution towards a memory stationary state and there is an optimal κ_0 that optimizes the evolution into such a state. Therefore, our results could explain why real world networks such as those in the brain do not create enormous numbers of synapses to begin with during early development. Moreover, being able to achieve eventual good performance with a limited density would also be preferable in terms of energy consumption. We have also shown that the transient heterogeneity determines the stationary state of the system. Given the aforementioned feedback loop, this depends on the transient memory m_Δ and κ_0, so that the stationary state of the system is ultimately determined by its physiological history.

We have also analyzed the robustness of the results to details of the model and the validity of the approximations considered. In particular, we have found a more realistic approximation such that the density of synaptic growth and death during the transient period of fixed connectivity is proportional to this connectivity. We have found that the qualitative behavior of the system does not depend on these details. Namely, there is also a discontinuous transition from a homogeneous non-memory state to a heterogeneous memory one as the duration Δ of the transient period increases, whereas there is a non-linear dependence on κ_0, and the stationary state of the system is ultimately determined by g_Δ. Therefore, the results presented in this chapter – namely the benefits of a transient high connectivity period, the second order effect of κ_0 and the crucial effect of g_Δ on the stationary state – are robust with respect to microscopic details of the model.

A question this work clarifies is why brain development produces an initial growth of a great many synapses which are then gradually pruned. If the final density is optimal for energy consumption, why should one go through a transient state of twice this density? Our neural network with an evolving structure based on some simple biological considerations shows that the memory performance of the system does indeed depend on whether it passed through a transient period of relatively high synaptic density. A feedback loop thus emerges between neural activity and network topology such that, beginning with a random network, a transient state of high density can allow for the subsequent pruning of synapses as the topology is optimized for memory performance. Why, though, should the brain not begin with both the low density and

high heterogeneity needed for good memory performance? We conjecture that much less genetic information is needed to build a random neural network that is subsequently shaped by its dynamics (under the influence of actual environmental conditions), than to specify a particular structure. This would also be a more robust developmental path. And why not begin with an even higher initial density? Apart from energetic considerations, we have also seen that there is an optimal initial synaptic density for a high performance neural network to emerge.

As in the previous chapters, the results presented here may serve as a starting point and a very suitable theoretical framework for studying the relationship that may exist between certain neurological disorders that appear during brain development, such as childhood autism and schizophrenia in young adults, and different synaptic pruning profiles, as has recently been suggested (Tang et al., 2014; Afroz et al., 2016; Sekar et al., 2016).

Chapter 5

Complex Network Geometry and Frustrated Synchronization.

Brain networks develop in a (bounded) 3D space that affects its development and structure, a fact that is nonetheless typically ignored by *in-vitro* studies, which usually consider 2D substrates. Interestingly, however, it was recently shown that the dynamics of *in-vitro* neural networks is strongly dependent on the network geometry, and that neuronal cultures grown on 3D scaffolds are able to display more varied regimes of synchronization, with a more stable synchronized regime (Severino et al., 2016). However, the question of how synchronization phenomena depend on the dimensionality and geometrical properties of the underlying network is yet to be explored from the theoretical point of view, and results from such study could have strong implications for the understaing of complex enural systems like the brain. With the goal of helping fill this gap, in this chapter we reveal the rich interplay between the geometrical properties of a network and the synchronization dynamics of coupled oscillators on top of it. In order to do so, we make use of the theoretical framework of a simplicial complex model of manifolds called Complex Network Manifold (Bianconi and Rahmede, 2015). This model allows us to generate networks that combine a highly modular structure and small-world properties, as indicated by an infinite Hausdorff dimension, with a finite and tunable spectral dimension that is related to the inherent geometrical substrate of the network. Within this set-up, we demonstrate that the synchronization properties of a network are directly affected by its the spectral properties and we show that, due to their highly modular

structure, CNMs also have de-localized eigenvectors so they can support that states of frustrated synchronization. In particular, we show the emergence of large regions of frustrated synchronization for spectral dimension $d_s \leq 4$, and that the synchronized regime is more stable in $d_s = 4$ than for $d_s = 2, 3$. Interestingly, we also demonstrate that CNMs with a given integer spectral dimension d_s can be embedded in a $d_s - 1$-dimensional manifold. Consequently, cortical networks, embedded in a 3D space, could display a spectral dimension equal to four, the critical dimension for the onset of a global synchronous phase. The study presented here has been published in Millán et al., 2018a.

5.1 Introduction

As we have seen in the previous chapters of this thesis, it is a well-known fact that network topology strongly affects the dynamics and function of complex networks (Watts and Strogatz, 1998; Barabási and Albert, 1999; Dorogovtsev and Mendes, 2002; Boccaletti et al., 2006; Fortunato, 2010; Newman, 2011; Barabási et al., 2016). Recent studies have started to suggest that a geometrical perspective is also necessary, and growing attention has been devoted to analyze networks from a geometrical viewpoint (Barthélemy, 2011; Serrano et al., 2011; Bianconi, 2015; Clough and Evans, 2017). Consequently, there has been an increasing number of works aiming at unveiling the hidden geometry of networks using statistical mechanics (Boguná et al., 2010; Krioukov et al., 2010; Bianconi and Rahmede, 2015; Wu et al., 2015; Bianconi and Rahmede, 2016, 2017; Mulder and Bianconi, 2018; Silva et al., 2018), discrete geometry (Jost and Liu, 2014) and machine learning tools (Bronstein et al., 2017; Muscoloni et al., 2017), to name a few.

Characterizing the geometry of complex networks is particularly relevant for brain research (Bullmore and Sporns, 2009; Giusti et al., 2016), where the embedding in a three-dimensional space is essential to understand the wiring diagram characterizing the connections between brain regions – or connectome (Sporns, 2011; Vértes et al., 2012; Ercsey-Ravasz et al., 2013) – and also at a more microscopic neuronal level. Interestingly, recent experimental results have shown that the synchronization properties of neuronal cultures grown on $2D$ slices differ considerably from those grown on $3D$ scaffolds. The latter turn out to be much more likely to maintain synchrony and present two operating regimes: a highly synchronized and a moderately synchronized one (Severino et al., 2016). This result can be compared with results obtained in the framework of the Blue Brain project where it has been observed that pairs of neurons have more significant correlations in their dynamics if they belong to higher

dimensional structures (Reimann et al., 2017).

These results reveal that not only network topology but also network geometry plays a crucial role in determining the dynamical properties of a complex network. However, the connection between network geometry and dynamics has been so far mostly unexplored from a theoretical point of view. In this chapter, we provide a theoretical framework based on simplicial complexes (Petri et al., 2014; Bianconi and Rahmede, 2015; Wu et al., 2015; Bianconi and Rahmede, 2016; Giusti et al., 2016; Bianconi and Rahmede, 2017; Mulder and Bianconi, 2018; see also section 1.3.3) to investigate the effect of network geometry on synchronization dynamics. Simplicial complexes are generalized network structures that go beyond pair-wise interactions. They are formed not only by nodes and links, but also by triangles, tetrahedra, hypercubes, orthoplexes, etc. They are thus made up by discrete geometrical building blocks, making them ideal structures to investigate and model network geometry and topology (Bianconi, 2015; Giusti et al., 2016; Salnikov et al., 2018). Modeling network geometry with simplicial and cell complexes has been for long the practice in quantum gravity approaches, including Causal Dynamical Triagulations, Regge calculus or Tensor networks, to name a few (Oriti, 2001; Ambjórn et al., 2005; Lionni, 2018). More recently, simplicial complexes (and also their generalization, cell complexes, as discussed in chapter 6) have become very popular to model also complex systems ranging from brain networks to social networks (Bianconi, 2015; Giusti et al., 2016; Iacopini et al., 2018; Millán et al., 2018a; Petri and Barrat, 2018; Salnikov et al., 2018), in part supported by the fact that their geometrical properties are often retained if one considers their network skeleton, i.e. the network formed exclusively by their nodes and links.

Similarly, synchronization phenomena are the subject of extensive research in physical, biological, chemical and social systems (Pikovsky et al., 2003; Arenas et al., 2008). In the case of brain networks, synchronization is thought to be essential for the integration and coordination of distributed information across different brain areas (Varela et al., 2001). The emergence of brain rhythms has been reported both on EEG and fMRI recording of the brain, with different frequencies of synchronized activity allegedly related to different brain functions (see section 1.4.2). Moreover, some brain disorders such as schizophrenia, autism spectrum disorder, epilepsy and Alzheimer and Parkison disease have been related to abnormal neural synchronization autism and Alzheimer and Parkinson disease have been associated with abnormal neural synchronization (Uhlhaas and Singer, 2006).

The synchronization properties of a network are known to be influenced by the network topology (Chavez et al., 2005) and by its spectral properties (Barahona and Pecora, 2002; Donetti et al., 2005). For instance, the stability of a fully synchronized state is known to depend crucially on the ratio between the Fiedler eigenvalue (i.e. the smallest non zero eigenvalue) and the largest

eigenvalue of Laplacian (Barahona and Pecora, 2002; Donetti et al., 2005). In this regard, network geometries are typically characterized by having a Fiedler eigenvalue that goes to zero in the large-size limit or, equivalently, by a finite spectral dimension d_S (Rammal and Toulouse, 1983; Burioni and Cassi, 1996; Jonsson and Wheater, 1998; Burioni and Cassi, 2005; Durhuus et al., 2007), which characterizes the return time distribution of the random walk. For instance, Euclidean lattices in dimension d have spectral dimension $d = d_S$, which is also equal to the Hausdorff dimension of the lattice, $d_S = d_H$. However, in general networks can have non-integer spectral dimension d_S not equal to their Hausdorff dimension.

Interestingly, non-trivial synchronization phenomena have been related to complex network topologies. For instance, the emergence of *frustrated synchronization*, characterized by large spatio-temporal fluctuations of the synchronization order parameter, has been related to a complex network topology characterized by a hierarchical modular structure (Moretti and Muñoz, 2013). Similarly, also in hierarchical modular networks it has been shown the appearance of rare-regions of activity in the contact processes, in correspondence with the so-called *Griffith phase* (Villegas et al., 2014; Safari et al., 2017; Cota et al., 2018). However, so far the considered network structures have a finite Hausdorff dimension (Moretti and Muñoz, 2013) (i.e. they are large-world networks), whereas a large number of brain networks are known to be small-world, that is, to have an infinite Hausdorff dimension (watts1998collective,bullmore2009; see also section 1.2). Therefore, exploring whether such dynamical phase can appear in small-world networks has particular relevance in the field of neuroscience and neural computation.

In this chapter we demonstrate that a finite spectral dimension of geometrical networks can be combined with a complex modular network structure to give rise to frustrated synchronization and spatio-temporal fluctuations of the order parameter of the synchronization dynamics (Bianconi and Rahmede, 2015, 2016, 2017; Mulder and Bianconi, 2018). In this way, we provide a clear evidence of the important effect that network geometry has on the dynamics of complex networks. For this we make use of the mathematical framework of **Complex Network Manifolds** (CNMs), which is a particular case of the Network Geometry with Flavor model presented in chapter 1 (see Sec. 1.3.3). We also discuss here the geometrical, spectral and topological dimensions of CNMs, and we demonstrate that, as a result of their complex network geometry, CNMs can sustain frustrated synchronization for a large range of their parameter values, with the stability of this phase crucially depending on the network dimensionality. We finally show that the observed spatio-temporal fluctuations of the order parameter associated with the frustrated synchronization regime appear when the dynamics is strongly affected by localized eigenvectors, identifying "rare" regions of activity, and driving global oscillations of the synchronization global

order parameter.

5.2 Complex Network Manifolds

The framework of Complex Network Manifolds (CNMs) is a particular case of the Network Geometry with Flavor (NGF) model (see Sec. 1.3.3), corresponding to NGFs with flavor $s = -1$. Moreover, here we also select $\beta = 0$, so that there is not intrinsic heterogeneity of the nodes[1].

Therefore, the framework of CNM (Bianconi and Rahmede, 2015, 2016, 2017) consists on a non-equilibrium growing model of simplicial complexes of dimension d that generates discrete manifolds by subsequently gluing d-dimensional simplices along their $(d-1)$ faces. At each time t a new simplex is added to a $(d-1)$-face α with probability

$$\Pi_\alpha = \frac{1 - n_\alpha}{\sum_{\alpha'}(1 - n_{\alpha'})}, \tag{5.1}$$

where n_α is the incidence number of the face, indicating the number of d-dimensional simplices incident to it minus one.

Many structural properties of CNMs have been studied. For instance, the degree distribution $p(k)$ is exponential for dimension $d = 2$ and scale-free for $d > 2$. The exact asymptotic expression has been derived by Bianconi and Rahmede, 2017 (see appendix C, and it is given for $d = 2$ by

$$p(k) = \frac{1}{d+1}\left(\frac{2}{3}\right)^{k-d}, \tag{5.2}$$

with $k \geq 2$, whereas for $d > 2$ it is given by

$$p(k) = \frac{d-1}{2d-1}\frac{\Gamma\left[(1 + (2d-1)/(d-2)\right]}{\Gamma\left[d/(d-2)\right]}\frac{\Gamma\left[k - d + d/(d-2)\right]}{\Gamma\left[k - d + 1 + (2d-1)/(d-2)\right]}, \tag{5.3}$$

with $k \geq d$. It is easy to see that, for $k \gg 1$,

$$p(k) \approx k^{-\gamma}, \tag{5.4}$$

with

$$\gamma = 2 + \frac{1}{d-2}, \tag{5.5}$$

so that CNMs are scale-free for $d > 2$. In particular, for $d = 3$ we obtain $\gamma = 3$, whereas for $d = 4$, $\gamma = 5/2$. In figure 5.2.1a we show the agreement between the analytic expression given by Eqs. $C.1$ and $C.2$ (in appendix C) (dashed lines) and the computational results (data points).

---

[1]The codes for generating the Complex Network Manifolds, which are equivalent to the Network Geometry with Flavor $s = -1$ (Bianconi and Rahmede, 2016), can be found in this public repository (Bianconi, n.d.).
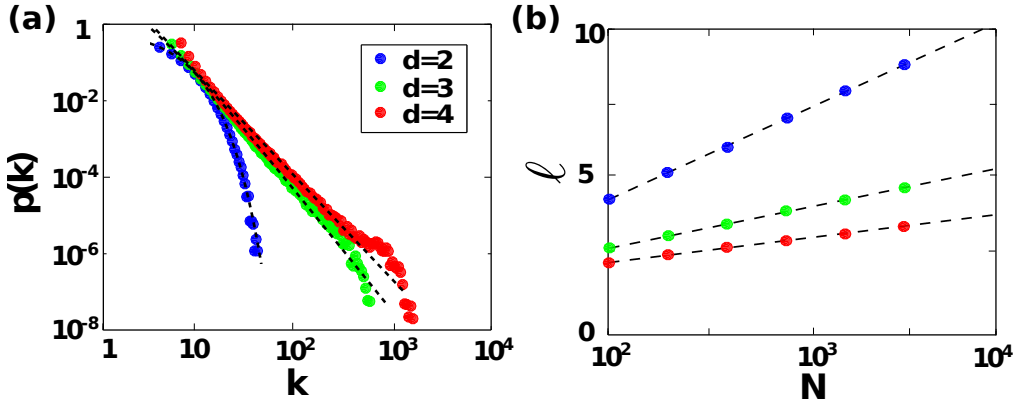
Figure 5.1: **Degree distribution and small-word properties of CNMs.**
The degree distribution $p(k)$ of CNMs of $N = 6400$ nodes and dimensions
$d = 2, 3$ and 4 is plotted in panel a. Points represent results from numeri-
cal simulations whereas dashed lines stand for the analytical result as given by
Eq. $C.1$ and $C.2$. The mean minimum path ℓ is plotted versus N for $d = 2$, 3, 4
in panel b. Data points are from simulation results whereas dashed lines cor-
respond to the logarithmic fit. Numeric results have been averaged over 100
network realizations in both panels.

5.2.1 Network dimensions

Topological dimension

CNMs are small-world networks with an infinite Hausdorff dimension d_H. This
can be seen by the logarithmic scaling of the mean minimum path (or charac-
teristic path length, as defined in table 1.1) ℓ between the nodes of the network
with the network size N, as shown in figure 5.2.1b, where points represent data
from numerical simulations of CNMs of dimension d and the solid lines stand
for the best logarithmic fit, as given by

$$\ell = a_d \log(N) + b_d. \tag{5.6}$$

The parameters from the fit are shown in table 5.1, and they clearly indicate that
CNMs of higher dimension d have a average shortest distance that grows always
logarithmically with the network size N but with different constant factor a_d.

Geometric dimension

CNMs can either be considered as manifolds of dimension d with all the nodes
placed on the boundary of the manifold or as $D = d - 1$ dimensional manifolds
without boundary, as we go on to show. Consider first a CNM of dimension

d	a_d	b_d	R^2
2	2.93(3)	$-1.45(9)$	0.983
3	1.32(2)	0.17(4)	0.964
4	0.78(1)	0.79(4)	0.954

Table 5.1: Fitted parameters a_d and b_d determining the logarithmic growth of the mean minimum path ℓ of CNMs of dimension d according to Eq. 5.6.
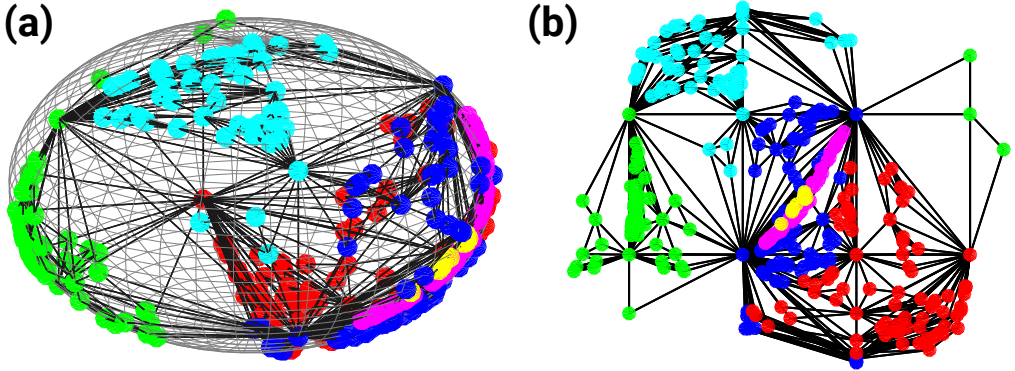

Figure 5.2: **Complex Network Manifold's dimensions.** The CNM constructed from d-dimensional simplicies with $d = 3$ can be interpreted either (panel a) as a $d = 3$ dimensional manifold with boundary (topologically equivalent to a sphere) or alternatively as a $D = 2$ dimensional manifold without boundary tessellating the $D = 2$ dimensional surface of the sphere. Panel b represents the projection of the $D = 2$ manifold on the plane with the Cartesian coordinates indicating the azimuth and elevation of point on the surface of the sphere, respectively. Note that for better visualization purposes we have omitted the links connecting nodes at the opposite sides of the plane. The node colors indicate different communities detected using the Gen-Louvain algorithm (Blondel et al., 2008; Mucha et al., 2010).

$d = 3$. The CNM can be embedded in a $d = 3$ dimensional sphere of radius one without any crossing of the faces. To this end, we inscribe the first tetrahedron (which is regular) in the 3D sphere, so that every node is placed on the sphere and at equal distances. Then, we glue every added tetrahedron to the corresponding existing face, and deform it so that the new node is also on the surface of the sphere. In this picture the CNM constitutes a 3D bounded manifold, with the links inside the ball and the nodes on the surface.

Interestingly, in this embedding all the nodes of the CNM are on the $D = 2$ dimensional surface of the sphere, so that the network can also be interpreted as a tessellation of the $D = 2$ dimensional manifold formed by the surface of the $d = 3$ sphere (see figure 5.2). In this $D = 2$ triangulated space, the elementary

move of adding a new tetrahedron corresponds to the placement of a new node in the middle of a randomly selected triangle of the $D = 2$ triangulation, and the establishment of three new links between the new node and each of the nodes of the selected triangle (in which case not only nodes but also links are on the 2D sphere). Most notably, this construction reveals that CNMs in $d = 3$ are random Apollonian Networks (Andrade Jr et al., 2005; Andrade and Herrmann, 2005; Zhang et al., 2006).

Similarly, a CNM of dimension $d = 4$ can be interpreted either as a 4D manifold with boundary or as the tessellation of a $D = 3$ space, in which case all the links are super-imposed to the circumference. In this case, the addition of a new 4-simplex corresponds to the selection of a tetrahedron forming the tessellation of the $D = 3$ space, the placement of a new node in the middle of it, and the establishment of four new links between the new nodes and each of the existing nodes of the selected tetrahedron. Finally, a CNM of dimension $d = 2$ can be interpreted as a 2D manifold with boundary, with the nodes placed on the circumference and the links inside the circle; or as the tessellation of the $D = 1$ circumference.

Therefore, one can naturally associate both dimension d and dimension D of its natural embedding spaces to the CNM formed by simplices of dimension d.

5.2.2 Spectral and localization properties

The spectral properties of complex networks have been shown to be particularly relevant to reveal the interplay between network structure and synchronization dynamics on the network. However, less is known about the relationship between the spectral and geometrical properties of complex networks. With the aim to help fill this gap, here we characterize the spectral properties of the normalized Laplacian matrix **L** associated with CNMs of dimension d. **L** has elements

$$L_{ij} = \delta_{ij} - e_{ij}/k_i, \tag{5.7}$$

where e_{ij} define the adjacency matrix (with 0 entries for non-connected nodes and 1 entries for connected ones) and k_i is the degree of node i in the associated network skeleton.

The normalized Laplacian has real eigenvalues $0 = \lambda_1 \leq \lambda_2 \leq \ldots \leq \lambda_N$. In a large number of complex networks, the second smallest (or Fiedler) eigenvalue λ_2 remains finite as the network size increases. In this case, the network is said to present a *spectral gap*. On the contrary, CNMs, like regular lattices, have a spectral gap that approaches zero for large network sizes (see figure 5.3). This ensures that one can define the **spectral dimension** d_S (see box 1.2.1), which characterizes the power-law scaling of the density of eigenvalues $\rho(\lambda)$ for $\lambda \ll 1$
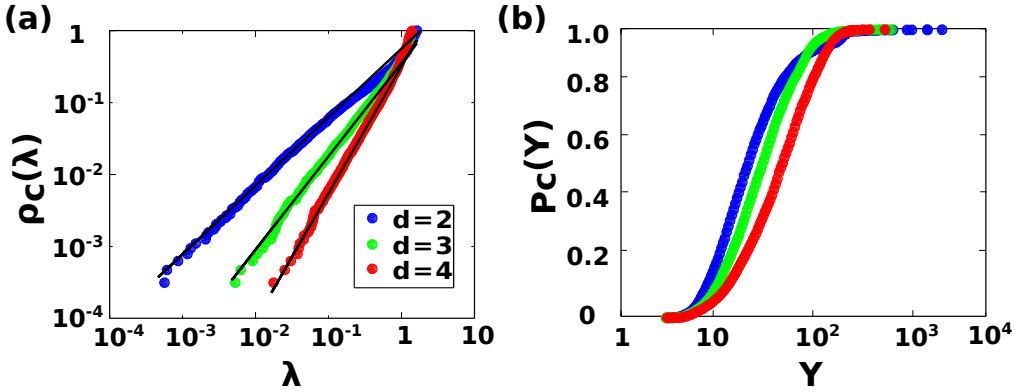
Figure 5.3: **Spectral properties of Complex Network Manifolds.** Panel *a* shows the cumulative distribution of eigenvalues $\rho_c(\lambda)$ for CNMs of dimension $d = 2, 3, 4$. Solid (black) lines indicate the power-law fit of $\rho_c(\lambda)$. Panel *b* shows the cumulative distribution $P_c(Y)$ of the participation ratio Y of the CNM modes (legend is the same as in panel *a*). Data are extracted from a single realization of CNMs of size $N = 6400$.

as (Rammal and Toulouse, 1983; Burioni and Cassi, 1996)

$$\rho(\lambda) \simeq \lambda^{d_S/2-1}. \tag{5.8}$$

d_s can be calculated starting from the associated cumulative distribution $\rho_c(\lambda)$ determining the probability that a random eigenvalue is less than λ, i.e.

$$\rho_c(\lambda) = \int_0^\lambda d\lambda' \rho(\lambda') \simeq \lambda^{d_S/2}. \tag{5.9}$$

For finite D-dimensional lattices, it holds that $d_S = D$ (where D is both the Euclidean and the Hausdorff dimension) but, in general, the spectral dimension does not have to coincide with the Hausdorff dimension of the network nor with the dimension of the space it tessellates (Rammal and Toulouse, 1983; Wu et al., 2015).

Remarkably, CNMs formed by d-dimensional simplices have spectral dimension

$$d_S \simeq d \tag{5.10}$$

as we have checked numerically for dimensions $d = 2, 3, 4$. Indeed, in figure 5.3*a*, we show the cumulative eigenvalue distribution $\rho_c(\lambda)$ and the fitted power-law behavior for small λ, which yields $d_S = 2.00(2)$ for $d = 2$, $d_S = 3.02(4)$ for $d = 3$, $d_S = 3.96(8)$ for $d = 4$.

The eigenvectors of the normalized Laplacian are also useful to reveal relevant properties of the CNMs. Given that the normalized Laplacian is an asymmetric matrix, it is characterized by a set of left $\mathbf{u}_L^\lambda$ and a set of right eigenvectors

$\mathbf{u}_R^\lambda$ which, in general, do not coincide. Left and right eigenvectors associated with the same eigenvalue are normalized according to the condition

$$\sum_{i=1}^{N} u_{i,L}^\lambda u_{i,R}^{\lambda'} = \delta_{\lambda,\lambda'}. \tag{5.11}$$

The localization of any given eigenvector can be quantified using the **participation ratio** Y, which is an indicator of the number of nodes on which such an eigenvector has a significantly different from zero value, i.e.

$$Y = \left[\sum_{i=1}^{N} \left(u_{i,L}^\lambda u_{i,R}^\lambda \right)^2 \right]^{-1}. \tag{5.12}$$

In figure 5.3*b* we show that a very large fraction of eigenvectors are localized on a small fraction of nodes, as indicated by a small value of their participation ratio Y compared with the total number of nodes of the network, N. This differs from what happens in regular lattices, where eigenfunctions (oscillation modes) are typically delocalized.

5.3   Synchronization dynamics

Synchronization of specialized groups of neurons is often regarded as a neural basis for binding and integrating distributed information in the brain (Sporns et al., 1989; Singer et al., 1997; Tononi et al., 1998), and it has been repeatedly reported both on EEG and fMRI recordings of brain activity. It is now commonly accepted that synchronization plays an important role in brain functioning and dysfunctioning (Glass, 2001; Varela et al., 2001; Schnitzler and Gross, 2005; Buzsaki, 2006; Uhlhaas and Singer, 2006) and some brain disorders such as schizophrenia, epilepsy, autism and Alzheimer and Parkinson disease have been associated with abnormal neural synchronization (Uhlhaas and Singer, 2006). For instance, a prominent example of pathophysiologic neuronal synchronization are epileptic seizures appearing in epilepsy, which affects approximately 1% of the world's population (Duncan et al., 2006).

The topological organization of brain connectomes has an important role in enabling complex functionality and synchronization, and the wiring architecture of mammalian and nematode neural systems shows several network attributes of an efficient processing and communication structure (Kaiser and Varier, 2011; Van Den Heuvel and Sporns, 2011), as discussed in section 1.2. For instance, a number of recent computational models of epileptic activity take into account the connectivity patterns of neural networks seen in the epileptic brain (Netoff et al., 2004; Percha et al., 2005; Dyhrfjeld-Johnsen et al., 2007; Morgan and Soltesz, 2008). Together with findings obtained from an *in-vitro* study (Srinivas et al., 2007), these stress the importance of non-random synaptic topologies for

hyper-excitability and synchronization, as well as for the emergence of certain types of epileptic seizures. Network approaches are also expected to help interpreting the complex synchronization phenomena seen on the EEG of epilepsy patients (Wendling et al., 2005; Feldt et al., 2007). However, little is known about the effect of the network dimensionality on the emerging synchronization phenomena. Consequently, here we go on to study the synchronization properties of coupled oscillators running on top of CNMs as a function of the network dimensionality.

5.3.1 Synchronization model

Here we make use of the Kuramoto model (Kuramoto, 1975) to study synchronization phenomena. This model is commonly used in brain research to simulate the interaction of cortical brain areas by means of coupled phase oscillators, as a way to model brain interactions through synchrony. Simulation studies employing the Kuramoto model have investigated synchronization patterns in the cortical brain networks of the cat (Gómez-Gardeñes et al., 2010), the macaque (Honey and Sporns, 2008) and the human (Kitzbichler et al., 2009; Villegas et al., 2014), for instance, showing correspondence with resting-state functional data supportive of the applicability of the model (Cabral et al., 2014; Vuksanović and Hövel, 2014).

The oscillators obey a normalized Kuramoto dynamics (Kuramoto, 1975; Strogatz, 2000; Pikovsky et al., 2003; Acebrón et al., 2005; Arenas et al., 2008). This is a particular case of the Kuramoto model presented in chapter 1 (section 1.4.2), so that the phase θ_i of each node changes in time according to

$$\dot{\theta}_i(t) = \omega_i + \sigma \sum_{j=1}^{N} \frac{e_{ij}}{k_i} \sin(\theta_j - \theta_i), \tag{5.13}$$

where σ is the control parameter tuning the overall coupling strength, and ω_i is the node's internal frequency, which is independently drawn from a normal distribution with mean 0 and variance 1, i.e. $\mathcal{N}(0,1)$ [2]. This definition corresponds to a specific case of the Kuramoto model in which the coupling strength between each pair of oscillators depends only on the degree of the input node: $\sigma_{ij} = \sigma/k_i$. This is done in order to attenuate the effect of the heterogeneous degree distributions and to emphasize that of network geometry.

In order to quantify the degree of synchronization, we employ the standard

---

[2] Previous studies on frustrated synchronization on complex networks have shown that whereas the particular choice of the distribution can affect quantitatively the phase transition between an asynchronous and a synchronous phases, its qualitative properties are quite robust (Villegas et al., 2014).

Kuramoto order parameter, defined as in Eq. 1.26, namely

$$Z(t) = R(t)e^{i\phi(t)} = \frac{1}{N}\sum_j e^{i\theta_j(t)}, \tag{5.14}$$

where $R(t) \in [0,1]$ is a real variable (function of t) that quantifies the level of global synchronization, and $\phi(t)$ gives the average global phase of collective oscillations (Kuramoto, 1975; Watts and Strogatz, 1998; Pikovsky et al., 2003).

   Several previous works have analyzed the effect that the underlying network topology has on the synchronization properties of Kuramoto oscillators:

   i) In fully connected networks, as well as in random Poissonian networks, the dynamics of the Kuramoto model yields a continuous phase transition from an incoherent state (with $R \simeq 0$) to a coherent one (with $R \simeq 1$) at the critical coupling σ_c (Kuramoto, 1975; Strogatz, 2000; Acebrón et al., 2005).

   ii) In regular lattices of dimension d it has been shown that global synchronization is only possible for $d > 4$; in dimensions $2 < d \leq 4$ only entrained frequency synchronization, but not phase synchronization, is observed, whereas in dimension $d \leq 2$ synchronization is not observed (Hong et al., 2005; Hong et al., 2007).

Furthermore, as mentioned above, it has been recently shown that also a regime of frustrated synchronization – akin to a Griffith phase (Moretti and Muñoz, 2013) – characterized by global oscillations of $R(t)$, can emerge in complex networks with hierarchical and modular structure (Villegas et al., 2014). This regime has been previously associated only with large-world networks, i.e. networks with a finite Hausdorff dimension (Moretti and Muñoz, 2013). In what follows we illustrate that it is the network spectral dimension what mostly determines the resulting synchronization properties, so that small-world networks – with an infinite Haussdorf dimension – of which CNMs are an example here, can also display a regime of frustrated synchronization.

5.3.2   Synchronization and Frustrated Synchronization

Numerical analysis of the Kuramoto dynamics on CNMs reveals, for a wide range of coupling values, a frustrated synchronization phase in which the global order parameter has large temporal fluctuations. In figure 5.4 we show the global order parameter $R(T_f)$ calculated at large times T_f for a given fixed CNM of size N and given internal frequencies $\{\omega_i\}_{i=1,2,...,N}$, and for different values of the coupling σ; the same figure (bottom panels) also shows some examples of typical time series of the global order parameter $R(t)$ for $D = 1, 2, 3$[3]. One can observe

---

[3]In the electronic supplementary material of Millán et al., 2018a we show activity movies depicting the oscillator dynamics on top of the CNMs for some representative cases.
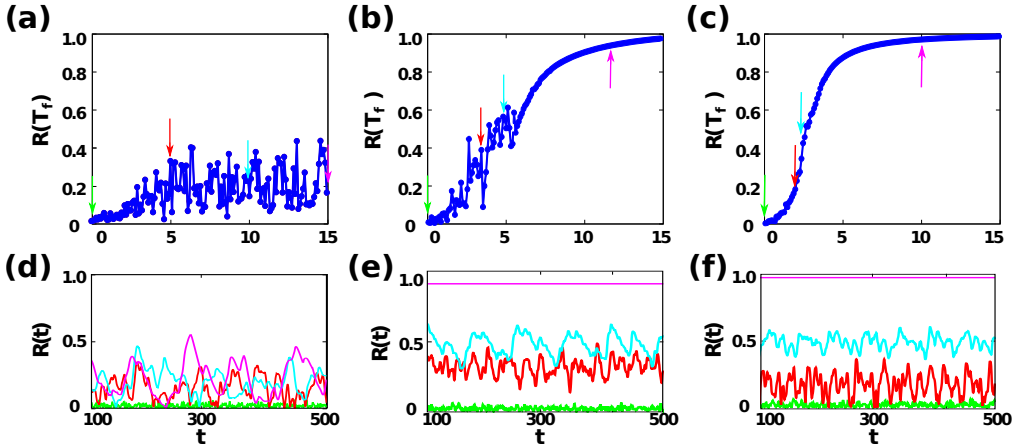
Figure 5.4: **Frustrated synchronization. (a-c)** Synchronization order parameter $R(T_f)$ plotted versus the coupling strength σ respectively for $D = 1$, $D = 2$ and $D = 3$, for a single network realization of $N = 1600$ nodes. Here, we have taken $T_f = 500$ in all graphs. **(d-f)** $R(t)$ time series respectively for $D = 1$, $D = 2$ and $D = 3$, for σ values as indicated with the arrows in the corresponding $a - c$ panels. Integration of system dynamics are carried out using the MATLAB ODE45 function, which uses a non-stiff 4-th order integration algorithm with adaptive steps.

that there are regimes (of values of the coupling strength σ) in all dimensions where the synchronization dynamics does not reach a steady state with small fluctuations around a mean value. However, the capability of the network to maintain a synchronized state depends on its dimension: while for $D = 1$ a synchronized steady state is never reached, for $D = 3$ a synchronized phase is observed (on a finite network) for large values of the coupling σ between the oscillators. The synchronization properties in the case $D = 2$ reveal an intermediate scenario with respect to the cases $D = 1$ and $D = 3$, with a wide region of large oscillations of the global synchronization parameter $R(T_f)$, i.e. frustrated synchronization.

In order to characterize the frustrated synchronization phase and to assess whether a true synchronization transition is observed for CNMs of $D = 2$ and $D = 3$, we have performed an extensive computational analysis of the considered Kuramoto dynamics averaged over different CNMs and different realizations of the internal frequencies. As a way to characterize network oscillations, in figure 5.5 the average order parameter R and its standard deviation σ_R, calculated after a transient time, are shown as a function of the coupling constant σ. The large values of the standard deviation indicate the region of the phase space in which frustrated synchronization is observed. Our finite size analysis (see figure 5.5) reveals the strong influence of the CNM dimension on the macroscopic

dynamics. In $D = 1$ global synchronization is never achieved for large network sizes, indicating that in the large-size (thermodynamic) limit synchronization is impossible. On the other hand, synchronization in CNMs with $D = 2$ and $D = 3$ is possible for small networks but gets delayed to higher couplings for increasing system sizes, and a much broader regime of large fluctuations is observed in the $D = 2$ case.

These numerical observations can be understood in connection with the spectral dimension of the corresponding CNM. In fact, by linearizing the Kuramoto dynamics, it is possible to extend the results obtained in Hong et al., 2005 for regular lattices to complex networks with finite spectral dimension (Mulder and Bianconi, 2018). These theoretical considerations reveal that for $d_S \leq 2$ networks cannot synchronize, whereas for $d_S > 4$ there is always a critical value of the coupling above which synchronization is possible. Finally, for $2 < d_S \leq 4$ global synchronization is not possible but an entrained synchronized state can be observed.

Interestingly, CNMs show that is possible to realize tessellations of a $D = 3$ space that have spectral dimension $d_S = 4$. These networks have the critical spatial dimension for the onset of the synchronized state. This suggests that it could be possible to have marginal synchronization in three-dimensionally embedded networks, such as cortical networks in the brain.

5.3.3 Spatio-temporal fluctuations of the order parameter

Here, we investigate further the regime of frustrated synchronization by characterizing the spatio-temporal fluctuations of the order parameter. As a matter of fact, CNMs are characterized by significantly modular structures that can be revealed by community detection methods. Due to the geometrical structure of the networks, nodes within each community are not only more densely connected, but they also are close in the embedding space. In order to give a visual representation of these communities, in figure 5.6 we visualize single instances of CNMs in $D = 1$, $D = 2$, $D = 3$ and plot, by employing different colors, the communities found by using a standard (Gen-Louvain) algorithm for community detection (Blondel et al., 2008; Mucha et al., 2010).

Given a community partition, one can explore the differences between the dynamical state of these communities with a "mesoscopic" synchronization parameter

$$Z_{mod,n}(t) = R_{mod}(t)e^{i\phi_{mod}(t)} = \frac{1}{|\mathcal{C}_n|} \sum_{i \in \mathcal{C}_n} e^{i\theta_i}, \qquad (5.15)$$

where $\mathcal{C}_n$ is the set of nodes in the nth community and $|\mathcal{C}_n|$ indicates the total number of nodes in the community. Here,

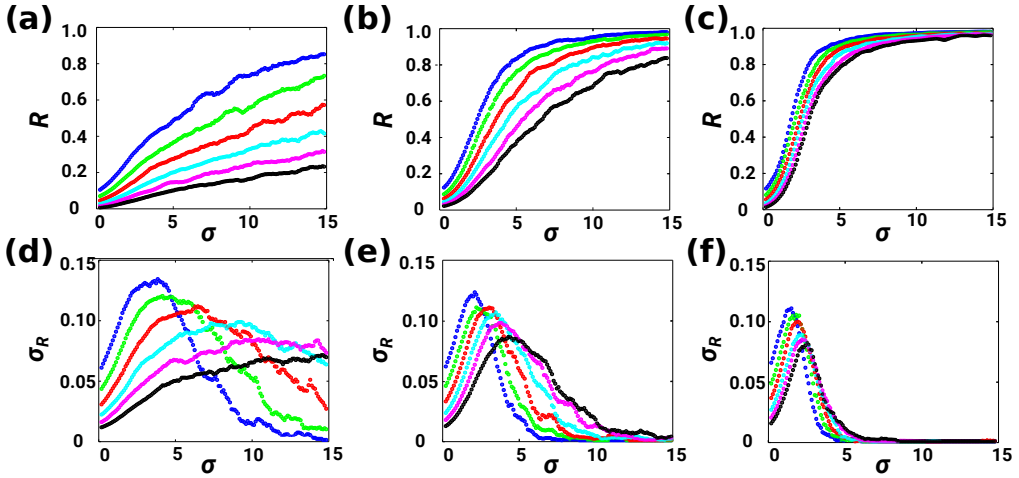$$R_{mod}(t) = |Z_{mod}(t)| \qquad (5.16)$$

Figure 5.5: **Synchronization transition. (a-c)** Synchronization order parameter R, and **(d-f)** its variance σ_R for $D = 1$ **(a,d)**, $D = 2$ **(b,e)** and $D = 3$ **(c,f)**. Different lines are drawn for different networks sizes: $N = 100$ (blue), 200 (green), 400 (red), 800 (cyan), 1600 (pink) and 3200 (black). The data are averaged over 50 realizations of the CNMs and the internal frequencies. A finite size scaling analysis shows decay in the synchronization order parameter with network size for every dimension (from 2 to 4) indicating that synchronization fades away in the infinite-network-size (thermodinamic) limit (Hong et al., 2007).

is a real variable taking values in the range $[0, 1]$.

Figure 5.7 displays the trajectory of $Z_{mod}(t)$ in the complex plane for some exemplary modules of CNMs in $D = 1$, 2, and $D = 3$, for coupling values that maximize σ_R as indicated in the caption. In these plots, a circular trajectory describes a situation in which $R_{mod}(t)$ is constant in time, with full synchronization of the module corresponding to $R_{mod}(t) = 1$. Random trajectories around $(0,0)$ describe unsynchronized modules. Partially synchronized modules, on the other hand, may describe more complex, i.e. chaotic, trajectories. We can distinguish between trajectories that oscillate within a circular crown of relatively large radius, in which $R_{mod}(t)$ oscillates between different states of partial synchronization, and trajectories that visit the center (unsynchronized state) too.

Figure 5.7 also displays the time series $R_{mod}(t)$ and the spectral decomposition $S(f)$ of the temporal series $R_{mod}(t) - \langle R_{mod}(t) \rangle$ for the considered exemplary modules. Interestingly, the spectral decomposition shows that, whereas some frequencies are in fact dominant, different modules can oscillate in rather different ways, indicating diverse synchronization states.

This numerical analysis reveals the relevant spatio-temporal fluctuations ob-
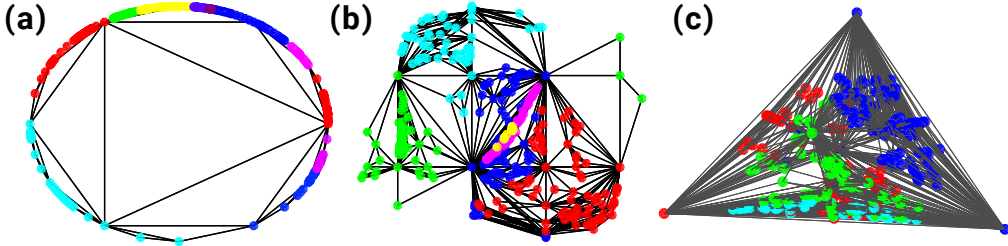
Figure 5.6: **Geometric representation and community structure of Complex Network Manifolds.** CNMs of $N = 400$ nodes and dimension $D = 1$ **(a)**, $D = 2$ **(b)** and $D = 3$ **(c)** are visualized and their corresponding community structures, as detected using the Gen-Louvain algorithm (Blondel et al., 2008; Mucha et al., 2010), are indicated by different colors. $D = 2$ and $D = 3$ CNMs are displayed by using their holographic representation, as indicated in section 5.2.1. In $D = 2$ the 2-dimensional coordinates indicate the elevation and azimuth of the nodes on the surface of a sphere, respectively. Finally, the $D = 1$ CNM is represented on a bounded 2-dimensional manifold. The holographic 1-dimensional representation is equivalent to this one but all links should be superimposed on the circumference.

served in the frustrated synchronization phase where different modules synchronize at different frequencies. Due to the geometrical structure of CNMs, these modules correspond to spatially localized regions.

5.3.4 Communities and localized eigenvectors

In order to reveal the relation between the community structure of CNMs and their spectral decomposition, we have characterized the localization properties of the eigenvectors on the network communities. To this end we have evaluated for each eigenvector λ the **community participation ratio Y_Q**, defined as

$$Y_Q = \left[\sum_{n=1}^{C} \left(\sum_{i \in \mathcal{C}_n} u_{i,L}^{\lambda} u_{i,R}^{\lambda} \right)^2 \right]^{-1}, \qquad (5.17)$$

where $\mathcal{C}_n$ indicates the nth community and C is the total number of communities. The community participation ratio $Y_Q \in [1, C]$ indicates the number of communities on which the eigenmode is localized. Figure 5.8 indicates that a large number of eigenvectors are localized in one or a few communities. Thus, diverse modes are activated at different communities (and at different local coupling strengths), justifying the emergence of local patches of synchronization and overall frustrated synchronization. This therefore explains the fact that in
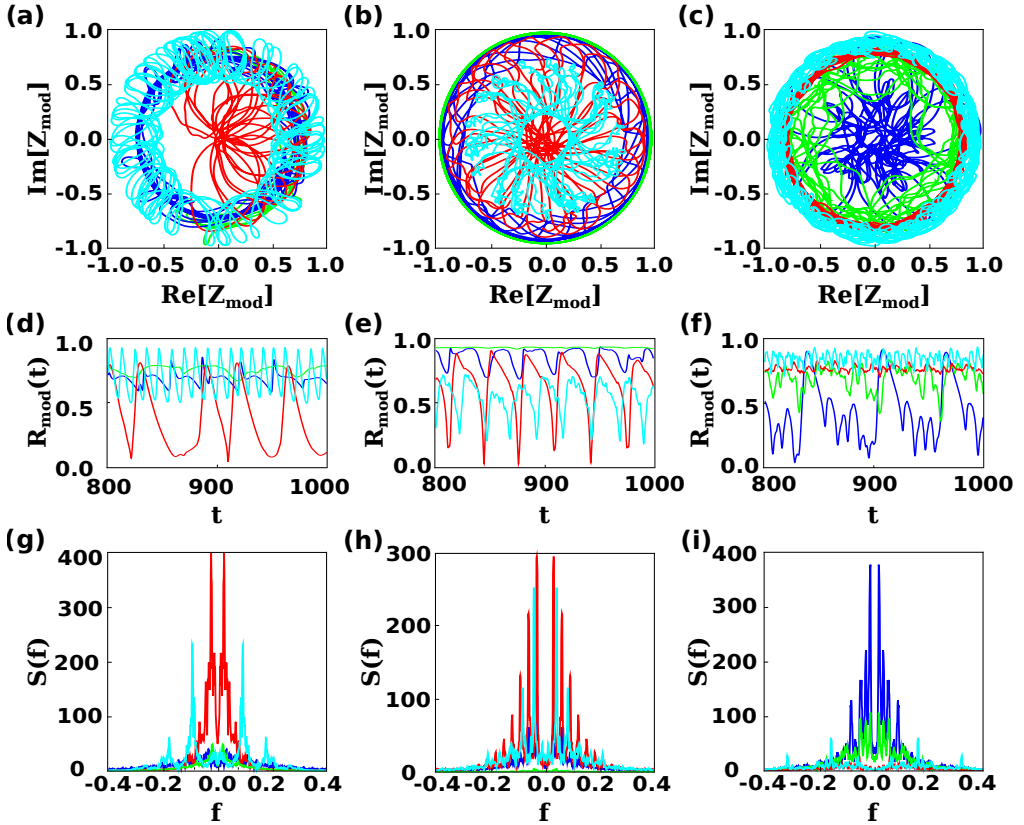
Figure 5.7: **Spatio-temporal fluctuations of the order parameter. (a-c)** Representative plots of the trajectory of the system on the phase space defined by $\mathrm{Re}[Z_{mod}], \mathrm{Im}[Z_{mod}]$ respectively for $D = 1$, $\sigma = 5.0$ (a), $D = 2$, $\sigma = 3.5$ (b) and $D = 3$, $\sigma = 3.0$ (c). **(d-f)** Corresponding time series of $R_{mod}(t)$, respectively for panels *a-c*, with the time t in seconds. **(g-i)** Spectral decomposition $S(f)$ of the previous time series, with the frequency f in units of $10^3[t]^{-1}$, respectively for $D = 1, 2, 3$.

the frustrated synchronization phase we observe a dynamics highly correlated with the modular structure of the network.

5.3.5   Coarse graining of the frustrated synchronization dynamics

As we have discussed on chapter 1, brain activity is typically measured by coarse graining brain dynamics to the level of brain regions and constructing a correlation matrices. Interestingly, different experiments might start from larger of smaller partitions of the brain, corresponding to different levels of coarse graining of the bottom level neuronal dynamics. Here we investigate the effect
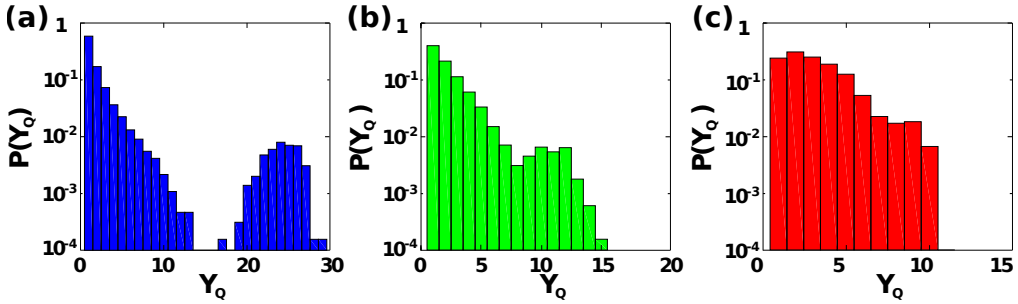
Figure 5.8: **Localization of the eigenmodes. (a-c)** Distribution $P(Y_Q)$ of the community participation ratio Y_Q of a single realization of $N = 6400$ nodes of a CNM respectively $D = 1$, 2 and 3. The total number of communities in these networks are: 30 (a), 18 (b) and 12 (c). Observe that Y can be larger in lower dimensions; this is because the modularity is smaller in lower dimensions and the community-detection algorithm divides the network in more communities. Modularity analyses are performed via the Generalized Louvain algorithm (Blondel et al., 2008; Mucha et al., 2010).
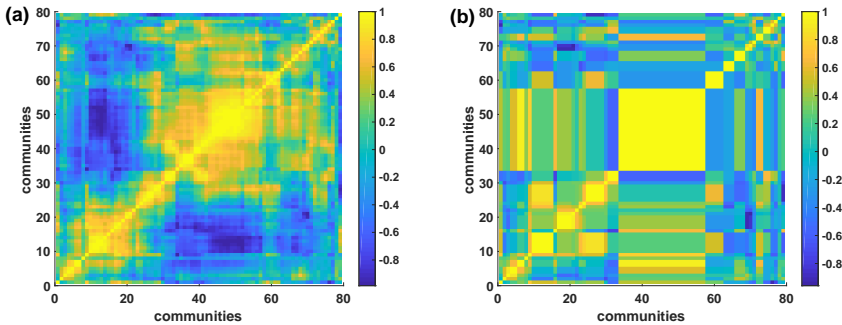
Figure 5.9: **Correlations between modules and coarse graining of the frustrated synchronization dynamics.** The matrix of Pearson correlations among the dynamical state of each pair of communities is reported for a fine grained partition **(a)** and a coarse grained one **(b)** of a CNM of $N = 1000$ nodes and dimension $D = 2$.

of coarse graining the frustrated synchronization dynamics on CNMs by using the local order parameter $R_{mod,n}$, which describes the internal synchronization of each module of the CNM, to compare the synchronization dynamics at different levels of network coarse graining.

Consequently, we run twice the Gen-Louvain algorithm in order to obtain a fine partition into modules of the CNM (with $D = 2$), whereas retaining high modularity. This fine-grain partition is formed by 79 communities and has $Q = 0.66$. We then measure the Pearson correlation coefficient between

the activity (as indicated by $R_{mod,n}$) of every pair of modules (see figure 5.9*a*). Subsequently, we coarse grain further these modules by reducing their number to about one half, by considering the aggregation generated by running a single linkage clustering to the correlation matrix (see figure 5.9*b*). The resulting coarse grained partition is formed by 30 communities and has $Q = 0.60$.

We observe that the modularity of the coarse grained partition remains high, thus revealing once more the coupling between the synchronization dynamics and the network topology. Moreover, we find that the coarse grained dynamics remains non-trivial, as revealed by a complex correlation matrix, indicating a sort of invariance under network hierarchical coarse graining. A similar behavior of the dynamics under coarse graining is observed in the frustrated synchronization phase of CNMs of other dimensions D.

5.4   Discussion

In this chapter we have shown the rich interplay between network geometry and synchronization dynamics by investigating the Kuramoto model running on top of Complex Network Manifolds (CNMs). We have shown that these networks – defined by discrete manifolds – combine the small-world property with a highly modular structure in which frustrated synchronization characterized by spatio-temporal fluctuations of the order parameter of the synchronization dynamics emerge (Bianconi and Rahmede, 2015, 2016, 2017; Mulder and Bianconi, 2018). Consequently, they provide an ideal theoretical setting to explore the interplay between network geometry and brain dynamics.

In this chapter we have first presented (some of) the geometrical, spectral and topological properties of CNMs build in dimension d. In doing so we have illustrated how a CNM build in dimension d can be seen as d-dimensional manifold with boundary (in which the nodes are placed), or equivalently as the tessellation of a $D = d - 1$ closed manifold. Furthermore, we have shown that, despite being small-world (that is, with an infinite Hausdorff dimension), CNMs have a spectral dimension equal to that of the embedding space, $d = d_S$, as lattices do. Interestingly, however, whereas the eigenvectors of lattices are de-localized over the network, CNMs have a hierarchical-modular structure and consequently their eigenvectors are localized in the network communities.

Given the determinant role of the spectral dimension of a network on its emergent synchronization capabilities, we have then compared the synchronization properties of CNMs of different dimensions. In particular, we observe that both CNMs with $D = 3$ and $D = 2$ sustain a regime of frustrated synchronization where spatio-temporal fluctuations of the order parameter are observed. Consequently, our work in this chapter reveals that non-trivial synchronization states can emerge even in small-world networks, with an infinite topological dimension, provided that the spectral dimension is finite. In this regime, network

modules are characterized by different synchronization frequencies. However, finite CNMs in $D = 3$ are much more favorable to sustain synchronized states than CNMs in $D = 2$. Regions of frustrated synchronization provide an ideal substrate for complex brain behavior, large dynamical repertoires, and optimal trade-offs between local segregation and global integration (Villegas et al., 2014).

Moreover, our study shows evidence that CNMs that can be embedded in dimension $D = 3$ may have spectral dimension $d_S = 4$, i.e. the critical spectral dimension for the onset of a global synchronous phase. This allows us to observe both a fully synchronized regime and a frustrated synchronization regime on a finite network. These results help shedding light on the experimental finding that 3D scaffolds of neuronal cultures favor neuronal network dynamics, as recorded in calcium activity experiments, with respect to 2D geometries. They further support the hypothesis that some relevant features of brain dynamics are a consequence of its 3D topology, as experimentally observed by Severino et al., 2016.

We finally show that the observed spatio-temporal fluctuations of the order parameter associated with the frustrated synchronization regime appear when the dynamics is strongly affected by localized eigenvectors. These identify "rare" regions of activity, and drive the global oscillations of the synchronization global order parameter. Consequently, on a wider perspective the work presented in this chapter reveals the important role of the spectral dimension and the localization of eigenvalues in promoting the frustrated synchronization phase. Moreover, it opens new research lines to relate network geometry and brain dynamics. In particular, whereas most previous studies have focused on the topological structure of the networks, these findings indicate that the spectral properties of cortical networks may also play a fundamental role in determining its synchronization abilities. In the following chapter we provide a theoretical framework for the numerical results presented here.

Chapter 6

Synchronization in Network Geometries with Finite Spectral Dimension

Recently there is a surge of interest in characterizing network geometry and topology and their effect on the dynamics running on top of them. This might be particularly relevant for the case of neural dynamics, in which the underlying network of connections is greatly influenced by the 3D limited space where it develops. In this chapter we show that the spectral dimension plays a fundamental role in establishing a clear relation between the topological and geometrical properties of a network and its dynamics. Specifically, we explore the role of the spectral dimension d_s in determining the synchronization properties of the Kuramoto model. We show that the synchronized phase can only be thermodynamically stable for spectral dimensions above four and that phase entrainment of the oscillators can only be found for spectral dimensions greater than two. Given that in the previous chapter we showed that networks with $d_s = 4$ can be embedded in a 3D space, this implies that cortical neural networks can have the critical dimension for the onset of full synchronization, while also being able to display regimes of partial synchronization. In order to prove the validity of our analytical predictions, we finally analyze the emerging synchronization phenomena on an extended version of the Complex Network Manifolds model used in chapter 5. As we show in this chapter, in this extended framework the networks can show a fractional spectral dimension too, giving rise to a more rich scenario. The work presented here has been published in Millán et al., 2019a.

6.1   Introduction

As we have seen in the previous chapter, CNMs made up by simplicial complexes have an infinite Hausdorff dimension together with a modular structure and a finite spectral dimension. Interestingly, it has been recently shown that is is also possible to built up CNMs considering not only simplicial complexes but also cell complexes made up by regular polytopes. This allows for more degrees of freedom and the creation of networks with different spectral and topological properties embedded in the same geometrical space (Bianconi and Rahmede, 2015, 2016, 2017). Much like CNMs made up by simplicial complexes, the network skeleton of cell complexes have also been show to display finite spectral dimension, heterogeneous degree distribution, the small-world property (infinite Hausdorff dimension $d_H = \infty$) and rich community structure on top of an emergent hyperbolic geometry (Mulder and Bianconi, 2018). This suggests that a finite spectral dimension is not only a very strong indication of a rich underlying geometry of network structures, but is also compatible with the main universal properties of complex networks, including brain networks (Bullmore and Sporns, 2009; Sporns, 2011; Reimann et al., 2017; see also 1.2).

Predicting the properties of synchronization dynamics on network geometries is a fundamental statistical mechanics problem that can be crucial to understanding the relationship between structural and functional brain networks (Ódor and Hartmann, 2018). Even though the interplay between complex network structure and synchronization dynamics has been extensively studied (Kuramoto, 1975; Strogatz, 2000; Barahona and Pecora, 2002; Pikovsky et al., 2003; Acebrón et al., 2005; Chavez et al., 2005; Arenas et al., 2008; Villegas et al., 2014; Expert et al., 2017; Cota et al., 2018), so far most works have only considered complex networks where the smallest non-zero eigenvalue of the Laplacian (the so called Fidler eigenvalue) is well separated from zero, i.e. the networks display a spectral gap and do not display a finite spectral dimension. Moreover, as we have largely argued in the previous chapter, and as recent work are starting to point out, network geometry can have a profound effect on synchronization dynamics (Severino et al., 2016; Reimann et al., 2017; Millán et al., 2018a). In particular, it has been found that neuronal cultures have synchronization properties strongly affected by their dimensionality, so that $2D$ neuronal cultures display weaker synchronization properties than neuronal cultures grown in $3D$ scaffolds (Severino et al., 2016). Additionally, large-scale numerical models of the brain generated in the framework of the Blue Brain project (Reimann et al., 2017) reveal that neurons in the brain can be thought of as forming a simplicial complex where neurons belonging to higher dimensional simplices are more correlated.

In chapter 5 we shown numerical evidence that the synchronization dynamics of Kuramoto oscillators (Kuramoto, 1975) running on top of CNMs are strongly

influenced by the dimensionality of the network, and that strong spatio-temporal fluctuations might appear depending on parameters (Millán et al., 2018a). In this chapter we shed light in these numerical results by developing a theoretical framework to investigate the synchronization properties of the Kuramoto model on networks with a finite spectral dimension.

In particular, in this chapter we first characterize the spectral properties of CNMs. We show that, despite having a finite spectral dimension as Euclidean lattices do, CNMs, with their underlying hyperbolic network geometry (Bianconi and Rahmede, 2017), are in fact very different from regular Euclidean lattices. Thus, we demonstrate that in general the spectral dimension of a CNM does not coincide with its geometrical dimension unless the underlying building blocks are simpleces. Furthermore, a notable difference with lattices is that the eigenvectors of CNMs are not in general de-localized over the network as the Fourier basis is on an Euclidean lattice. Instead, they can be very localized on a small fraction of nodes, reflecting the symmetries and hierarchical-modular structure of the network.

We then derive analytically general results on the predicted stability of the synchronized phase in the linear approximation of the Kuramoto model, depending on the spectral dimension of the underlying network. We thus extend the known result for Euclidean lattices of dimension d, where the synchronized phase of the Kuramoto model is thermodynamically stable only for $d > 4$ (Hong et al., 2005; Hong et al., 2007), and show that in complex networks with finite spectral dimension, the Kuramoto model can yield a synchronized state in the infinite network limit only for spectral dimensions $d_S > 4$. For spectral dimensions $d_S \in (2, 4]$ instead, only an entrained synchronization phase can be observed in the large network limit, whereas we also prove that for $d_S \leq 2$ the linear approximation is not valid due to the divergence of the correlations.

We analyze the effect of the localization of the eigenvectors of CNMs on the properties of the entrained phase synchronization, which is known to display strong spatio-temporal fluctuations of the order parameter (Millán et al., 2018a). This phase, also called frustrated synchronization (Villegas et al., 2014; Cota et al., 2018), has a very rich structure and can be interpreted as an extended critical region to be related to the smeared phase observed in critical phenomena on hyperbolic networks, such as percolation (Boettcher et al., 2012; Bianconi and Ziff, 2018). Finally, we test our analytical results numerically and show evidence that CNMs can display entrained phase synchronization also for dimensions $d > 4$ as long as that the spectral dimension $d_S \leq 4$.

6.2   The spectral dimension

Diffusion on network structures is typically studied using the properties of suitably defined Laplacian operators. On an undirected network of N nodes and

adjacency matrix $\mathbf{e}$, the normalized Laplacian $\mathbf{L}$ is a $N \times N$ matrix of elements

$$L_{ij} = \delta_{ij} - \frac{e_{ij}}{k_i}. \tag{6.1}$$

The normalized Laplacian operator is typically used for characterizing the random walk on a given network, or a diffusion dynamics in which, starting from each node i, there is a well defined probability of diffusion to every neighbor node. For instance, the random walk can be characterized by studying the equation for the probability $\pi_i(t)$ that a random walker is at node i at time t given by

$$\pi_i(t) = -\sum_j L_{ji} \pi_j(t-1). \tag{6.2}$$

Given the initial condition $\pi_i(0) = \delta_{i,i_0}$, this equation has solution

$$\pi_i(t) = \sum_\lambda e^{-\lambda t} u_i^\lambda v_{i_0}^\lambda, \tag{6.3}$$

where $\mathbf{v}^\lambda$ and $\mathbf{u}^\lambda$ are the right and left eigenvectors corresponding to the eigenvalue λ.

While $\mathbf{L}$ is asymmetric, an alternative definition of the normalized Laplacian considers the symmetric matrix $\hat{\mathbf{L}}$ of elements

$$\hat{L}_{ij} = \delta_{ij} - \frac{e_{ij}}{\sqrt{k_i k_j}}. \tag{6.4}$$

Interestingly, is it easy to show that the spectrum of $\mathbf{L}$ and the spectrum of $\hat{\mathbf{L}}$ are the same. Therefore, although the normalized Laplacian $\mathbf{L}$ is asymmetric, it has a real spectrum and non-negative eigenvalues. Additionally, the normalized Laplacian $\mathbf{L}$ has the following spectral properties:

i) $\mathbf{L}$ has always one zero eigenvalue $\lambda = 0$ with degeneracy equal to the number of components of the network. So if a network is connected the zero eigenvalue has degeneracy one.

ii) In a connected network the right and left eigenvectors corresponding to the zero eigenvalue $\lambda = 0$ are given by

$$\begin{aligned} v_i^{\lambda=0} &= \frac{1}{\sqrt{\langle k \rangle N}} (1, 1, \dots 1), \\ u_i^{\lambda=0} &= \sqrt{\langle k \rangle N} (\mu_1, \mu_2, \dots, \mu_N), \end{aligned} \tag{6.5}$$

where

$$\mu_i = \frac{k_i}{\langle k \rangle N} \tag{6.6}$$

is the invariant measure of the random walk on the network. The right $\mathbf{v}^\lambda$ and left $\mathbf{u}^\lambda$ eigenvectors of $\mathbf{L}$ are related to the eigenvectors $\mathbf{w}^\lambda$ of $\hat{\mathbf{L}}$ by

$$
\begin{aligned}
u_i^\lambda &= \sqrt{k_i} w_i^\lambda, \\
v_i^\lambda &= \frac{1}{\sqrt{k_i}} w_i^\lambda.
\end{aligned}
\tag{6.7}
$$

Therefore, if follows that the elements u_i^λ and v_i^λ are simply related as

$$
u_i^\lambda = k_i v_i^\lambda.
\tag{6.8}
$$

Moreover, since the eigenvectors $\mathbf{w}^\lambda$ are orthogonal, we have

$$
\sum_{i=1}^{N} u_i^\lambda v_i^{\lambda'} = \sum_{i=1}^{N} \left(w_i^\lambda \right)^2 = \delta(\lambda, \lambda').
\tag{6.9}
$$

iii) The effective number of nodes over which the λ eigenmode is localized can be measured using the **participation ratio** Y (Millán et al., 2018a; see also Sec. 5.2.2 in the previous chapter) defined as

$$
Y = \left[\sum_{i=1}^{N} (u_i^\lambda v_i^\lambda)^2 \right]^{-1} = \left[\sum_{i=1}^{N} (w_i^\lambda)^4 \right]^{-1}.
$$

In networks with distinct geometrical properties, the density of eigenvalues $\rho(\lambda)$ of the normalized Laplacian follows the scaling relation

$$
\rho(\lambda) \simeq \lambda^{d_S/2-1}
\tag{6.10}
$$

for $\lambda \ll 1$, where d_S is called the **spectral dimension** of the network. In d-dimensional Euclidean lattices, $d_S = d$. More in general, it can be shown that d_S is related to the Hausdorff dimension d_H of the network by the dis-inequalities (Jonsson and Wheater, 1998; Durhuus et al., 2007)

$$
d_H \geq d_S \geq 2\frac{d_H}{d_H + 1}.
\tag{6.11}
$$

Therefore, for small-world networks, which have infinite Hausdorff dimension $d_H = \infty$, it is only possible to have finite spectral dimension $d_S \geq 2$.

We observe here that, in presence of a finite spectral dimension, the cumulative distribution $\rho_c(\lambda)$ evaluating the density of eigenvalues $\lambda' \leq \lambda$ follows the scaling

$$
\rho_c(\lambda) \simeq \lambda^{d_S/2},
\tag{6.12}
$$

for $\lambda \ll 1$. In presence of a finite spectral dimension it is possible to evaluate the scaling with the network size of the smallest non-zero eigenvalue λ_2 of a connected network (also called the the Fidler eigenvalue) by imposing that

$$\rho_c(\lambda_2) = \frac{1}{N}, \tag{6.13}$$

i.e. the eigenvalue λ_2 is the smallest non zero eigenvalue. From this relation and the scaling of the cumulative density of eigenvalues we get

$$\lambda_2 \propto N^{-2/d_S}. \tag{6.14}$$

Therefore, the Fidler eigenvalue $\lambda_2 \to 0$ as $N \to \infty$ and we say that in the large network limit the spectral gap closes.

6.3 Complex Network Manifolds: a model with tunable spectral dimension

As we have seen in the previous chapter, simplicial complexes and cell complexes are natural objects to be considered when investigating network geometry. In fact, they can be intuitively interpreted as geometrical network structures built from geometrical building blocks. A pure d-dimensional simplicial complex, as defined in chapter 1 (Sec. 1.3.3) is formed by d-dimensional simplices (fully connected networks of $d + 1$ nodes) such as nodes ($d = 0$), links ($d = 1$), triangles ($d = 2$) , tetrahedra ($d = 3$) etc., glued along their $d - 1$-faces[1]. Interestingly, instead of simpleces, one can also construct geometrical complexes by subsequently gluing together *regular polytopes* along their faces, constituting the so-called **cell complexes** (Mulder and Bianconi, 2018).

The framework of Complex Network Manifolds (CNMs) can also be extended to cell complexes in general, considering regular polytopes as their building blocks. Therefore, initially (at time $t = 1$), the CNM is formed by a single d-dimensional polytope. At any subsequent step (at time $t > 1$), a new d-dimensional polytope is glued to a $(d-1)$- face α with probability

$$\Pi_\alpha = \frac{1 - n_\alpha}{\sum_{\alpha'}(1 - n_{\alpha'})}, \tag{6.15}$$

where n_α is the incidence number of face α, given by the number of d-dimensional polytopes incident to it minus one. Since in dimension $d > 4$ there are only three types of convex regular polytopes, namely the simplices, the hypercubes and the orthoplexes, here we focus on CNM formed by these d-dimensional building blocks.

---

[1] A δ-face of a d-dimensional simplex, is a δ-dimensional simplex with $\delta < d$ formed by a subset of its nodes, as defined in section 1.3.3.

The resulting CNMs (Mulder and Bianconi, 2018) have exponential degree distribution for $d = 2$ and power-law degree distribution for $d > 2$, with power-law exponent γ given by

$$\gamma = 1 + \frac{F - 2}{f - 2}, \tag{6.16}$$

where F and f are respectively the number of faces of the regular polytope and the number of $(d-1)$-faces incident to each node. By using the fact that F and f are given for the different regular polytopes of dimension d by

$$\begin{array}{lll} F = d + 1, & f = d, & \text{simplices,} \\ F = 2d, & f = d, & \text{hypercubes,} \\ F = 2^d, & f = 2^{d-1}, & \text{orthoplexes,} \end{array} \tag{6.17}$$

we derive that the power-law exponent γ of the degree distribution is given by

$$\begin{array}{ll} \gamma = 2 + \frac{1}{d-2}, & \text{simplices,} \\ \gamma = 3 + \frac{2}{d-2}, & \text{hypercubes,} \\ \gamma = 3 + \frac{1}{2^{(d-2)}-1}, & \text{orthoplexes.} \end{array} \tag{6.18}$$

Interestingly, we notice that only CNM built using simplices have a scale-free degree distribution with $\gamma \in (2,3]$ in dimension $d > 2$.

6.3.1   Spectral properties of CNMs

CNMs follow simple combinatorial rules that do not take into account any embedding space. However, these structures display an emergent hyperbolic geometry characterized by an infinite Hausdorff dimension $d_H = \infty$ (the networks are small-world, Millán et al., 2018a) together with a finite spectral dimension $d_S \geq 2$.

In this section we investigate numerically the spectral properties of the skeleton of CNMs, that is, the network formed exclusively by its nodes and links. Figure 6.1 shows the cumulative distribution of eigenvalues $\rho_c(\lambda)$ as obtained for the simplices (panel a), hypercubes (panel b) and orthoplexes (panel c), and for dimensions $d = 2$, 3, 4 and 5, as indicated in the legend. A finite size study of this spectrum reveals that λ_2 approaches zero in the large network limit, as predicted in presence of a finite spectral dimension d_S. Moreover, $\rho_c(\lambda)$ obeys Eq. 6.12 for $\lambda \ll 1$, which allows us to obtain the spectral dimension d_S as a function of d (see figure 6.1d) by performing a power-law fit to $\rho_c(\lambda)$ for $\lambda \ll 1$. We notice that the spectral dimension d_S increases with the dimension of the regular polytope d for simplices, hypercubes and orthoplex as well. However, the growth of d_S with d saturates for hypercubes and orthoplexes, while it does not appear to saturate for simplices. Therefore, we conclude that the spectral
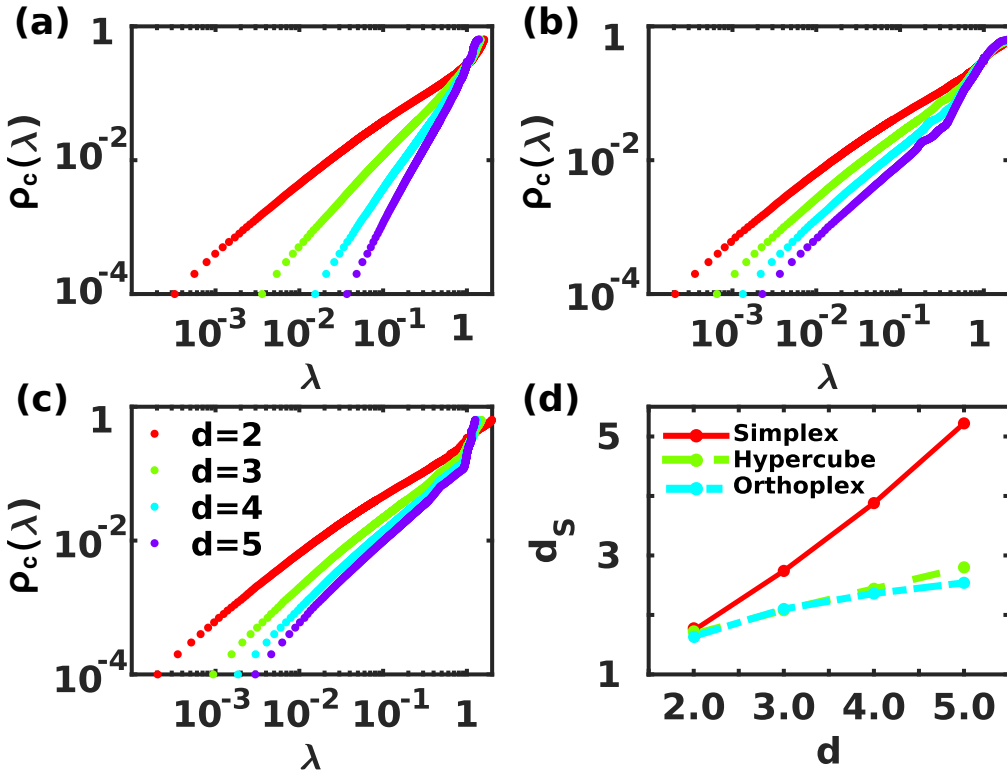
Figure 6.1: **Cumulative distribution of eigenvalues and spectral dimension.** **(a-c)** $\rho_c(\lambda)$ for CNM of dimension $d = 2,\ 3,\ 4$ and 5, respectively for the simplex, hypercube and orthoplex. **(d)** Fitted spectral dimension of CNMs as a function of the dimension d of their building blocks. Results are for $N = 6400$ and the cumulative distribution of eigenevalue $\rho_c(\lambda)$ is averaged over 100 realizations of the network.

dimension d_S does not only depend on the dimension d of the polytopes forming the building blocks of the cell complex, but also on the specific nature and symmetry of these polytopes.

Finally, we also extend the results of the localization of the eigenvectors of CNMs, obtained in the previous chapter for simplicial complexes, in figure 6.2. This reveals that the participation ratio Y follows a very heterogeneous distribution $P(Y)$ (panels a, d and g of figure 6.2), including many eigenvectors localized on a small number of nodes compared to the total number of nodes of the network, as opposed to the Fourier basis of Euclidean lattices, for with $Y = N$ for all eigenmodes. Consequently, the cumulative distribution $P_c(Y)$ can be significantly high also for values of Y much smaller than the number of nodes N of the network, i.e. $Y \ll N$ (panels b, e and h of Fig. 6.2). Finally, notice also that the dependence of the participation ratio Y on λ can be highly
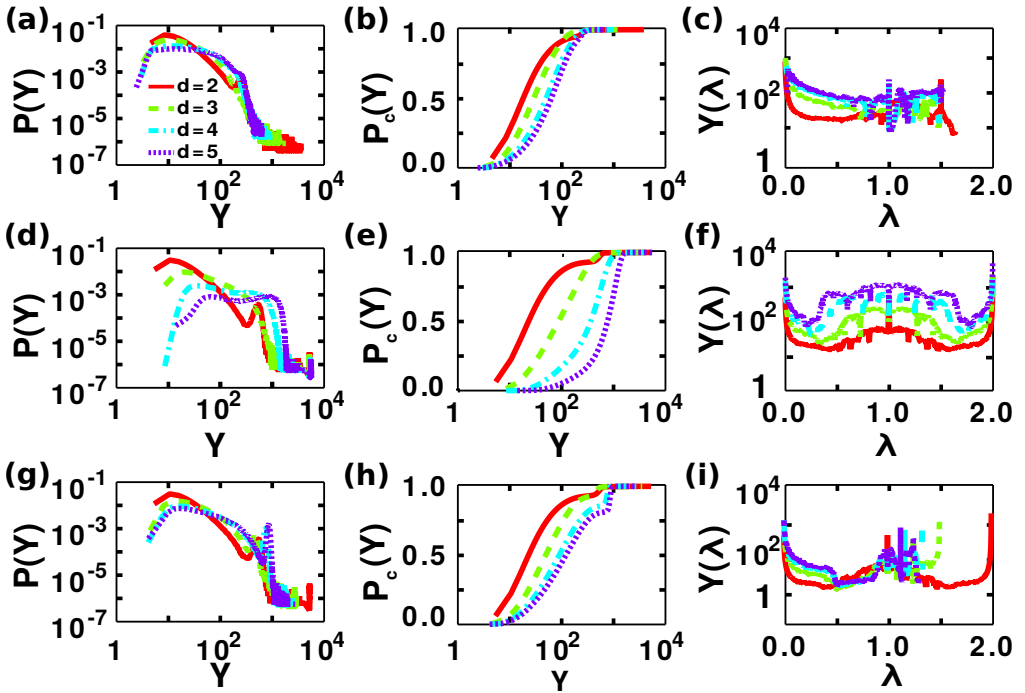
Figure 6.2: **Participation ratio Y of CNMs.** Probability distribution $P(Y)$ **(a,d,g)**, cumulative distribution $P_c(Y)$ **(b,e,h)**, and the average value of $Y(\lambda)$ **(c,f,i)**, for CNMs formed by simplices (panels a, b, c), hypercubes (panels d, e, f) and orthoplexes (panels g, h, i) of dimension $d = 2, 3, 4, 5$ as indicated in the label.

non-trivial (panels c, f and i of Fig. 6.2) and it is likely to be affected by the symmetries of the CNM (Sanchez-Garcia, 2018).

6.4 Kuramoto dynamics on networks with finite spectral dimension

In order to study synchronization dynamics on CNMs – which we take as an archetypal model of networks with finite spectral dimension – we consider the Kuramoto model, as in chapter 5 (see also section 1.4.2). In particular, consider a system of N coupled oscillators $i = 1, 2, \ldots, N$ with phases $\theta_i(t)$ obeying the following dynamical equation,

$$\dot{\theta}_i(t) = \omega_i + \sigma \sum_{j=1}^{N} \frac{e_{ij}}{k_i} \sin(\theta_j - \theta_i), \qquad (6.19)$$

where k_i is the degree of node i, e_{ij} the adjacency matrix of the network, and σ the control parameter tuning the strength of the coupling between nodes. Each internal frequency ω_i is independently drawn from a normal distribution with mean 0 and variance 1, i.e. $\mathcal{N}(0,1)$. We note that sometimes the Kuramoto model is defined by omitting k_i in Eq. 6.19, however our choice here is dictated by the desire to screen out the effect of having heterogeneous degree distributions. Therefore, the considered dynamics is designed to be independent of the degree distribution so that the effect of having networks with different spectral dimension can be revealed.

6.4.1 Theoretical predictions

In order to study the stability of the synchronized phase, we have linearized the Kuramoto dynamics in Eq. 6.19 assuming that $|\theta_i - \theta_j| \ll 1$ for every pair of neighbor nodes. In this way we get the linear system of equations

$$\dot{\theta}_i(t) = \omega_i - \sigma \sum_{j=1}^{N} L_{ij}\theta_j, \tag{6.20}$$

for $i = 1, 2, \ldots, N$, where $\mathbf{L}$ is defined in Eq. 6.1.

In order to evaluate the stability of the synchronized state, we use an approach already established for finite lattices (Hong et al., 2005; Hong et al., 2007). Specifically we calculate the average fluctuation of the phases over the entire network by evaluating W^2 given by

$$W^2 = \frac{1}{N} \left\langle \sum_{i=1}^{N} [\theta_i(t) - \overline{\theta}]^2 \right\rangle, \tag{6.21}$$

where in Eq. 6.21 $\overline{\theta}$ is given by

$$\overline{\theta} = \frac{1}{N} \sum_{i=1}^{N} \theta_i(t), \tag{6.22}$$

in the linear approximation. In presence of a thermodynamically stable synchronized phase, the **average fluctuations of the phases** W^2 should remain bounded. Therefore, if W^2 diverges with the network size N, the synchronized phase is unstable. By considering networks having a finite spectral dimension d_S we obtain (see appendix D) that, in the large network limit ($N \to \infty$), W^2 diverges as long as $d_S \leq 4$. Specifically we can show that W^2 obeys the scaling

$$W^2 \sim \begin{cases} N^{4/d_S - 1} & \text{if } d_S < 4, \\ \ln(N) & \text{if } d_S = 4, \\ \text{const} & \text{if } d_S > 4. \end{cases} \tag{6.23}$$

It follows from this derivation that the synchronized state cannot be thermodynamically stable in networks with spectral dimension $d_S \leq 4$.

The linear approximation is valid only if the coupling term of each oscillator with the phases of the linked oscillators is small. Therefore in order for the linear approximation to hold we must require that the vector $\mathbf{L}\boldsymbol{\theta}$ has small elements. A global parameter that can establish the sufficient condition for the failure of the linear approximation is the **correlation** C defined as

$$C = \frac{1}{N}\left\langle \boldsymbol{\theta}^T \mathbf{L}\boldsymbol{\theta} \right\rangle. \tag{6.24}$$

In fact, if the correlation C diverges the linear approximation cannot be valid. In a network with finite spectral dimension d_S we have obtained (see detailed derivation in appendix D) that C obeys the following scaling with N,

$$C \sim \begin{cases} N^{2/d_S - 1} & \text{if } d_S < 2, \\ \ln(N) & \text{if } d_S = 2, \\ \text{const} & \text{if } d_S > 2. \end{cases} \tag{6.25}$$

Therefore, for spectral dimension $d_S \leq 2$ the correlations among the phases of nearest neighbor nodes diverge and the linear approximation fails.

So far we have shown that for spectral dimension $d_S < 2$ the linear approximation fails, while for spectral dimensions $d_S \in (2, 4]$ the linear approximation can be valid but the synchronized phase is not thermodynamically stable. In order to uncover the phenomenology for spectral dimensions $d_S \in (2, 4]$, we follow the approach used by Hong et al., 2005; Hong et al., 2007 for regular lattices. We start by characterizing the fluctuations observed in phase velocities across the nodes of the network

$$V^2 = \frac{1}{N}\sum_{i=1}^{N}\left\langle \left[\psi_i - \bar{\psi}\right]^2 \right\rangle, \tag{6.26}$$

where ψ_i indicates the phase velocity of node i,

$$\psi_i = \dot{\theta}_i, \tag{6.27}$$

and $\bar{\psi}$ the average of the phase velocities over the network

$$\bar{\psi} = \frac{1}{N}\sum_{i=0}^{N}\psi_i. \tag{6.28}$$

In appendix D we show that, as long as the linear approximation is valid, i.e. $d_S > 2$, the fluctuations observed in phase velocities vanish in the large network limit, i.e.

$$V^2 \to 0 \quad \text{as} \quad N \to \infty. \tag{6.29}$$

This analysis therefore reveals that for spectral dimensions $d_S \in (2, 4]$ phase entrainment takes place as long as the linear approximation is valid.

In summary, in this section we have shown that the stability of the synchronized phase depends crucially on spectral dimension of the network. In particular, we have shown that the linear approximation is only valid for $d_S > 2$, since the correlations among the phases of the nodes diverge otherwise. For $d_S > 4$ the synchronized phase is thermodynamically stable, and finally for $d_s \in (2, 4]$ the synchronized phase is not thermodynamically stable and phase entrainment of the oscillators occurs instead.

6.5   Kuramoto model on Complex Network Manifolds

In this section we test out theoretical predictions with numerical simulations of the Kuramoto dynamics running over CNMs, which have a tunable spectral dimension, as previously discussed (Sec. 6.2). The macroscopic state of synchronization of the system at each time t is characterized by the Kuramoto order parameter

$$Z(t) = R(t)e^{i\phi(t)} = \frac{1}{N}\sum_{j=1}^{N} e^{i\theta_j(t)}, \tag{6.30}$$

where $R(t) \in [0, 1]$ is a real variable that quantifies the level of global synchronization, and $\phi(t)$ gives the average global phase of collective oscillations (Kuramoto, 1975; Pikovsky et al., 2003). Therefore, $R(t) \approx 0$ corresponds to the noisy or non-coherent state, whereas $R(t) \approx 1$ corresponds to the coherent or synchronized state.

We simulated the Kuramoto dynamics by integrating the system of Eqs. 6.19 in MATLAB using the ode45 function, which uses a non-stiff 4-th order integration algorithm with adaptive time steps. Simulations are run for a total time T_f, and for different realizations of the CNMs, formed by d-dimensional simplices, hypercubes and orthoplexes.

As expected from results in chapter 5 and our previous theoretical discussion, our numerical analysis reveals that CNMs can display a frustrated synchronization phase with fully entrained phases in which the global order parameter $R(t)$ has large temporal fluctuations. The typical range of values of the coupling constants where we observe this phase depends both on the spectral dimension d_S and the network size N. In figure 6.4 we show single instances of the time series $R(t)$ of the global order parameter defined on CNMs of size $N = 3200$ for representative values of the coupling σ and for the different polytopes and dimensions. Characteristic states of frustrated synchronization can be observed for $\sigma = 5.0$ (red lines) and $d = 3, 4$ for CNMs formed by simplex, hypercubes and orthoplex (panels d-i); and also for $d = 5$ for CNMs formed by hypercubes
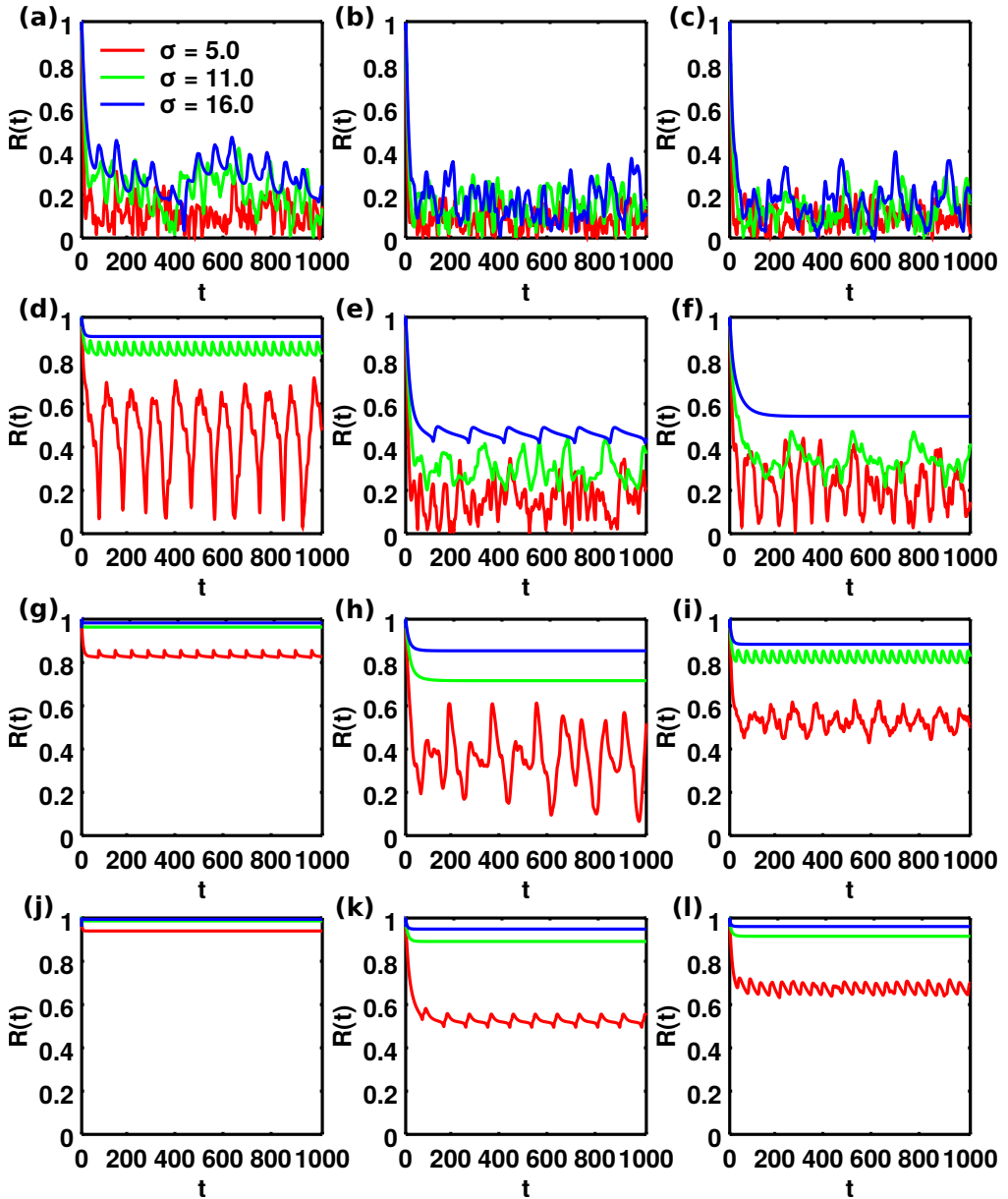
Figure 6.3: **Exemplary time series of the synchronization parameter.** The time series are for $\sigma = 5$, 11 and 16, as indicated in the legend, and CNM formed by simplices **(a,d,g,j)**, hypercubes **(b,e,h,k)**, and orthoplex **(c,f,i,l)** of dimensions $d = 2$ **(a-c)**, $d = 3$ **(d-f)**, $d = 4$ **(g-i)**, and $d = 5$ **(j-l)**.
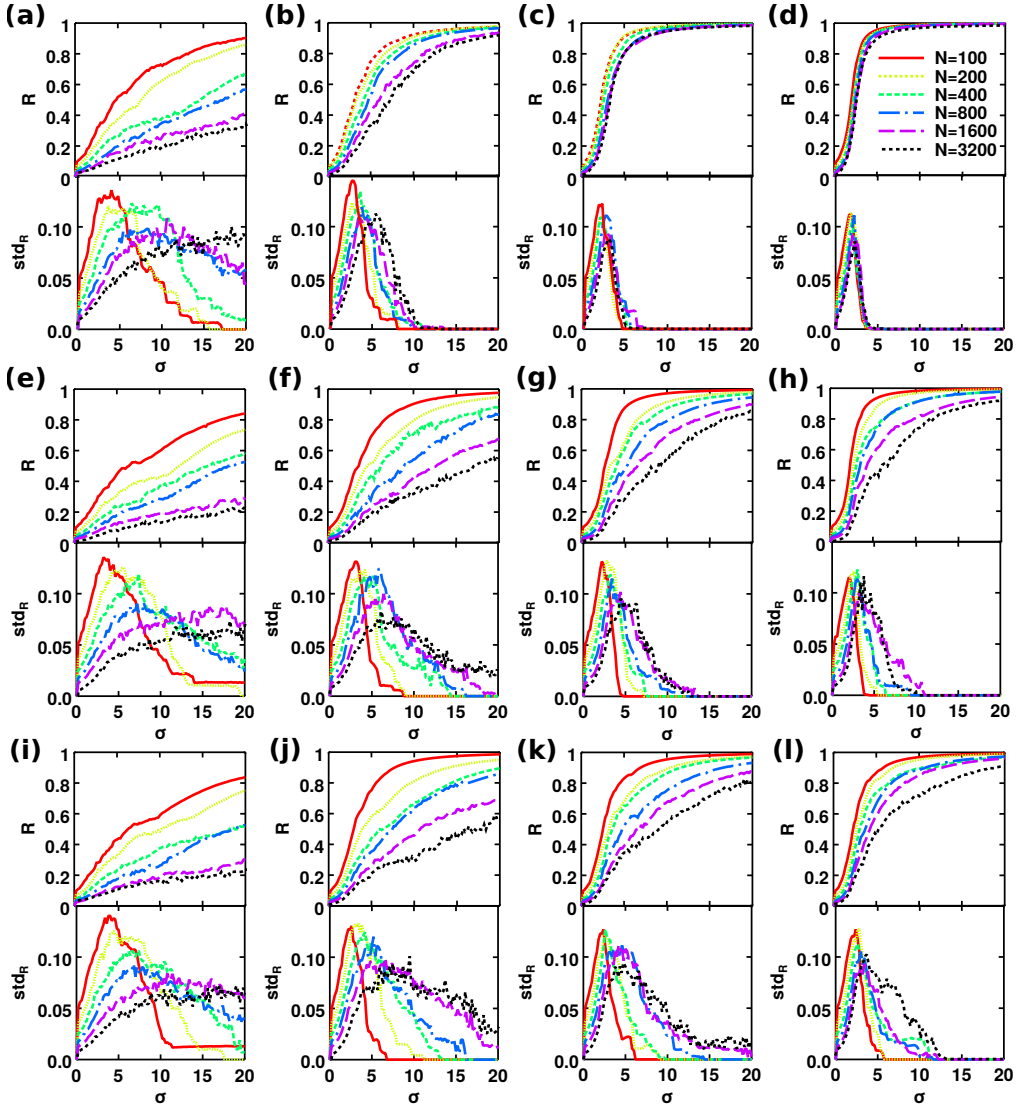
Figure 6.4: **Synchronization transition.** Average order parameter $\bar{R}$ and its standard deviation std_R as functions of the coupling constant σ for CNM formed by simplices **(a-d)**, hypercubes **(e-h)**, and orthoplexes **(i-l)**, for dimension $d = 2$ **(a,e,i)**, $d = 3$ **(b,f,j)**, $d = 4$ **(c,g,k)**, and $d = 5$ **(d,h,l)**. Results are shown for different network sizes $N = 100,\ 200,\ 400,\ 800,\ 1600$ and 3200 as indicated in the legend. Results are for $T_f = 1000$ and have been averaged after equilibration for 20 realizations of the networks and internal frequencies.

and orthoplex (panels k and l).

In general, for CNMs formed by a finite number of nodes N, as the coupling constant σ increases we can generally distinguish between three phases:

i) For very small values of the coupling constant σ, the order parameter $R(t) \approx 0$, i.e. the oscillators are not coherent (as shown for example in panels a and b of figure 6.3).

ii) For large values of the coupling constant σ we observe a synchronized phase and a stationary time-series of $R(t)$ with large values of $R(t)$ [see for instance $\sigma = 11.0$ (green lines) and $\sigma = 16.0$ (blue lines) in panels a and b of figure 6.4].

iii) In the intermediate range of values of the coupling constant σ, we observe the frustrated synchronization regime of phase entrainment where the order parameter $R(t)$ is not stationary [see for instance $\sigma = 5.0$ (red lines) in panels $d - f$ of figure 6.4].

We now seek to investigate the thermodynamical stability of these phases in the large network limit as a function of the spectral dimension d_S. According to the results in section 6.2, for $d = 2$ CNMs have spectral dimension $d_S \approx 2$, whereas for $2 < d \leq 5$ CNMs formed by simplices have spectral dimension d_S that in first approximation can be assumed to be $d_S \approx d$ and CNM formed by hypercubes and orthoplexes have spectral dimension $d_S \in (2,3)$. Consequently, our theoretical expectation is that for $d = 2$ we cannot observe entrained phases, that for $2 < d \leq 4$ we can observe entrained phases and the synchronized phase cannot be thermodynamically stable. Moreover for $d = 5$ our predictions are that CNMs formed by simplices can display a thermodynamically stable synchronized phase while CNM formed by hypercubes and orthoplexes cannot display a thermodynamically stable synchronized phase.

In order to test these predictions we have numerically studied as functions of the coupling σ the mean value $\bar{R}$ and the standard deviation std_R of the order parameter $R(t)$, averaged after the transient evolution over different realizations of CNMs. In particular, in figure 6.4 we display $\bar{R}$ and std_R for CNM formed by simplices, hypercubes and orthoplex of dimension $d = 2, 3, 4, 5$ and increasing network sizes N. The de-coherent or unsynchronized phase corresponds to the regime where $\bar{R}$ is low. The synchronized phase corresponds to the regime where $\bar{R}$ is high and the fluctuations std_R are low. Finally, the frustrated synchronization phase corresponds to values of the coupling where both $\bar{R}$ and std_R have significantly high values. As the network size N increases we observe different scenarios depending on the value of the spectral dimension d_S. For spectral dimension $d_S \approx 2$ in the large network limit the system remains in the de-coherent state. This occurs for all considered CNM of dimension $d = 2$. For spectral dimension $d_S \in (2, 4]$ we observe that the synchronized phase is not

Figure 6.5:   **Orbit diagrams of the Kuramoto dynamics on CNMs.**
The diagrams correspond to CNMs formed by simplices **(a,d,g,j)**, hypercubes
(b,e,h,k), and orthoplexes **(c,f,i,l)** for $d = 2,\ 3,\ 4$ and 5, respectively from top
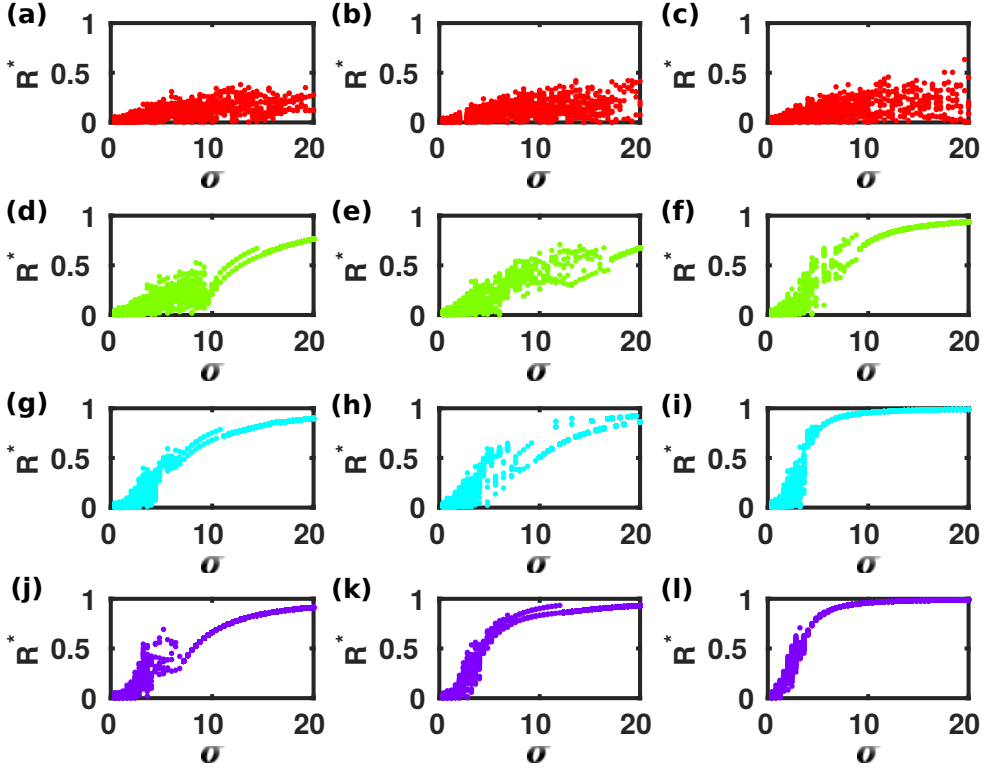to bottom. The orbit diagrams are represented by the extremes (maxima and
minima) R^* taken by $R(t)$ for $t > 0.8T_f$. Results are for $N = 3200$, $T_f = 1000$
and a given realization of the networks structure.

thermodynamically stable as the values of coupling constant where the onset of
this phase is observed increase with the network size and do not converge to
a finite value. It occurs for CNM formed by simplices of dimension $d = 3, 4$
and for CNM formed by hypercubes and orthoplexes of dimension $d = 3, 4, 5$.
Finally for spectral dimension $d_S > 4$ we observe that the synchronized phase
is thermodynamically stable as the onset of this phase occurs at a finite value
of σ in the large network limit (this is only observed for simpleces with $d = 5$).

The properties of the frustrated synchronization phase observed in CNMs are
here furthermore investigated by means of the orbit diagrams (Strogatz, 2018)
(see figure 6.5). These are measured as the extrema R^* (maximum and mini-
mum) of the time series $R(t)$ for each coupling σ. Therefore, a fixed stationary
state is represented by one point corresponding to the mean value, as it appears
in the synchronized state observed for high values of σ provided that $d > 2$.

This situation corresponds to one of full synchronization if $R^* = 1$ or to partial synchronization if $R^* < 1$, in which some nodes remain unsynchronized. For spectral dimensions $d_S \in (2, 4]$, on the other hand, we observe that as the value of the coupling constant σ is lowered and we enter in the frustrated synchronization phase, oscillatory states appear with a given number of extrema that depends on the network and frequency realization. These typically correspond to interereference among different locally synchronized regions, whose sizes scale as N (Millán et al., 2018a), which gives rise to a chaotic behavior as the coupling constant σ is decreased. Finally, in the case $d_S \approx d = 2$ the synchronized state is never reached.

> In summary our numerical study of the synchronization properties of CNM indicates that the phase diagram of the model depends critically on the spectral dimension d_S as predicted by our theoretical investigation.

6.6   Conclusions

This work investigates the role of the spectral dimension d_S on the synchronization properties of the Kuramoto model. Using a linear approximation we have shown that the synchronized phase cannot be thermodynamically stable for spectral dimension $d_S \leq 4$. Therefore a necessary condition to observe a synchronized regime in the thermodynamic limit is that $d_S > 4$. We have also shown that the considered linear approximations cannot be valid for $d_S \leq 2$, since the correlations C diverge. Finally, we have shown that a for spectral dimension $d_S \in (2, 4]$ phase entrainment takes place in the large network limit as long as the linear approximation is valid, i.e. the fluctuations in phase velocities, V^2, vanish asymptotically in time, so that the phases of the nodes are totally entrained.

In order to consider a concrete example where to test these theoretical derivations, we have characterized the synchronization dynamics of the normalized Kuramoto model taking place on Complex Network Manifolds which have a tunable spectral dimension. These networks define discrete manifolds with the small-world property (infinite Hausdorff dimension) and highly modular structure, and provide an ideal theoretical setting to explore the interplay between network geometry and synchronization dynamics (Millán et al., 2018a).

CNMs have significant spectral properties and display a finite spectral dimension. In particular, we have found that CNMs based on simplicial complexes have a spectral dimension d_S increasing almost linearly with the dimension d of the simplices, whereas CNMs formed by d-dimensional hypercubes and orthoplexes have a spectral dimension d_S that saturates with d. Having a tunable spectral dimension, CNMs can be compared to Euclidean lattices that have a

spectral dimension d_S equal to their Hausdorff dimension, i.e. $d_S = d_H$. However, CNMs have a hyperbolic structure with $d_H = \infty$ and we always observe $d_S < d_H$. Moreover, a closer look at the localization properties of the eigenvectors of CNMs reveals more significant differences with respect to Euclidean lattices. In fact, contrarily to the Fourier eigenvector of Euclidean lattices, a large fraction of eigenmodes of CNMs are highly localized on few nodes of the network, reflecting the symmetries of the building block structure.

We have subsequently studied numerically the Kuramoto dynamics on CNMs testing our theoretical predictions on the nature of the synchronization dynamics as a function of the spectral dimension d_S. We have shown that an entrained synchronization regime emerges for spectral dimensions $d_S \in (2, 4]$ and that, for this range of values of the spectral dimension, finite CNMs with high coupling constant σ reach also a synchronized phase but this phase is not thermodynamically stable. Moreover we show that for spectral dimension $d_S = 5$ the synchronized phase is thermodynamically stable.

In conclusion our work reveals that non-trivial synchronization states can emerge even in small-world networks, with an infinite Hausdorff dimension provided that the spectral dimension is finite. These results reveal deep connections between geometry and synchronization dynamics and are potentially very useful to further investigate the relation between structural and functional brain networks.

Final conclusions and outlook

"For the many, not the few"
Jeremy Corbyn

The brain is a paradigmatic example of a complex system with a wide and rich dynamical repertoire arising from the non-linear dynamics of its billions of constituents, connected in a non-trivial manner. As we presented in the introduction to this thesis, approaches to understanding brain dynamics were first made in a behavioral manner to then become increasingly precise in a microscopic scale. It has been made clear, however, that an integrated view of brain dynamics will be necessary if one seeks to explain how memory, speech, or consciousness may emerge from those little cells and the connections among them.

In this thesis we have tackled in the problem of the interplay between brain structure and function, and how this may affect its emergent cognitive abilities. We have thus considered the framework of biologically inspired neural networks, that have long provided a means of relating cognitive processes, such as memory or brain rhythms, with biophysical dynamics at the cellular level. In particular, we have studied two fundamental problems in this thesis. Firstly, how the complex structure of brain networks might develop from simple rules based on the microscopical activity, and how this developing structure in turn affects neuronal activity. Secondly, the establishment of a link between the inherent geometrical structure of cortical networks and brain – and in particular synchronization – dynamics.

Interplay between form and function in developing neural networks

In **chapter** 2 we have presented a mathematical description of how neural networks might be formed during infancy and continue to develop through adulthood, and in particular during the process of synaptic pruning (SP). The presented model takes into account the intrinsic coupling of the developing network – as given by a tunable preferential attachment model of SP (Johnson et al., 2010a) – with neuronal physiology – as modeled by the Amari-Hopfield (AH)

model (Amit, 1989). Taken separately, each of these models exhibits continuous phase transitions between ordered and disordered phases: between memory and noise in the AH model, and between heterogeneous and homogeneous networks in the synaptic pruning one. Interestingly, the phases of the AH model are known to depend on the underlying structure, so that, in the case of hetero- geneous networks, the transition from memory to noise is delayed and occurs at higher noise levels, eventually diverging with the size of the system (Torres et al., 2004; Boccaletti et al., 2006; Oshima and Odagaki, 2007).

As a consequence of the form and function interplay, a feed-back loop ap- pears in the coupled model such that heterogeneous networks can only develop when the system is in a memory – or ordered – phase. Otherwise, the neu- ronal currents leading synaptic growth and death become randomly distributed and uncorrelated with the degrees of the nodes, eventually leading to a Poisson (homogeneous) degree distribution. Interestingly, this memory-heterogeneity coupling leads in the high noise region to the existence of a discontinuous tran- sition with an associated region of bi-stability or co-existence of phases. In particular, we have found the structure of the underlying network at the onset of synaptic pruning to be determinant for the eventual structure and memory capabilities of the system, so that an initially relatively heterogeneous neural network is able to maintain a memory state despite the presence of high noise in the system. The existing memory will in turn allow the network to become more heterogeneous, thus stabilizing the memory state even further. On the contrary, a homogeneous network in the same conditions will fall into the noisy state (due to the high noise) and consequently remain homogeneous. The state of the network prior SP is that crucial for its development. Our picture thus addresses how neural activity can impact on early brain development.

In **chapter** 3 we explore further how learning a larger number of memories – or patterns of activity – in a situation with thermal and structural noise affects the emergent behavior of the system. We have found that heterogeneous network can greatly improve the stability of the memory patterns, since its structure is optimized to preserve information about them in the network hubs. These correspond to the active neurons of the retrieved memories during the recall process and play a central role in memory maintenance. Moreover, due to the structural plasticity, once a pattern is retrieved, the ability of the system to recall it again increases thanks to pruning optimization. This illustrates the constructive role of synaptic pruning to consolidate memories in the memory phase of the system.

Moreover, we have found that, due to the interplay between thermal noise, the interference among stored patterns and the dynamics driving the evolution of the topology, the memory attractors become unstable under certain condi- tions, leading to oscillations of the activity of the system among different stored memories. The reported oscillations appear on the homogeneous networks phase

of the system, but they are associated with an increased heterogeneity. This is caused by the transient existence of some relatively-high degree nodes, that appear distributed through the network, creating a non-trivial time-dependent competition among the different memories. Interestingly, the oscillations are not periodic but present a power spectrum that decays as $f^{-0.9}$ – so that there are no preferred frequencies. This is to be related to experimental studies reporting the so-called $1/f$ noise in brain activity under healthy conditions (Chialvo, 2010).

The stability of the reported phases depends crucially on the stationary synaptic density, so that a deficit on synaptic pruning, leading to increased synaptic density, can cause an absence of dynamical memories. Similarly, high frequency oscillations among patterns – and more tendency towards noisy behavior – occur in our model when there is a pruning excess that leads to a decreased connectivity. Interestingly, the existence of this oscillatory phase could be relevant to enhance the learning and recalling of sequences of patterns of activity, as in episodic memories, without invoking any external input (Marro et al., 2008; Torres et al., 2008). Remarkably, short-term and episodic memory are imparied in ASD subjects (Poirier et al., 2011; Lind et al., 2014), where also a pruning defect has been observed (Tang et al., 2014), two independent observations that are linked by the results presented here. Similarly, schizophrenia and related disorders are usually associated with erratic behavior, and also an excessive pruning has been reported in some brain areas (Loh et al., 2007; Sekar et al., 2016). Curiously, these results suggest that a lightly pruned brain – as in the case of ASD – could be forced out of the memory phase into an oscillatory regime by increasing the number of stored patterns, an observation that could help experimental psychologists to design new cognitive strategies that might help improving the cognitive abilities of patients with ASD. On the contrary, in the case of schizophrenia a more convenient strategy would consist on stabilizing some of the memory states, as for instance a few old useful memories.

In **chapter** 4, finally, we have analyzed the fundamental role of the high synaptic density period that the brain goes through during infancy, inspired by the finding in chapter 2 that the evolution of the system is strongly dependent on the state in which synaptic pruning starts. We have thus introduced a high fixed-density transient at the beginning of network evolution, which can allow the network to maintain memory and heterogenize even under noisy conditions, in a situation of high noisy and high pruning control parameter α (so that the system can heterogenize). We have found a discontinuous transition as the duration and intensity of the initial transient of high synaptic density increase, in such a way that the stationary state of the system is determined by the degree of heterogeneity when synaptic pruning begins. Interestingly, we have also found that are is an optimal value of the initial high connectivity that allows for a faster and more stable evolution towards the memory state, requiring a shorter time

in the high density state. This is convenient in terms of energy consumption, since less synapses have to be grown, maintained, and pruned. Therefore, it could explain why brain networks do not create enormous numbers of synapses during development.

A question this part of the thesis aimed to clarify is why brain development proceeds via a severe synaptic pruning – that is, with an initial overgrowth of synapses, followed by the subsequent atrophy of approximately half of them throughout infancy. It is clear that fewer synapses require less metabolic energy, but why not start with the optimal synaptic density? Our adaptive neural network model shows that the memory performance of the system does indeed depend on whether it passed through a transient period of relatively high synaptic density. Furthermore, it also provides a simple demonstration of how network structure can be optimized by pruning with a rule that only depends on local information at each synapse – the intensity of electrical current – that is consistent with empirical results on synaptic growth and death (Lee et al., 1980; Klintsova and Greenough, 1999; De Roo et al., 2007). In this view, a neural network would begin life as a more or less random structure with a sufficiently high synaptic density that is capable of memory performance. Throughout infancy, certain memory patterns are stored, and pruning gradually eliminates synapses experiencing less electrical activity. Eventually, a network architecture emerges which has lower mean synaptic density but is still capable, thanks to a more optimal structure, of retrieving memories. Moreover, the network structure will be optimized for the specific patterns it stored. This seems consistent with the fact that young children can acquire memory patterns (such as languages or artistic skills) which remain with them indefinitely, yet as adults they struggle to learn new ones (Gómez and Gerken, 2000; Kolb and Gibb, 2011).

Interestingly, the reported feed-back loop between form and function might be relevant not only to neural networks but also to other biological and engineering systems that also evolve in time and activity dependent manner. In particular, we have shown in chapter 2 that networks of proteins – which change in an evolutionary time scale – show evidences of sharing the topological features that emerge naturally from the adaptive network model presented in this thesis, and may thus also benefit from the reported feedback loop between structure and function.

Finally, it is worth noting that the model can be extended in various ways, such as the consideration of learning or short-term synaptic plasticity, or more realistic choices of neuronal and synaptic dynamics (Fares and Stepanyants, 2009; Knoblauch et al., 2014). Moreover, more elaborated definitions of the probabilities of growth and death of synapses could also be considered, such as a mechanism of self-organization towards the stationary mean connectivity (Chechik et al., 1999; Arcangelis et al., 2006; Tetzlaff et al., 2010). Interestingly, one could also consider biologically inspired pruning functions, character-

izing specific dependences on the concentration of different proteins and growth factors, that could be obtained experimentally – although to the best of our knowledge it has not yet been done. Results in these chapters could thus motivate neurobiologists to design experiments to describe the exact probabilities involved in synaptogenesis and pruning, information that could be easily incorporated in our theoretical framework.

Effect of network dimensionality on brain networks

In chapters 5 and 6 we have explored another aspect of the structure of neural networks that might affect their emergent cognitive capabilities, which is that of the network *dimensionality*. According to recent experimental works, the synchronization properties of *in-vitro* neuronal cultures strongly depend on the dimensionality of the substrate, so that 3D systems are able to display a more varied regime of synchronization than 2D ones, and that they are also more likely to display highly synchronized states (Severino et al., 2016). Following these observations, we have studied synchronization dynamics, as defined by the Kuramoto model, on top of a complex networks model called Complex Networks Manifolds (CNMs) that characterizes networks with a inherent geometrical nature and relevant properties for neural networks. In particular, CNMs combine the small-world (SW) property (i.e. infinite Hausdorff dimension) and hierarchical-modular structure with a finite and tunable spectral dimension.

In this context, in **chapter** 5 we have studied CNMs based on simplicial complexes of dimension d, which have relevant spectral properties. In particular, we have shown that:

i) CNMs have a finite spectral dimension $d_S = d$. Interestingly, we also show that CNMs build in dimension d can be embedded in a $d - 1$-dimensional manifold, so that one could hypothesize that cortical networks in a 3D space could actually have $d_S = 4$.

ii) The eigenvectors of CNMs are localized in the network communities, as opposed to those of regular lattices, which are de-localized over the entire network.

We have then shown the fundamental role of these properties on synchronization dynamics:

i) We have found the emergence of a wide region of *frustrated synchronization* – where spatio-temporal fluctuations of the order parameter are observed – due to the localization of the eigenvectors on the network communities. This demonstrates that frustrated synchronization can emerge even in SW networks with an infinite Hausdorff dimension as long as the spectral dimension is finite.

ii) CNMs with $d = 4$ are more likely to sustain synchronized states than CNMs in $d = 3, 2$ when the system size increases. Together with the finding that CNMs with $d_s = d$ can be embedded in $(d-1)$-dimensional spaces, this suggest that *in-vivo* brain networks could present enhanced synchronization properties due to their non-trivial geometrical structure.

Finally, in **chapter** 6 we have demonstrated theoretically that the synchronization state of the Kuramoto model in the thermodynamical limit depends crucially on the spectral dimension d_S. Using a linear approximation, we have shown that the synchronized phase cannot be thermodynamically stable for spectral dimension $d_S \leq 4$, whereas for $d_S \in (2, 4]$ only phase entrainment can take place in the large network limit as long as the linear approximation is valid. Finally we have shown that the considered linear approximation cannot be applied for $d_S \leq 2$, since the correlations C diverge. We have then tested our theoretical results with numerical simulations of the Kuramoto model running on top of an extended version of the Complex Network Manifolds framework that considers not only simplicial complexes but also cell complexes made up by hypercubes and orthoplexes. This allows for a more tunable (and fractional) spectral dimension, thus providing an ideal theoretical setting to explore the interplay between network geometry and synchronization dynamics. In particular, whereas for CNMs based on simplicial complexes $d_S \approx d$, the spectral dimension of CNMs formed by d-dimensional hypercubes and orthoplexes eventually saturates. We have also found that a large fraction of eigenmodes of CNMs are highly localized on a few nodes of the network, reflecting the symmetries of the building blocks structure. We have then studied numerically the Kuramoto dynamics running on top of CNMs. We have found that a frustrated synchronization regime with entrained phases emerges for spectral dimensions $d_S \in (2, 4]$. For this range of values of d_S, finite CNMs with high coupling constant σ also reach a synchronized phase. However, this phase is not thermodynamically stable as the minimum coupling σ necessary to reach the synchronized state diverges with the network size. On contrary, we have shown that for spectral dimension $d_S = 5$ the synchronized phase is thermodynamically stable.

In conclusion, our work in chapters 5 and 6 exposes that non-trivial synchronization states can emerge even in small-world networks, with an infinite Hausdorff dimension provided that the spectral dimension is finite. These results reveal deep connections between geometry and synchronization dynamics and might provide an useful approach to further investigate, for instance, the relation between structural and functional brain networks.

Some of the fundamental problems in science and society reside in finding an appropiate description of real systems when these involve complex non-linear dynamics, or are too large, or not large enough; i.e., the problem to move from

the few – the detailed microscopical description of individual elements – to the many – the collectivity, e.g. the brain. With the models and results presented in this thesis we hope to have highlighted the necessary interplay between a system's activity dynamics and structure, when both are heterogeneous and non-linear. In such situation, we have seen that non-equilibrium phases can emerge, with the associated phase transitions, suggesting novel paths to unveil, for instance, different brain functions or cognitive deficit associated to neurological disorders. This is of intrinsic relevance for the statitiscal physicist – it is *fun* – but it seems also fundamental to understand how thoughts are thought... and how theses are written.

Publications derived from this thesis

Matias, F. et al. (2015). "On the basic mechanisms of anticipated synchronization in neuronal circuits." *BMC neuroscience* 16.1.

Millán, A. P., J. J. Torres, and G. Bianconi (2018a). "Complex Network Geometry and Frustrated Synchronization." *Scientific Reports* 8.9910.

Millán, A. P., J. J. Torres, S. Johnson, and J. Marro (2018b). "Growth strategy determines network performance." arXiv:1806.01878.

Millán, A. P., J. J. Torres, S. Johnson, and J. Marro (2018c). "Concurrence of form and function in developing networks and its role in synaptic pruning." *Nature Communications* 9.1.

Haney, S. et al. (2019). "Olfactory receptor neuron response heterogeneity increases available information in temporally complex plumes." in preparation.

Millán, A. P., J. J. Torres, and G. Bianconi (2019a). "Synchronization in network geometries with finite spectral dimension." *Physical Review E* 99.2.

Millán, A. P., J. J. Torres, and J. Marro (2019b). "How Memory Conforms to Brain Development." *Frontiers in Computational Neuroscience* 13.

Williams, O., L. Lacasa, A. P. Millán, and V. Latora (2019a). "Measuring the memory of a temporal network." in preparation.

Bibliography

Abbott, L. F. and S. B. Nelson (2000). "Synaptic plasticity: taming the beast." *Nature Neuroscience* 3.11s.

Abbott, L. F., J. Varela, K. Sen, and S. Nelson (1997). "Synaptic depression and cortical gain control." *Science* 275.5297.

Abbott, L. and T. B. Kepler (1990). "Model neurons: From hodgkin-huxley to hopfield." *Statistical Mechanics of Neural Networks*. Springer.

Abbott, L. and G. LeMasson (1993). "Analysis of neuron models with dynamically regulated conductances." *Neural Computation* 5.6.

Abbott, L. and W. G. Regehr (2004). "Synaptic computation." *Nature* 431.7010.

Abrams, D. M., R. Mirollo, S. H. Strogatz, and D. A. Wiley (2008). "Solvable model for chimera states of coupled oscillators." *Physical Review Letters* 101.8.

Abrams, D. M. and S. H. Strogatz (2004). "Chimera states for coupled oscillators." *Physical Review Letters* 93.17.

Acebrón, J. A. et al. (2005). "The Kuramoto model: A simple paradigm for synchronization phenomena." *Reviews of Modern Physics* 77.1.

Acerra, N. E. and G. L. Moseley (2005). "Dysynchiria: Watching the mirror image of the unaffected limb elicits pain on the affected side." *Neurology* 65.5. eprint: http://n.neurology.org/content/65/5/751.full.pdf.

Achard, S. and E. Bullmore (Feb. 2007). "Efficiency and Cost of Economical Brain Functional Networks." *PLoS Computational Biology* 3.2.

Achard, S. et al. (2006). "A resilient, low-frequency, small-world human brain functional network with highly connected association cortical hubs." *Journal of Neuroscience* 26.1.

Afroz, S., J. Parato, H. Shen, and S. S. Smith (2016). "Synaptic pruning in the female hippocampus is triggered at puberty by extrasynaptic GABAA receptors on dendritic spines." *Elife* 5.

Akam, T. and D. M. Kullmann (2014). "Oscillatory multiplexing of population codes for selective communication in the mammalian brain." *Nature Reviews Neuroscience* 15. Perspective.

Albert, R. (2005). "Scale-free networks in cell biology." *Journal of Cell Science* 118.21.

Albert, R., H. Jeong, and A.-L. Barabási (1999). "Internet: Diameter of the world-wide web." *Nature* 401.6749.

Amaral, L. A. N., A. Scala, M. Barthelemy, and H. E. Stanley (2000). "Classes of small-world networks." *Proceedings of the national academy of sciences* 97.21.

Amari, S.-i. (1972). "Characteristics of Random Nets of Analog Neuron-Like Elements." *IEEE Trans. Systems, Man, and Cybernetics* 2.

Ambjörn, J., J. Jurkiewicz, and R. Loll (2005). "Reconstructing the universe." *Physical Review D* 72.6.

Amit, D. J. (1989). *Modeling Brain Function: the World of Attractor Neural Networks*. New York, NY, USA: Cambridge University Press.

Andrade Jr, J. S., H. J. Herrmann, R. F. Andrade, and L. R. Da Silva (2005). "Apollonian networks: Simultaneously scale-free, small world, Euclidean, space filling, and with matching graphs." *Physical Review Letters* 94.1.

Andrade, R. F. and H. J. Herrmann (2005). "Magnetic models on Apollonian networks." *Physical Review E* 71.5.

Anteneodo, C. and D. Chialvo (2009). "Unraveling the fluctuations of animal motor activity." *Chaos: An Interdisciplinary Journal of Nonlinear Science* 19.3.

Arcangelis, L. de, C. Perrone-Capano, and H. J. Herrmann (2006). "Self-organized criticality model for brain plasticity." *Physical Review Letters* 96.2.

Arenas, A. et al. (2008). "Synchronization in complex networks." *Physics Reports* 469.3.

Avena-Koenigsberger, A., B. Misic, and O. Sporns (2018). "Communication dynamics in complex brain networks." *Nature Reviews Neuroscience* 19.1.

Azouz, R. and C. M. Gray (2000). "Dynamic spike threshold reveals a mechanism for synaptic coincidence detection in cortical neurons in vivo." *Proceedings of the National Academy of Sciences* 97.14.

— (2003). "Adaptive coincidence detection and dynamic gain control in visual cortical neurons in vivo." *Neuron* 37.3.

Bak, P. (2013). *How Nature Works: the Science of Self-Organized Criticality*. Springer Science & Business Media.

Bak, P., C. Tang, and K. Wiesenfeld (1987). "Self-organized criticality: An explanation of the 1/f noise." *Physical Review Letters* 59.4.

Baliki, M. N., P. Y. Geha, A. V. Apkarian, and D. R. Chialvo (2008). "Beyond feeling: chronic pain hurts the brain, disrupting the default-mode network dynamics." *Journal of Neuroscience* 28.6.

Barabási, A.-L. et al. (2016). *Network science*. Cambridge University press.

Barabási, A.-L. and R. Albert (1999). "Emergence of scaling in random networks." *Science* 286.5439.

Barahona, M. and L. M. Pecora (2002). "Synchronization in small-world systems." *Physical Review Letters* 89.5.

Barrat, A., M. Barthélemy, R. Pastor-Satorras, and A. Vespignani (2004). "The architecture of complex weighted networks." *Proceedings of the National Academy of Sciences* 101.11. eprint: https://www.pnas.org/content/101/11/3747.full.pdf.

Barthélemy, M. (2011). "Spatial networks." *Physics Reports* 499.1-3.

Bassett, D. S. et al. (2006). "Adaptive reconfiguration of fractal small-world human brain functional networks." *Proceedings of the National Academy of Sciences* 103.51.

Bassett, D. S. et al. (2008). "Hierarchical organization of human cortical networks in health and schizophrenia." *Journal of Neuroscience* 28.37.

Baxter, R. J. (2016). *Exactly Solved Models in Statistical Mechanics.* Elsevier.

Bazhenov, M., I. Timofeev, M. Steriade, and T. J. Sejnowski (2002). "Model of thalamocortical slow-wave sleep oscillations and transitions to activated states." *Journal of neuroscience* 22.19.

Bear, M. F., B. W. Connors, and M. A. Paradiso (2007). *Neuroscience.* Vol. 2. Lippincott Williams & Wilkins.

Beckers, R., J.-L. Deneubourg, S. Goss, and J. M. Pasteels (1990). "Collective decision making through food recruitment." *Insectes Sociaux* 37.3.

Beggs, J. M. and D. Plenz (2003). "Neuronal avalanches in neocortical circuits." *Journal of Neuroscience* 23.35.

— (2004). "Neuronal avalanches are diverse and precise activity patterns that are stable for many hours in cortical slice cultures." *Journal of Neuroscience* 24.22.

Berg, J., M. Lässig, and A. Wagner (2004). "Structure and evolution of protein interaction networks: a statistical model for link dynamics and gene duplications." *BMC Evolutionary Biology* 4.1.

Bertram, R., A. Sherman, and E. F. Stanley (1996). "Single-domain/bound calcium hypothesis of transmitter release and facilitation." *Journal of Neurophysiology* 75.5.

Bianconi, G. (n.d.). https://github.com/ginestrab.

— (2015). "Interdisciplinary and physics challenges of network theory." *Europhysics Letters* 111.5.

Bianconi, G. and C. Rahmede (2015). "Complex quantum network manifolds in dimension d> 2 are scale-free." *Scientific Reports* 5.

— (2016). "Network geometry with flavor: From complexity to quantum geometry." *Physical Review E* 93.3.

— (2017). "Emergent hyperbolic network geometry." *Scientific Reports* 7.

Bianconi, G., C. Rahmede, and Z. Wu (2015). "Complex quantum network geometries: Evolution and phase transitions." *Physical Review E* 92 (2).

Bianconi, G. and R. M. Ziff (2018). "Topological percolation on hyperbolic simplicial complexes." *Physical Review E* 98.5.

Blanton, R. E. et al. (2001). "Mapping cortical asymmetry and complexity patterns in normal children." *Psychiatry Research: Neuroimaging* 107.1.

Bliss, T. V. and G. L. Collingridge (1993). "A synaptic model of memory: long-term potentiation in the hippocampus." *Nature* 361.6407.

Blondel, V. D., J.-L. Guillaume, R. Lambiotte, and E. Lefebvre (2008). "Fast unfolding of communities in large networks." *Journal of Statistical Mechanics: Theory and Experiment* 2008.10.

Boccaletti, S. et al. (2006). "Complex networks: Structure and dynamics." *Physics Reports* 424.4-5.

Boccaletti, S. et al. (2014). "The structure and dynamics of multilayer networks." *Physics Reports* 544.1.

Boettcher, S., V. Singh, and R. M. Ziff (2012). "Ordinary percolation with discontinuous transitions." *Nature Communications* 3.

Boguna, M., D. Krioukov, and K. C. Claffy (2009). "Navigability of complex networks." *Nature Physics* 5.1.

Boguná, M., F. Papadopoulos, and D. Krioukov (2010). "Sustaining the internet with hyperbolic mapping." *Nature Communications* 1.

Bonachela, J. A., S. De Franciscis, J. J. Torres, and M. A. Muñoz (2010). "Self-organization without conservation: are neuronal avalanches generically critical?" *Journal of Statistical Mechanics: Theory and Experiment* 2010.02.

Bortz, A. B., M. H. Kalos, and J. L. Lebowitz (1975). "A new algorithm for Monte Carlo simulation of Ising spin systems." *Journal of Computational Physics* 17.1.

Boto, E. et al. (2018). "Moving magnetoencephalography towards real-world applications with a wearable system." *Nature* 555.7698.

Brandes, U. (2001). "A faster algorithm for betweenness centrality." *The Journal of Mathematical Sociology* 25.2. eprint: https://doi.org/10.1080/0022250X.2001.9990249.

Bronstein, M. M. et al. (2017). "Geometric deep learning: going beyond euclidean data." *IEEE Signal Processing Magazine* 34.4.

Brown, R. A. and J. A. Nelson (2016). "The invention and early history of the N-localizer for stereotactic neurosurgery." *Cureus* 8.6.

Brunel, N. and V. Hakim (2008). "Sparsely synchronized neuronal oscillations." *Chaos: An Interdisciplinary Journal of Nonlinear Science* 18.1.

Brunel, N. and F. Lavigne (2009). "Semantic priming in a cortical network model." *Journal of Cognitive Neuroscience* 21.12.

Brunel, N. and M. C. Van Rossum (2007). "Lapicque's 1907 paper: from frogs to integrate-and-fire." *Biological Cybernetics* 97.5-6.

Brunel, N. and X.-J. Wang (2003). "What determines the frequency of fast network oscillations with irregular neural discharges? I. Synaptic dynamics and excitation-inhibition balance." *Journal of Neurophysiology* 90.1.

Brush, S. G. (1967). "History of the Lenz-Ising model." *Reviews of Modern Physics* 39.4.

Buia, C. I. and P. H. Tiesinga (2005). "Rapid temporal modulation of synchrony in cortical interneuron networks with synaptic plasticity." *Neurocomputing* 65.

Bullmore, E. and O. Sporns (2009). "Complex brain networks: graph theoretical analysis of structural and functional systems." *Nature Reviews Neuroscience* 10. Review Article.

— (2012). "The economy of brain network organization." *Nature Reviews Neuroscience* 13.5.

Bullock, T., M. McClune, and J. Enright (2003). "Are the electroencephalograms mainly rhythmic? Assessment of periodicity in wide-band time series." *Neuroscience* 121.1.

Burioni, R. and D. Cassi (1996). "Universal properties of spectral dimension." *Physical Review Letters* 76.7.

— (2005). "Random walks on graphs: ideas, techniques and results." *Journal of Physics A: Mathematical and General* 38.8.

Burns, G. A. and M. P. Young (2000). "Analysis of the connectional organization of neural systems associated with the hippocampus in rats." *Philosophical Transactions of the Royal Society of London B: Biological Sciences* 355.1393.

Buzsaki, G. (2006). *Rhythms of the Brain*. Oxford University Press.

Cabral, J., M. L. Kringelbach, and G. Deco (2014). "Exploring the network dynamics underlying brain activity during rest." *Progress in neurobiology* 114.

Cardin, J. A., L. A. Palmer, and D. Contreras (2008). "Cellular mechanisms underlying stimulus-dependent gain modulation in primary visual cortex neurons in vivo." *Neuron* 59.1.

Castellano, C., M. A. Muñoz, and R. Pastor-Satorras (2009). "Nonlinear q-voter model." *Physical Review E* 80.4.

Castillo, I. P. et al. (2004). "Analytic solution of attractor neural networks on scale-free graphs." *Journal of Physics A: Mathematical and General* 37.37.

Cavagna, A. et al. (2010). "Scale-free correlations in starling flocks." *Proceedings of the National Academy of Sciences* 107.26.

Chavez, M. et al. (2005). "Synchronization is enhanced in weighted complex networks." *Physical Review Letters* 94.21.

Chechik, G., I. Meilijson, and E. Ruppin (1998). "Synaptic Pruning in Development: A Computational Account." *Neural Computation* 10.7.

— (1999). "Neuronal Regulation: A Mechanism for Synaptic Pruning During Brain Maturation." *Neural Computation* 11.

Chen, S.-K. et al. (2010). "Hematopoietic origin of pathological grooming in Hoxb8 mutant mice." *Cell* 141.5.

Chialvo, D. R. (2004). "Critical brain networks." *Physica A: Statistical Mechanics and its Applications* 340.4.

— (2006). "Psychophysics: Are our senses critical?" *Nature Physics* 2.5.

— (2010). "Emergent complex neural dynamics." *Nature Physics* 6.10.

Chialvo, D. R., P. Balenzuela, and D. Fraiman (2008). "The brain: what is critical about it?" *AIP Conference Proceedings.* Vol. 1028. 1. AIP.

Chklovskii, D. B., B. Mel, and K. Svoboda (2004). "Cortical rewiring and information storage." *Nature* 431.7010.

Clough, J. R. and T. S. Evans (2017). "Embedding graphs in Lorentzian spacetime." *PLoS One* 12.11.

Commons, W. (2018). *File: Diagram showing the brain stem which includes the medulla oblongata, the pons and the midbrain (2) CRUK 294.* [Online; accessed 8-April-2019].

— (2019). *File: Neuron description.*

Connors, B. W. and M. A. Long (2004). "Electrical synapses in the mammalian brain." *Annual Review of Neuroscience* 27.

Cortés, J. M. et al. (2006). "Effects of Fast Presynaptic Noise in Attractor Neural Networks." *Neural Computation* 18.

Cortes, J. M. et al. (2006). "Effects of fast presynaptic noise in attractor neural networks." *Neural Computation* 18.3.

Cota, W., G. ódor, and S. C. Ferreira (2018). "Griffiths phases in infinite-dimensional, non-hierarchical modular networks." *Scientific Reports* 8.1.

Courtney, O. T. and G. Bianconi (2016). "Generalized network structures: The configuration model and the canonical ensemble of simplicial complexes." *Physical Review E* 93.6.

Cowan, W. M., J. W. Fawcett, D. D. O'Leary, and B. B. Stanfield (1984). "Regressive events in neurogenesis." *Science* 225.4668.

Crick, F. and E. Jones (1993). "Backwardness of human neuroanatomy." *Nature* 361.6408.

Critchley, M. and E. A. Critchley (1998). *John Hughlings Jackson: Father of English Neurology.* Oxford University Press.

Crossley, N. A. et al. (2014). "The hubs of the human connectome are generally implicated in the anatomy of brain disorders." *Brain* 137.8.

Damoiseaux, J. S. and M. D. Greicius (2009). "Greater than the sum of its parts: a review of studies combining structural connectivity and resting-state functional connectivity." *Brain Structure and Function* 213.6.

Danon, L., A. Díaz-Guilera, J. Duch, and A. Arenas (2005). "Comparing community structure identification." *Journal of Statistical Mechanics: Theory and Experiment* 2005.09.

De Franciscis, S., J. Torres, and J. Marro (2010). "Unstable dynamics, nonequilibrium phases, and criticality in networked excitable media." *Physical Review E* 82.4.

De Roo, M. et al. (2007). "Activity-dependent PSD formation and stabilization of newly formed spines in hippocampal slice cultures." *Cerebral Cortex* 18.1.

Dean III, D. C. et al. (2014). "Modeling healthy male white matter and myelin development: 3 through 60 months of age." *Neuroimage* 84.

DeFelipe, J. (2015). "The dendritic spine story: an intriguing process of discovery." *Frontiers in neuroanatomy* 9.

Deger, M., M. Helias, S. Rotter, and M. Diesmann (2012). "Spike-timing dependence of structural plasticity explains cooperative synapse formation in the neocortex." *PLoS Computational Biology* 8.9.

Deger, M., A. Seeholzer, and W. Gerstner (2016). "Multi-contact synapses for stable networks: a spike-timing dependent model of dendritic spine plasticity and turnover." *arXiv preprint arXiv:1609.05730.*

Derecki, N. C. et al. (2012). "Wild-type microglia arrest pathology in a mouse model of Rett syndrome." *Nature* 484.7392.

Descartes, R. (1984). *The philosophical writings of Descartes.* Vol. 2. Cambridge University Press.

Destexhe, A. (2009). "Self-sustained asynchronous irregular states and up–down states in thalamic, cortical and thalamocortical networks of nonlinear integrate-and-fire neurons." *Journal of Computational Neuroscience* 27.3.

Deuker, L. et al. (2009). "Reproducibility of graph metrics of human brain functional networks." *Neuroimage* 47.4.

Dodel, S., J. M. Herrmann, and T. Geisel (2002). "Functional connectivity by cross-correlation clustering." *Neurocomputing* 44.

Donetti, L., P. I. Hurtado, and M. A. Muñoz (2005). "Entangled networks, synchronization, and optimal network topology." *Physical Review Letters* 95.18.

Dormann, C. F., J. Fründ, N. Blüthgen, and B. Gruber (2009). "Indices, graphs and null models: analyzing bipartite ecological networks." *The Open Ecology Journal* 2.1.

Dorogovtsev, S. N. and J. F. Mendes (2002). "Evolution of networks." *Advances in Physics* 51.4.

Duncan, J. S., J. W. Sander, S. M. Sisodiya, and M. C. Walker (2006). "Adult epilepsy." *The Lancet* 367.9516.

Durhuus, B., T. Jonsson, and J. F. Wheater (2007). "The spectral dimension of generic trees." *Journal of Statistical Physics* 128.5.

Dyhrfjeld-Johnsen, J. et al. (2007). "Topological determinants of epileptogenesis in large-scale structural and functional models of the dentate gyrus derived from experimental data." *Journal of neurophysiology* 97.2.

Eguiluz, V. M. et al. (2005). "Scale-free brain functional networks." *Physical Review Letters* 94.1.

Ercsey-Ravasz, M. et al. (2013). "A predictive network model of cerebral cortical connectivity based on a distance rule." *Neuron* 80.1.

Evergren, E., F. Benfenati, and O. Shupliakov (2007). "The synapsin cycle: a view from the synaptic endocytic zone." *Journal of Neuroscience Research* 85.12.

Expert, P., S. de Nigris, T. Takaguchi, and R. Lambiotte (2017). "Graph spectral characterization of the X Y model on complex networks." *Physical Review E* 96.1.

Expert, P. et al. (2010). "Self-similar correlation function in brain resting-state functional magnetic resonance imaging." *Journal of The Royal Society Interface* 8.57.

Eyal, G. et al. (2018). "Human cortical pyramidal neurons: From spines to spikes via models." *Frontiers in Cellular Neuroscience* 12.

Eytan, D. and S. Marom (2006). "Dynamics and effective topology underlying synchronization in networks of cortical neurons." *Journal of Neuroscience* 26.33.

Fagiolo, G. (2007). "Clustering in complex directed networks." *Physical Review E* 76 (2).

Faludi, G. and K. Mirnics (2011). "Synaptic changes in the brain of subjects with schizophrenia." *International Journal of Developmental Neuroscience* 29.3. Schizophrenia.

Fares, T. and A. Stepanyants (2009). "Cooperative synapse formation in the neocortex." *Proceedings of the National Academy of Sciences* 106.38.

Feldt, S. et al. (2007). "Internetwork and intranetwork communications during bursting dynamics: applications to seizure prediction." *Physical Review E* 76.2.

Felleman, D. J. and D. E. Van (1991). "Distributed hierarchical processing in the primate cerebral cortex." *Cerebral cortex* 1.1.

Field, S., J. Witt, F. Nori, and X. Ling (1995). "Superconducting vortex avalanches." *Physical review letters* 74.7.

FitzHugh, R. (1961). "Impulses and physiological states in theoretical models of nerve membrane." *Biophysical Journal* 1.6.

Fornito, A., B. J. Harrison, A. Zalesky, and J. S. Simons (2012). "Competitive and cooperative dynamics of large-scale brain functional networks supporting recollection." *Proceedings of the National Academy of Sciences* 109.31.

Fornito, A., A. Zalesky, and M. Breakspear (2015). "The connectomics of brain disorders." *Nature Reviews Neuroscience* 16.3.

Fortunato, S. (2010). "Community detection in graphs." *Physics Reports* 486.3-5.

Foss, J. M., A. V. Apkarian, and D. R. Chialvo (2006). "Dynamics of pain: fractal dimension of temporal variability of spontaneous pain differentiates between pain states." *Journal of Neurophysiology* 95.2.

Fox, M. D. and M. E. Raichle (2007). "Spontaneous fluctuations in brain activity observed with functional magnetic resonance imaging." *Nature Reviews Neuroscience* 8.9.

Fraiman, D., P. Balenzuela, J. Foss, and D. R. Chialvo (2009). "Ising-like dynamics in large-scale functional brain networks." *Physical Review E* 79.6.

Franciscis, S. de, S. Johnson, and J. J. Torres (2011). "Enhancing neural-network performance via assortativity." *Physical Review E* 83.3.

Frank, E. (1997). "Synapse Elimination–For Nerves It's All or Nothing." *Science* 275.5298.

Fricker, D., J. A. Verheugen, and R. Miles (1999). "Cell-attached measurements of the firing threshold of rat hippocampal neurones." *The Journal of Physiology* 517.3.

Friston, K. J. (1994). "Functional and effective connectivity in neuroimaging: a synthesis." *Human Brain Mapping* 2.1-2.

Galarreta, M. and S. Hestrin (2001). "Electrical synapses between GABA-releasing interneurons." *Nature Reviews Neuroscience* 2.6.

Gallos, L. K., H. A. Makse, and M. Sigman (2012). "A small world of weak ties provides optimal global integration of self-similar modules in functional brain networks." *Proceedings of the National Academy of Sciences* 109.8.

Garcia-Ojalvo, J., M. B. Elowitz, and S. H. Strogatz (2004). "Modeling a synthetic multicellular clock: repressilators coupled by quorum sensing." *Proceedings of the National Academy of Sciences* 101.30.

Gardiner, C. W. et al. (1985). *Handbook of stochastic methods.* Vol. 3. Springer Berlin.

Gastner, M. T. and G. ódor (2016). "The topology of large Open Connectome networks for the human brain." *Scientific Reports* 6.

Geschwind, D. H. and P. Levitt (2007). "Autism spectrum disorders: developmental disconnection syndromes." *Current Opinion in Neurobiology* 17.1. Development.

Gireesh, E. D. and D. Plenz (2008). "Neuronal avalanches organize as nested theta-and beta/gamma-oscillations during development of cortical layer 2/3." *Proceedings of the National Academy of Sciences* 105.21.

Girvan, M. and M. E. J. Newman (2002). "Community structure in social and biological networks." *Proceedings of the National Academy of Sciences* 99.12.

Giusti, C., R. Ghrist, and D. S. Bassett (2016). "Two's company, three (or more) is a simplex." *Journal of Computational Neuroscience* 41.1.

Glass, L. (2001). "Synchronization and rhythmic processes in physiology." *Nature* 410.6825.

Gollo, L. L. and M. Breakspear (2014). "The frustrated brain: from dynamics on motifs to communities and networks." *Philosophical Transactions of the Royal Society B: Biological Sciences* 369.1653.

Gómez-Gardeñes, J., G. Zamora-López, Y. Moreno, and A. Arenas (2010). "From modular to centralized organization of synchronization in functional areas of the cat cerebral cortex." *PLoS One* 5.8.

Gómez, R. L. and L. Gerken (2000). "Infant artificial language learning and language acquisition." *Trends in Cognitive Sciences* 4.5.

Gotelli, N. J. and G. R. Graves (1996). *Null models in ecology.*

Greicius, M. D., G. Srivastava, A. L. Reiss, and V. Menon (2004). "Default-mode network activity distinguishes Alzheimer's disease from healthy aging: Evidence from functional MRI." *Proceedings of the National Academy of Sciences* 101.13. eprint: https://www.pnas.org/content/101/13/4637.full.pdf.

Greicius, M. D. et al. (2007). "Resting-state functional connectivity in major depression: abnormally increased contributions from subgenual cingulate cortex and thalamus." *Biological Psychiatry* 62.5.

Greiner, W., L. Neise, and H. Stöcker (2012). *Thermodynamics and statistical mechanics.* Springer Science & Business Media.

Griffin, L. D. (1994). "The intrinsic geometry of the cerebral cortex." *Journal of Theoretical Biology* 166.3.

Griffiths, R. B. (1969). "Nonanalytic behavior above the critical point in a random Ising ferromagnet." *Physical Review Letters* 23.1.

Gross, T. and B. Blasius (2007). "Adaptive coevolutionary networks: a review." *Journal of The Royal Society Interface* 5.20. eprint: http://rsif.royalsocietypublishing.org/content/5/20/259.full.pdf.

Gruart, A., M. D. Muñoz, and J. M. Delgado-García (2006). "Involvement of the CA3–CA1 synapse in the acquisition of associative learning in behaving mice." *Journal of Neuroscience* 26.4.

Guillery, R. W. (2004). "Observations of synaptic structures: origins of the neuron doctrine and its current status." *Philosophical Transactions of the Royal Society B: Biological Sciences* 360.1458.

Guimerà, R. and L. A. N. Amaral (2005). "Cartography of complex networks: modules and universal roles." *Journal of Statistical Mechanics: Theory and Experiment* 2005.02.

Ha, G. E. and E. Cheong (2017). "Spike frequency adaptation in neurons of the central nervous system." *Experimental Neurobiology* 26.4.

Hagmann, P. (2005). "From Diffusion MRI to Brain Connectomics."

Hagmann, P. et al. (2008). "Mapping the structural core of human cerebral cortex." *PLoS Biology* 6.7.

Hahn, G. et al. (2010). "Neuronal avalanches in spontaneous activity in vivo." *Journal of Neurophysiology* 104.6.

Haimovici, A., E. Tagliazucchi, P. Balenzuela, and D. R. Chialvo (2013). "Brain organization into resting state networks emerges at criticality on a model of the human connectome." *Physical Review Letters* 110.17.

Haney, S. et al. (2019). "Olfactory receptor neuron response heterogeneity increases available information in temporally complex plumes." in preparation.

Harris, T. E. (2002). *The theory of branching processes.* Courier Corporation.

He, Y., Z. J. Chen, and A. C. Evans (2007). "Small-world anatomical networks in the human brain revealed by cortical thickness from MRI." *Cerebral Cortex* 17.10.

Hebb, D. O. (1949). "The organization of behavior. A neuropsychological theory."

Heuvel, M. P. van den, R. S. Kahn, J. Goñi, and O. Sporns (2012). "High-cost, high-capacity backbone for global brain communication." *Proceedings of the National Academy of Sciences* 109.28.

Hilgetag, C. C. and S. Grant (2000). "Uniformity, specificity and variability of corticocortical connectivity." *Philosophical Transactions of the Royal Society of London B: Biological Sciences* 355.1393.

Hilgetag, C. C. et al. (2000). "Anatomical connectivity defines the organization of clusters of cortical areas in the macaque and the cat." *Philosophical Transactions of the Royal Society of London B: Biological Sciences* 355.1393.

Hobbiss, A. F., Y. R. Cortes, and I. Israely (2018). "Homeostatic plasticity scales dendritic spine volumes and changes the threshold and specificity of Hebbian plasticity." *bioRxiv.*

Hodgkin, A. L. and A. F. Huxley (1939). "Action potentials recorded from inside a nerve fibre." *Nature* 144.3651.

Holcman, D. and M. Tsodyks (2006). "The emergence of up and down states in cortical networks." *PLoS Computational Biology* 2.3.

Holme, P. and J. Saramäki (2012). "Temporal networks." *Physics Reports* 519.3.

Holtmaat, A. J. et al. (2005). "Transient and persistent dendritic spines in the neocortex in vivo." *Neuron* 45.2.

Holtmaat, A. and K. Svoboda (2009). "Experience-dependent structural synaptic plasticity in the mammalian brain." *Nature Reviews Neuroscience* 10. Review Article.

Honey, C. J., R. Kötter, M. Breakspear, and O. Sporns (2007). "Network structure of cerebral cortex shapes functional connectivity on multiple time scales." *Proceedings of the National Academy of Sciences* 104.24.

Honey, C. J. and O. Sporns (2008). "Dynamical consequences of lesions in cortical networks." *Human brain mapping* 29.7.

Honey, C. et al. (2009). "Predicting human resting-state functional connectivity from structural connectivity." *Proceedings of the National Academy of Sciences* 106.6.

Hong, H., H. Park, and M. Choi (2005). "Collective synchronization in spatially extended systems of coupled oscillators with random frequencies." *Physical Review E* 72.3.

Hong, H., H. Chaté, H. Park, and L.-H. Tang (2007). "Entrainment transition in populations of random frequency oscillators." *Physical Review Letters* 99.18.

Hopfield, J. J. (1982). "Neural networks and physical systems with emergent collective computational abilities." *Proceedings of the National Academy of*

Sciences 79.8. eprint: http://www.pnas.org/content/79/8/2554.full.pdf.

Horn, D. and M. Usher (1989). "Neural networks with dynamical thresholds." *Physical Review A* 40.2.

Horwitz, B. (2003). "The elusive concept of brain connectivity." *Neuroimage* 19.2.

Huttenlocher, P. R. and A. S. Dabholkar (1997). "Regional differences in synaptogenesis in human cerebral cortex." *Journal of Comparative Neurology* 387.2.

Iacopini, I., G. Petri, A. Barrat, and V. Latora (2018). "Simplicial models of social contagion." *arXiv preprint arXiv:1810.07031.*

Iglesias, J. et al. (2005). "Dynamics of pruning in simulated large-scale spiking neural networks." *Biosystems* 79.1-3.

Irons, H. R. et al. (2008). "Three-dimensional neural constructs: a novel platform for neurophysiological investigation." *Journal of neural engineering* 5.3.

Ising, E. (1925). "Beitrag zur theorie des ferromagnetismus." *Zeitschrift für Physik A Hadrons and Nuclei* 31.1.

Itskov, V., C. Curto, E. Pastalkova, and G. Buzsáki (2011). "Cell assembly sequences arising from spike threshold adaptation keep track of time in the hippocampus." *Journal of Neuroscience* 31.8.

Izhikevich, E. M. (2004). "Which model to use for cortical spiking neurons?" *IEEE Transactions on Neural Networks* 15.5.

Jensen, H. J. (1998). *Self-organized criticality: emergent complex behavior in physical and biological systems.* Vol. 10. Cambridge University Press.

Jirsa, V. K. and J. S. Kelso (2000). "Spatiotemporal pattern formation in neural systems with heterogeneous connection topologies." *Physical Review E* 62.6.

Johnson, S., J. Marro, and J. J. Torres (2010a). "Evolving networks and the development of neural systems." *Journal of Statistical Mechanics: Theory and Experiment* 2010.03.

Johnson, S., J. J. Torres, J. Marro, and M. A. Muñoz (2010b). "Entropic origin of disassortativity in complex networks." *Physical Review Letters* 104.10.

— (2011). "Why are so many networks disassortative?" *AIP Conference Proceedings.* Vol. 1332. 1. AIP.

Johnson, S., J. J. Torres, and J. Marro (2009). "Nonlinear preferential rewiring in fixed-size networks as a diffusion process." *Physical Review E* 79.5.

Jonsson, T. and J. F. Wheater (1998). "The spectral dimension of the branched polymer phase of two-dimensional quantum gravity." *Nuclear Physics B* 515.3.

Jost, J. and S. Liu (2014). "Ollivier's Ricci curvature, local clustering and curvature-dimension inequalities on graphs." *Discrete & Computational Geometry* 51.2.

Kaiser, M. and C. C. Hilgetag (2004). "Modelling the development of cortical systems networks." *Neurocomputing* 58.

Kaiser, M. and S. Varier (2011). "Evolution and development of brain networks: from Caenorhabditis elegans to Homo sapiens." *Network: Computation in Neural Systems* 22.1-4.

Kandel, E. R. et al. (2000). *Principles of Neural Science*. Vol. 4. McGraw-hill New York.

Karmarkar, U. R. and D. V. Buonomano (2007). "Timing in the absence of clocks: encoding time in neural network states." *Neuron* 53.3.

Kauffman, S. A. (1993). *The origins of order: Self-organization and selection in evolution*. OUP USA.

Kennedy, D. P., E. Redcay, and E. Courchesne (2006). "Failing to deactivate: Resting functional abnormalities in autism." *Proceedings of the National Academy of Sciences* 103.21. eprint: https://www.pnas.org/content/103/21/8275.full.pdf.

Keshavan, M. S., S. Anderson, and J. W. Pettergrew (1994). "Is Schizophrenia due to excessive synaptic pruning in the prefrontal cortex? The Feinberg hypothesis revisited." *Journal of Psychiatric Research* 28.3.

Kiselev, V. G., K. R. Hahn, and D. P. Auer (2003). "Is the brain cortex a fractal?" *Neuroimage* 20.3.

Kitzbichler, M. G., M. L. Smith, S. R. Christensen, and E. Bullmore (2009). "Broadband criticality of human brain network synchronization." *PLoS computational biology* 5.3.

Kiyono, K. et al. (2005). "Phase transition in a healthy human heart rate." *Physical review letters* 95.5.

Klintsova, A. Y. and W. T. Greenough (1999). "Synaptic plasticity in cortical systems." *Current Opinion in Neurobiology* 9.2.

Knoblauch, A., E. Körner, U. Körner, and F. T. Sommer (2014). "Structural synaptic plasticity has high memory capacity and can explain graded amnesia, catastrophic forgetting, and the spacing effect." *PLoS One* 9.5.

Knoblauch, A. and G. Palm (2002). "Scene segmentation by spike synchronization in reciprocally connected visual areas. I. Local effects of cortical feedback." *Biological Cybernetics* 87.3.

Knoblauch, A., G. Palm, and F. T. Sommer (2010). "Memory capacities for synaptic and structural plasticity." *Neural Computation* 22.2.

Knoblauch, A. and F. T. Sommer (2016). "Structural plasticity, effectual connectivity, and memory in cortex." *Frontiers in Neuroanatomy* 10.

Kobayashi, R., Y. Tsubo, and S. Shinomoto (2009). "Made-to-order spiking neuron model equipped with a multi-timescale adaptive threshold." *Frontiers in Computational Neuroscience* 3.

Koch, C. (2004). *Biophysics of Computation: Information Processing in Single Neurons*. Oxford University Press.

Koch, C. and I. Segev (1998). *Methods in Neuronal Mdeling: from Ions to Networks*. MIT press.

Kolb, B. and R. Gibb (2011). "Brain plasticity and behaviour in the developing brain." *Journal of the Canadian Academy of Child and Adolescent Psychiatry* 20.4.

Kolb, B. et al. (2012). "Experience and the developing prefrontal cortex." *Proceedings of the National Academy of Sciences.*

Komin, N., A. C. Murza, E. Hernández-García, and R. Toral (2010). "Synchronization and entrainment of coupled circadian oscillators." *Interface Focus.*

Kötter, R. and K. E. Stephan (2003). "Network participation indices: characterizing component roles for information processing in neural networks." *Neural Networks* 16.9.

Krioukov, D. et al. (2010). "Hyperbolic geometry of complex networks." *Physical Review E* 82.3.

Kuehn, E. and M. I. Sereno (2018). "Modelling the Human Cortex in Three Dimensions." *Trends in cognitive sciences* 22.12.

Kuramoto, Y. (1975). "Self-entrainment of a population of coupled non-linear oscillators." *International Symposium on Mathematical Problems in Theoretical Physics.* Springer.

— (2003). *Chemical oscillations, waves, and turbulence.* Courier Corporation.

Lago-Fernández, L. F., R. Huerta, F. Corbacho, and J. A. Sig´uenza (2000). "Fast response and temporal coherent oscillations in small-world networks." *Physical Review Letters* 110.84.

Laing, C. R. (2009). "Chimera states in heterogeneous networks." *Chaos: An Interdisciplinary Journal of Nonlinear Science* 19.1.

Lapicque, L. (1907). "Recherches quantitatives sur l'excitation electrique des nerfs traitee comme une polarization." *Journal de Physiologie et de Pathologie Generalej* 9.

Latora, V. and M. Marchiori (2001). "Efficient behavior of small-world networks." *Physical Review Letters* 87.19.

Lee, K. S., F. Schottler, M. Oliver, and G. Lynch (1980). "Brief bursts of high-frequency stimulation produce two types of structural change in rat hippocampus." *Journal of Neurophysiology* 44.2.

Leicht, E. A. and M. E. J. Newman (2008). "Community Structure in Directed Networks." *Physical Review Letters* 100 (11).

Leistedt, S. J. et al. (2009). "Altered sleep brain functional connectivity in acutely depressed patients." *Human Brain Mapping* 30.7.

Lenz, W. (1920). "Beitrag zum Verständnis der magnetischen Erscheinungen in festen Körpern." *Z. Phys.* 21.

Leone, M., A. Vázquez, A. Vespignani, and R. Zecchina (2002). "Ferromagnetic ordering in graphs with arbitrary degree distribution." *The European Physical Journal B-Condensed Matter and Complex Systems* 28.2.

Leung, C. and H. Chau (2007). "Weighted assortative and disassortative networks model." *Physica A: Statistical Mechanics and its Applications* 378.2.

Levina, A., J. M. Herrmann, and T. Geisel (2007). "Dynamical synapses causing self-organized criticality in neural networks." *Nature physics* 3.12.

Lewis, M. D. and R. M. Todd (2007). "The self-regulating brain: Cortical-subcortical feedback and the development of intelligent action." *Cognitive Development* 22.4.

Li, S. et al. (2004). "A map of the interactome network of the metazoan C. elegans." *Science.*

Lind, S. E., D. M. Williams, D. M. Bowler, and A. Peel (2014). "Episodic memory and episodic future thinking impairments in high-functioning autism spectrum disorder: An underlying difficulty with scene construction or self-projection?" *Neuropsychology* 28.1.

Linkenkaer-Hansen, K., V. V. Nikouline, J. M. Palva, and R. J. Ilmoniemi (2001). "Long-range temporal correlations and scaling behavior in human brain oscillations." *Journal of Neuroscience* 21.4.

Lionni, L. (2018). *Colored discrete spaces: higher dimensional combinatorial maps and quantum gravity.* Springer.

Litwin-Kumar, A. and B. Doiron (2014). "Formation and maintenance of neuronal assemblies through synaptic plasticity." *Nature Communications* 5.

Liu, G. et al. (2017). "Functional diversity of topological modules in human protein-protein interaction networks." *Scientific Reports* 7.1.

Loh, M., E. T. Rolls, and G. Deco (Nov. 2007). "A Dynamical Systems Hypothesis of Schizophrenia." *PLoS Computational Biology* 3.11.

Low, L. K. and H.-J. Cheng (2006). "Axon pruning: an essential step underlying the developmental plasticity of neuronal connections." *Philosophical Transactions of the Royal Society of London B: Biological Sciences* 361.1473.

Luo, L. and D. D. O'Leary (2005). "Axon retraction and degeneration in development and disease." *Annual Review of Neuroscience* 28.

Lux, T. and M. Marchesi (1999). "Scaling and criticality in a stochastic multi-agent model of a financial market." *Nature* 397.6719.

Malamud, B. D., G. Morein, and D. L. Turcotte (1998). "Forest fires: an example of self-organized critical behavior." *Science* 281.5384.

Markram, H., J. Lübke, M. Frotscher, and B. Sakmann (1997). "Regulation of synaptic efficacy by coincidence of postsynaptic APs and EPSPs." *Science* 275.5297.

Marro, J., J. Torres, and J. Cortes (2008). "Complex behavior in a network with time-dependent connections and silent nodes." *Journal of Statistical Mechanics: Theory and Experiment* 2008.02.

Marro, J. and D. R. Chialvo (2017). *La mente es crítica: descubriendo la admirable complejidad del cerebro.* Universidad de Granada.

Marro, J. and R. Dickman (2005). *Nonequilibrium phase transitions in lattice models.* Cambridge University Press.

Marro, J., J. J. Torres, and J. M. Cortés (2007a). "Chaotic hopping between attractors in neural networks." *Neural Networks* 20.2.

Marro, J., J. J. Torres, and J. M. Cortés (2007b). "Chaotic hopping between attractors in neural networks." *Neural Networks* 20.2.

Maslov, S. and K. Sneppen (2002). "Specificity and stability in topology of protein networks." *Science* 296.5569.

Masoli, S., S. Solinas, and E. D'Angelo (2015). "Action potential processing in a detailed Purkinje cell model reveals a critical role for axonal compartmentalization." *Frontiers in Cellular Neuroscience* 9.

Masuda, N. and K. Aihara (2004). "Global and local synchrony of coupled neurons in small-world networks." *Biological Cybernetics* 90.4.

Matias, F. et al. (2015). "On the basic mechanisms of anticipated synchronization in neuronal circuits." *BMC neuroscience* 16.1.

McCulloch, W. S. and W. Pitts (1943). "A logical calculus of the ideas immanent in nervous activity." *The Bulletin of Mathematical Biophysics* 5.4.

Mejías, J. F. (2009). "Short-term synaptic plasticity: computational implications in the emergent behavior of neural systems." PhD thesis. Universidad de Granada.

Mejías, J. F., B. Hernandez-Gomez, and J. J. Torres (2012). "Short-term synaptic facilitation improves information retrieval in noisy neural networks." *Europhysics Letters* 97.4.

Mejías, J. F., H. J. Kappen, and J. J. Torres (2010). "Irregular dynamics in up and down cortical states." *PLoS One* 5.11.

Mejías, J. F. and J. J. Torres (2009). "Maximum memory capacity on neural networks with short-term synaptic depression and facilitation." *Neural Computation* 21.3.

— (2011). "Emergence of resonances in neural systems: the interplay between adaptive threshold and short-term synaptic plasticity." *PLoS One* 6.3.

Melamed, O. et al. (2008). "Slow oscillations in neural networks with facilitating synapses." *Journal of Computational Neuroscience* 25.2.

Millán, A. P., J. J. Torres, and G. Bianconi (2018a). "Complex Network Geometry and Frustrated Synchronization." *Scientific Reports* 8.9910.

Millán, A. P., J. J. Torres, S. Johnson, and J. Marro (2018b). "Growth strategy determines network performance." arXiv:1806.01878.

Millán, A. P., J. J. Torres, S. Johnson, and J. Marro (2018c). "Concurrence of form and function in developing networks and its role in synaptic pruning." *Nature Communications* 9.1.

Millán, A. P., J. J. Torres, and G. Bianconi (2019a). "Synchronization in network geometries with finite spectral dimension." *Physical Review E* 99.2.

Millán, A. P., J. J. Torres, and J. Marro (2019b). "How Memory Conforms to Brain Development." *Frontiers in Computational Neuroscience* 13.

Millán, A., J. Torres, S. Johnson, and J. Marro (2015). "Evolution of brain network structure under a critical condition as induced by local currents." *Int. J. Complex Systems in Science* 5.1.

Millman, D., S. Mihalas, A. Kirkwood, and E. Niebur (2010). "Self-organized criticality occurs in non-conservative neuronal networks during 'up' states." *Nature physics* 6.10.

Mimura, K., T. Kimoto, and M. Okada (2003). "Synapse efficiency diverges due to synaptic pruning following overgrowth." *Physical Review E* 68.3.

Mitra, B., N. Ganguly, S. Ghose, and F. Peruani (2008). "Generalized theory for node disruption in finite-size complex networks." *Physical Review E* 78.2.

Miyamoto, A., H. Wake, A. J. Moorhouse, and J. Nabekura (2013). "Microglia and synapse interactions: fine tuning neural circuits and candidate molecules." *Frontiers in cellular neuroscience* 7.

Modha, D. S. and R. Singh (2010). "Network architecture of the long-distance pathways in the macaque brain." *Proceedings of the National Academy of Sciences* 107.30.

Mongillo, G., O. Barak, and M. Tsodyks (2008). "Synaptic theory of working memory." *Science* 319.5869.

Morelli, L. G., G. Abramson, and M. N. Kuperman (2004). "Associative memory on a small-world neural network." *The European Physical Journal B-Condensed Matter and Complex Systems* 38.3.

Moretti, P. and M. A. Muñoz (2013). "Griffiths phases and the stretching of criticality in brain networks." *Nature Communications* 4.

Morgan, R. J. and I. Soltesz (2008). "Nonrandom connectivity of the epileptic dentate gyrus predicts a major role for neuronal hubs in seizures." *Proceedings of the National Academy of Sciences* 105.16.

Mori, S. and J.-D. Tournier (2013). *Introduction to diffusion tensor imaging: And higher order models.* Academic Press.

Morrison, A., M. Diesmann, and W. Gerstner (2008). "Phenomenological models of synaptic plasticity based on spike timing." *Biological cybernetics* 98.6.

Moussaïd, M. et al. (2009). "Experimental study of the behavioural mechanisms underlying self-organization in human crowds." *Proceedings of the Royal Society B: Biological Sciences* 276.1668.

Mucha, P. J. et al. (2010). "Community structure in time-dependent, multiscale, and multiplex networks." *Science* 328.5980.

Mulder, D. and G. Bianconi (2018). "Network Geometry and Complexity." *Journal of Statistical Physics* 173.3-4.

Muñoz, M. A. (2018). "Colloquium: Criticality and dynamical scaling in living systems." *Reviews of Modern Physics* 90.3.

Muñoz, M. A., R. Juhász, C. Castellano, and G. ódor (2010). "Griffiths phases on complex networks." *Physical Review Letters* 105.12.

Muscoloni, A. et al. (2017). "Machine learning meets complex networks via coalescent embedding in the hyperbolic space." *Nature Communications* 8.1.

Nakamura, T. et al. (2007). "Universal scaling law in human behavioral organization." *Physical Review Letters* 99.13.

Navlakha, S., A. L. Barth, and Z. Bar-Joseph (July 2015). "Decreasing-Rate Pruning Optimizes the Construction of Efficient and Robust Distributed Networks." *PLoS Computational Biology* 11.7.

Netoff, T. I. et al. (2004). "Epilepsy in small-world networks." *Journal of neuroscience* 24.37.

Newman, M. E. J. (2006). "Modularity and community structure in networks." *Proceedings of the National Academy of Sciences* 103.23.

Newman, M. E. J. (2002). "Assortative Mixing in Networks." *Physical Review Letters* 89 (20).

— (2004). "Fast algorithm for detecting community structure in networks." *Physical Review E* 69 (6).

Newman, M. E. (2003). "The structure and function of complex networks." *SIAM Review* 45.2.

— (2011). *Networks: an introduction.* Oxford University Press.

Niedermeyer, E. and F. L. da Silva (2005). *Electroencephalography: basic principles, clinical applications, and related fields.* Lippincott Williams & Wilkins.

Nimmerjahn, A., F. Kirchhoff, and F. Helmchen (2005). "Resting microglial cells are highly dynamic surveillants of brain parenchyma in vivo." *Science* 308.5726.

Noest, A. J. (1986). "New universality for spatially disordered cellular automata and directed percolation." *Physical review letters* 57.1.

Norton, L. et al. (2012). "Disruptions of functional connectivity in the default mode network of comatose patients." *Neurology.*

Nykter, M. et al. (2008). "Gene expression dynamics in the macrophage exhibit criticality." *Proceedings of the National Academy of Sciences* 105.6.

Ódor, G. (2013). "Spectral analysis and slow spreading dynamics on complex networks." *Physical Review E* 88.3.

Ódor, G. and B. Hartmann (2018). "Heterogeneity effects in power grid network models." *Physical Review E* 98.2.

Oh, S. W. et al. (2014). "A mesoscale connectome of the mouse brain." *Nature* 508.7495.

Onnela, J.-P., J. Saramäki, J. Kertész, and K. Kaski (2005). "Intensity and coherence of motifs in weighted complex networks." *Physical Review E* 71 (6).

Onsager, L. (1944). "Crystal statistics. I. A two-dimensional model with an order-disorder transition." *Physical Review* 65.3-4.

Oppenheim, R. W. (1989). "The neurotrophic theory and naturally occurring motoneuron death." *Trends in Neurosciences* 12.7.

Oriti, D. (2001). "Spacetime geometry from algebra: spin foam models for non-perturbative quantum gravity." *Reports on Progress in Physics* 64.12.

Oshima, H. and T. Odagaki (2007). "Storage capacity and retrieval time of small-world neural networks." *Physical Review E* 76.3.

Palla, G., I. Derényi, I. Farkas, and T. Vicsek (2005). "Uncovering the overlapping community structure of complex networks in nature and society." *Nature* 435.814.

Panaggio, M. J. and D. M. Abrams (2015). "Chimera states: coexistence of coherence and incoherence in networks of coupled oscillators." *Nonlinearity* 28.3.

Pantic, L., J. J. Torres, H. J. Kappen, and S. C. A. M. Gielen (2002). "Associative Memory with Dynamic Synapses." *Neural Computation* 14.12.

Paolicelli, R. C. et al. (2011). "Synaptic pruning by microglia is necessary for normal brain development." *science* 333.6048.

Papadopoulos, L., M. A. Porter, K. E. Daniels, and D. S. Bassett (2018). "Network analysis of particles and grains." *Journal of Complex Networks* 6.4.

Pastor-Satorras, R., A. Vázquez, and A. Vespignani (2001). "Dynamical and Correlation Properties of the Internet." *Physical Review Letters* 87 (25).

Pearce, J. (2009). "Marie-Jean-Pierre flourens (1794–1867) and cortical localization." *European neurology* 61.5.

Percha, B., R. Dzakpasu, M. Żochowski, and J. Parent (2005). "Transition from local to global phase synchrony in small world neural network and its possible implications for epilepsy." *Physical Review E* 72.3.

Peretto, P. (1992). *An introduction to the modeling of neural networks*. Vol. 2. Cambridge University Press.

Perry, V. H. and V. O'Connor (2010). "The role of microglia in synaptic stripping and synaptic degeneration: a revised perspective." *ASN neuro* 2.5.

Petanjek, Z. et al. (2011). "Extraordinary neoteny of synaptic spines in the human prefrontal cortex." *Proceedings of the National Academy of Sciences* 108.32.

Petermann, T. et al. (2009). "Spontaneous cortical activity in awake monkeys composed of neuronal avalanches." *Proceedings of the National Academy of Sciences* 106.37.

Peters, O. and J. D. Neelin (2006). "Critical phenomena in atmospheric precipitation." *Nature Physics* 2.6.

Petri, G. and A. Barrat (2018). "Simplicial Activity Driven Model." *arXiv preprint arXiv:1805.06740*.

Petri, G. et al. (2014). "Homological scaffolds of brain functional networks." *Journal of The Royal Society Interface* 11.101.

Pikovsky, A., M. Rosenblum, and J. Kurths (2003). *Synchronization: a universal concept in nonlinear sciences*. Vol. 12. Cambridge University Press.

Piraveenan, M., M. Prokopenko, and A. Y. Zomaya (2008). "Local assortativeness in scale-free networks." *Europhysics Letters* 84.2.

Poil, S.-S., R. Hardstone, H. D. Mansvelder, and K. Linkenkaer-Hansen (2012). "Critical-state dynamics of avalanches and oscillations jointly emerge from balanced excitation/inhibition in neuronal networks." *Journal of Neuroscience* 32.29.

Poirier, M., J. S. Martin, S. B. Gaigg, and D. M. Bowler (2011). "Short-term memory in autism spectrum disorder." *Journal of Abnormal Psychology* 120.1.

Presumey, J., A. R. Bialas, and M. C. Carroll (2017). "Advances in Immunology." Vol. 135. Academic Press. Chap. Chapter Two - Complement System in Neural Synapse Elimination in Development and Disease.

Purves, D. et al. (2018). *Neuroscience.* Oxford University Press.

Puschmann, T. B. et al. (2013). "Bioactive 3D cell culture system minimizes cellular stress and maintains the in vivo-like morphological complexity of astroglial cells." *Glia* 61.3.

Rabinovich, M. I., P. Varona, A. I. Selverston, and H. D. Abarbanel (2006). "Dynamical principles in neuroscience." *Reviews of Modern Physics* 78.4.

Raichle, M. E. (2011). "The restless brain." *Brain Connectivity* 1.1.

Raichle, M. E. and M. A. Mintun (2006). "Brain Work and Brain Imaging." *Annual Review of Neuroscience* 29.1. PMID: 16776593. eprint: https://doi.org/10.1146/annurev.neuro.29.051605.112819.

Raichle, M. E. et al. (2001). "A default mode of brain function." *Proceedings of the National Academy of Sciences* 98.2. eprint: https://www.pnas.org/content/98/2/676.full.pdf.

Rakic, P. et al. (1986). "Concurrent overproduction of synapses in diverse regions of the primate cerebral cortex." *Science* 232.4747.

Rammal, R. and G. Toulouse (1983). "Random walks on fractal structures and percolation clusters." *Journal de Physique Lettres* 44.1.

Ramón y Cajal, S. (1911). "Histologie du syste me nerveux de I'Homme et des verte be s." *Maloine (Paris)* 2.

— (1995). *Histology of the Nervous System of Man and Vertebrates (History of Neuroscience, No 6)(2 Volume Set).* Oxford: Oxford University Press.

Rauch, E. M., M. M. Millonas, and D. R. Chialvo (1995). "Pattern formation and functionality in swarm models." *arXiv preprint adap-org/9507003.*

Reimann, M. W. et al. (2017). "Cliques of neurons bound into cavities provide a missing link between structure and function." *Frontiers in Computational Neuroscience* 11.

Ren, J., J. Wang, M. Li, and L. Wang (2013). "Identifying protein complexes based on density and modularity in protein-protein interaction network." *BMC Systems Biology* 7.4.

Romani, S., D. J. Amit, and G. Mongillo (2006). "Mean-field analysis of selective persistent activity in presence of short-term synaptic depression." *Journal of Computational Neuroscience* 20.2.

Rubinov, M. and E. Bullmore (2013). "Fledgling pathoconnectomics of psychiatric disorders." *Trends in Cognitive Sciences* 17.12.

Sadek, R. A. (2013). "Regional atrophy analysis of MRI for early detection of alzheimer's disease." *International Journal of Signal Processing, Image Processing and Pattern Recognition* 6.1.

Safari, A., P. Moretti, and M. A. Muñoz (2017). "Topological dimension tunes activity patterns in hierarchical modular networks." *New Journal of Physics* 19.11.

Salnikov, V., D. Cassese, and R. Lambiotte (2018). "Simplicial complexes and complex systems." *European Journal of Physics* 40.1.

Sanchez-Garcia, R. J. (2018). "Exploiting symmetry in network analysis." *arXiv preprint arXiv:1803.06915.*

Santo, S. di, P. Villegas, R. Burioni, and M. A. Muñoz (2018). "Landau–Ginzburg theory of cortex dynamics: Scale-free avalanches emerge at the edge of synchronization." *Proceedings of the National Academy of Sciences* 115.7.

Santos, E. and C. A. Noggle (2011). "Synaptic Pruning." *Encyclopedia of Child Behavior and Development.* Ed. by S. Goldstein and J. A. Naglieri. Boston, MA: Springer US.

Sayama, H. et al. (2013). "Modeling complex systems with adaptive networks." *Computers & Mathematics with Applications* 65.10. Grasping Complexity.

Scannell, J. et al. (1999). "The connectional organization of the cortico-thalamic system of the cat." *Cerebral Cortex* 9.3.

Schiller, F. (1992). *Paul Broca: Founder of French anthropology, explorer of the brain.* Oxford University Press, USA.

Schnitzler, A. and J. Gross (2005). "Normal and pathological oscillatory communication in the brain." *Nature reviews neuroscience* 6.4.

Sekar, A. et al. (2016). "Schizophrenia risk from complex variation of complement component 4." *Nature* 530. Article.

Serrano, M. Á., M. Boguná, and F. Sagués (2012). "Uncovering the hidden geometry behind metabolic networks." *Molecular Biosystems* 8.3.

Serrano, M. Á., D. Krioukov, and M. Boguñá (2011). "Percolation in self-similar networks." *Physical Review Letters* 106.4.

Severino, F. P. U. et al. (2016). "The role of dimensionality in neuronal network dynamics." *Scientific Reports* 6.

Shen, K. et al. (2015). "Network structure shapes spontaneous functional connectivity dynamics." *Journal of Neuroscience* 35.14.

Sherrington, D. and S. Kirkpatrick (1975). "Solvable model of a spin-glass." *Physical Review Letters* 35.26.

Shmulevich, I., S. A. Kauffman, and M. Aldana (2005). "Eukaryotic cells are dynamically ordered or critical but not chaotic." *Proceedings of the National Academy of Sciences* 102.38.

Shulman, G. L. et al. (1997). "Common blood flow changes across visual tasks: II. Decreases in cerebral cortex." *Journal of Cognitive Neuroscience* 9.5.

Silva, D. C. da et al. (2018). "Complex network view of evolving manifolds." *Physical Review E* 97.3.

Singer, W. et al. (1997). "Neuronal assemblies: necessity, signature and detectability." *Trends in cognitive sciences* 1.7.

Singh, K. K. and F. D. Miller (2005). "Activity regulates positive and negative neurotrophin-derived signals to determine axon competition." *Neuron* 45.6.

Sjostrom, P. J., E. A. Rancz, A. Roth, and M. Hausser (2008). "Dendritic excitability and synaptic plasticity." *Physiological Reviews* 88.2.

Smith, S. M. et al. (2009). "Correspondence of the brain's functional architecture during activation and rest." *Proceedings of the National Academy of Sciences* 106.31.

Sompolinsky, H. and I. Kanter (1986). "Temporal association in asymmetric neural networks." *Physical Review Letters* 57.22.

Song, S., K. D. Miller, and L. F. Abbott (2000). "Competitive Hebbian learning through spike-timing-dependent synaptic plasticity." *Nature Neuroscience* 3.9.

Sossin, W. S., A. Sweet-Cordero, and R. H. Scheller (1990). "Dale's hypothesis revisited: different neuropeptides derived from a common prohormone are targeted to different processes." *Proceedings of the National Academy of Sciences* 87.12.

Sowell, E. R. et al. (2003). "Mapping cortical change across the human life span." *Nature Neuroscience* 6.3.

Sporns, O. (2004). "Complex neural dynamics." *Coordination Dynamics: Issues and Trends*. Springer.

— (2011). *Networks of the brain*. MIT Press.

— (2012). *Discovering the Human Connectome*. MIT press.

Sporns, O., J. A. Gally, G. N. Reeke, and G. M. Edelman (1989). "Reentrant signaling among simulated neuronal groups leads to coherency in their oscillatory activity." *Proceedings of the National Academy of Sciences* 86.18.

Sporns, O., G. Tononi, and G. M. Edelman (2000). "Theoretical neuroanatomy: relating anatomical and functional connectivity in graphs and cortical connection matrices." *Cerebral Cortex* 10.2.

Sporns, O., G. Tononi, and R. Kötter (2005). "The human connectome: a structural description of the human brain." *PLoS Computational Biology* 1.4.

Sporns, O. and J. D. Zwi (2004). "The small world of the cerebral cortex." *Neuroinformatics* 2.2.

Squire, L. et al. (2012). *Fundamental neuroscience*. Academic Press.

Srinivas, K. V., R. Jain, S. Saurav, and S. K. Sikdar (2007). "Small-world network topology of hippocampal neuronal network is lost, in an in vitro glutamate injury model of epilepsy." *European Journal of Neuroscience* 25.11.

Stafford, J. M. et al. (2014). "Large-scale topology and the default mode network in the mouse connectome." *Proceedings of the National Academy of Sciences* 111.52.

Stam, C. et al. (2008). "Graph theoretical analysis of magnetoencephalographic functional connectivity in Alzheimer's disease." *Brain* 132.1.

Stam, C. J. et al. (2006). "Small-world networks and functional connectivity in Alzheimer's disease." *Cerebral Cortex* 17.1.

Stauffer, D., A. Aharony, L. da Fontoura Costa, and J. Adler (2003). "Efficient Hopfield pattern recognition on a scale-free neural network." *The European Physical Journal B-Condensed Matter and Complex Systems* 32.3.

Steinmetz, P. N. et al. (2000). "Attention modulates synchronized neuronal firing in primate somatosensory cortex." *Nature* 404.6774.

Stepanyants, A., P. R. Hof, and D. B. Chklovskii (2002). "Geometry and structural plasticity of synaptic connectivity." *Neuron* 34.2.

Stephan, K. E. et al. (2000). "Computational analysis of functional connectivity between areas of primate cerebral cortex." *Philosophical Transactions of the Royal Society of London B: Biological Sciences* 355.1393.

Strogatz, S. H. (2000). "From Kuramoto to Crawford: exploring the onset of synchronization in populations of coupled oscillators." *Physica D: Nonlinear Phenomena* 143.1-4.

— (2018). *Nonlinear dynamics and chaos: with applications to physics, biology, chemistry, and engineering.* CRC Press.

Strotzer, M. (2009). "One century of brain mapping using Brodmann areas." *Clinical Neuroradiology* 19.3.

Su, G., Z. Ruan, S. Guan, and Z. Liu (2013). "Explosive synchronization on co-evolving networks." *Europhysics Letters* 103.4.

Sun, T. and R. F. Hevner (2014). "Growth and folding of the mammalian cerebral cortex: from molecules to malformations." *Nature Reviews Neuroscience* 15.4.

Šuvakov, M., M. Andjelković, and B. Tadić (2018). "Hidden geometries in networks arising from cooperative self-assembly." *Scientific Reports* 8.1.

Tagliazucchi, E., P. Balenzuela, D. Fraiman, and D. R. Chialvo (2012). "Criticality in large-scale brain fMRI dynamics unveiled by a novel point process analysis." *Frontiers in Physiology* 3.

Takayasu, M., H. Takayasu, and K. Fukuda (2000). "Dynamic phase transition observed in the Internet traffic flow." *Physica A: Statistical Mechanics and its Applications* 277.1-2.

Tang, G. et al. (2014). "Loss of mTOR-Dependent Macroautophagy Causes Autistic-like Synaptic Pruning Deficits." *Neuron* 83.5.

Telesford, Q. K. et al. (2011). "The brain as a complex system: using network science as a tool for understanding the brain." *Brain Connectivity* 1.4.

Tetzlaff, C. et al. (2010). "Self-organized criticality in developing neuronal networks." *PLoS Computational Biology* 6.12.

Tian, L. et al. (2006). "Altered resting-state functional connectivity patterns of anterior cingulate cortex in adolescents with attention deficit hyperactivity disorder." *Neuroscience Letters* 400.1-2.

Tononi, G., G. M. Edelman, and O. Sporns (1998). "Complexity and coherency: integrating information in the brain." *Trends in Cognitive Sciences* 2.12.

Tononi, G., O. Sporns, and G. M. Edelman (1994). "A measure for brain complexity: relating functional segregation and integration in the nervous system." *Proceedings of the National Academy of Sciences* 91.11.

Toro, R. et al. (2008). "Brain size and folding of the human cerebral cortex." *Cerebral cortex* 18.10.

Torres, J. (2010). "Modeling Biological Neural Networks." *Handbook of natural computing.* Ed. by G. Rozenberg, T. Bäck, and J. N. Kok. Editorial Springer Verlag.

Torres, J. J., J. M. Cortes, J. Marro, and H. J. Kappen (2007a). "Competition Between Synaptic Depression and Facilitation in Attractor Neural Networks." *Neural Computation* 19.10.

Torres, J. J., J. Marro, J. M. Cortes, and B. Wemmenhove (2008). "Instabilities in Attractor Networks with Fast Synaptic Fluctuations and Partial Updating of the Neurons Activity." *Neural Networks* 21.9.

Torres, J. J., J. M. Cortes, J. Marro, and H. J. Kappen (2007b). "Attractor neural networks with activity-dependent synapses: The role of synaptic facilitation." *Neurocomputing* 70.10-12.

Torres, J. J. and J. Marro (2015). "Brain performance versus phase transitions." *Scientific Reports* 5.

Torres, J. J., M. A. Muñoz, J. Marro, and P. Garrido (2004). "Influence of topology on the performance of a neural network." *Neurocomputing* 58.

Torres, J. J., L. Pantic, and H. J. Kappen (2002). "Storage capacity of attractor neural networks with depressing synapses." *Physical Review E* 66.6.

Travers, J. and S. Milgram (1967). "The small world problem." *Phychology Today* 1.1.

Tremblay, M.-È., R. L. Lowery, and A. K. Majewska (2010). "Microglial interactions with synapses are modulated by visual experience." *PLoS biology* 8.11.

Treviño III, S., Y. Sun, T. F. Cooper, and K. E. Bassler (2012). "Robust detection of hierarchical communities from Escherichia coli gene expression data." *PLoS computational biology* 8.2.

Tsodyks, M. V. and H. Markram (1997). "The neural code between neocortical pyramidal neurons depends on neurotransmitter release probability." *Proceedings of the National Academy of Sciences* 94.2.

Tsodyks, M., K. Pawelzik, and H. Markram (1998). "Neural networks with dynamic synapses." *Neural Computation* 10.4.

Turanalp, M. E. and T. Can (2008). "Discovering functional interaction patterns in protein-protein interaction networks." *BMC Bioinformatics* 9.1.

Turrigiano, G. G. et al. (1998). "Activity-dependent scaling of quantal amplitude in neocortical neurons." *Nature* 391.6670.

Uhlhaas, P. J. and W. Singer (2006). "Neural synchrony in brain disorders: relevance for cognitive dysfunctions and pathophysiology." *neuron* 52.1.

Uhlig, M., A. Levina, T. Geisel, and M. Herrmann (2013). "Critical dynamics in associative memory networks." *Frontiers in Computational Neuroscience* 7.

Valverde, S. et al. (2015). "Structural determinants of criticality in biological networks." *Frontiers in physiology* 6.

Van Den Heuvel, M. P. and O. Sporns (2011). "Rich-club organization of the human connectome." *Journal of Neuroscience* 31.44.

Van Kampen, N. G. (1992). *Stochastic processes in physics and chemistry*. Vol. 1. Elsevier.

Vandermeer, J., I. Perfecto, and S. M. Philpott (2008). "Clusters of ant colonies and robust criticality in a tropical agroecosystem." *Nature* 451.7177.

Varela, F., J.-P. Lachaux, E. Rodriguez, and J. Martinerie (2001). "The brainweb: phase synchronization and large-scale integration." *Nature reviews neuroscience* 2.4.

Varshney, L. R. et al. (2011). "Structural properties of the Caenorhabditis elegans neuronal network." *PLoS Computational Biology* 7.2.

Vazquez, F., V. M. Eguíluz, and M. S. Miguel (2008). "Generic Absorbing Transition in Coevolution Dynamics." *Physical Review Letters* 100 (10).

Vértes, P. E. et al. (2012). "Simple models of human brain functional networks." *Proceedings of the National Academy of Sciences*.

Villegas, P., P. Moretti, and M. A. Muñoz (2014). "Frustrated hierarchical synchronization and emergent complexity in the human connectome network." *Scientific Reports* 4.

Voges, N. and L. U. Perrinet (2012). "Complex dynamics in recurrent cortical networks based on spatially realistic connectivities." *Frontiers in Computational Neuroscience* 6.

Vojta, T. (2006). "Rare region effects at classical, quantum and nonequilibrium phase transitions." *Journal of Physics A: Mathematical and General* 39.22.

Volman, V., M. Perc, and M. Bazhenov (2011). "Gap junctions and epileptic seizures–two sides of the same coin?" *PLoS One* 6.5.

Voytek, B. et al. (2015). "Age-related changes in 1/f neural electrophysiological noise." *Journal of Neuroscience* 35.38.

Vuksanović, V. and P. Hövel (2014). "Functional connectivity of distant cortical regions: role of remote synchronization and symmetry in interactions." *NeuroImage* 97.

Wake, H. et al. (2009). "Resting microglia directly monitor the functional state of synapses in vivo and determine the fate of ischemic terminals." *Journal of Neuroscience* 29.13.

Wan, C. et al. (2015). "Panorama of ancient metazoan macromolecular complexes." *Nature* 525.7569.

Wang, L. et al. (2009). "Altered small-world brain functional networks in children with attention-deficit/hyperactivity disorder." *Human Brain Mapping* 30.2.

Ward, L. M. (2002). *Dynamical Cognitive Science.* MIT press.

— (2003). "Synchronous neural oscillations and cognitive processes." *Trends in Cognitive Sciences* 7.12.

Wasserman, S. and K. Faust (1994). *Social Network Analysis: Methods and Applications.* Vol. 8. Cambridge University Press.

Watts, D. J. and S. H. Strogatz (1998). "Collective dynamics of "small-world" networks." *Nature* 393.6684.

Wendling, F. et al. (2005). "Interictal to ictal transition in human temporal lobe epilepsy: insights from a computational model of intracerebral EEG." *Journal of Clinical Neurophysiology* 22.5.

Wiedermann, M. et al. (2015). "Macroscopic description of complex adaptive networks coevolving with dynamic node states." *Physical Review E* 91.5.

Williams, O., L. Lacasa, A. P. Millán, and V. Latora (2019a). "Measuring the memory of a temporal network." in preparation.

Williams, O. E., F. Lillo, and V. Latora (2019b). "Effects of memory on spreading processes in non-Markovian temporal networks." *New Journal of Physics.*

Williams, O. and C. I. Del Genio (2014). "Degree correlations in directed scale-free networks." *PLoS One* 9.10.

Williamson, P. (May 2007). "Are Anticorrelated Networks in the Brain Relevant to Schizophrenia?" *Schizophrenia Bulletin* 33.4. eprint: http://oup.prod.sis.lan/schizophreniabulletin/article-pdf/33/4/994/5426555/sbm043.pdf.

Wu, Z., G. Menichetti, C. Rahmede, and G. Bianconi (2015). "Emergent complex network geometry." *Scientific Reports* 5.

Xiong, W., L. Xie, S. Zhou, and J. Guan (2014). "Active learning for protein function prediction in protein–protein interaction networks." *Neurocomputing* 145.

Young, M. P. (1992). "Objective analysis of the topological organization of the primate cortical visual system." *Nature* 358.152.

Yuan, J., M. Lipinski, and A. Degterev (2003). "Diversity in the mechanisms of neuronal cell death." *Neuron* 40.2.

Zenke, F., E. J. Agnes, and W. Gerstner (2015). "Diverse synaptic plasticity mechanisms orchestrated to form and retrieve memories in spiking neural networks." *Nature Communications* 6.

Zhang, L. I. et al. (1998). "A critical window for cooperation and competition among developing retinotectal synapses." *Nature* 395.6697.

Zhang, Z., F. Comellas, G. Fertin, and L. Rong (2006). "High-dimensional Apollonian networks." *Journal of Physics A: Mathematical and General* 39.8.

Zhou, C. et al. (2006). "Hierarchical organization unveiled by functional connectivity in complex brain networks." *Physical Review Letters* 97.23.

Zucker, R. S. and W. G. Regehr (2002). "Short-term synaptic plasticity." *Annual Review of Physiology* 64.1.

Appendix A

Supplementary Information for Chapter 2

In this appendix we discuss the effect of the topological parameter γ on the emergent behavior of the adaptive neural network model presented in chapter 2.

A.1 Effect of γ on the emerging phases of the system

In panels a, b and c of figure $A.1$ we show the phase diagrams of the system respectively for $\gamma = 0.5$, 1.0 and 1.5; and for $n = 10$, $\kappa_0 = 20$, $\kappa_\infty = 10$ and $N = 1600$. Results for $\gamma = 1.0$ hold qualitatively for other values, but the region corresponding to each phase depends on γ. Due to the structure-memory coupling, the critical value α_c is depends slightly on the temperature, as shown in the main paper for $\gamma = 1.0$. Data has been averaged over 20 realizations.

In panel d we show $p_\infty(k)$ in some representative cases:

- **Main plot.** Three (T, α) points corresponding respectively to the homogeneous memory $(0.5, 0.5)$, homogeneous noise $(1.5, 0.5)$ and heterogeneous memory $(0.5, 1.5)$, as indicated in the caption. The homogeneous distributions are fairly similar, whereas the heterogeneous one is bimodal.

- **Inset i1.** Comparison between homogeneous (red circles) and heterogeneous (blue squares) IC in the bistability region ($T = \alpha = 1.5$). Homogeneous IC fall into the noisy homogeneous phase, whereas heterogeneous ones maintain memory and organize into a bimodal distribution.

- **Inset i2.** Examples of $p_\infty(k)$ along the critical transition $\alpha_c^t(T)$ for $T = 0.5$ and different values of γ, as indicated in the caption. Results are are mostly independent on γ, showing a heterogeneous and roughly scale-free

behaviour, but given the finite size of the system the exponent cannot be measured.

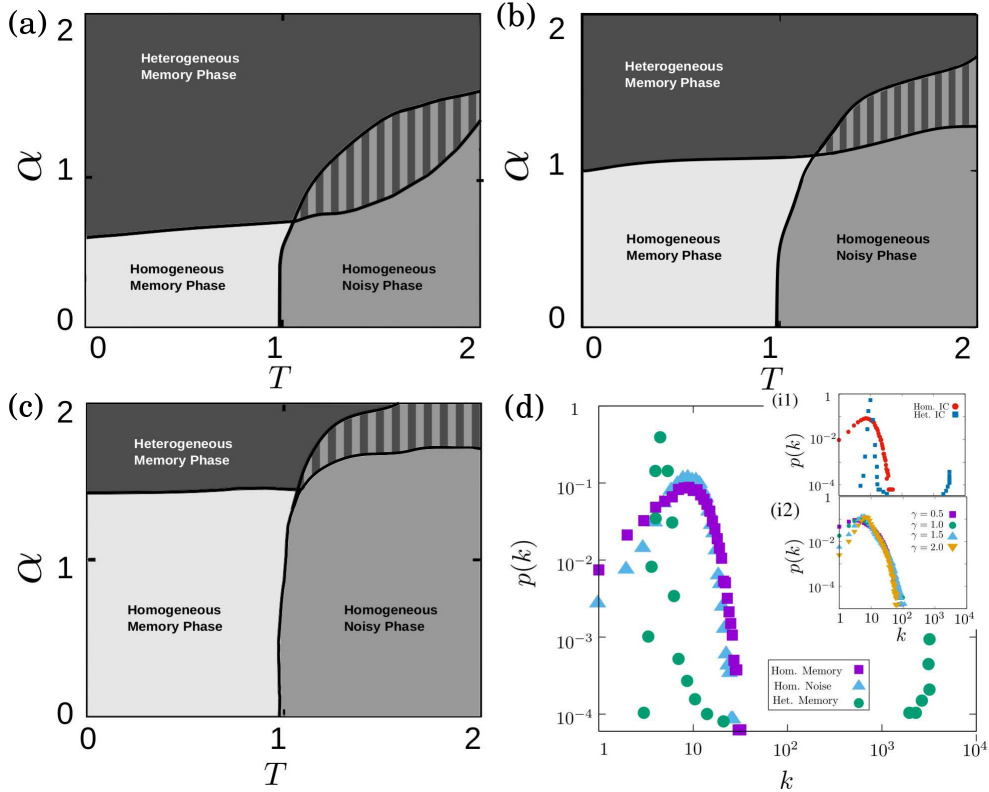Data in this panel has been averaged over 100 realizations.

Figure A.1: **Parameter analysis.**

Appendix B

Supplementary Information for Chapter 3

In this appendix we include some supplementary information and figures for chapter 3.

B.1   Behavior of the system at $T = 0$

Figure $B.1$ shows the (P, α) phase diagrams of the system in the absence of thermal noise $(T = 0)$, representing the fraction of recovered patterns g_p, the average overlap with these patterns, m_p, and the stationary homogeneity in the network, $\bar{g}$. The diagrams are for three values of $\kappa_\infty = 20$, 40 and 60 as indicated in the caption. Similarly, figure $B.2$ shows the phase diagrams indicating the number of recovered patterns $P_r(P, \alpha)$ for the same set of values of κ_∞.

B.2   Behavior of the system at $T > 0$

Figure $B.3$ shows the phase diagrams of the system with respect to α and T, $T > 0$, for $P = 5$, 10, 15 and 20, and for $\kappa_\infty = 20$, 40, 60. In each case we show three diagrams: g_p, m_p and $\bar{g}$, as indicated in the label of the color bar. In this figure a memory phase appears as a blue region in the diagram of g_p and a high value of m_p, indicated by a yellow or green color. A SG phase appears as an orange region in g_p and a lower value of m_p, indicated by a green or blue color, whereas a noisy phase appears as black in g_p and dark-blue in m_p. Finally, the oscillatory phase appears for high values of g_p, (light yellow regions in the corresponding diagrams) and relatively low values of m_p (associated blue regions of the corresponding diagrams). Similarly, homogeneous structures take place for high values of $\bar{g}$, indicated by a yellow region in the corresponding diagram, whereas heterogeneous structures are for low values of $\bar{g}$, indicated by
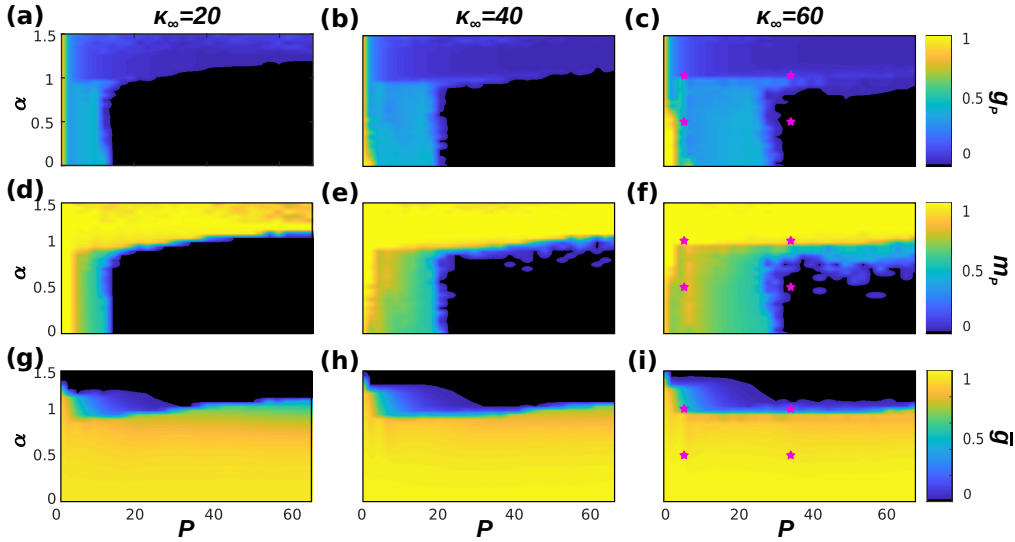
Figure B.1: **Phase diagrams at** $T = 0$. These depict the steady-state of the system with respect to P and α at $T = 0$ and $\kappa_\infty = 20$, 40 and 60, respectively from left to right. The top panels (a-c) show the fraction of patterns, g_p, retrieved after a given transient, and the middle ones (d-f) the average overlap with these different patterns, m_p, and finally the bottom ones (g-i) the stationary homogeneity of the network $\bar{g}$. The network size was set here to $N = 1600$ and each point has been averaged over 10 realizations of the dynamics.
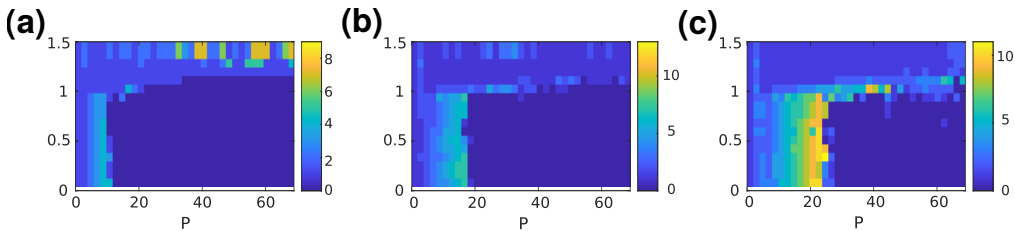

Figure B.2: **(a-c)** Diagrams indicating the number of recovered patterns P_r with respect to P and α at $T = 0$ and respectively for $\kappa_\infty = 20$, 40 and 60.

a black or dark blue region.

Finally, figure $B.4$ shows some representative time series of the overlap $m^\mu(t)$ corresponding to the points marked in the diagrams of figure $B.3$ with pink stars.
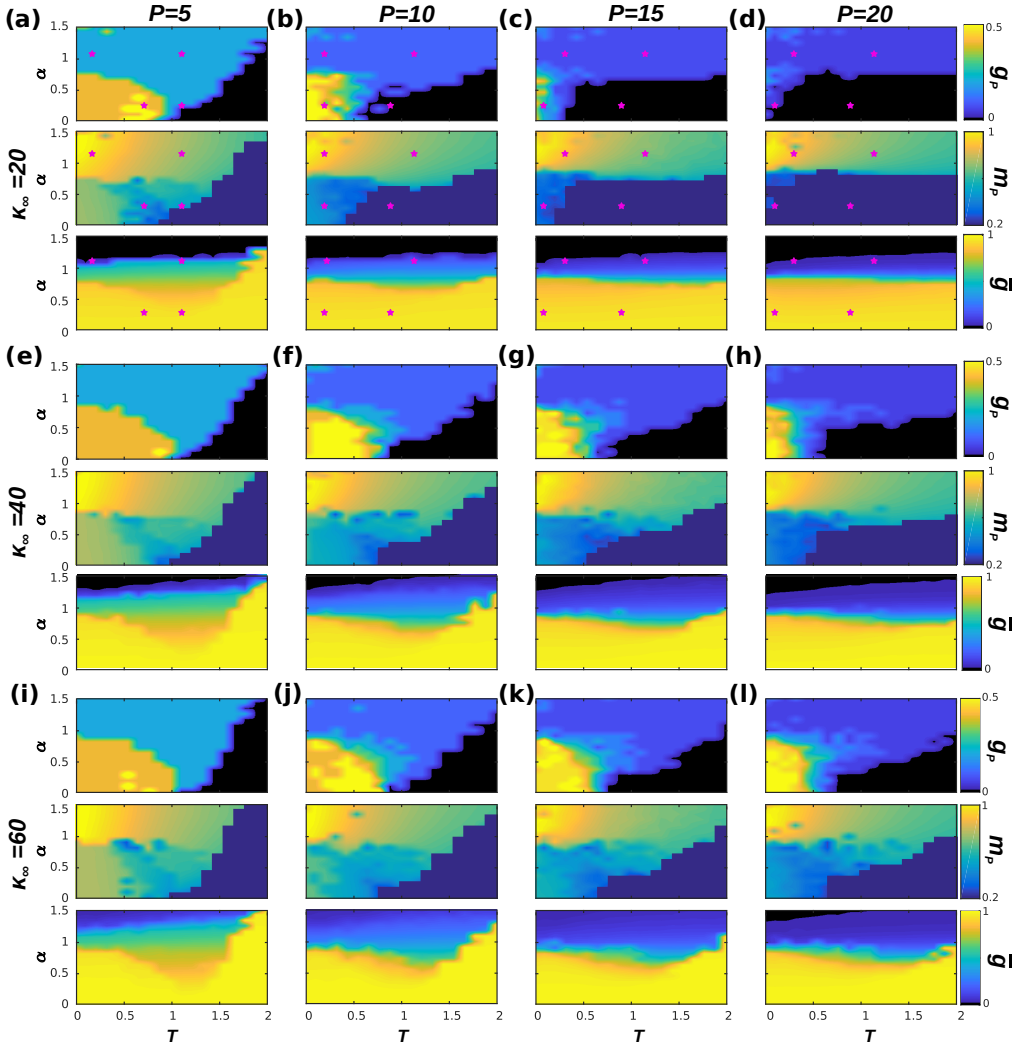
Figure B.3: Phase diagrams of the system with respect to α and T for four different values of P, in particular for $P = 5$, 10, 15 and 20 respectively from left to right, and for three values of $\kappa_\infty = 20$, 40, 60, respectively from top to bottom. In each panel we show three diagrams: g_p, m_p and $\bar{g}$, as indicated in the label of the color bar. Pink stars in panels (a) to (d) indicate the (T, α) point of the corresponding time series in figure 3.4. Results are for $N = 1600$ and have been averaged over 5 realizations of the system dynamics.
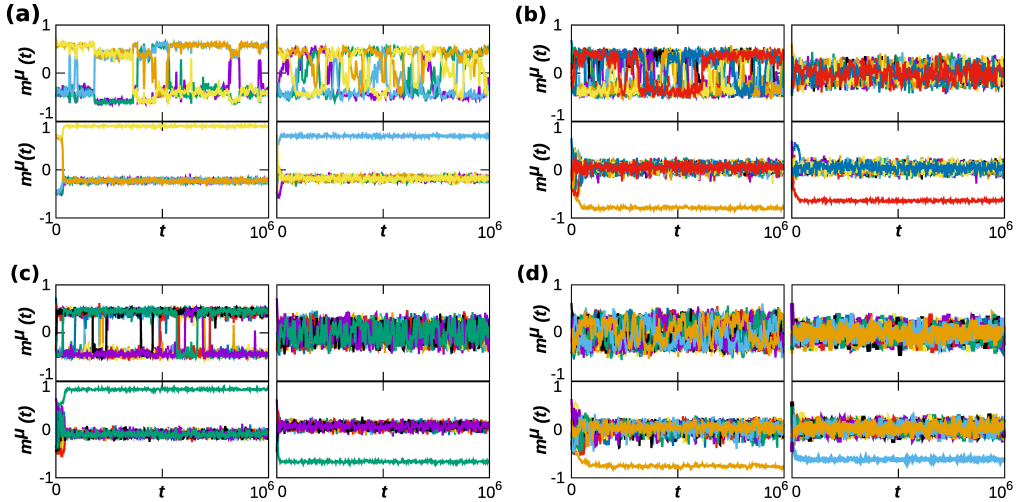
Figure B.4: Time series of the overlap $m^{\mu}(t)$ for some representative cases of the system dynamical behavior, corresponding to $\kappa_{\infty} = 20$ and to $P = 5$, 10, 15 and 20, respectively from panel a to d. In each composite panel, we illustrate the behavior of the system on for 4 points of the (T, α) space, as indicated by pink starts in the corresponding phase diagrams of figure 3.3. Namely, panel a is for the points $(0.7, 0.3)$, $(0.9, 0.3)$, $(0.3, 1.1)$, $(1.1, 1.1)$; panel b is for $(0.3, 0.3)$, $(0.9, 0.3)$, $(0.3, 1.1)$, $(1.1, 1.1)$; and finally panels c and d are for the points $(0.1, 0.3)$, $(0.9, 0.3)$, $(0.3, 1.1)$, $(1.1, 1.1)$. We have selected slightly different points for each P so as to show an example of the oscillatory behavior in each case, and the region of its appearance depends on P. Results are for $N = 1600$.

Appendix C

Supplementary Information for Chapter 5

In this appendix we provide additional information about the structure of Complex Network Manifolds regarding their degree distribution and small-word characteristic. Moreover we report additional information on the Complex Network Manifolds that have been used in the activity movies in Millán et al., 2018a.

C.1 Degree distribution and Hausdorff dimension of Complex Network Manifolds

The degree distribution $p(k)$ of Complex Network Manifold (Bianconi and Rahmede, 2015, 2016) is exponential for dimension $d = 2$ and scale-free for $d > 2$. The exact asymptotic expression has been derived in Bianconi and Rahmede, 2017 and is given for $d = 2$ by

$$p(k) = \frac{1}{d+1} \left(\frac{2}{3}\right)^{k-d},$$

(C.1)

with $k \geq 2$ whereas for $d > 2$ it is given by

$$p(k) = \frac{d-1}{2d-1} \frac{\Gamma\left[(1+(2d-1)/(d-2)\right]}{\Gamma\left[d/(d-2)\right]} \frac{\Gamma\left[k-d+d/(d-2)\right]}{\Gamma\left[k-d+1+(2d-1)/(d-2)\right]},$$

(C.2)

with $k \geq d$. Therefore, for $d > 2$ Complex Network Manifolds are scale-free with a power-law scaling

$$p(k) \approx k^{-\gamma},$$

(C.3)

valid for $k \gg 1$, and power-law exponent γ

$$\gamma = 2 + \frac{1}{d-2}.$$

(C.4)

Therefore, for $d = 3$ we obtain $\gamma = 3$ and for $d = 4$ we obtain $\gamma = 5/2 = 2.5$. In Fig. *C.2a* we show the agreement between the analytic expression (dashed lines) and the computational results (data points).
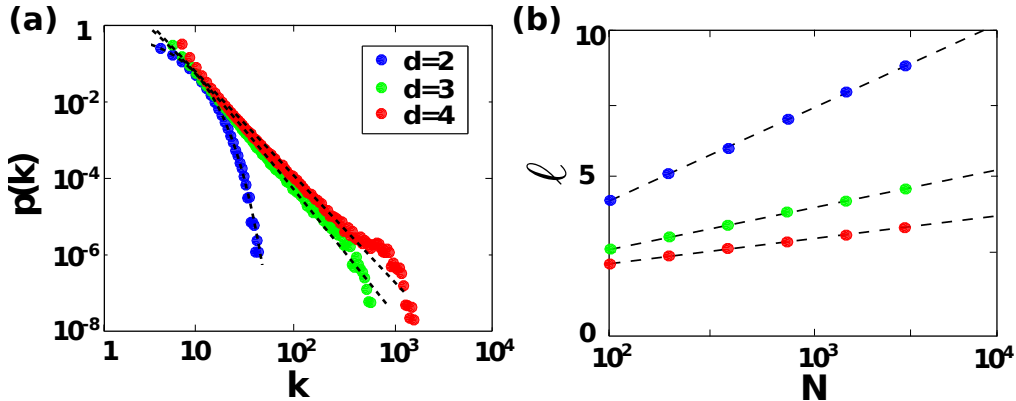

Figure C.1: **Degree distribution and small-word properties of Complex Network Manifolds.** **(a)** Degree distribution $p(k)$ of CNMs of $N = 6400$ nodes and dimensions $d = 2, 3$ and 4. Points represent results from numerical simulations whereas dashed lines stand for the analytical result as given by Eq. *C.*1 and *C.*2. **(b)** Network diameter D versus the network size N for dimensions $d = 2$, 3, 4. Data points are from simulation results whereas dashed lines correspond to the logarithmic fit. Numeric results have been averaged over 100 network realizations in both plots.

The logarithmic scaling of the average shortest (hopping) distance ℓ between the nodes of the network with the network size N, is known to reveal the small-world (Watts and Strogatz, 1998) nature of a network. By investigating numerically the scalling of ℓ with N we show that Complex Network Manifolds are small world. Our result are reported in Fig. *C.2b* where points represent data from numerical simulations of Complex Network Manifold of dimension d, whereas the solid lines stand for the best logarithmic fit, as given by

$$\ell = a_d \log(N) + b_d. \tag{C.5}$$

The parameters from the fit are shown in the Table *C.I*, and they clearly indicate that the Complex Network Manifolds of higher dimension d have a average shortest distance that grows always logarithmically with the network size N but with different constant prefactor a_d.

d	a_d	b_d	R^2
2	2.93(3)	$-1.45(9)$	0.983
3	1.32(2)	0.17(4)	0.964
4	0.78(1)	0.79(4)	0.954

Table C.I: Fitted parameters a_d and b_d determining the logarithmic growth of the average shortest (hopping) distance ℓ of Complex Network Manifolds in dimension d according to Eq. $C.5$.

C.2   Complex Network Manifolds that have been used for the movies of temporal activity

Further Supplementary Materials include the movies for the temporal activity of three Complex Network Manifolds in $D = 1$, $D = 2$ and $D = 3$ respectively. These networks have $N = 200$ nodes and random assignment of their internal frequencies. The activity of the nodes is recorded for different values of the coupling constant σ by coloring the nodes according to a color code depending on $\cos(\theta)$.

In figure $C.2$ as a reference we plot the $R(T)$ curve as a function of the coupling constant σ as recorded for the Complex Network Manifolds captured by the movies.
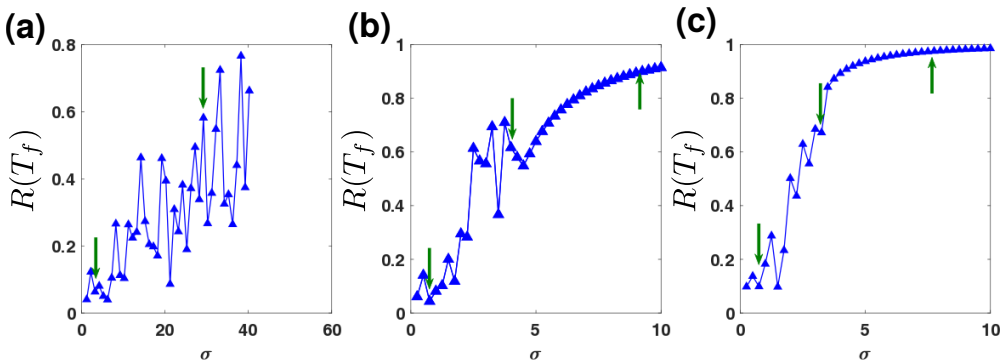

Figure C.2: **Frustrated synchronization for the CNMs shown in the movies.** The synchronization order parameter $R(T)$ is plotted versus the coupling strength σ for $D = 1$ **(a)**, $D = 2$ **(b)** and $D = 3$ **(c)**, for a single network realization of $N = 200$ nodes. The arrows indicate the coupling constants σ at which the movies are recorded (for $D = 1$, $\sigma = 3, 29$ for $D = 2$ $\sigma = 0.75, 4.00, 8.74$ for $D = 3$ $\sigma = 0.75, 3.25, 7.25$).

Appendix D

Supplementary Information for Chapter 6

In this appendix we will investigate the stability of the synchronized phase by considering the linearized dynamical system given by Eqs. 6.20. The normalized Laplacian $\mathbf{L}$ appearing in Eqs. 6.20 and defined in Eq. 6.1 is diagonalizable with eigenvalues $\{\lambda_i\}_{i=1,2,\ldots,N}$, numbered in increasing order, $0 = \lambda_1 < \lambda_2 \leq \lambda_3, \ldots, \leq \lambda_N$, and therefore can be written as

$$\mathbf{P}^{-1}\mathbf{L}\mathbf{P} = \mathbf{D}, \tag{D.1}$$

where $\mathbf{P}$ is the matrix whose columns are the right eigenvectors $\mathbf{v}^\lambda$ and and $\mathbf{P}^{-1}$ is the matrix whose rows are the left eigenvectors $\mathbf{u}^\lambda$ of $\mathbf{L}$. Notice that we always have $\mathbf{P}^{-1}\mathbf{P} = \mathbf{I}$, where $\mathbf{I}$ indicates the identity matrix, due to the normalization condition of the eigenvectors given by Eq. 6.9.

The vector $\boldsymbol{\theta} = (\theta_1, \theta_2, \ldots, \theta_N)^T$ can be projected both in the base of the right and left eigenvectors, so θ_i can either be expressed as

$$
\begin{aligned}
\theta_i &= \sum_\lambda \theta_\lambda^R v_i^\lambda, \\
\theta_i &= \sum_\lambda \theta_\lambda^L u_i^\lambda,
\end{aligned}
\tag{D.2}
$$

or, equivalently,

$$
\begin{aligned}
\boldsymbol{\theta} &= \mathbf{P}\boldsymbol{\theta}^R, \\
\boldsymbol{\theta} &= [\mathbf{P}^{-1}]^T \boldsymbol{\theta}^L,
\end{aligned}
\tag{D.3}
$$

where we have indicated with $\boldsymbol{\theta}^R$ and $\boldsymbol{\theta}^L$ the column vector of elements θ_λ^R and θ_λ^L, respectively. Inverting these relations we have that $\boldsymbol{\theta}^R$ and $\boldsymbol{\theta}^L$ are given by

$$
\begin{aligned}
\boldsymbol{\theta}^R &= \mathbf{P}^{-1}\boldsymbol{\theta}, \\
\boldsymbol{\theta}^L &= \mathbf{P}^T\boldsymbol{\theta}.
\end{aligned}
\tag{D.4}
$$

Similarly, we can also consider the vector $\boldsymbol{\omega}$ of elements ω_i, and project it along the bases of the right and the left eigenvectors,

$$
\begin{aligned}
\boldsymbol{\omega} &= \mathbf{P}\boldsymbol{\omega}^R, \\
\boldsymbol{\omega} &= [\mathbf{P}^{-1}]^T\boldsymbol{\omega}^L.
\end{aligned}
\tag{D.5}
$$

Inverting these relations we obtain

$$
\begin{aligned}
\boldsymbol{\omega}^R &= \mathbf{P}^{-1}\boldsymbol{\omega}, \\
\boldsymbol{\omega}^L &= \mathbf{P}^T\boldsymbol{\omega},
\end{aligned}
\tag{D.6}
$$

where the elements $\boldsymbol{\omega}^{R,L}$ have the averages

$$
\begin{aligned}
\left\langle \omega_\lambda^{R,L} \right\rangle &= 0. \\
\left\langle \omega_\lambda^R \omega_{\lambda'}^L \right\rangle &= \sum_{i=1}^N \sum_{j=1}^N \langle \omega_i \omega_j \rangle\, u_i^\lambda v_j^{\lambda'} = \delta_{\lambda,\lambda'}.
\end{aligned}
\tag{D.7}
$$

The linearized Eq. 6.20 can also be projected along the bases of right and left eigenvectors, obtaining

$$
\begin{aligned}
\frac{d\theta_\lambda^R}{dt} &= \omega_\lambda^R - \sigma\lambda\theta_\lambda^R, \\
\frac{d\theta_\lambda^L}{dt} &= \omega_\lambda^L - \sigma\lambda\theta_\lambda^L.
\end{aligned}
\tag{D.8}
$$

These equations can be solved obtaining, for $\lambda \neq 0$,

$$
\theta_\lambda^{R/L}(t) = e^{-\sigma\lambda t}\theta_\lambda^{R/L}(0) + \frac{\omega_\lambda^{R/L}}{\sigma\lambda}(1 - e^{-\sigma\lambda t}),
\tag{D.9}
$$

and, for $\lambda = 0$,

$$
\theta_\lambda^{R/L}(t) = \theta_{\lambda=0}^{R/L}(0) + \omega_{\lambda=0}^{R/L}t.
\tag{D.10}
$$

D.1   Stability of the synchronized phase

In order to evaluate the stability of the synchronized state, we use an approach already established for finite lattices (Hong et al., 2005; Hong et al., 2007) and calculate the **average fluctuation of the phases** over the entire network by evaluating W^2 given by

$$
W^2 = \frac{1}{N}\left\langle \sum_{i=1}^N [\theta_i(t) - \bar{\theta}]^2 \right\rangle,
\tag{D.11}
$$

where

$$\bar{\theta} = \frac{1}{N} \sum_{i=1}^{N} \theta_i(t). \tag{D.12}$$

In presence of a thermodynamically stable synchronized phase, the average fluctuations of the phases W^2 should remain bounded. Therefore, if W^2 diverges with the network size N, the synchronized phase is unstable.

Since $\boldsymbol{\theta}$ can be expressed equivalently in the base of right and left eigenvectors as expressed in Eqs. $D.3$, and the right eigenvector is given by the first of Eqs. 6.5, we can calculate $\bar{\theta}$ in terms of $\boldsymbol{\theta}^L$ and $\boldsymbol{\theta}^R$ as

$$\bar{\theta} = \sqrt{\frac{\langle k \rangle}{N}} \theta^L_{\lambda=0}(t)$$
$$\bar{\theta} = \sum_{\lambda} \theta^R_{\lambda}(t) \frac{1}{N} \sum_{i} v_i^{\lambda} \tag{D.13}$$

Using the explicit solution of $\theta^L_{\lambda}(t)$ and $\theta^R_{\lambda}(t)$ given by Eq. $D.9$ and Eq. $D.10$, and using Eqs. $D.7$ we can express $\left\langle \bar{\theta}^2 \right\rangle$ as

$$\left\langle \bar{\theta}^2 \right\rangle = \frac{1}{N} \left\langle \theta^L_{\lambda=0}(t)\theta^R_{\lambda=0}(t) \right\rangle + \sqrt{\frac{\langle k \rangle}{N}} \theta^L_{\lambda=0}(0)\theta^R_{\lambda=0}(0)$$
$$\times \sum_{\lambda \neq 0} e^{-\sigma\lambda t} \frac{1}{N} \sum_{i=1}^{N} v_i^{\lambda}. \tag{D.14}$$

Therefore asymptotically in time, for $t \to \infty$, we obtain

$$\left\langle \bar{\theta}^2 \right\rangle = \frac{1}{N} \left\langle \theta^L_{\lambda=0}(t)\theta^R_{\lambda=0}(t) \right\rangle. \tag{D.15}$$

We now note that W^2 can be equivalently expressed as

$$W^2 = \frac{1}{N} \left\langle \boldsymbol{\theta}^T \boldsymbol{\theta} \right\rangle - \left\langle \bar{\theta}^2 \right\rangle. \tag{D.16}$$

Using Eq. $D.4$ we note that $\left\langle \boldsymbol{\theta}^T \boldsymbol{\theta} \right\rangle$ has a simple expression in terms of $\boldsymbol{\theta}^L$ and $\boldsymbol{\theta}^R$, i.e.

$$\left\langle \boldsymbol{\theta}^T \boldsymbol{\theta} \right\rangle = \left\langle [\boldsymbol{\theta}^L]^T \mathbf{P}^{-1} \mathbf{P} [\boldsymbol{\theta}^R] \right\rangle = \left\langle [\boldsymbol{\theta}^L]^T \boldsymbol{\theta}^R \right\rangle. \tag{D.17}$$

Using the solution of the Kuramoto dynamics Eq. $D.9$ and Eqs. $D.7$ we get

$$\left\langle [\boldsymbol{\theta}^L]^T \boldsymbol{\theta}^R \right\rangle = \left\langle \theta^L_{\lambda=0}(t)\theta^R_{\lambda=0}(t) \right\rangle$$
$$+ \sum_{\{\lambda\}|\lambda\neq 0} \left[e^{-2\sigma\lambda t}\theta^R_{\lambda}(0)\theta^L_{\lambda}(0) + \frac{1}{(\sigma\lambda)^2}(1 - e^{-\sigma\lambda t})^2 \right]. \tag{D.18}$$

Finally using Eq. *D*.16 together with Eqs. *D*.15-*D*.18, it results that asymptotically in time for $t \to \infty$

$$W^2 = \int_{\lambda_2}^{\lambda_{max}} d\lambda \rho(\lambda) \frac{1}{(\sigma\lambda)^2}. \tag{D.19}$$

Since the Fidler eigenvalue λ_2 satisfies the scaling expressed in Eq. 6.14 and goes to zero in the infinite network limit, using the scaling in Eq. 6.10 for the density of eigenvalues $\rho(\lambda)$ we obtain the following results.

i) For spectral dimension $d_S < 4$ the average fluctuation of the phases W^2 diverges as

$$W^2 \simeq O\left(\lambda_2^{d_S/2-2}\right) \tag{D.20}$$

ii) For spectral dimension $d_S = 4$ the average fluctuation of the phases W^2 diverges as

$$W^2 \simeq O(-\ln \lambda_2). \tag{D.21}$$

iii) Only for spectral dimension $d > 4$ the average fluctuation of the phases W^2 converges.

Specifically, by inserting the scaling of the Fidler eigenvalue Eq. 6.14 with the network size N we obtain

$$W^2 \sim \begin{cases} N^{4/d_S-1} & \text{if } d_S < 4 \\ \ln(N) & \text{if } d_S = 4 \\ \text{const} & \text{if } d_S > 4. \end{cases} \tag{D.22}$$

It follows from this derivation that the synchronized state cannot be thermodynamically stable in networks with spectral dimension $d_S \leq 4$.

D.2   Correlations between phases and validity of the linear approximation

The linear approximation is valid only if the coupling term of each oscillator with the phases of the linked oscillators is small. Therefore in order for the linear approximation to hold we must require that the vector $\mathbf{L}\boldsymbol{\theta}$ has small elements. A global parameter that can establish the sufficient condition for the failure of the linear approximation is the **correlation** C defined as

$$C = \frac{1}{N} \left\langle \boldsymbol{\theta}^T \mathbf{L} \boldsymbol{\theta} \right\rangle. \tag{D.23}$$

In fact, if the correlation C diverges the linear approximation cannot be valid.

The correlation can be expressed in the basis of eigenvalues of the normalized Laplacian getting the simple expression

$$C = \frac{1}{N} \sum_{\lambda} \left\langle \theta_\lambda^L \lambda \theta_\lambda^R \right\rangle. \tag{D.24}$$

By using the explicit expression for $\theta_\lambda^{L/R}$ given by Eq. *D.9* it is easy to show that

$$C = \frac{1}{N} \sum_{\{\lambda\}|\lambda \neq 0} \lambda \left[e^{-2\sigma\lambda t} \theta_\lambda^R(0)\theta_\lambda^L(0) + \frac{1}{(\sigma\lambda)^2}(1 - e^{-\sigma\lambda t})^2 \right]$$

which gives in the asymptotic limit $t \to \infty$

$$C = \int_{\lambda_2}^{\lambda_N} \rho(\lambda) \frac{1}{\sigma^2 \lambda} d\lambda. \tag{D.25}$$

> By inserting the scaling of the Fidler eigenvalue with the network size N given by Eq. 6.14, we obtain
>
> $$C \sim \begin{cases} N^{2/d_S - 1} & \text{if } d_S < 2 \\ \ln(N) & \text{if } d_S = 2 \\ \text{const} & \text{if } d_S > 2. \end{cases} \tag{D.26}$$
>
> Therefore, for spectral dimension $d_S \leq 2$ the correlations among the phases of nearest neighbor nodes diverge and the linear approximation fails.

D.3 Entrained phases

So far we have shown that for spectral dimension $d_S < 2$ the linear approximation fails, while for spectral dimensions $d_S \in (2,4]$ the linear approximation can be valid but the sychronized phase is not thermodynamically stable. In order to uncover the phenomenology for spectral dimensions $d_S \in (2,4]$, we follow the approach used by Hong et al., 2005; Hong et al., 2007 for regular lattices. This analysis will reveal that for spectral dimensions $d_S \in (2,4]$ phase entrainment takes place as long as the linear approximation is valid.

We start by characterizing the fluctuations observed in phase velocities across the nodes of the network

$$V^2 = \frac{1}{N} \sum_{i=1}^{N} \left\langle \left[\psi_i - \bar{\psi} \right]^2 \right\rangle \tag{D.27}$$

where ψ_i indicates the phase velocity of node i

$$\psi_i = \dot{\theta}_i, \tag{D.28}$$

and $\bar{\psi}$ the average of the phase velocities over the network

$$\bar{\psi} = \frac{1}{N} \sum_{i=0}^{N} \psi_i. \tag{D.29}$$

The phase velocities $\boldsymbol{\psi} = (\psi_1, \psi_2, \ldots, \psi_N)^T$ can be projected into the basis of right and left eigenvectors of the normalized Laplacian getting

$$\begin{aligned}
\boldsymbol{\psi}^R &= \mathbf{P}^{-1}\boldsymbol{\psi}, \\
\boldsymbol{\psi}^L &= \mathbf{P}^T\boldsymbol{\psi}.
\end{aligned} \tag{D.30}$$

By using the solution of the linearized dynamics, Eqs. *D*.9 and *D*.10, it is easy to show that with the linear approximation we have

$$\psi_\lambda^{R/L}(t) = \dot{\theta}_\lambda^{R/L} = -\sigma\lambda e^{-\sigma\lambda t}\theta_\lambda^{R/L}(0) + \omega_\lambda^{R/L}e^{-\sigma\lambda t}, \tag{D.31}$$

and for $\lambda = 0$

$$\psi_\lambda^{R/L}(t) = \omega_{\lambda=0}^{R/L}. \tag{D.32}$$

Using the same procedure used previously for the derivation of $\bar{\theta}$, it is easy to show that the average phase velocity $\bar{\psi}$ can be expressed equivalently as

$$\begin{aligned}
\bar{\psi} &= \sqrt{\frac{\langle k \rangle}{N}}\psi_{\lambda=0}^L(t), \\
\bar{\psi} &= \sum_\lambda \psi_\lambda^R(t)\frac{1}{N}\sum_i v_i^\lambda.
\end{aligned} \tag{D.33}$$

From these expressions, and using Eqs. *D*.7, it follows that

$$\left\langle \bar{\psi}^2 \right\rangle = \frac{1}{N}\left\langle \psi_{\lambda=0}^L(t)\psi_{\lambda=0}^r(t) \right\rangle. \tag{D.34}$$

Finally using again Eq. *D*.7 we get that

$$V^2 = \frac{1}{N}\left\langle [\boldsymbol{\psi}^L]^T\boldsymbol{\psi}^R \right\rangle - \left\langle \bar{\psi}^2 \right\rangle \tag{D.35}$$

scales in the asymptotic limit $t \to \infty$ as

$$V^2 \sim \int_{\lambda_2}^{\lambda_{max}} d\lambda\rho(\lambda)e^{-2\sigma\lambda t} \sim t^{-d_S/2}.$$

This result implies that asymptotically in time the fluctuations in the phase velocities vanish, i.e.

$$V^2 \to 0 \tag{D.36}$$

as $t \to \infty$. This result implies that the phases of the oscillators are totally entrained as long as the linear approximation is valid.